The Role of XBP1 in Necroptosis-Induced Intestinal Inflammation

Inaugural-Dissertation

zur

Erlangung des Doktorgrades

der Mathematisch-Naturwissenschaftlichen Fakultät

der Universität zu Köln

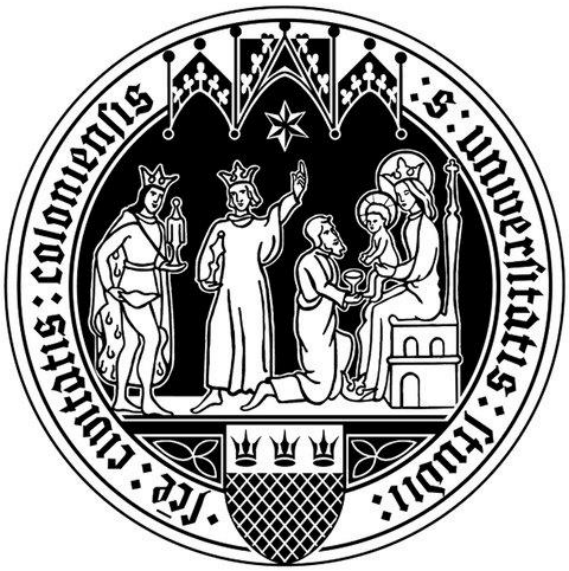

vorgelegt von

Göksu Gökberk Kaya

aus Ankara

Köln, 2024

Berichterstatter:
Prof. Dr. Manolis Pasparakis

Prof. Dr. Hamid Kashkar

Prof. Dr. Philip Rosenstiel

Vorsitzender der Prüfungskommission:
Prof. Dr. Matthias Hammerschmidt

Tag der mündlichen Prüfung: 21.11.2024

Abstract

Intestinal epithelial cells (IECs) form an epithelial barrier which is covered and reinforced with the mucus layer. The intestinal epithelium and the mucus layer play critical roles in the regulation of intestinal immune homeostasis by establishing a stratified, protective barrier against luminal microbiota. Dysregulated epithelial cell death and a bacteria-permeable mucus layer were implicated in inflammatory bowel disease (IBD). While environmental factors including gut microbiota are thought to contribute to the disease pathology, the host's genetic background is a significant determinant of predisposition to IBD. Specifically, hypomorphic variants of X-box binding protein 1 (*XBP1)*, a gene encoding a critical transcription factor in response to endoplasmic reticulum (ER) stress, were identified in IBD patients. Meanwhile, humans deficient in caspase-8, a protein inhibiting necroptosis, were reported to develop intestinal inflammation. The polygenic risk score is a critical tool for assessing the predisposition to IBD, however, the crosstalk of multiple genetic variants and their pathways remains to be elucidated. In this study, we investigated the interaction between XBP1 deletion-induced ER stress and necroptosis triggered by the ablation of caspase-8 (Casp8) or Fas-associated with death domain (FADD) in IECs. Our results revealed that colitis but not ileitis in mice lacking epithelial-specific Casp8 or FADD was exaggerated by XBP1 deficiency. We showed that genetic inhibition of IEC necroptosis rescued the severe colitis in mice lacking XBP1 and Casp8 or XBP1 and FADD. IEC-derived Tumor necrosis factor (TNF) did not play an important role in the exacerbation of colitis, however, colitis was driven by epithelial-intrinsic TNF receptor 1 (TNFR1) in mice lacking XBP1 and Casp8. Importantly, we found that MUCIN-2 (MUC2), a gel-forming mucin crucially required for the formation of bacteria-impermeable mucus layer in the colon, was strongly downregulated in the colons of XBP1 deficient mice. Mice lacking XBP1 in IECs showed an intact intestinal epithelium covered by a dysfunctional mucus layer leading to increased contact between luminal bacteria and the apical regions of colonic epithelial cells. Whereas XBP1 deficiency-induced mucus barrier impairment did not culminate in spontaneous colon inflammation, it strongly synergised with epithelial necroptosis and exaggerated the colitis in mice lacking Casp8 or FADD. Furthermore, we showed that the impairment of the mucus layer in XBP1 deficiency was independent of extrinsic apoptosis and necroptosis of IECs. Taken together, this study revealed a hitherto unidentified link between ER stress, necroptosis and mucus layer in intestinal inflammation, which could contribute to understanding the pathogenesis of IBD.

Table of Contents

Table of Figures ..... *V*

List of Tables ..... *VI*

List of Abbreviations ..... *VII*

Abbreviation of units ..... *X*

1. Introduction *1*

1.1 Innate immune system and inflammation **1**

1.2 DAMPs, cell death and inflammation **3**

1.2.1 DAMPs and inflammation 3

1.2.2 Cell death 3

1.3 Endoplasmic reticulum and Unfolded protein response **9**

1.3.1 Structure and function of Endoplasmic reticulum 9

1.3.2 ER stress and Unfolded protein response 10

1.4 The mammalian intestine **13**

1.4.1 Anatomy and physiology of the mammalian intestine 13

1.4.2 Intestinal epithelial cells and intestinal epithelium 14

1.4.3 Paneth cells 16

1.4.4 Goblet cells, mucins and the mucus layer 17

1.4.5 Inflammatory bowel disease 19

1.5 Objective of the study **23**

2. Results *24*

2.1 IEC-specific XBP1 suppresses the colitis in *Casp8*$^{IEC-KO}$ mice **24**

2.1.1 Characterization of *Xbp1*$^{IEC-KO}$ mice 24

2.1.2 *Xbp1*$^{IEC-KO}$ *Casp8*$^{IEC-KO}$ mice exhibit severe colitis compared to *Casp8*$^{IEC-KO}$ mice 28

2.2 XBP1 deficiency aggravates colitis in *Casp8*$^{IEC-KO}$ and *Fadd*$^{IEC-KO}$ mice necroptosis-dependent manner **33**

2.2.1 Ubiquitous RIPK3 or MLKL deletion inhibits severe colitis in *Xbp1*$^{IEC-KO}$ *Casp8*$^{IEC-KO}$ mice 33

2.2.2 IEC-specific XBP1 deletion exaggerates the necroptosis-induced colitis in *Fadd*$^{IEC-KO}$ mice 35

2.3 IEC-specific XBP1 does not play an important role in necroptosis-induced or -driven ileitis **39**

2.3.1 Ablation of IEC-specific XBP1 does not increase the severity of ileitis in *Casp8*$^{IEC-KO}$ mice 39

2.3.2 Epithelial XBP1 does not protect from severe ileitis in *Fadd*$^{IEC-KO}$ mice 41
2.3.3 IEC-specific XBP1 deficiency leads to Paneth cell impairment and crypt hyperplasia independent of extrinsic apoptosis and necroptosis 42
2.4 The contribution of IEC-specific TNF and TNFR1 to necroptosis-induced intestinal inflammation in *Xbp1*$^{IEC-KO}$ *Casp8*$^{IEC-KO}$ mice 44
2.4.1 Epithelial TNFR1 drives the exacerbated colitis in *Xbp1*$^{IEC-KO}$ *Casp8*$^{IEC-KO}$ mice 44
2.4.2 Epithelial cell-intrinsic TNF and TNFR1 do not drive necroptosis-induced ileitis in *Xbp1*$^{IEC-KO}$ *Casp8*$^{IEC-KO}$ mice 48
2.5 Epithelial-specific XBP1 is required for the formation of the functional mucus layer in the colon 49
2.5.1 MUC2 is strongly reduced in the colons of *Xbp1*$^{IEC-KO}$ mice 49
2.5.2 XBP1 deficiency impairs the inner mucus layer in the colon 52
2.5.3 Epithelial-specific XBP1 but not Casp8 regulates mucin levels in the colon 55
2.5.4 XBP1 suppresses the translocation of luminal bacteria into colonic sublayers and prevents systemic inflammation in *Casp8*$^{IEC-KO}$ mice 57
2.6 XBP1 deficiency leads to the dysfunctional mucus layer independent of extrinsic apoptosis, necroptosis and TNFR1 signalling in IECs 59
2.6.1 Combined inhibition of extrinsic apoptosis and necroptosis do not restore the mucus barrier impairment 59
2.6.2 IEC-specific TNFR1 does not contribute to the impairment of the mucus layer in *Xbp1*$^{IEC-KO}$ mice 63
2.6.3 Glycosylation reactions are not completely lost in the colons of mice lacking XBP1 66
2.7 Increased bacterial translocation and systemic inflammation in *Xbp1*$^{IEC-KO}$ *Casp8*$^{IEC-KO}$ mice depends on IEC necroptosis 70
2.8 Epithelial XBP1 deficiency causes reduced mucin production in the ileum independent of extrinsic apoptosis and necroptosis 72
3. Discussion 74
3.1 XBP1 suppresses necroptosis-induced colitis by regulating the formation of bacteria-impermeable mucus barrier 74
3.1.1 XBP1-deletion-induced impaired mucus barrier per se aggravates necroptosis-induced colitis 74
3.1.2 Epithelial XBP1 deficiency might alter the composition of colonic microbiota driving the exaggeration of necroptosis-induced Colitis 78
3.2 The possible mechanisms by which XBP1 deficiency impairs the mucus layer 79
3.2.1 Death of Goblet cells and mucus layer 79

3.2.2 Contribution of the cell death-independent pathways to the impaired mucus layer in XBP1 deficiency....80
3.2.3 The regulatory role of epithelial XBP1 in other mucins and mucus-associated proteins....86
3.3 Differential effects of epithelial TNFR1 and TNF on necroptosis-induced colitis....86
3.4 Effect of epithelial-specific XBP1 on ileitis in *Casp8*$^{IEC-KO}$ and *Fadd*$^{IEC-KO}$ mice....88
4. Concluding Remarks....90
5. Materials and Methods....91
5.1 Materials....91
5.1.1 Antibodies, chemicals, commercial kits and equipment....91
5.1.2 Buffers and solutions....96
5.1.3 Software....96
5.2 Methods....97
5.2.1 Animal Experiments....97
5.2.2 Histology....98
5.2.3 Molecular Biology....101
5.2.4 Cell Culture....106
6. References....109
7. Acknowledgement....141
8. Erklärung zur Dissertation.... *Error! Bookmark not defined.*

Table of Figures

Figure 1-1 The formation of complex I and complex II under TNFR1. 5
Figure 1-2 TNFR1-induced apoptosis and necroptosis. 7
Figure 1-3 IRE1α-mediated Unfolded protein response. 12
Figure 1-4 Intestinal epithelial cells, the intestinal epithelium and the layers of the intestine in the small intestine and colon. 15
Figure 1-5 Discrepancy between the mucus layers in the small intestine and colon. 18
Figure 2-1 Indirect confirmation of XBP1 deletion in the intestines of Xbp1^{IEC-KO} mice. 26
Figure 2-2 Xbp1^{IEC-KO} mice show mild hyperplasia and impaired Paneth cells in the ileum. 27
Figure 2-3 Xbp1^{IEC-KO} mice do not show an observable pathology in the colon. 28
Figure 2-4 *Xbp1*$^{IEC-KO}$ *Casp8*$^{IEC-KO}$ mice have reduced body weight compared to *Casp8*$^{IEC-KO}$. 29
Figure 2-5 Deletion of XBP1 aggravates colitis in Casp8^{IEC-KO} mice. 30
Figure 2-6 *Xbp1*$^{IEC-KO}$ *Casp8*$^{IEC-KO}$ mice develop more severe colitis compared to *Casp8*$^{IEC-KO}$ mice. 31
Figure 2-7 Histopathological assessment and RNA sequencing analysis of colons from control, Xbp1^{IEC-KO}, Casp8^{IEC-KO} and Xbp1^{IEC-KO} Casp8^{IEC-KO} mice. 32
Figure 2-8 Ablation of RIPK3 or MLKL restores the body weight of Xbp1^{IEC-KO} Casp8^{IEC-KO} mice. 33
Figure 2-9 Inhibition of RIPK3-MLKL-dependent IEC necroptosis prevents the development of colitis in Xbp1^{IEC-KO} Casp8^{IEC-KO} mice. 34
Figure 2-10 The severe colitis in Xbp1^{IEC-KO} Casp8^{IEC-KO} mice completely depends on epithelial necroptosis. 35
Figure 2-11 IEC-specific XBP1 protects Fadd^{IEC-KO} mice from severe colitis. 36
Figure 2-12 Xbp1^{IEC-KO} Fadd^{IEC-KO} mice have more severe colitis compared to Fadd^{IEC-KO} mice. 37
Figure 2-13 The severe colitis in Xbp1^{IEC-KO} Fadd^{IEC-KO} mice completely depends on epithelial necroptosis. 38
Figure 2-14 Epithelial-specific XBP1 ablation does not exaggerate necroptosis-induced ileitis in Casp8^{IEC-KO} mice. 40
Figure 2-15 Epithelial XBP1 does not play an important role in ileitis in Fadd^{IEC-KO} mice. 42
Figure 2-16 Chronic deficiency of XBP1 does not cause an increased number of CC3- and TUNEL-positive IECs in the ileum. 44
Figure 2-17 IEC-specific TNFR1 but not TNF drives the exacerbation of colitis in *Xbp1*$^{IEC-KO}$ *Casp8*$^{IEC-KO}$ mice. 46
Figure 2-18 Histopathological assessment and RNA sequencing analysis of colons from Xbp1^{IEC-KO} Casp8^{IEC-KO} Tnf^{IEC-KO} and Xbp1^{IEC-KO} Casp8^{IEC-KO} Tnfr1^{IEC-KO} mice. 47
Figure 2-19 IEC-Specific TNF and TNFR1 do not contribute to ileitis in Xbp1^{IEC-KO} Casp8^{IEC-KO} mice. 49
Figure 2-20 Ablation of XBP1 in IECs causes diminished Muc2 expression in the colon. 50
Figure 2-21 Epithelial XBP1 regulates the production of MUC2 in the colon. 51
Figure 2-22 Xbp1^{IEC-KO} mice have impaired inner mucus layer in the colon. 53
Figure 2-23 Luminal bacteria are not separated from the colonic epithelial cells with XBP1 deficiency. 54
Figure 2-24 ZG16 production is reduced in the colons of Xbp1^{IEC-KO} mice. 55
Figure 2-25 Deficiency of XBP1 but not caspase-8 reduces MUC2 expression in the colonic epithelium. 56
Figure 2-26 Epithelial-specific XBP1 restricts bacterial translocation into colonic submucosa in Casp8^{IEC-KO} mice. 58
Figure 2-27 Xbp1^{IEC-KO} Caps8^{IEC-KO} mice exhibit markers of systemic inflammation. 59

Figure 2-28 XBP1 deficiency does not lead to increased caspase-3- and TUNEL-positive IECs in the colon compared to control mice. 60
Figure 2-29 Extrinsic apoptosis and necroptosis do not contribute to the formation of the impaired mucus barrier in the colons of Xbp1^{IEC-KO} mice. 62
Figure 2-30 Xbp1^{IEC-KO} Casp8^{IEC-KO} Ripk3$^{-/-}$ and Xbp1^{IEC-KO} Casp8^{IEC-KO} Mlkl$^{-/-}$ mice do not show increased numbers of cleaved caspase-3- and TUNEL-positive colonic IECs compared to control mice. 63
Figure 2-31 TNFR1 signalling in epithelium does not play an important role in reduced mucin production in the colons of Xbp1^{IEC-KO} mice. 65
Figure 2-32 Xbp1^{IEC-KO} Tnfr1^{IEC-KO} mice show an impaired mucus layer in the colon. 66
Figure 2-33 XBP1 deficiency does not lead to complete loss of certain glycosylation reactions in Goblet cells. 68
Figure 2-34 XBP1-deficient colon organoids have strongly reduced Muc2 expression upon differentiation into Goblet cells. 69
Figure 2-35 Inhibition of IEC necroptosis prevents bacterial translocation into the colonic sublayers and systemic inflammation in *Xbp1*$^{IEC-KO}$ *Casp8*$^{IEC-KO}$ mice. 71
Figure 2-36 XBP1 deficiency results in impaired mucin production in the ileum independent of extrinsic apoptosis and necroptosis. 72
Figure 3-1 The main proposed mechanism by which epithelial-specific XBP1 protects from severe necroptosis-induced colitis in mice with IEC-Specific Casp8 or FADD deficiency. 76
Figure 3-2 The possible mechanisms by which XBP1 deletion in IECs could lead to reduced MUC2 production. 83

List of Tables

Table 5-1. Antibodies, chemicals, commercial kits, and equipment used in this thesis. 96
Table 5-2 Genotyping PCR primers and the expected band sizes of the genotyping PCRs. 103

List of Abbreviations

APAF-1	Apoptotic protein-activating factor-1
ATF6	Activating transcription factor 6
BAK	Bcl-2 antagonist/killer-1
BAX	Bcl-2 associated X
Bcl-2	B-cell lymphoma 2
BH-3	Bcl-2 homology region 3
BID	BH-3 interacting domain death agonist
BOK	Bcl-2-related ovarian killer
Casp8	caspase-8
CBCs	Crypt-base columnar cells
CD	Crohn’s disease
CFTR	chloride and bicarbonate ion channel transmembrane regulator
cIAP1/2	cellular inhibitors of apoptosis1/2
DAB	3,3'Diaminobenzidine
DAMPs	Damage-associated molecular patterns
DAPT	N-[N-(3,5-Difluorphenacetyl)-L-alanyl]-S-phenylglycin-tert-butylester
DRs	Death receptors
DSS	Dextran sulfate sodium
EIF2AK3	eukaryotic translation initiation factor 2 alpha kinase 3
ER	Endoplasmic Reticulum
ERAD	ER-associated protein degradation
ERN1	Endoplasmic Reticulum to nucleus signalling 1
ERN2	Endoplasmic Reticulum to nucleus signalling 2
FADD	Fas-associated with death domain

FISH	fluorescence *in situ* hybridization
GALT	Gut-associated lymphoid tissues
GWAS	Genome-wide association studies
IBD	Inflammatory Bowel Disease
IECs	Intestinal epithelial cells
IF	Immunofluorescence
IFN	Interferon
IgA^+	Immunoglobulin A-positive
IHC	Immunohistochemistry
IκB	Inhibitor of NF-κB
IKK1/α	IκB-kinase-1
IKK2/β	IκB-kinase-2
IL	Interleukin
ILF	Isolated lymphoid follicles
IRAK	Interleukin-1 associated-receptor kinase
IRE1α	Inositol requiring enzyme 1α
LGR5	Leucine-rich repeat-containing G protein-coupled receptor 5
LRR	Leucine-rich repeat
LUBAC	Linear ubiquitin chain assembly complex
M cells	Microfold cells
MAPK	Mitogen-activated protein kinase
MCS	Membrane contact sites
MLKL	Mixed lineage kinase domain-like pseudokinase
MOMP	mitochondrial outer membrane permeabilization
MUC2	MUCIN-2
MTX	Methotrexate

MyD88	Myeloid differentiation primary response 88
NEMO	NF-κB essential modulator
NF-κB	Nuclear factor κ-light-chain-enhancer of activated B cells
NOD	Nucleotide-binding oligomerisation domain
NLRP6	NOD-like receptor family pyrin domain containing 6
PAS	Periodic Acid Schiff
PCR	Polymerase chain reaction
PFA	Paraformaldehyde
PERK	Protein kinase-like RNA kinase
PRR	Pattern-recognition receptors
PTS	Proline-Threonine-Serine
RIDD	Regulated Ire1-dependent decay
RIPK1	Receptor-interacting protein kinase 1
RHIM	RIP homotypic interaction motif
RT-PCR	Reverse transcriptase-PCR
SMAC	Second mitochondria-derived activator of caspase
TA	Transit-amplifying cells
TAB1/2	TAK1 binding protein-1/2
TAK1	TGF-beta activating kinase-1
TICAM	TIR containing adaptor molecule
TIR	Toll-IL-1 receptor
TFF3	Trefoil factor 3
TLRs	Toll-like Receptors
TNF	Tumour necrosis factor
TNFR1	TNF Receptor 1
TRADD	TNFR1-associated DD

TRAF2	TNFR-associated factor 2
TRIF	TIR-domain containing adaptor inducing IFN-β
qRT-PCR	Quantitative Real Time PCR
UC	Ulcerative colitis
XBP1	X-box Binding Protein 1
XIAP	X-linked inhibitor of apoptosis protein
ZG16	Zymogen granule protein 16

Abbreviation of units

V, mV	Volt, millivolt
°C	Degree Celsius
g, mg, μg, ng	gram, milligram, microgram, nanogram
l, ml, μl	litre, millilitre, microlitre

1. Introduction

1.1 Innate immune system and inflammation

The innate immune system had been believed to initiate its signalling cascades in a nonspecific way such as the roles of Alum and Freund's adjuvant in vaccines[1]. Charles Janeway came up with a revolutionary hypothesis, in which innate immune cells are capable of recognising non-host patterns by their receptors[2]. He coined the Pathogen-associated molecular patterns (PAMPs) and Pattern-recognition receptors (PRRs) terms[2]. After this, many PRRs including Toll-like Receptors (TLRs)[3-5] and Nucleotide-binding oligomerisation domain (NOD)-like receptors (NLRs)[6-8] have been identified and characterised.

TLRs can be found either on the cell surface or endosomes, where their corresponding ligands are sensed by their Leucine-rich repeats (LRRs), and the downstream signalling is mediated through their cytoplasmic Toll-interleukin (IL)-1 receptor (TIR) domains[9]. TIR domains of activated TLRs interact with cytoplasmic adaptor proteins containing TIR domains including Myeloid differentiation primary response 88 (MyD88)[10] and TIR-domain containing adaptor inducing interferon (IFN)-β (TRIF or TIR containing adaptor molecule (TICAM))[11]. Adaptor proteins recruited to TLRs activate the signalling cascades, which primarily lead to the production of inflammatory cytokines, chemokines, and type I IFNs[12]. In addition to the localisation, TLRs can be grouped based on which adaptor protein mediates their signalling: MyD88 or TRIF[9,12]. However, TLR4 was found to be an exception, utilizing both MyD88- and TRIF-mediated signalling[12].

Among other ligands[13,14], TLR4-mediated inflammatory response is activated by Lipopolysaccharide (LPS) as macrophages isolated from TLR4 deficient mice do not produce and secrete Tumor necrosis factor (TNF) and Nitric oxide[15]. Overexpression of MyD88, (Interleukin-1 associated-receptor kinase) IRAK and TNF-associated factor 6 (TRAF6) was found to activate Nuclear Factor κ-light-chain-enhancer of activated B cells (NF-κB, p65/p50 heterodimers) as well as mitogen-activated protein kinase (MAPK) pathway, suggesting TLR4 employs MyD88-IRAK-TRAF6 complex to induce inflammatory cytokine production[16]. Indeed, mice lacking MyD88 are protected from lethality and cannot produce inflammatory cytokines upon LPS injection[17]. Further characterizations of this pathway reveal that the interaction between MyD88-IRAKs-TRAF6 and TLR4 is established by TIR-domain containing adaptor protein (TIRAP)[18-20]. While TRAF6

generates K63-linked polyubiquitin chains[21], Linear ubiquitin chain assembly complex (LUBAC) recruited upon K63-linked ubiquitination provides M1-linked linear ubiquitin chains[22-24] which are crucial for the recruitment of NF-κB essential modulator (NEMO)[25] and Growth factor-beta (or TGF-β) activating kinase-1 (TAK1) via TAK1 binding proteins (TAB1/2)[26]. Inhibitor of NF-κB (IκB) kinase-1 and -2 (IKK1 and IKK2) are recruited with NEMO and activated by TAK1-mediated phosphorylation, and active IKK1/2 complex catalyses the phosphorylation of IκBα, targeting it to ubiquitin-mediated proteosome-dependent degradation[27,28]. As IκBα interacts with p65/p50 and restricts their activation by preventing their nuclear translocation, degradation of IκBα allows p65/p50 to translocate into the nucleus, inducing the expression of pro-inflammatory and pro-survival genes[29]. Meanwhile, TAK1 induces the activation of MAPKs in which a series of phosphorylation events take place, culminating in the induction of inflammatory cytokines by allowing the translocation of transcription factors including AP-1 and c-Jun into the nucleus[12].

It was found that upon LPS challenge, activation of NF-κB lags in cells lacking MyD88, and they can still express IFN-β, showing MyD88-independent pathway exists under TLR4[17,30,31]. Indeed, TRIF was found to be recruited to TLR4-TRAM on endosomes and activate the TANK-binding protein kinase-1 (TBK1)/IKKε-IRF3 pathway, leading to the induction of IFN-β[32-35]. Meanwhile, TRAF6 recruited to TRIF activates MAPK and NF-κB pathways[36]. Importantly, Receptor interacting-protein serine/threonine-kinase 1 (RIPK1) can be recruited to TRIF via their RIP homotypic interaction motif (RHIM) domains and contributes to the activation of NF-κB pathway[37,38]. Of note, TRIF-RIPK1 interaction is critical for pathogen and PAMPs induced cell death pathways as well[37].

TLR2/1-2/6-5-7-9 and TLR3 utilize similar proteins of the cascades to elicit responses upon their corresponding ligand engagement, as described in MyD88- and TRIF-dependent signalling cascades of TLR4, respectively[12].

1.2 DAMPs, cell death and inflammation

1.2.1 DAMPs and inflammation

It has been known that a flare-up of inflammation can still happen without an infection, and this phenomenon is termed sterile inflammation[39]. After a series of discussions in the field[40-42], the term Damage-associated molecular pattern (DAMPs) is shaped to define the host-derived molecules/ions that can initiate an immune response[43]. The DAMP model places the cellular and tissue level damage in the centre of immune induction, however, this does not contradict Janeway's model, rather PAMP and DAMP-based models coexist, and the inflammation aroused from PAMPs/DAMPs is thought to be critical for the pathogen clearance and tissue restoration[42].

DAMPs can be classified based on their molecular nature such as nucleic acids, metabolites, and proteins[43]. For example, Heat shock proteins (HSPs)[44,45] as well as histones[46] in extracellular environment are found to be recognised by TLR4 and induce the expression of inflammatory cytokines. As HSPs and histones can be found within different cellular comportments, the loss of spatial confinement of host-derived molecules is one route to achieve DAMP-mediated inflammation, and cell death plays a pivotal role in the induction of immune responses by allowing DAMPs to be released[43].

1.2.2 Cell death

It is accepted that cell death can happen accidentally or unregulated manner, however, regulated cell death is the major focus of ongoing research[47]. In this thesis, cell death term refers to regulated cell death. Cell death is known to critically contribute to organogenesis, maintenance of tissue homeostasis, immune system ripening and intracellular communication by disposal of redundant, impaired, self-intolerant and infected cells[48].

Several different cell death modalities were identified, and they are broadly classified based on whether plasma membrane permeabilization is involved in the process[49]. Therefore, a superfluous number of cell death can lead to inflammation, as discussed in section 1.2.1 self-derived molecules are capable of triggering the immune responses[48]. Apoptosis is regarded to be a cell death type that does not mount aberrant activation of the immune system as it is almost always non-lytic cell death[49]. The apoptotic cascade

can be initiated by various signals and take different routes (discussed below, Section 1.2.2.1 and 1.2.2.2.). Cysteinyl proteases, caspases, that can cleave target proteins after certain amino acid sequence, play vital roles in apoptosis[50]. Initiator caspases including caspase-8 and -9 integrate upstream signalling cues into the apoptotic cascade leading to cleave of executioner/effector caspases (caspase-3, -7)[51]. It is accepted that hundreds of proteins in a cell committed to apoptosis are being cleaved by active effector caspases, leading to characteristic morphological features of apoptosis including cell shrinkage, pyknosis (nuclear condensation), karyorrhexis (DNA fragmentation) and membrane blebbing[47,48]. In contrast to apoptosis, necroptosis is caspase-independent, lytic cell death, leading to inflammation[52]. RIPK1, RIPK3 and Mixed lineage kinase domain-like pseudokinase (MLKL) are critical regulators and mediators of necroptosis[48]. The roles of RIPK1 and RIPK3 in necroptosis are discussed below (Section 1.2.2.1). Phosphorylation of MLKL by active RIPK3 is a critical event in the necroptosis pathway as phosphorylated MLKL is translocated to the plasma membrane and oligomerises, leading to membrane rupture[49,53-55]. Whereas a large body of evidence put forward two hypotheses[48,49], the exact mechanism by which MLKL elicits membrane rupture is still under investigation[56-60].

1.2.2.1 TNFR1-induced signalling, apoptosis and necroptosis

Extrinsic apoptosis and necroptosis can be triggered under death receptors (DRs), which belong to the TNF superfamily[61]. While DRs are activated at their extracellular regions, they elicit intracellular signalling pathways via a critical domain at their cytoplasmic regions: death domain (DD)[62]. One of the most extensively studied DRs is TNF receptor-1 (TNFR1), which trimerizes and recruits two cytoplasmic proteins containing DD, TNFR1-associated DD (TRADD) and RIPK1, upon TNF engagement[63-66]. The recruitment of TRADD is pivotal as it brings TNFR-associated factor 2/5 (TRAF2/5) which subsequently recruits cellular inhibitors of apoptosis1/2 (cIAP-1/2)[67,68]. cIAP-1 and -2, together, provide lysine-63 polyubiquitination (K63) on certain proteins including itself and RIPK1[69-71]. K63 ubiquitination is critical for the recruitment of LUBAC and TAB2/3. TAB2/3 recruits TAK1 to the complex. LUBAC catalyses methionine-1 (M1), linear, ubiquitin chains on K63-linked ubiquitination chains of RIPK1[26], on which IKK1/2 are recruited via NEMO[64,72-75]. In addition, TBK1 and IKKε are found to be recruited to these linear ubiquitin chains via NEMO and their adaptor proteins[76]. Similar to Myd88-dependent TLR signalling (section 1.1), TAK1 phosphorylates itself and IKK1/2. While TAK1 activates the MAPK pathway,

the phosphorylation of IKK1/2 leads to the induction of NF-κB[48,77]. Importantly, TAK1[78], IKK1/2[79] and TBK1/IKKε[76] negatively regulate RIPK1 by phosphorylating it. This whole complex upon TNF induction is called complex I[51].

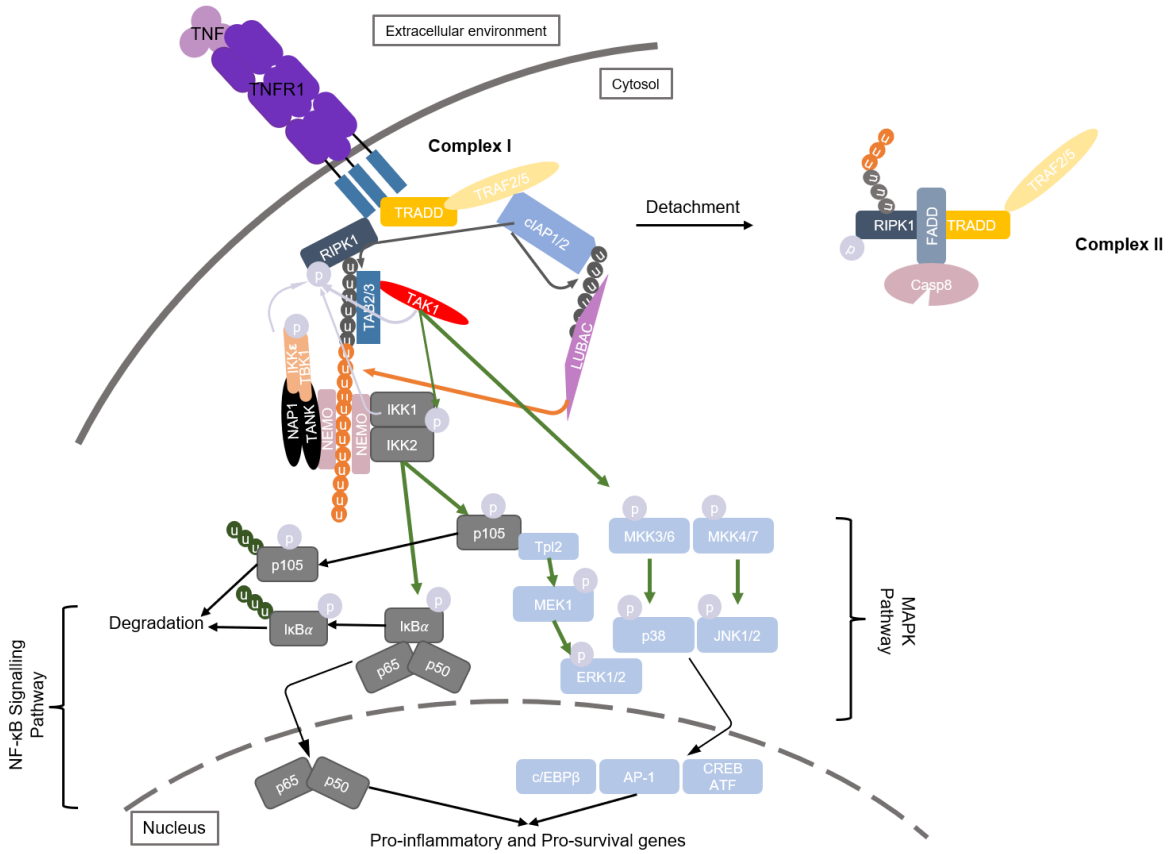

Figure 1-1 The formation of complex I and complex II under TNFR1.

Upon TNF engagement, complex I is assembled and leads to the induction of pro-survival proteins and inflammatory genes through NF-κB and MAPK pathways. TRAF2, RIPK1 and TRADD dissociate from complex I and form cytosolic complex II[65]. Dark grey circles represent K63-linked ubiquitination K63- and M1-linked ubiquitination as well as phosphorylation of RIPK1 are critical for the inhibition of TNFR1-mediated cell death. Dark grey arrows represent the catalysation of K63-linked ubiquitination. Orange circles represent M1-linked ubiquitination. Orange arrows represent the catalysation of M1-linked ubiquitination. Light grey arrows represent phosphorylation events, negatively regulating the activation of RIPK1. Green arrows represent phosphorylation events, activating the proteins. Dark green circles represent K48-linked ubiquitination. Adapted from [80].

It was shown that after TNF engagement, TRADD, TRAF2 and RIPK1, dissociate from complex I and form a cytosolic complex (complex II) with a protein containing DD (FAS-associated with death domain, FADD) and caspase-8[65]. Several checkpoints on complex I, as well as complex II, were identified and shown to regulate cell death under TNFR1 tightly[80]. Interestingly, the inhibition or relinquishment of the distinct checkpoints renders

TNFR1-induced cell death modalities different[80]. One checkpoint in complex II is achieved by NF-κB-induced pro-survival protein that has a short half-life and alters the activity of caspase-8 via direct interaction: cellular FLICE-like inhibitory protein (cFLIP)[81-83]. TNF stimulation in the presence of a protein translation inhibitor, cycloheximide, was shown to induce caspase-8-mediated RIPK1-independent apoptosis, which was rescued upon cFLIP-overexpression in cells, suggesting the modulation of caspase-8 activity by cFLIP is critical in TNFR1-induced RIPK1-independent apoptosis[84]. This complex eliciting RIPK1-independent, caspase-8-initiated caspase-3/7 dependent apoptosis is termed complex IIa[48].

Another vital checkpoint regulating TNFR1-induced cell death is post-translational modifications on RIPK1 such as ubiquitination and phosphorylation[85]. These post-translational modifications on RIPK1 have been shown to regulate RIPK1 kinase-dependent apoptosis and necroptosis which are mediated by complex IIb and necrosome complexes, respectively[85,86]. Chemical degradation and knockdown of cIAPs in cellular systems were shown to reduce ubiquitination on RIPK1 and cause RIPK1-Casp8-dependent apoptosis[69]. Mice lacking cIAP-1/2[87] can only be born in the background of ubiquitous TNF deficiency, demonstrating the essential role of non-linear ubiquitination events on RIPK1 in the regulation of cell death pathways under TNFR1. The lethality of cIAP-1/2 deficient mice was further demonstrated to be dependent on caspase-8-mediated apoptosis without profound RIPK3 activation, suggesting cIAP-1/2 protects from TNF-induced RIPK1-dependent apoptosis (complex IIb)[88]. Interestingly, knock-in mice expressing RIPK1 that cannot be K63-ubiquitinated on a lysine residue (K376R; K377 in human RIPK1) die *in utero*, which can be rescued by combined inhibition of apoptosis and necroptosis[89,90]. In line with the critical role of K63-linked ubiquitination on RIPK1 in the regulation of cell death pathways, M1-linked ubiquitination on RIPK1, which is catalysed on K63-linked ubiquitination, is vital as indicated by the cell death-driven lethality and/or pathologies in mice lacking components of LUBAC (HOIL-1L[73,91], HOIL-1L interacting protein (HOIP)[92], SHANK-associated RH domain-interacting protein (SHARPIN)[22,23]). For example, TNFR1-induced, caspase-8- and the kinase activity of RIPK1-mediated apoptosis was shown to drive skin pathology in *Sharpin*^{cpdm} mice[93-96].

K63 and M1 ubiquitination events are vital for the recruitment of the negative regulators of RIPK1 including TAK1[78], IKK1/2[79], TBK1/IKKε[76]. Serine 25 was identified to be a critical phosphorylation site by IKK1/2, whose point mutation into aspartic acid in mice protects from RIPK1 kinase-driven inflammatory pathologies[97]. Serine 14, 15, 161, 166 and threonine 169 residues were discovered to be the autophosphorylation sites on RIPK1[95-99]. Importantly, there is no evidence showing RIPK1 can phosphorylate other proteins in the cell death pathways[80] although RIPK3 was shown to phosphorylate RIPK1 *in vitro*[100]. Whereas it remains to be elucidated how the kinase activity of RIPK1 mediates apoptosis and necroptosis under TNFR1, the conformational change of RIPK1 upon activation is thought to mediate apoptosis and necroptosis by forming complexes with (Death domain-dependent manner) FADD and (RHIM domain-dependent manner) RIPK3, respectively[52,101].

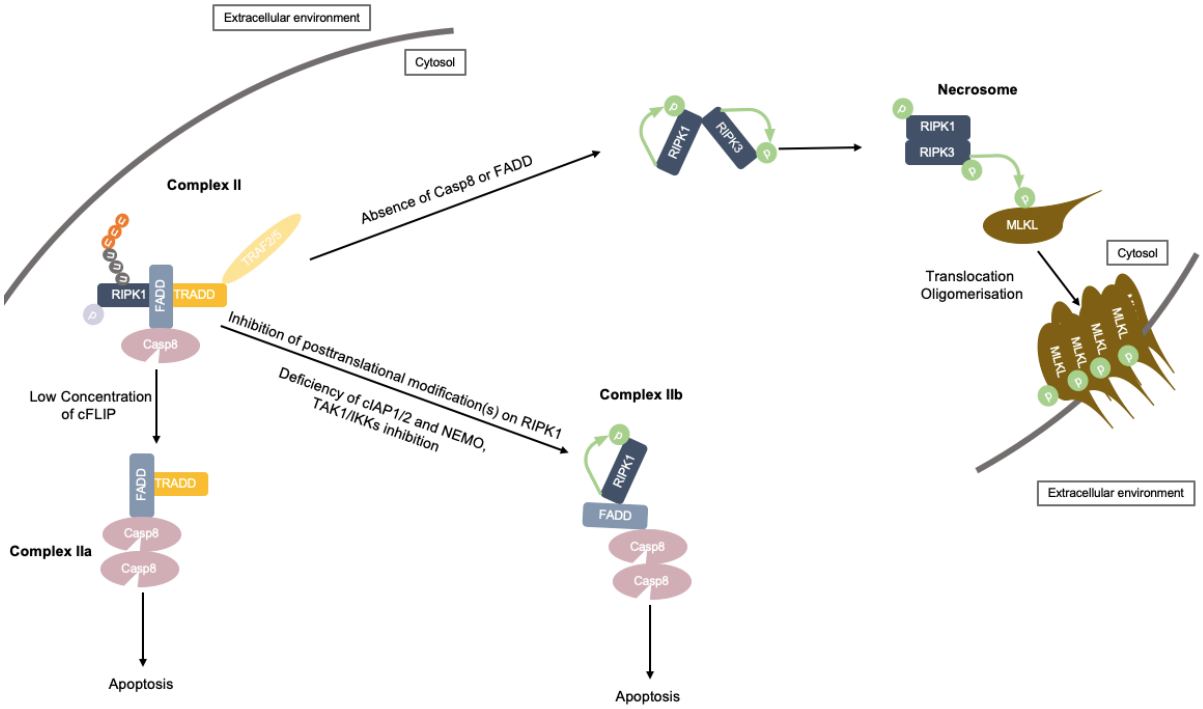

Figure 1-2 TNFR1-induced apoptosis and necroptosis.

Complex II can induce apoptosis and/or necroptosis under certain conditions. The concentration of cFLIP and posttranslational modifications on RIPK1 are critical to inhibit apoptosis. The absence of Casp8 or FADD, which interacts with Casp8 in complex II, leads to RIPK3-MLKL-mediated necroptosis. The relinquishment of certain checkpoints such as the complete loss of K63-linked ubiquitination on RIPK1 (*Ripk1*^{K376R}) can culminate in apoptosis as well as necroptosis. Adapted from [80,86].

Whereas the kinase activity of RIPK1 can mediate apoptosis and/or necroptosis, the presence of caspase-8 or its catalytic activity can dictate the type of cell death as well[48,80].

Mice ubiquitously lacking Casp8 or FADD which interacts with caspase-8 via the death-effector domain(DED)-dependent manner is embryogenically lethal[102,103] and can be born in the absence of RIPK3 or MLKL[104-108], demonstrating that RIPK3-MLKL-dependent necroptosis is triggered when the interaction between Casp8-RIPK1 is broken. Upon inhibition of caspase-8, autophosphorylated/active RIPK1 can engage RIPK3 through RHIM-RHIM domain interaction forming an amyloid structure and activating it[48,100,109-111]. Then, RIPK3 phosphorylates itself as well as MLKL, which translocates to the plasma membrane and leads to cell rupture[53,112,113]. RIPK1-RIPK3-MLKL complex inducing necroptosis is termed necrosome[48]. Importantly, mice expressing catalytically inactive caspase-8 (C362S) die before birth, and immunostaining experiments showed the active RIPK3 in the tissues of these mice[114,115]. Whereas RIPK3 ablation in these mice rescued the embryonic lethality, *Casp8*$^{C362S/C362S}$ *Mlkl*$^{-/-}$ mice die at birth[114,115], showing that the catalytic activity of caspase-8 prevents multiple cell death pathways including necroptosis. In line with this, knock-in mice expressing RIPK1 that cannot be cleaved by caspase-8 are embryonically lethal, and the embryonic lethality in these mice is mediated by FADD- and RIPK1-kinase-dependent cell death[116]. Therefore, these extensive reports over the years demonstrate that caspase-8 plays a vital role in the regulation of cell death pathways under TNFR1.

1.2.2.2 Intrinsic apoptosis

The impaired integrin signalling[117] (further in 1.4.5.1 section, as anoikis), absence of growth factors, mitochondrial and DNA damage are reported to induce apoptosis independent of a death receptor participation, and this type of regulated cell death is termed intrinsic apoptosis[51]. Integration of these various insults into the intrinsic apoptosis pathway and its regulation are mediated by the parity between groups of proteins belonging to the B-cell lymphoma 2 (Bcl-2) protein family[118]. Specifically, Bcl-2 homology region 3 (BH-3)-only proteins counteract the Bcl-2 proteins, which inhibit the activation of effector Bcl-2 proteins: Bcl-2 associated X (BAX) and Bcl-2 antagonist/killer-1 (BAK)[119]. While BAK predominantly stays at mitochondria under a steady state, upon activation BAX localizes and precipitates on mitochondria with BAK[120-122]. BAK and BAX, redundantly, form pores in the outer membrane of mitochondria and lead to mitochondrial outer membrane permeabilization (MOMP), discharging proteins including cytochrome *c*[123-125].

The release of cytochrome *c* is a critical step in intrinsic apoptosis as it binds to apoptotic protein-activating factor-1 (APAF-1), allowing its heptameric structure to be formed in the presence of ATP[126,127]. Oligomerized APAF-1/apoptosome integrates the upstream signalling pathway into caspase-9, which activates effector caspases: caspase-3/7[128]. Besides cytochrome *c*, the second mitochondria-derived activator of caspase (SMAC) is released upon MOMP, which prevents the activation of a caspase-3/7/9 inhibitor protein (X-linked inhibitor of apoptosis protein, XIAP) and promotes intrinsic apoptosis[129]. In addition to BAX and BAK, Bcl-2-related ovarian killer (BOK), whose regulation is independent of Bcl-2 and BH-3-only proteins, was shown to participate in MOMP under certain conditions[130].

Importantly, mice lacking effector proteins of the Bcl-2 family, *Bax*$^{-/-}$ *Bak*$^{-/-}$[131,132] as well as *Bax*$^{-/-}$ *Bak*$^{-/-}$ *Bok*$^{-/-}$[131], are born at a reduced rate compared to wild-type mice, and only some of those mice can survive through adulthood with deformed development in the central nervous system, female reproductive system, and abnormality in the immune system. Therefore, intrinsic apoptosis critically contributes to mammalian development. Of note, the Fas ligand-induced cell death pathway is intact in *Bax*$^{-/-}$ *Bak*$^{-/-}$ mice[132], however, Fas- and TNF/cycloheximide-induced active caspase-8 can process a BH-3-only protein: BH-3 interacting domain death agonist (BID) and culminate in the activation of the intrinsic apoptosis pathway[133]. Thus, the effector proteins of the intrinsic apoptosis pathway are dispensable for extrinsic apoptosis while extrinsic apoptosis can the initiate intrinsic apoptosis pathway.

Meanwhile, BAX and/or BAK were reported to establish growing pores on mitochondria that can lead to mitochondrial DNA discharge, and the recognition of mitochondria-derived DNA in the cytosol by cGAS-STING is proposed to contribute to inflammation in apoptosis, arguing against the generally accepted immunologically silent notion of apoptosis[134-136].

1.3 Endoplasmic reticulum and Unfolded protein response

1.3.1 Structure and function of Endoplasmic reticulum

A study published in 1945 observed tissues from chicken embryos under the electron microscope and reported the presence of a meshwork of reticular structure within the cytoplasm[137]. Further studies expanded the knowledge of this structure as well as the

presence of it in different types of cells[138,139]. In 1954, 'Endoplasmic Reticulum' (ER) was coined to define the largest membranous organelle in eukaryotes[140].

ER spans across the entire eukaryotic cell, nucleus to the plasma membrane. ER possesses one single lumen, enclosed by an uninterrupted bilipid layer in monolayers, ER membrane[141]. Whereas ER is one single continuous organelle, structurally its domains are divided into two major classes: nuclear and peripheral, and the latter is further classified into ER sheets (cisternae) and ER tubules[142]. Membrane curvature is the most important difference between tubules and cisternae, the nomenclature based on structure is more than a mere location-based classification, rather reflecting the functionality of these dynamic domains[143].

ER is an organelle with diverse tasks playing vital roles in several essential functions of cells, such as protein synthesis, folding, quality control, degradation and navigation of them to the final destinations, lipid biosynthesis, metabolism and controlling intracellular Ca^{2+} concentration[143]. Furthermore, ER is the most prominent organelle involved in membrane contact sites (MCS) where membranes of at least two organelles establish intricate contacts without being fused and merged physically[144]. The sites between tubules of ER and mitochondria were shown to be critical for mitochondrial fission, demonstrating the essential contribution of ER in the fundamental functions of eukaryotic cells[145].

1.3.2 ER stress and Unfolded protein response

It is roughly estimated that 33% of the entire protein output is produced within the ER of cells[146]. Furthermore, the protein production process from a gene is relatively loosely checked for errors compared to DNA replication, which can lead proteins to fold improperly and/or aggregate at high rates[147-150]. In addition, dysregulated biochemical processes controlling protein abundance such as ubiquitination and autophagy can cause an increment in the unfolded, aggregated protein concentration[151]. The plethora of misfolded proteins in the ER lumen is called ER Stress[152]. Persistent ER stress or inability to respond to the ER stress constitutes potentially detrimental consequences for the cells as well as the entire organism[151,153,154], ER harbours three different receptors that can sense the ER stress: inositol requiring enzyme 1 (IRE1), eukaryotic translation initiation factor 2 alpha kinase 3 (EIF2AK3) (also, Protein kinase-like RNA kinase, PERK) and activating transcription factor 6 (ATF6)[155]. The triggered receptors initiate a series of intricate

cascades, and this collective reaction of cells is called unfolded protein response (UPR)[155]. Cells employ these signalling pathways to alleviate the deleterious consequences of ER stress by increasing the abundance of certain transcription factors which induce UPR target genes[152]. UPR target proteins regulate the protein synthesis rate[156,157], folding[158,159], ER expansion[160], lipogenesis[161], autophagy[162] and ER-associated protein degradation (ERAD)[163].

Two pioneering studies conducted in yeast identified Ire1p as an ER stress receptor[164,165]. A couple of years later mammalian homologue of Ire1p was described: IRE1 or Endoplasmic Reticulum to Nucleus signalling (ERN1)[166,167]. These studies predicted a paralog of ERN1: ERN2 or IRE1β, which was characterized and found to be expressed only in lung and intestinal mucosal epithelial cells, in contrast to the ubiquitous expression of ERN1[168]. Further investigations uncovered that metazoans do express additional ER stress receptors: PERK[156,157] and ATF6[169], revealing that IRE1 is the archaic ER stress receptor conserved from yeast to mammalians.

IRE1 is a protein spanning the ER membrane and possesses two important portions: luminal and cytosolic, which accommodates serine/threonine kinase and endonuclease domains[170]. The exact mechanism by which IRE1-mediated signalling is initiated at the luminal domain is still under debate[171,172], however, upon activation IRE1α monomers oligomerise, leading to transautophosphorylation at serine 724, serine 726 and serine 729[173] and proceeding with splicing of X-box binding protein 1 (*XBP1)* mRNA by endonuclease domain in the cytoplasm[174]. IRE1-endonuclease domain-dependent *XBP1* mRNA splicing is a sequence-specific unconventional event in which two open reading frames of *XBP1* are merged after 26 nucleotides within an intron are excised[175]. The splicing event leads to a frameshift in *XBP1* mRNA without altering its protein stability[175] and generates a Spliced XBP1 (XBP1s) transcription factor participating in the induction of certain sets of proteins such as chaperones and ERAD proteins[158].

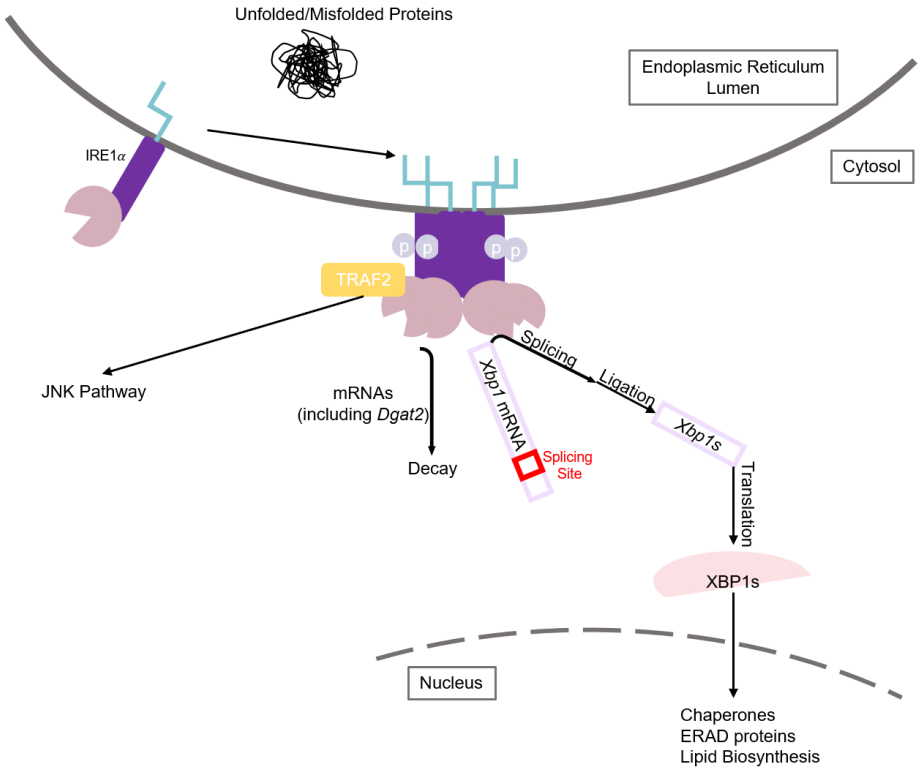

Figure 1-3 IRE1α-mediated Unfolded protein response.

The endonuclease domain of activated IRE1α processes *Xbp1* mRNA by performing unconventional splicing via its endonuclease domain, leading to the production of the XBP1s transcription factor. XBP1s induces the expression of certain sets of genes that are critical to mount unfolded protein response. In addition, certain mRNAs can be degraded by a process called Regulated Ire1-dependent mRNA decay (RIDD) upon activation of IRE1α. Under certain conditions, IRE1α can activate the JNK pathway. Grey circles represent the transautophosphorylation of IRE1α. The red section in *Xbp1* mRNA indicates the splicing site of *Xbp1u*. Adapted from[152,155].

In addition to *XBP1* splicing, it was reported that IRE1 is capable of degrading certain sets of mRNAs, a process called Regulated Ire1-dependent mRNA decay (RIDD)[176-178]. Although the localization, sequence and stem-loop structure of mRNAs are thought to be critical for RIDD, it remains to be revealed further which mRNAs are targeted by IRE1[170,179]. By utilising RIDD, IRE1 is thought to suppress mRNA-protein load during ER stress[174]. Moreover, TRAF2 was shown to interact with IRE1 and can activate the JNK pathway upon chemical induction of ER stress in certain types of cells[180].

1.4 The mammalian intestine

1.4.1 Anatomy and physiology of the mammalian intestine

The mammalian intestine is a multifunctional organ performing essential tasks of the gastrointestinal system such as digestion of foods, selective absorption and transportation of nutrients as well as separation of the diverse luminal microbes from the rest of the body[181-183]. The intestine is categorized into two major parts: the small intestine and the large intestine[184]. From the pyloric sphincter to the ileocecal valve, the small intestine spans[184]. The large intestine is the part between the ileocecal valve and the anus. There are three segments of the small intestine: duodenum, jejunum and ileum. Meanwhile, the large intestine is composed of caecum, colon and rectum[184]. The colon can be further divided into proximal and distal parts[184]. Whereas the small intestine performs the digestion and absorption, the large intestine is majorly responsible for the uptake of water and electrolytes as well as defecation[185].

In addition to being a tubular hollow organ, the intestine is composed of transverse layers. Monolayered squamous epithelial cells compose the outermost layer, the serosa. Above the serosa layer, muscularis externa (or muscularis propria) is located, in which longitudinal and circular layers of smooth muscles reside. The muscle layers are followed by the submucosa, a connective tissue layer, containing nerve cells, blood and lymphatic vessels. The area in between the submucosa and lumen is named mucosa. As a part of the mucosa, the lamina propria is a connective tissue layer supported by mucosal immune cells, lymph nodes[181]. The lamina propria is covered by single-layered epithelial cells, intestinal epithelial cells (IECs).

The intestinal epithelium does not cover the lamina propria as a straightforward line, but rather, forms the folds on it, ‘crypts of Lieberkühn’, named after Johann Nathanael Lieberkühn as he first described them[186,187]. In addition, IECs of the small intestine elongate into the lumen, forming villi. Importantly, villi are confined to the small intestine. That is, the colon does not contain villi[188]. Furthermore, organelles, proteins as well as the orientation of the secretory pathway in IECs are not uniformly distributed but polarised[189]. At the apical part of IECs in the small intestine as well as the colon have microvilli[190].

Villi and microvilli remarkably increase the area of the small intestinal surface, facing the lumen. It is estimated that the surface area of the small intestine in humans ranges from 200 m^2 to 400 m^2 [183,191,192]. The expansion of the surface area is thought to play a pivotal

role in the digestion and absorption tasks[193]. However, increased mucosal surface area elevates the contact region between the intestinal epithelium and microorganisms. Whereas bacteria are the most abundant microorganisms in the gut lumen[182], viruses, fungi, archaea and yeast embody the rest of the diversity[194,195]. The cumulative group of these microorganisms in the lumen are defined as the luminal microbiota[183]. On the one hand, the microbiota is a critical contributor to the digestion in the intestine[196], but on the other hand, the high load of the microbiota with immense diversity poses a threat to the host[183]. The mucosal immune system in the intestine is responsible for the surveillance of microorganisms and the initiation of an immune response upon an invasion or the loss of intestinal barrier homeostasis[197,198]. Thereby, the microorganisms breaching into the lamina propria can be restricted to the intestinal tissue and prevented from spreading into other tissues, leading to an aberrant systemic immune response[183].

1.4.2 Intestinal epithelial cells and intestinal epithelium

IECs restrict luminal microorganisms from the intestinal immune system by establishing an immunological barrier and regulating the accessibility of their antigens by mucosal immune cells[183]. In addition, IECs are in charge of digestion, and absorption tasks. Performing these diverse and challenging functions is thought to be achieved by the cellular heterogeneity of IECs[186]. IECs are composed of several different cell types. Crypt-base columnar cells (CBCs) expressing leucine-rich repeat-containing G protein-coupled receptor 5 (LGR5), whose location is strictly restricted to the bottom of crypts, are the stem cells in the epithelium of the small intestine as well as colon[199,200]. CBCs give rise to secretory cells and transit-amplifying cells (TA)[201]. TAs differentiate into enterocytes, which perform the essential function of the intestine, absorbing nutrients and water. Cells with high secretory capacity are Paneth cells, Goblet cells, Tuft cells and enteroendocrine cells. Paneth cells and Goblet cells provide chemical barriers by secreting antimicrobial peptides and mucins[202]. Meanwhile, Tuft cells are pivotal initiators of the immune response in the course of helminth and protists infection[203-205]. Enteroendocrine cells are vital composers of the hormone regulation in the intestine[206]. $LGR5^{+}$ CBCs also generate a specialized cell type in the small intestine, Microfold cells (M cells)[207-209]. Along with enterocytes, M cells comprise the columnar epithelial barrier lining two components of gut-associated lymphoid tissues (GALT), Peyer's patches and isolated lymphoid follicles (ILF)[210]. In addition to immune cells in the lamina propria as well as intraepithelial cells,

Peyer's patches and ILF, which are composed of T-cells, B-cells and dendritic cells, are the major sites for the initiation and maturation of the immune responses against dense luminal communities of microorganisms[211]. In contrast to other secondary lymphoid organs such as lymph nodes or spleen, Peyer's patches and ILF do receive luminal antigens necessary to initiate immune responses via M cells[212,213]. For example, mice lacking the receptor for binding antigens on M cells were shown to have less *Salmonella* burden in Peyer's patches as well as mesenteric lymph nodes, demonstrating the contribution of M cells to transcytosis of antigens[214].

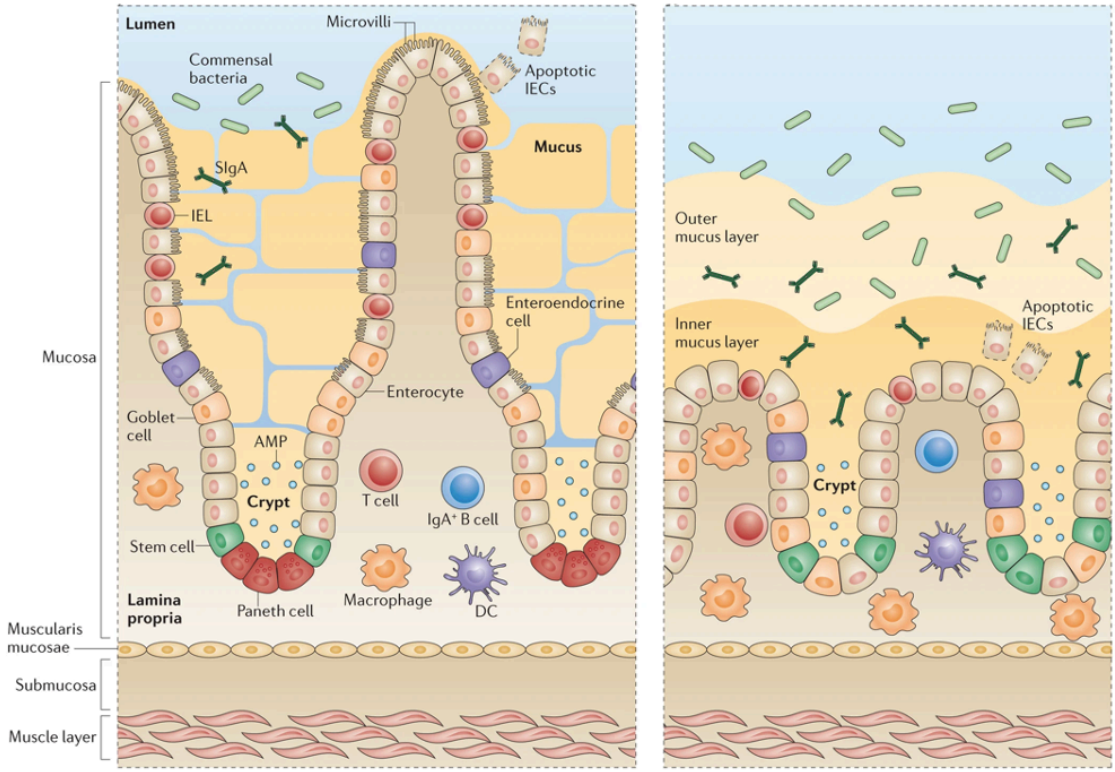

Figure 1-4 Intestinal epithelial cells, the intestinal epithelium and the layers of the intestine in the small intestine and colon.

Intestinal epithelial cells (IECs) establish a monolayered epithelium (left: the small intestine; right: the colon). Intestinal epithelium covers the Lamina propria and segregates the mucosal immune system from luminal bacteria. The intestinal epithelium folds into invaginations, crypts, invading through Lamina propria. Intestinal stem cells are located at the bottom of the crypts in the intestinal epithelium and give rise to other IECs including enterocytes, Paneth cells and Goblet cells. Enterocytes are critical for nutrient absorption. In contrast to other non-stem cell types, Paneth cells are located at the small intestinal crypts and secrete antimicrobial proteins/peptides into the lumen, which reinforce the intestinal barrier. Goblet cell is another type of secretory cell in the intestinal epithelium. They produce and secrete glycosylated proteins, called mucins, into the lumen. Secreted mucins expand, leading to the formation of a bacteria-impermeable layer in the colon. The intestinal epithelium and the mucus layer establish a stratified barrier against luminal microbiota. Taken from [211].

CBCs renew the entire intestinal epithelium every 3 to 5 days[215]. The rapid turnover of the intestinal epithelium is thought to be essential for the maintenance of the barrier function, which is under constant challenge by biological, chemical threats and substantial mechanical forces[186]. WNT, Notch, EGF and BMP signalling cascades, whose ligand concentrations change from crypt to villus, firmly regulate the proliferation and the differentiation of CBCs[216]. While CBCs proliferate and replenish their population within the crypt, some of the generated daughter cells localise at the upper part of the crypt, named border cells[217]. They are exposed to changing environment of WNT, Notch, EGF and BMP ligands during this displacement, which is critical for the loss of stemness, and stochastic lineage commitment, the differentiation as well as the maturation of IECs[218-220]. IECs shed off at the tip of the villi in the small intestine or at the apex of the colonic crypt after 3-5 days of maturation[215]. As cells are dislodged into the lumen by the pushing force from cells beneath, they lose integrin-mediated signalling and subsequently undergo a specific type of regulated cell death, anoikis[221-223].

1.4.3 Paneth cells

Paneth cells, first discovered by Gustav Schwalbe and Josef Paneth, reside at the bottom of the small intestinal crypts along with CBCs[187]. That is, Paneth cells are an exception in terms of cellular localisation and migration as they are terminally differentiated cells[224]. Besides the unconventional localisation, studies identified the large granulae clustered at the apical region of Paneth cells, which were further characterised to contain anti-microbial peptides including lysozyme, defensins[225-227]. It was elegantly demonstrated that Paneth cells induce the expression of antimicrobial peptides Myd88-[228] and NOD-2[229,230] dependent manner and secrete them in the presence of bacteria as well as components of bacteria such as LPS[231]. This constitutes a critical feature of Paneth cells: providing the chemical barrier against microbiota and protecting CBCs in the crypt[232]. Furthermore, it was reported that anti-microbial peptides of Paneth cells can shape the content of luminal microbiota without altering their total numbers[233]. Intestinal mesenchymal cells including fibroblast and myofibroblast[234] are critical reinforcers of the stemness in the intestine by providing ligands of WTN[235], RSPO[236] and BMP[237]. In addition to the stroma, a key study identified Paneth cells as another intestinal stem niche supporter as they secrete ligands of WNT, EGF, and NOTCH[238]. As Paneth cells govern critical roles in the maintenance of intestinal homeostasis, dysregulation of cellular pathways including ER stress[162,239] and

autophagy[240-242] in Paneth cells are associated with inflammatory disorders of the intestine. Paneth cells can live for up to 60 days[243], and intestine-resident macrophages are thought to remove them by efferocytosis at the base of the crypts[216].

1.4.4 Goblet cells, mucins and the mucus layer

The mammalian intestine harbours a mucus layer over the epithelium, reinforcing the epithelial barrier against the tremendous loads of microbiota[244]. Whereas the small intestine and colon possess the mucus layer, their mucus layers do show distinction in certain features: The colon has two layers of mucus, inner and outer layers, yet the mucus layer in the small intestine is single-layered[202]. While the outer mucus layer in the colon sustains microbiota, the compact inner mucus layer attached to the epithelium is impervious to bacteria[244]. This difference is thought to originate from the stratification intensities of the inner and outer mucus layers as well as unexplored host-and microbiota-mediated regulations such as enzymatic degradation[245]. In contrast, the monolayered small intestinal mucus coat is uncondensed and motile, which can be pervaded by luminal bacteria[246]. The underlying reason why the mucus layer in the small intestine is permeable to bacteria remains elusive[245].

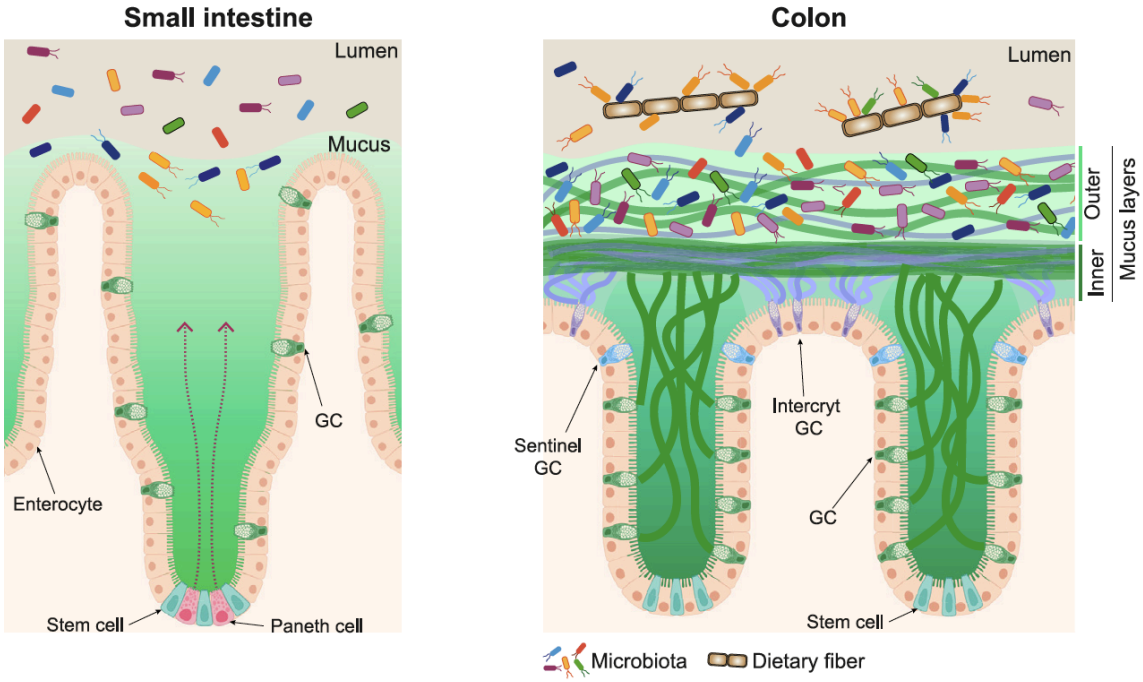

Figure 1-5 Discrepancy between the mucus layers in the small intestine and colon.

Goblet cells in the intestinal epithelium produce and secrete gel-forming proteins, called mucins. After being secreted into the intestinal lumen, mucins form the mucus layer. Two layers of the mucus layer exist in the colon. Luminal bacteria reside within the outer mucus layer in the colon. However, the inner mucus layer is stratified, and bacteria cannot penetrate it in homeostasis. In contrast, the small intestine harbours a mucus layer, which does not provide a clear separation of luminal bacteria from the small intestinal epithelium. Goblet cell (GC). Taken from[245].

Goblet cells, vigorously provide the mucus layer by producing, storing and secreting special proteins called mucins, which are the building blocks of the mucus layer[247]. Mice lacking a specific mucin, MUCIN-2 (MUC2), were shown to be devoid of the mucus layer and have increased bacterial presence in the mucosa as well as spontaneous intestinal inflammation, demonstrating that MUC2 is indispensable for the formation of mucus layer, stratification of microbiota and regulation of mucosal inflammation[244,248]. In addition to MUC2, Goblet cells in the intestinal epithelium secrete mucus-associated proteins to reinforce the functionality of the mucus layer such as calcium-activated chloride channel regulator-1 (CLCA1)[249], IgGFc-binding protein (FCGBP)[250], Trefoil factor 3 (TFF3)[251] and Zymogen granule membrane protein (ZG16)[252]. Interestingly, some mucins (MUCIN-13[253], MUCIN-17[254,255]) expressed by enterocytes are documented to contain transmembrane domain and cover their surfaces by directly tethered to the plasma membrane on the luminal side[247].

Apart from establishing the mucus layer, luminal antigens can be transported to dendritic cells residing in the lamina propria via Goblet cells of small intestinal epithelium (and to a lesser extent at the distal colonic epithelium)[256], demonstrating that Goblet cells not only contribute to the separation of microbes but also actively promote mucosal immune responses.

1.4.4.1 Mucins, ER and ER stress

Besides being a large protein (approximately 5200 amino acids), MUC2 is massively subjected to *O*- and *N*-glycosylations of diverse glycans on one of its domains composed of Proline-Threonine-Serine repetitions (PTS domain)[247]. MUC2 contains additional domains including von Willebrand D and cystine-knot domains, which enable disulphide bonds to form between two MUC2 monomers in ER[257]. While *N*-glycosylation of MUC2 occurs in ER, *O*-glycans are attached to MUC2 throughout the entire Golgi route [245,258]. Interestingly, the presence of unfolded regions of the PTS domain is thought to be crucial while glycosyltransferases perform *O*-linked glycosylations on MUC2, indicating folding and glycosylation of MUC2 are continuous and entangled rather than discrete and sequential events[245]. Importantly, pH levels in Golgi as well as the storage granules were found to be linked with the proper assembly of MUC2[259].

These findings at the molecular level indicate that ER as well as the entire secretory pathway of Goblet cells play an essential role in the translation-folding-glycosylation-dimerization-storage-secretion route of MUC2[245]. Indeed, studies in transgenic mice demonstrated that impaired ER or loss of one of ER stress receptors could lead to reduced mucin production/secretion and defective mucus layer[168,239,260-265], providing evidence that healthy functioning ER is critical for proper mucus layer establishment.

1.4.5 Inflammatory bowel disease

The intestine is remarkably an intricate organ in which stromal cells, IECs, the immune system and microbiota are in constant interaction[266]. Yet, this interplay is precarious, and the breakdown of it can culminate in inflammatory disorders of the intestine, including Inflammatory bowel disease (IBD)[266]. IBD is superficially grouped into two subsets: Crohn's disease (CD) and ulcerative colitis (UC)[267]. UC localizes throughout the entire

colon with focal ulcer formation (complete loss of the epithelial barrier integrity) along with bleeding[266]. In contrast, CD can be observed within any part of the gastrointestinal tract, which can be identified as focal abscesses, abrupt fistular inflammation coupled with fibrosis[266].

Starting from the late 20th century, reports based on IBD patients with their relatives provided evidence that the host's genetic factor is a critical aspect of IBD[268-275]. Furthermore, genome-wide association studies (GWAS) revealed more than 200 risk genes for IBD such as the most renowned linkage, *NOD2*[276]. However, ample evidence also shows that the genetic susceptibility of the host fails to fully resolve the culprit of IBD[267]. For example, the severity spectrum of CD and UC cannot be attributed to the gene associations up to 87% and 93%, respectively[277]. Critically, clinical studies recruiting monozygotic and dizygotic IBD patients dismantled the genetic background as the only culprit of IBD since the occurrence of UC and CD in those patients do not follow the ratio of either %100 or 50%[278-280]. Meanwhile, studies focusing on the linkage between IBD occurrence and socioeconomic parameters of the countries highlight the role of lifestyle including diet in the incidence rate of the disease[281]. In parallel, the profound alteration in the microbiota composition of the host is found in IBD[282-284] and suggested to contribute to the disease pathology[285]. Taken together, the accumulation and stratification of genetic as well as environmental factors are thought to be the basis of IBD[266].

1.4.5.1 Epithelial cell death in IBD

The regulatory role of epithelial cell death in the intestinal barrier had been enigmatic until the identification of an IEC-specific type of cell death, anoikis[221]. Anoikis occurs at the most apical regions of the intestinal layer[286]. As the monolayered integrity of epithelium is not lost, and IEC-free gaps are not formed, this process is thought to be induced by the direct physical forces applied by IECs beneath[222]. In line with this, a mechanistic study performed by injecting TNF into mice revealed that shedding of IECs relies on prejunctional as well as apical junctional complexes[223]. Whereas caspase-3 and caspase-7 were thought to play roles in anoikis, a recent report demonstrated that intestinal epithelium is capable of renewing itself independent of executionary caspases[287]. Moreover, other types of regulated cell death such as apoptosis[288,289], pyroptosis[290-292] of IECs play vital roles in the homeostasis and inflammation of the intestine.

IBD patients and their relatives, showing no signs of complications, show elevated permeability in the intestine, marking the importance of the genetic predisposition and the barrier loss in the pathogenesis of IBD[293-298]. In parallel, clinical studies provided clear evidence of increased epithelial death in the intestines of IBD patients[299-303]. Yet, it was unknown whether increased death of IECs is a cause of the inflammation by disrupting the intestinal barrier integrity or a mere result of the disease pathogenesis[286]. Transgenic mice models of intestinal inflammation show that dysregulated epithelial cell death can lead to inflammatory pathologies in the intestine, linking the genetic background of the host, increased IEC death and the loss of intestinal barrier in the pathogenesis of IBD[48,288,289,304-306]. Specifically, mice lacking caspase-8[307,308] or FADD[309] in IECs develop spontaneous intestinal inflammation, manifested by increased IEC death and loss of the colonic epithelial barrier. Casp8-ablation-induced ileitis as well as colitis completely depend on IEC-necroptosis, as additional ablation of RIPK3 or MLKL in these mice rescues the intestinal inflammation[307,310,311]. Whereas mice lacking IEC-specific FADD do develop necroptosis-dependent colitis, Casp8-mediated cell death contributes to ileitis in these mice[307]. Importantly, Casp8[312] or FADD[309] deficient mice treated with antibiotics or raised under germ-free conditions or lacking Myd88 do not show inflammation signs in the colon, demonstrating that luminal microbiota is a critical mediator of colitis but not ileitis. Patients harbouring mutations in the genes encoding regulatory proteins of cell death pathways such as RIPK1[313-315] and CASP8[303,316] were identified and showed spontaneous intestinal inflammation. Studies in mice and clinical reports provide evidence that dysregulation of epithelial cell death contributes to the pathogenesis of IBD.

1.4.5.2 UPR and the mucus layer in IBD

Impaired protein homeostasis was found to be implicated in IBD[317-319]. Several different genes encoding proteins of the UPR pathway are linked to CD and UC, including *ORMDL3*[320,321], *AGR2*[322] and *XBP1*[323]. Mice lacking XBP1 specifically in IECs show spontaneous small intestinal inflammation along with increased ER stress including IRE1α activation, impaired Paneth cells and impaired Goblet cell phenotype[323]. Although XBP1-deficiency does not lead to spontaneous phenotype in the colon, DSS administration to these mice culminates in microbiota-dependent severe colitis[323]. The protective role of XBP1-mediated UPR in the intestinal epithelium was further delineated by additional studies, uncovering the role of selective autophagy in the clearance of activated IRE1α

and suppressing intestinal inflammation[162,239]. Surprisingly, Paneth cell-specific XBP1 ablation causes dysfunctional secretory granulae of Paneth cells and leads to spontaneous ileitis, demonstrating the vital role of XBP1-mediated UPR in secretory cells of the intestine and the pathogenesis of IBD[162].

Proteomic analysis of the mucus isolated from UC patients demonstrated that mucins and mucus-associated proteins were diminished compared to control individuals, and the mucus layer of active UC patients showed increased permeability, suggesting defective mucus layer contributes to the pathogenesis of UC[324]. However, interestingly no mutation in *MUC2* has been linked to IBD up to date, which is attributed to the sequence complexity of MUC2 (discussed in section 1.3.4.1)[325]. Nevertheless, mice lacking proteins playing critical roles in the UPR pathway such as XBP1[323], ERN2[264,265], ATF6[263] and AGR2[326,327] show reduced mucin production and/or defective mucus layer, emphasising the tangled interaction between UPR and mucin production/secretion in the context of intestinal inflammation.

1.5 Objective of the study

Intestinal epithelial cells establish a protective barrier against luminal microbiota by forming the intestinal epithelium, and dysfunctional intestinal epithelium can culminate in inflammatory disorders of the intestine including IBD[181]. It is thought that the host's genetic background is critically linked to the pathogenesis of IBD[266]. Whereas identification of multiple genetic variants in individuals is an important tool for assessing the IBD risk[328,329], the impact of multiple genetic variants and their pathways on the pathogenesis of IBD remains to be studied. The overarching aim of this study is to elucidate the interaction between XBP1 ablation-induced ER stress and necroptosis triggered by Casp8 or FADD deficiency in the intestinal epithelium.

2. Results

2.1 IEC-specific XBP1 suppresses the colitis in *Casp8*$^{IEC\text{-}KO}$ mice

2.1.1 Characterization of *Xbp1*$^{IEC\text{-}KO}$ mice

To investigate the epithelial-specific role of XBP1 in intestinal inflammation induced by epithelial cell death, the spatial-conditional gene targeting strategy[330] was employed. Exon 2 of *Xbp1* is flanked by two *loxP* sites in *Xbp1*$^{fl/fl}$ mice. *Xbp1*$^{fl/fl}$ mice were crossed to mice carrying P1 bacteriophage cyclization recombination (*Cre*) under a specific promoter, *Villin-1*[331]. *Villin-1* is prominently expressed in brush border cells of the intestinal epithelium[332]. Therefore, transgenic CRE expression causes the excision of exon 2 in *Xbp1* and a frameshift mutation, leading to the formation of a stop codon at the third exon of *Xbp1*[323]. Attempts to demonstrate ablation of XBP1 protein by utilising commercially available antibodies failed. Nonetheless, XBP1 deficiency in IECs was shown to cause increased activation of the upstream receptor, IRE1α, as indicated by phosphorylated-IRE1α (pIRE1α) at Ser724[162]. To show activated IRE1α in the intestines of *Xbp1*$^{IEC\text{-}KO}$ mice and indirectly confirm deficiency of XBP1, the small intestinal as well as colon sections from *Xbp1*$^{IEC\text{-}KO}$ and control mice were immunostained with antibodies specific for pIRE1α at Ser724. Results demonstrated that *Xbp1*$^{IEC\text{-}KO}$ mice exhibited an increased number of pIRE1α^+ IECs compared to *Xbp1*$^{fl/fl}$ mice (Figure 2-1A).

After transgenic CRE expression, epithelial cells in *Xbp1*$^{IEC\text{-}KO}$ mice still express mutant *Xbp1* mRNA containing IRE1-splicing site (unspliced *Xbp1*, *Xbp1u*) preceded by premature translational stop codon[323]. Therefore, activated IRE1α can splice mutant *Xbp1* mRNA and generate the spliced variant of *Xbp1* (*Xbp1s)* in the epithelium of *Xbp1*$^{IEC\text{-}KO}$ mice. As mice lacking XBP1 in IECs had increased IRE1α activation compared to control mice (Figure 2-1A), it is expected to detect more *Xbp1s* compared to *Xbp1u* in the epithelial cells of *Xbp1*$^{IEC\text{-}KO}$ mice[323]. To assess levels of *Xbp1u* and *Xbp1s*, Xbp1 splicing assay[175] was performed. Colonic crypts were isolated from control and *Xbp1*$^{IEC\text{-}KO}$ mice, and colon organoids were established[333]. Control and XBP1-deficient colonoids were treated with either DMSO or an inhibitor (G03089668 or G'9668) that was previously found in a screen and shown to inhibit the kinase activity of IRE1α as well as *Xbp1* splicing[334]. After total RNAs were isolated from organoids, PCR with reverse transcription (RT-PCR) followed by Xbp1u/s-specific PCR was performed. Gel electroporation results

demonstrated that organoids lacking XBP1 showed more *Xbp1s* compared to *Xbp1u*. Inhibition of IRE1 led to reduced *Xbp1* splicing in colon organoids lacking XBP1 as indicated by a more prominent *Xbp1u*-specific band compared to *Xbp1u* band. In contrast, control organoids showed bands only specific to *Xbp1u* (Figure 2-1B). These data indicate that XBP1 is deleted in the intestinal epithelium of *Xbp1*$^{IEC\text{-}KO}$ mice.

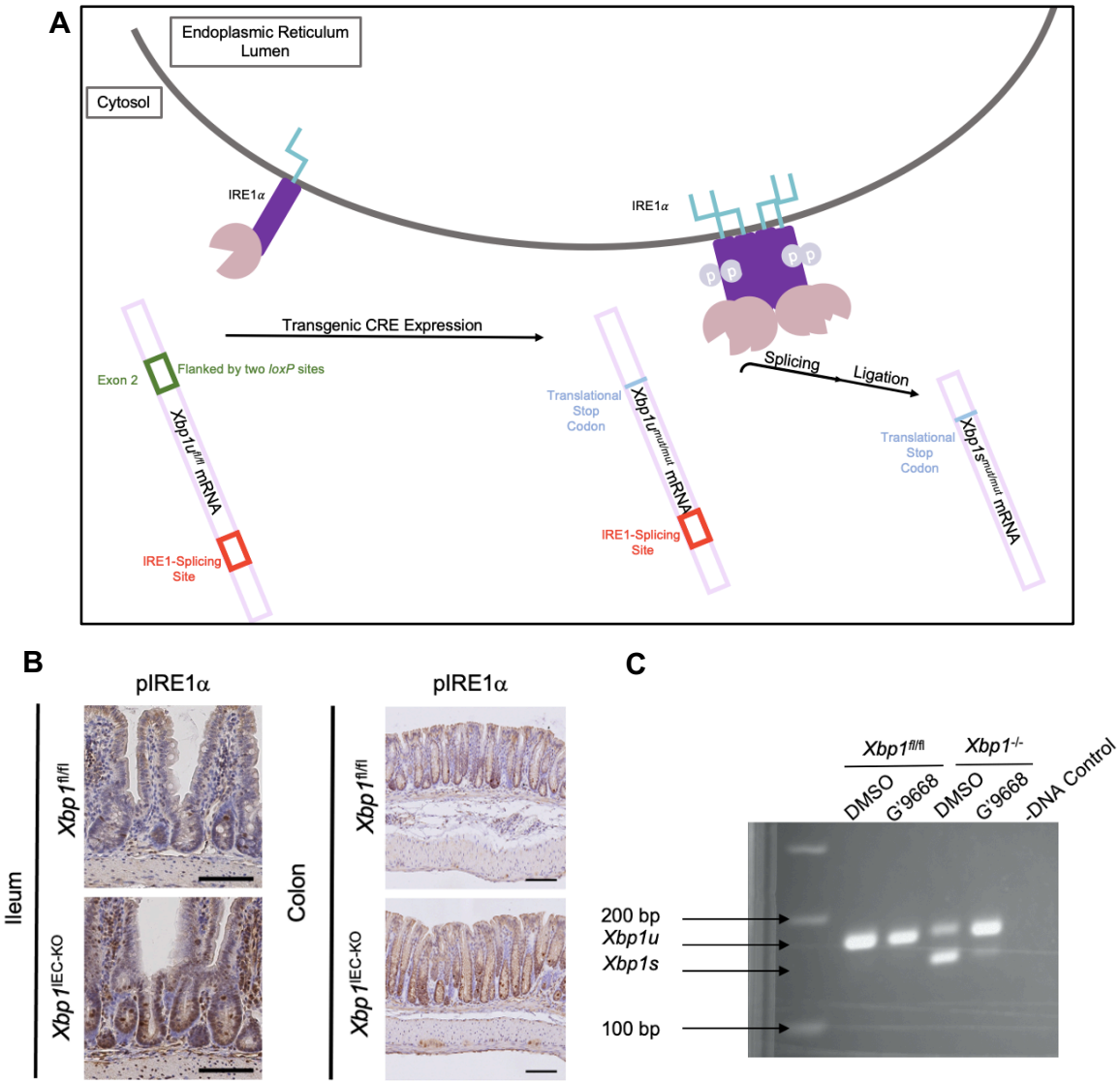

Figure 2-1 Indirect confirmation of XBP1 deletion in the intestines of *Xbp1*$^{IEC-KO}$ mice.

(A) Upon transgenic CRE expression in IECs, excision of Exon 2 in *Xbp1*$^{fl/fl}$ mRNA leads to the generation of the translational premature stop codon at the third exon. Activated IRE1α splices mutated *Xbp1* (*Xbp1*$^{mut/mut}$) mRNA containing splicing site (unspliced *Xbp1*, *Xbp1u*$^{mut/mut}$), leading to the generation of spliced *Xbp1* (*Xbp1s*$^{mut/mut}$). **(B)** Representative pictures of ileal and colon sections from indicated mouse lines immunostained for Phospho-IRE1 alpha (pIRE1α, Ser724). **(C)** Gel electrophoresis results showing spliced and unspliced versions of *Xbp1* in control and Xbp1-deficient colon organoids treated with DMSO or IRE1 inhibitor (G'9668) for 16 hours. Scale bars, 100 μm.

It was reported that *Xbp1*$^{IEC-KO}$ mice showed ER stress-mediated ileitis manifesting with hypomorphic Paneth cells, increased crypt hyperplasia, IEC death leading to obvious ulcerations and granulations, and crypt abscesses[323]. The histological analysis of haematoxylin & eosin (H&E) stained intestinal sections from *Xbp1*$^{IEC-KO}$ mice, generated

in this study, revealed that the deletion of XBP1 in IECs led to mild ileitis. Specifically, these mice showed increased crypt length and the absence of Paneth cells' dense granules. Epithelial hyperplasia and Paneth cell impairment in the ilea of XBP1 deficient mice were confirmed by performing immunostaining on the section slides with Ki-67 and Lysozyme antibodies, respectively. The number of cells at the crypt that were positively stained with Ki-67, which is expressed at a protein level during the S, G2 and M phases of the cell cycle and thereby, is regularly utilised as a marker for the dividing cells [335], was increased in the small intestinal sections from *Xbp1*$^{IEC\text{-}KO}$ mice compared to controls, confirming the crypt hyperplasia in these mice (Figure 2-2). Meanwhile, Lysozyme staining, which colocalises with the secretion granules of Paneth cells [336], revealed that IEC-specific XBP1 deletion severely affected the Paneth cells without complete loss[162,323]. Moreover, to check whether *Xbp1*$^{IEC\text{-}KO}$ mice had increased infiltration of immune cells in the mucosa, small intestinal sections from *Xbp1*$^{IEC\text{-}KO}$ mice were stained against CD45 antibody, a pan immune cell marker. Immunohistochemistry (IHC) results demonstrated that XBP1 deletion in IECs did not lead to an increased influx of immune cells in the small intestine compared to control mice, in contrast to the previous report (Figure 2-2) [323].

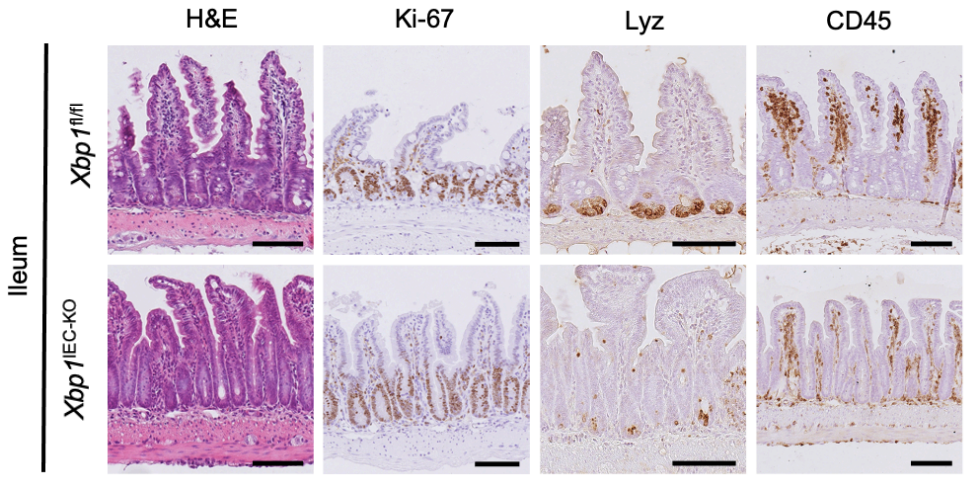

Figure 2-2 *Xbp1*$^{IEC\text{-}KO}$ mice show mild hyperplasia and impaired Paneth cells in the ileum.

Representative images of Swiss-roll ileal sections from 8-12 week-old mice with the indicated genotypes stained with haematoxylin & eosin (H&E) or immunostained for Lysozyme, CD45, Ki67, Phospho-IRE1 alpha (pIRE1α, Ser724). Scale bars, 100 μm.

In addition to the small intestines of *Xbp1*$^{IEC-KO}$ mice, the colons of *Xbp1*$^{IEC-KO}$ mice were analysed. Examination of H&E-stained colon sections did not reveal an observable phenotype in these mice (Figure 2-3), which was confirmed by performing immunostainings for Ki-67 and CD45 on colon sections from *Xbp1*$^{IEC-KO}$ and control mice (Figure 2-3). Collectively, these results show that XBP1 ablation in IECs leads to Paneth cell impairment, and mild hyperplasia in the small intestine.

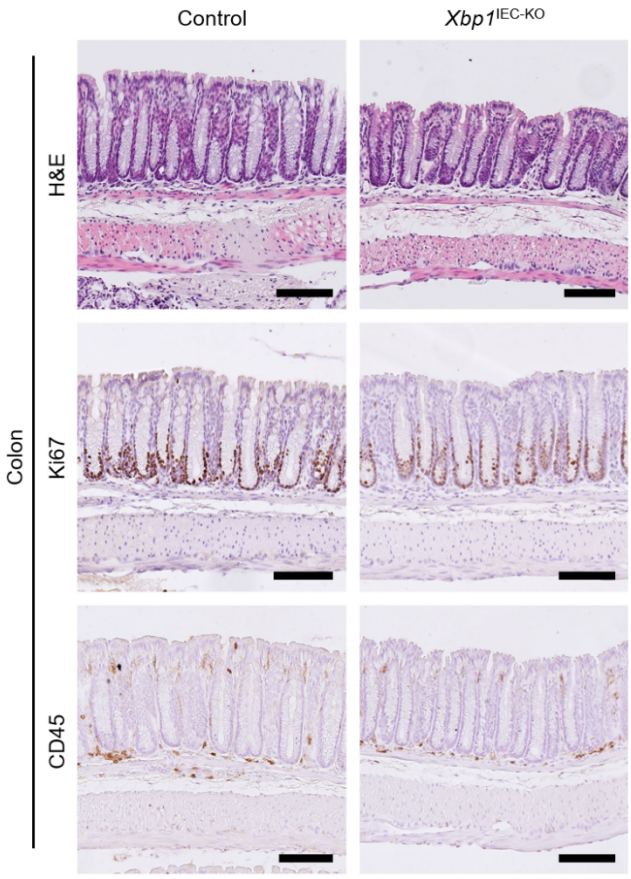

Figure 2-3 *Xbp1*$^{IEC-KO}$ mice do not show an observable pathology in the colon.

Representative images of Swiss-roll colon sections from 8-12 week-old mice with the indicated genotypes stained with H&E or immunostained for Ki67, CD45 and pIRE1α.

2.1.2 *Xbp1*$^{IEC-KO}$ *Casp8*$^{IEC-KO}$ mice exhibit severe colitis compared to *Casp8*$^{IEC-KO}$ mice

To study whether XBP1-deletion induced ER-stress and necroptosis pathways crosstalk in the intestine, *Xbp1*$^{IEC-KO}$ mice were crossed to *Casp8*$^{fl/fl}$ mice[337] carrying two *loxP*

recombination sites flanking exon 3 of *Casp8*. leading to the generation of the mice lacking XBP1 and Casp8 specifically in IECs (hereafter, *Xbp1*$^{IEC\text{-}KO}$ *Casp8*$^{IEC\text{-}KO}$). Strikingly, mice lacking both XBP1 and Casp8 in IECs had reduced relative body weight between 5-12 weeks of age compared to control, *Casp8*$^{IEC\text{-}KO}$ and *Xbp1*$^{fl/fl}$ *Villin*-cre$^{tg/wt}$ *Casp8*$^{wt/fl}$ (hereafter, *Xbp1*$^{IEC\text{-}KO}$ *Casp8*$^{IEC\text{-}Het}$) mice (Figure 2-4), indicating *Xbp1*$^{IEC\text{-}KO}$ *Casp8*$^{IEC\text{-}KO}$ mice could have the severe intestinal phenotype.

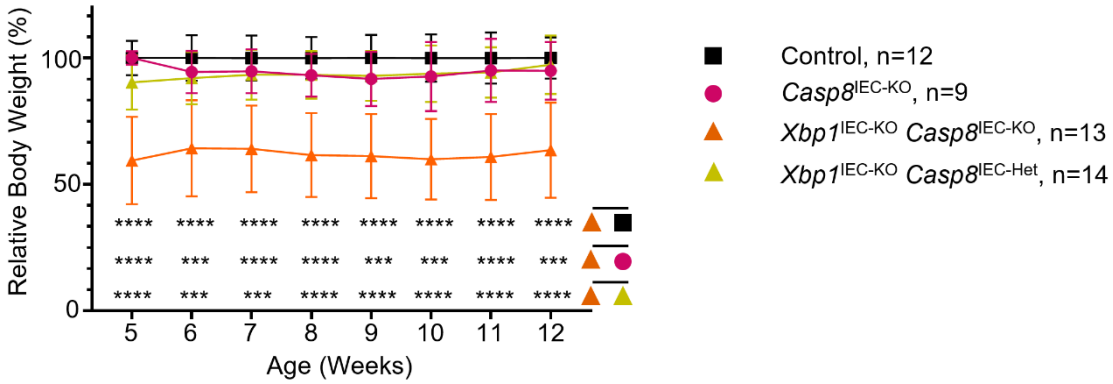

Figure 2-4 *Xbp1*$^{IEC\text{-}KO}$ *Casp8*$^{IEC\text{-}KO}$ mice have reduced body weight compared to *Casp8*$^{IEC\text{-}KO}$.

Graph depicting relative body weight of indicated mouse lines at 5-12 weeks of age. Age and sex-matched *Villin*-cre$^{wt/wt}$ mice, shown as control mice, were used as normalisation. ***p≤0.005 ****p≤0.0001 (Two-way ANOVA multiple comparisons).

As the reduced body weight in *Xbp1*$^{IEC\text{-}KO}$ *Casp8*$^{IEC\text{-}KO}$ mice could be a consequence of severe colitis, the colon sections from 8-12 weeks old *Casp8*$^{IEC\text{-}KO}$ and *Xbp1*$^{IEC\text{-}KO}$ *Casp8*$^{IEC\text{-}KO}$ mice were examined. As previously shown [307,308,310,312], the histological assessment revealed that *Casp8*$^{IEC\text{-}KO}$ mice developed spontaneous colitis which manifested itself as hyperplastic epithelium, dying IECs leading to mild epithelial injury, rarely leading to ulcerations, increased infiltration of immune cells which was largely confined to the mucosa (Figure 2-5 and 2-6). Meanwhile, histological scoring based on parameters such as hyperplasia, epithelial erosion, cell death and inflammation demonstrated that the severity of the colitis in *Casp8*$^{IEC\text{-}KO}$ mice varied between individuals in the spectrum of mild to severe (Figure 2-7A).

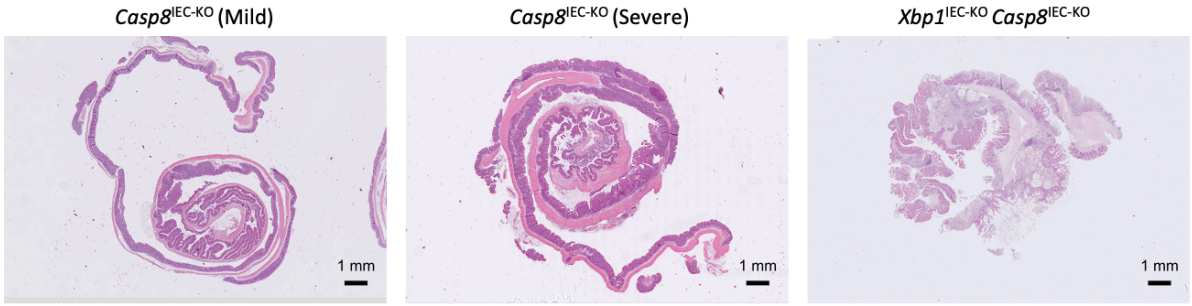

Figure 2-5 Deletion of XBP1 aggravates colitis in Casp8^{IEC-KO} mice.

Representative images of Swiss-roll ileal sections from 8-12 week-old mice with the indicated genotypes stained with H&E.

Histological investigation of colon sections from *Xbp1*$^{IEC-KO}$ *Casp8*$^{IEC-KO}$ mice revealed that mice lacking XBP1 and Casp8 developed severe colitis, characterized by a copious number of dying IECs which led to severe colonic epithelial injury (Figure 2-5 and 2-6). Importantly, the extent of the epithelial injury was leading to patchy epithelial erosions and clear ulcerations, spanning throughout the entire colon in *Xbp1*$^{IEC-KO}$ *Casp8*$^{IEC-KO}$ mice. In contrast, ulcerations were only observed at the proximal colons of *Casp8*$^{IEC-KO}$ mice (Figure 2-5 and 2-6). Furthermore, Ki-67 and CD45 immunostainings confirmed that *Xbp1*$^{IEC-KO}$ *Casp8*$^{IEC-KO}$ mice exhibited extensive hyperplasia and increased immune cell influx in the layers of the colon with the formation of crypt abscesses, respectively. (Figure 2-6).

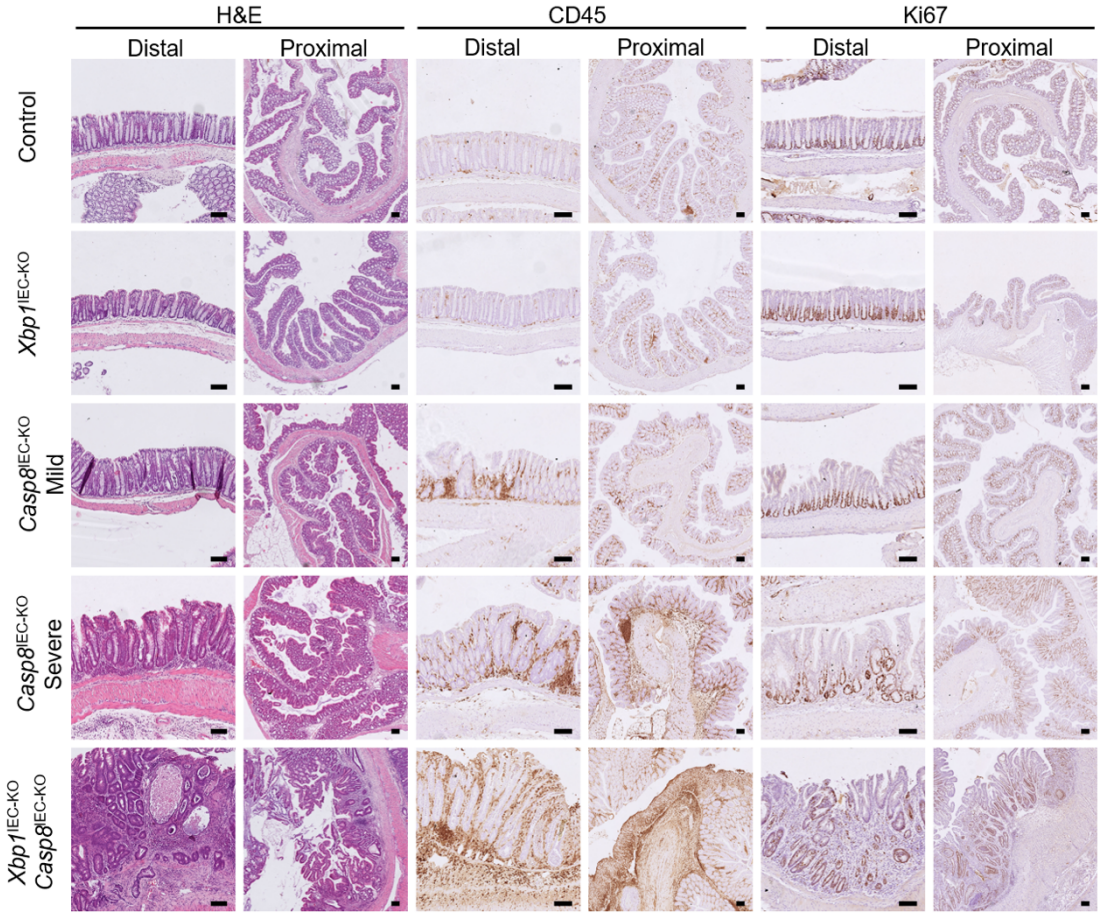

Figure 2-6 *Xbp1*$^{IEC\text{-}KO}$ *Casp8*$^{IEC\text{-}KO}$ mice develop more severe colitis compared to *Casp8*$^{IEC\text{-}KO}$ mice.

Representative images of Swiss-roll colon sections from 8-12 week-old mice with the indicated genotypes stained with H&E or immunostained for CD45, Ki67. Scale bars, 100 μm.

Blind histological scoring of the colon sections from *Casp8*$^{IEC\text{-}KO}$ and *Xbp1*$^{IEC\text{-}KO}$ *Casp8*$^{IEC\text{-}KO}$ mice revealed that *Xbp1*$^{IEC\text{-}KO}$ *Casp8*$^{IEC\text{-}KO}$ mice developed more severe colitis compared to *Casp8*$^{IEC\text{-}KO}$ mice (Figure 2-7A). In line with this, almost all of *Xbp1*$^{IEC\text{-}KO}$ *Casp8*$^{IEC\text{-}KO}$ mice showed ulcer formation in the colon, as opposed to 27% of *Casp8*$^{IEC\text{-}KO}$ mice. To unbiasedly evaluate the colitis in *Xbp1*$^{IEC\text{-}KO}$ *Casp8*$^{IEC\text{-}KO}$ mice, RNA sequencing analysis of total RNAs isolated from distal colon tissues was performed. The result revealed that RNA expression profile from the colons of *Xbp1*$^{IEC\text{-}KO}$ *Casp8*$^{IEC\text{-}KO}$ mice distinctly grouped compared to mouse lines from control, *Xbp1*$^{IEC\text{-}KO}$ and *Casp8*$^{IEC\text{-}KO}$ mice (Figure 2-7B). Furthermore, expression of genes involved inflammatory pathways were upregulated in the colons of *Xbp1*$^{IEC\text{-}KO}$ *Casp8*$^{IEC\text{-}KO}$ mice when it was compared to the colons of *Casp8*$^{IEC\text{-}KO}$ mice (Figure 2-7C), confirming more severe colitis in *Xbp1*$^{IEC\text{-}KO}$ *Casp8*$^{IEC\text{-}KO}$ mice compared to *Casp8*$^{IEC\text{-}KO}$ mice. Taken together, these results

demonstrate that IEC-specific deletion of XBP1 exaggerates the severity of colitis in *Casp8*$^{IEC\text{-}KO}$ mice.

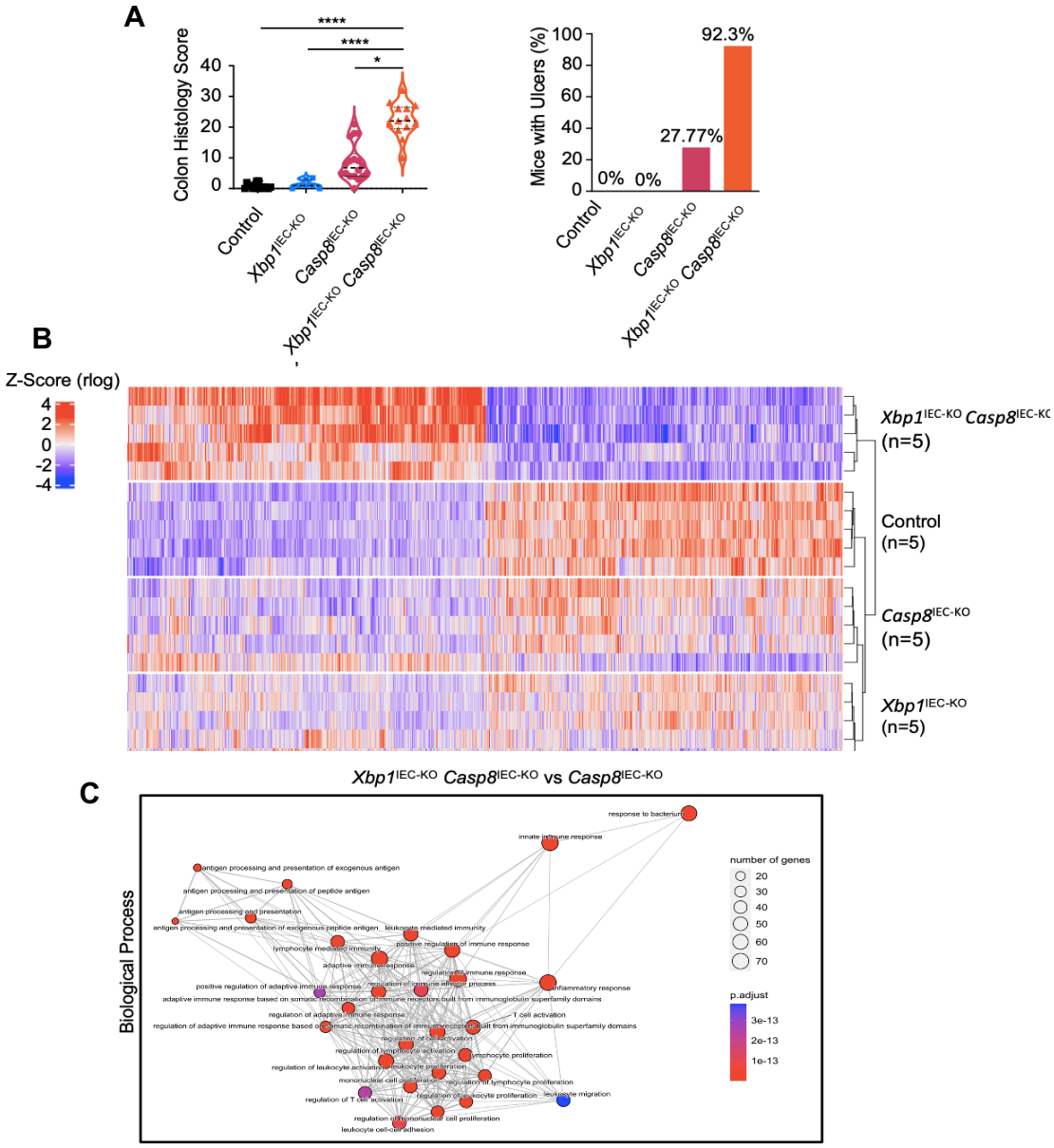

Figure 2-7 Histopathological assessment and RNA sequencing analysis of colons from control, *Xbp1*$^{IEC\text{-}KO}$, *Casp8*$^{IEC\text{-}KO}$ and *Xbp1*$^{IEC\text{-}KO}$ *Casp8*$^{IEC\text{-}KO}$ mice.

(A) Graphs showing colon histology score (left), percent of the mice with colonic ulcers (right) from 8-12 weeks old mice with indicated genotypes. Each dot represents one mouse. $*p < 0.05$, $**p < 0.01$, $***p < 0.005$, $****p < 0.0001$. **(B)** Heatmap depicting RNA expression profile of distal colons from 8-12 weeks old mice with indicated genotypes. **(C)** Emap plots showing enrichment of genes in gene ontology of Biological process in the colons of *Xbp1*$^{IEC\text{-}KO}$ *Casp8*$^{IEC\text{-}KO}$ mice compared to *Casp8*$^{IEC\text{-}KO}$ mice. 5 mice per mouse line were analysed.

2.2 XBP1 deficiency aggravates colitis in *Casp8*$^{IEC\text{-}KO}$ and *Fadd*$^{IEC\text{-}KO}$ mice necroptosis-dependent manner

2.2.1 Ubiquitous RIPK3 or MLKL deletion inhibits severe colitis in *Xbp1*$^{IEC\text{-}KO}$ *Casp8*$^{IEC\text{-}KO}$ mice

Caspase-8 cleaves RIPK1 [116,338-340] and inhibits RIPK3-MLKL-mediated necroptosis[104-106]. Specifically, ubiquitous deletion of RIPK3 prevents spontaneous colon inflammation in *Casp8*$^{IEC\text{-}KO}$ mice, showing IEC necroptosis induces colitis in Casp8 deficient mice[310].

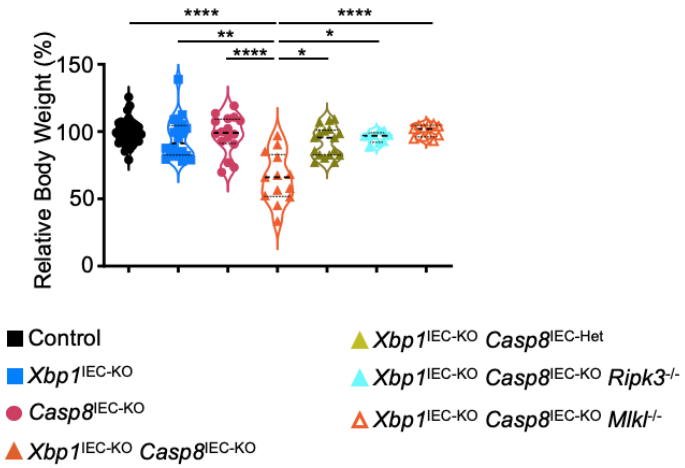

Figure 2-8 Ablation of RIPK3 or MLKL restores the body weight of *Xbp1*$^{IEC\text{-}KO}$ *Casp8*$^{IEC\text{-}KO}$ mice.

Graph showing the relative body weight of 8-12 weeks old mice with indicated genotypes. Age and sex-matched *Villin*-cre$^{wt/wt}$ mice, shown as control mice, were used as normalisation. Each dot represents one mouse. ∗p < 0.05, ∗∗p < 0.01, ∗∗∗p < 0.005, ∗∗∗∗p < 0.0001 (One-way ANOVA).

To study whether IEC-specific XBP1 deletion could increase the severity of colitis in *Casp8*$^{IEC\text{-}KO}$ mice epithelial necroptosis-dependent manner, *Xbp1*$^{IEC\text{-}KO}$ *Casp8*$^{IEC\text{-}KO}$ mice were crossed to RIPK3 full-body knock-out mice (*Ripk3*$^{-/-}$ mice)[341]. The generated mice (*Xbp1*$^{IEC\text{-}KO}$ *Casp8*$^{IEC\text{-}KO}$ *Ripk3*$^{-/-}$) were devoid of RIPK3 protein ubiquitously whereas XBP1 and Casp8 were specifically absent in the intestines of these mice. Strikingly, ablation of RIPK3 normalised the body weight of *Xbp1*$^{IEC\text{-}KO}$ *Casp8*$^{IEC\text{-}KO}$ mice (Figure 2-8).

Histopathological analysis of colon sections demonstrated that *Xbp1*$^{IEC\text{-}KO}$ *Casp8*$^{IEC\text{-}KO}$ *Ripk3*$^{-/-}$ mice did not develop colitis (Figure 2-9 and 2-10).

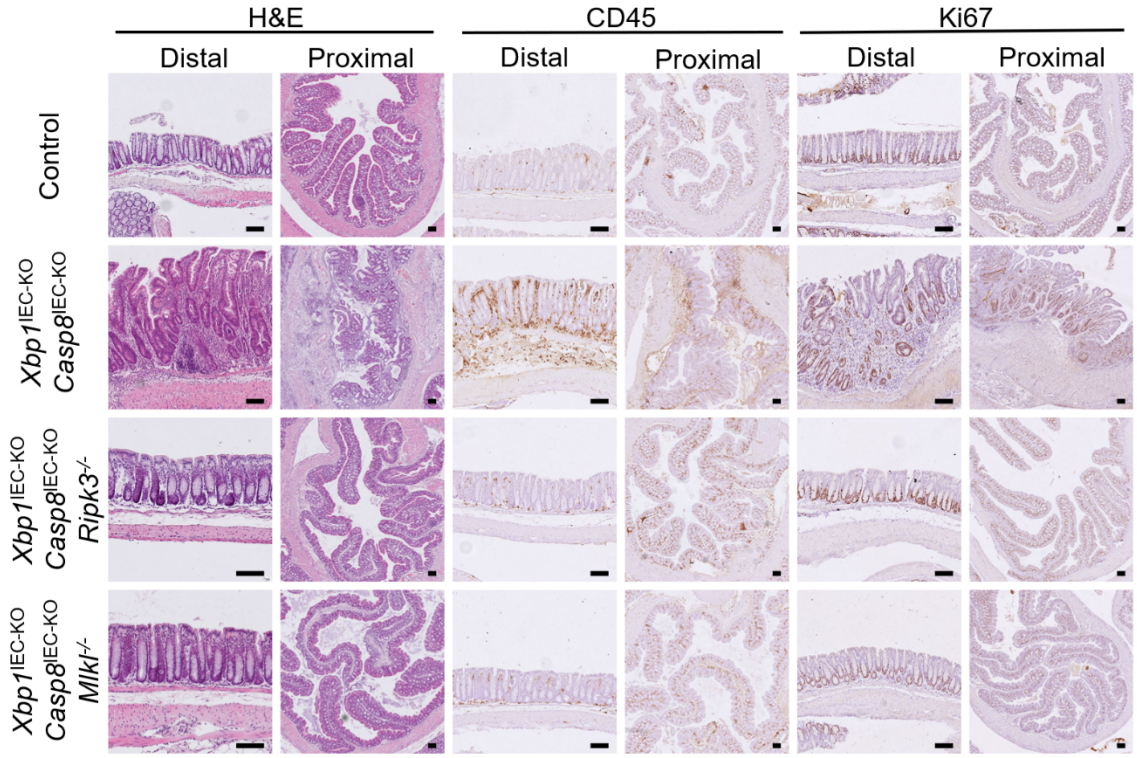

Figure 2-9 Inhibition of RIPK3-MLKL-dependent IEC necroptosis prevents the development of colitis in *Xbp1*$^{IEC\text{-}KO}$ *Casp8*$^{IEC\text{-}KO}$ mice.

Representative images of Swiss-roll colon sections from 8-12 week-old mice with the indicated genotypes stained with H&E or immunostained for CD45, Ki67. Scale bars, 100 µm.

It was previously demonstrated that RIPK3 expression in haemopoietic cells plays a role in DSS-induced colitis[342]. To exclude the contribution of RIPK3 deletion in immune cells while inhibiting IEC-necroptosis, *Xbp1*$^{IEC\text{-}KO}$ *Casp8*$^{IEC\text{-}KO}$ mice were crossed to mice with MLKL full-body knock-out (*Mlkl*$^{-/-}$ mice)[343]. MLKL is the executor of necroptosis[112,344]. Ablation of MLKL restored the body weight of *Xbp1*$^{IEC\text{-}KO}$ *Casp8*$^{IEC\text{-}KO}$ mice (Figure 2-8). Histopathological analysis revealed that *Xbp1*$^{IEC\text{-}KO}$ *Casp8*$^{IEC\text{-}KO}$ *Mlkl*$^{-/-}$ mice did not develop colitis, similar to *Xbp1*$^{IEC\text{-}KO}$ *Casp8*$^{IEC\text{-}KO}$ *Ripk3*$^{-/}$ mice (Figure 2-9 and 2-10A). Furthermore, RNA-sequencing analysis confirmed that MLKL ablation prevented the colitis in *Xbp1*$^{IEC\text{-}KO}$ *Casp8*$^{IEC\text{-}KO}$ as indicated by similar RNA expression profile in the colons of *Xbp1*$^{IEC\text{-}KO}$ and *Xbp1*$^{IEC\text{-}KO}$ *Casp8*$^{IEC\text{-}KO}$ *Mlkl*$^{-/-}$ mice (Figure 2-10B). Collectively,

these results show the severe colitis in *Xbp1*$^{IEC\text{-}KO}$ *Casp8*$^{IEC\text{-}KO}$ mice completely depends on RIPK3-MLKL-dependent epithelial necroptosis.

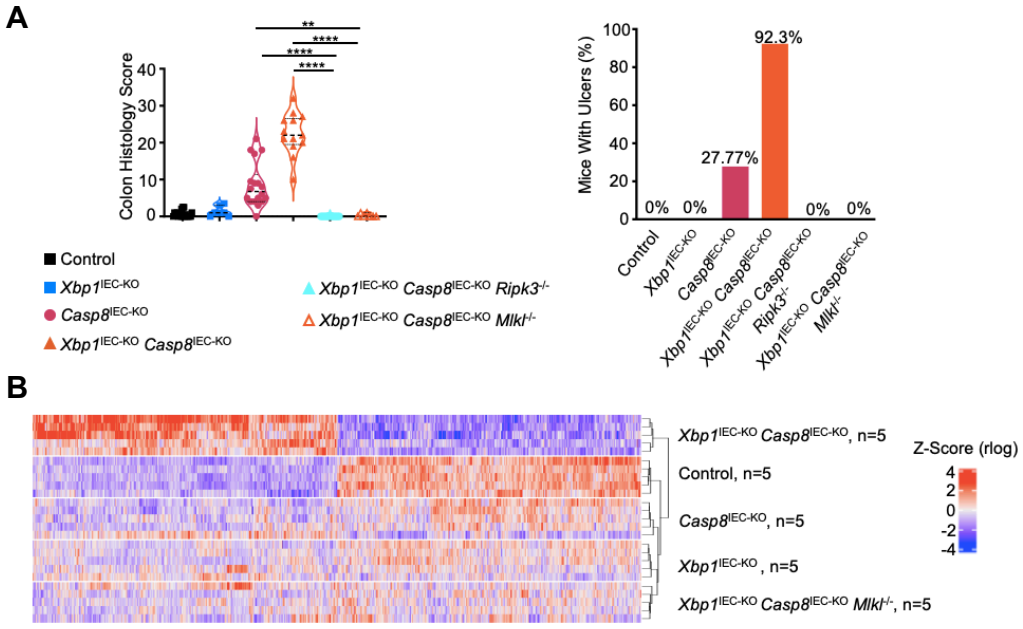

Figure 2-10 The severe colitis in *Xbp1*$^{IEC\text{-}KO}$ *Casp8*$^{IEC\text{-}KO}$ mice completely depends on epithelial necroptosis.

(A) Graphs showing colon histology score (left), percent of the mice with colonic ulcers (right) from 8-12 week-old mice with indicated genotypes. Each dot represents one mouse. $*p < 0.05$, $**p < 0.01$, $***p < 0.005$, $****p < 0.0001$.(One-way ANOVA). **(B)** Heatmap depicting RNA expression profile of distal colons from 8-12 weeks old mice with indicated genotypes. 5 mice per mouse line were analysed. RNA-sequencing was analysed by Ulrike Goebel.

2.2.2 IEC-specific XBP1 deletion exaggerates the necroptosis-induced colitis in *Fadd*$^{IEC\text{-}KO}$ mice

The death receptors induce Caspase-8-mediated apoptosis through the adaptor protein FADD[345,346]. Moreover, it was demonstrated that FADD has a critical function in preventing necroptosis [309,347,348]. Specifically, mice lacking FADD in IECs develop RIPK3-MLKL-dependent spontaneous colitis[307,309]. To answer whether IEC-specific ablation of XBP1 could exaggerate colitis in *Fadd*$^{IEC\text{-}KO}$ mice, *Xbp1*$^{IEC\text{-}KO}$ mice were crossed to mice carrying *Fadd* whose exon 2 are flanked by *loxP* recombination sites (*Fadd*$^{fl/fl}$ mice). As a result, mice lacking XBP1 and FADD in IECs were generated (*Xbp1*$^{IEC\text{-}KO}$ *Fadd*$^{IEC\text{-}KO}$). Observations based on the colon sections stained with H&E revealed that *Xbp1*$^{IEC\text{-}KO}$

Fadd$^{IEC\text{-}KO}$ mice developed spontaneous colitis. Specifically, the colons of *Xbp1*$^{IEC\text{-}KO}$ *Fadd*$^{IEC\text{-}KO}$ mice exhibited epithelial erosions with ulcerations, hyperplastic epithelium and an elevated influx of immune cells into mucosa and submucosa with crypt abscesses (Figure 2-11).

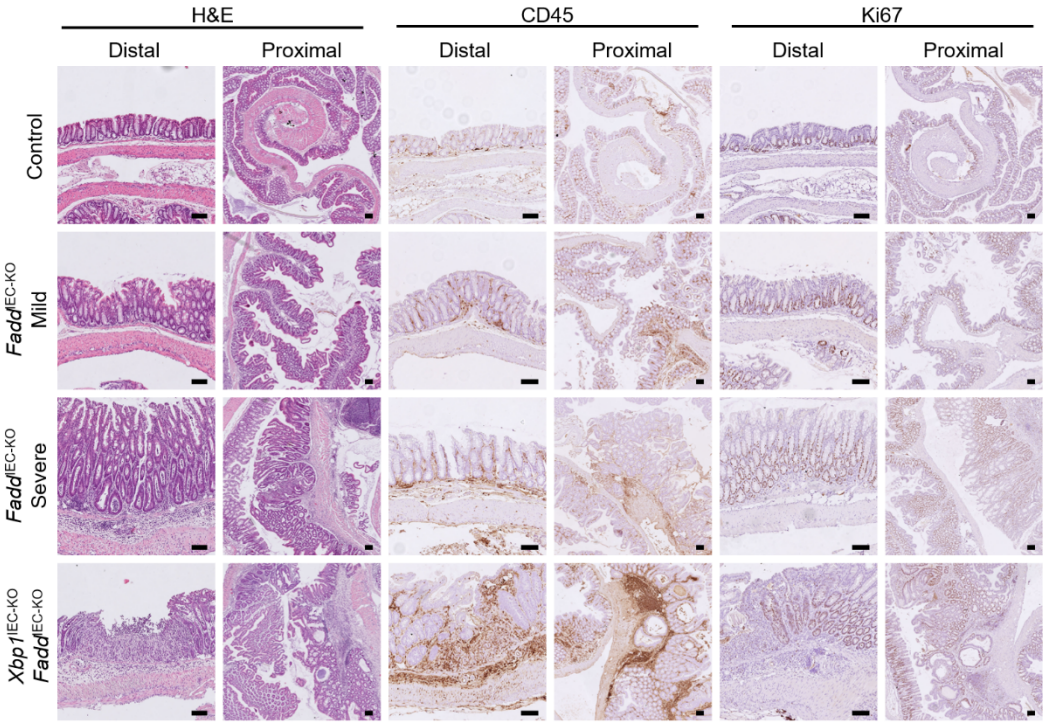

Figure 2-11 IEC-specific XBP1 protects *Fadd*$^{IEC\text{-}KO}$ mice from severe colitis.

Representative images of Swiss-roll colon sections from 8-12 week-old mice with the indicated genotypes stained with H&E or immunostained for CD45, Ki67. Scale bars, 100 μm.

Immunostainings with antibodies against CD45 and Ki-67 confirmed the inflammation and epithelial hyperplasia in the colons of *Xbp1*$^{IEC\text{-}KO}$ *Fadd*$^{IEC\text{-}KO}$ mice (Figure 2-11). The severity of colitis in *Fadd*$^{IEC\text{-}KO}$ mice showed variability. However, *Xbp1*$^{IEC\text{-}KO}$ *Fadd*$^{IEC\text{-}KO}$ mice did not show colitis severity spectrum, as all the observed *Xbp1*$^{IEC\text{-}KO}$ *Fadd*$^{IEC\text{-}KO}$ mice had severe colitis. The blind histopathological scoring demonstrated that XBP1 deletion exaggerated the colitis in *Fadd*$^{IEC\text{-}KO}$ mice (Figure 2-12). Counting the number of mice possessing ulcers in the colon revealed that all the analysed *Xbp1*$^{IEC\text{-}KO}$ *Fadd*$^{IEC\text{-}KO}$ mice showed ulcers, as opposed to only 60% of *Fadd*$^{IEC\text{-}KO}$ mice, further demonstrating that *Xbp1*$^{IEC\text{-}KO}$ *Fadd*$^{IEC\text{-}KO}$ mice had exacerbated colitis compared to *Fadd*$^{IEC\text{-}KO}$ mice (Figure 2-12).

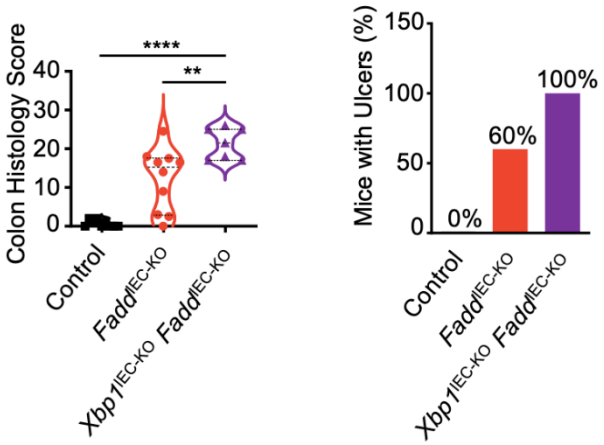

Figure 2-12 *Xbp1*$^{IEC-KO}$ *Fadd*$^{IEC-KO}$ mice have more severe colitis compared to *Fadd*$^{IEC-KO}$ mice.

Graphs showing colon histology score (left), percent of the mice with colonic ulcers (right) from 8-12 weeks old mice with indicated genotypes. Each dot represents one mouse. $*p < 0.05$, $**p < 0.01$, $***p < 0.005$, $****p < 0.0001$.(One-way ANOVA).

Inhibition of IEC-necroptosis by RIPK3 full-body deletion completely inhibits the development of colitis in *Fadd*$^{IEC-KO}$ mice[309]. Moreover, the previous results in this thesis showed that severe colitis in *Xbp1*$^{IEC-KO}$ *Casp8*$^{IEC-KO}$ mice completely depends on RIPK3-MLKL-mediated necroptosis (Figure 2-9 and 2-10). To check whether XBP1 exaggerates colitis in *Fadd*$^{IEC-KO}$ mice IEC necroptosis-dependent manner, *Xbp1*$^{IEC-KO}$ *Fadd*$^{IEC-KO}$ *Ripk3*$^{-/-}$ mice were generated. Histopathological assessment of the colon sections from *Xbp1*$^{IEC-KO}$ *Fadd*$^{IEC-KO}$ *Ripk3*$^{IEC-KO}$ mice demonstrated that ablation of RIPK3 in *Xbp1*$^{IEC-KO}$ *Fadd*$^{IEC-KO}$ mice completely prevented the development of colitis (Figure 2-13B and 2-13C). All in all, these results demonstrate that XBP1 ablation exacerbates necroptosis-induced colitis in *Casp8*$^{IEC-KO}$ and *Fadd*$^{IEC-KO}$ mice.

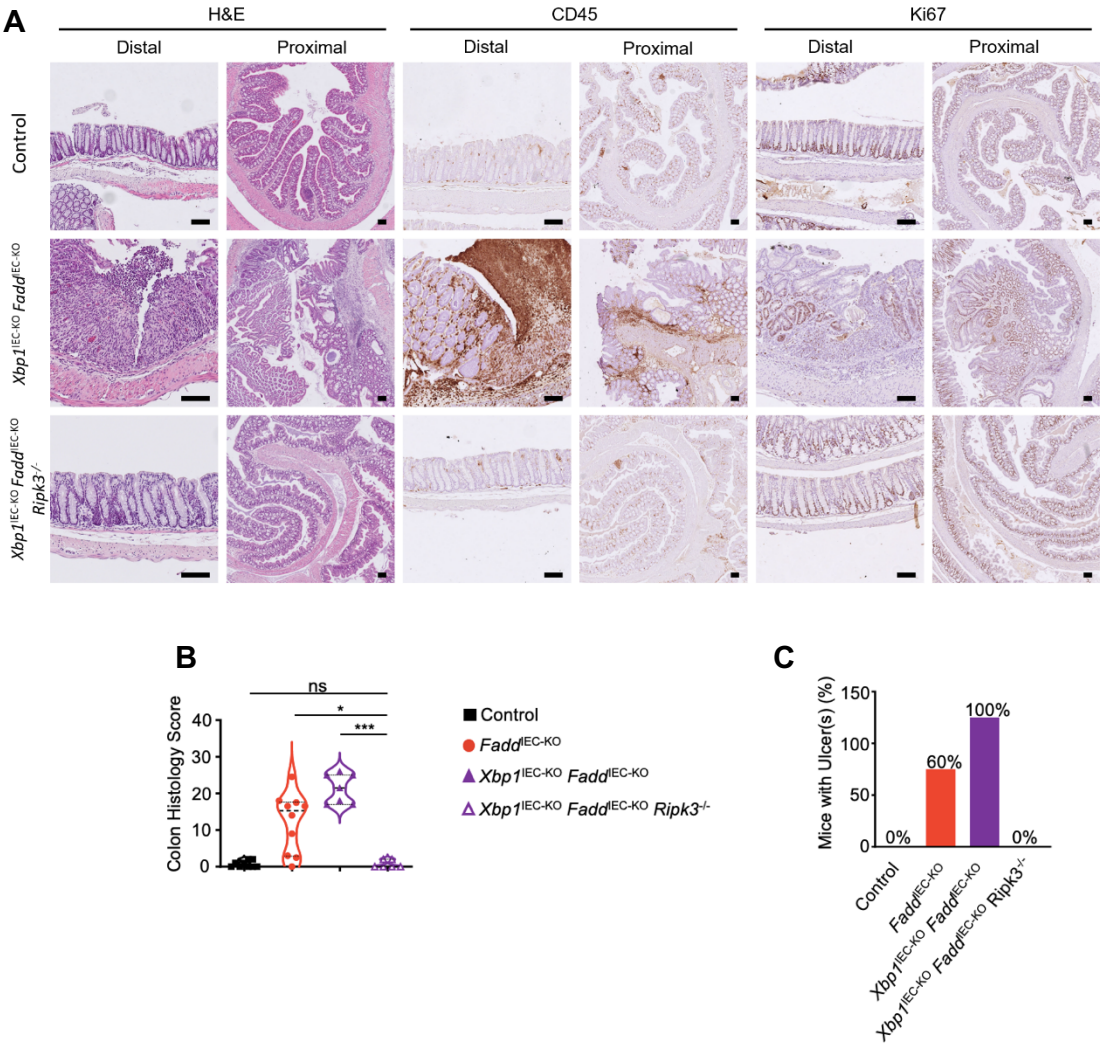

Figure 2-13 The severe colitis in *Xbp1*$^{IEC\text{-}KO}$ *Fadd*$^{IEC\text{-}KO}$ mice completely depends on epithelial necroptosis.

(A) Representative images of Swiss-roll colon sections from 8-12 week-old mice with the indicated genotypes stained with haematoxylin & eosin (H&E) or immunostained for CD45, Ki67. Graphs showing colon histology score **(B)**, percent of the mice with colonic ulcers **(C)** from 8-12 weeks old mice with indicated genotypes. Each dot represents one mouse. $*p < 0.05$, $**p < 0.01$, $***p < 0.005$, $****p < 0.0001$.(One-way ANOVA). Scale bars, 100 μm.

2.3 IEC-specific XBP1 does not play an important role in necroptosis-induced or -driven ileitis

2.3.1 Ablation of IEC-specific XBP1 does not increase the severity of ileitis in *Casp8*$^{IEC\text{-}KO}$ mice

Xbp1$^{IEC\text{-}KO}$ mice generated in this study showed mild crypt hyperplasia and reduced Paneth cells in the ileum (Figure 2-2). *Casp8*$^{IEC\text{-}KO}$ mice develop spontaneous ileitis, which is characterised by alteration in crypt structures, almost complete absence of Paneth cells, and increased presence of $CD4^+$ T cells and granulocytes in the lamina propria [308]. Having found out that XBP1 exacerbates the colitis in *Casp8*$^{IEC\text{-}KO}$ and *Fadd*$^{IEC\text{-}KO}$ mice, it was asked whether deletion of XBP1 could increase the severity of ileitis in *Casp8*$^{IEC\text{-}KO}$ and *Fadd*$^{IEC\text{-}KO}$ mice. Small intestinal sections from *Casp8*$^{IEC\text{-}KO}$ and *Xbp1*$^{IEC\text{-}KO}$ *Casp8*$^{IEC\text{-}KO}$ mice were analysed. As it was previously reported, H&E-stained ileal sections from *Casp8*$^{IEC\text{-}KO}$ mice showed increased IEC death and mild villi injury as observed by thinning of epithelium without ulceration, lacking the dense granules that are associated with Paneth cell[187], crypt hyperplasia, increased influx of cells in lamina propria, leading to thickening of mucosa as well as Mucosa serosa, showing these mice developed spontaneous ileitis (Figure 2-14A). Examination of H&E-stained ileal sections from *Xbp1*$^{IEC\text{-}KO}$ *Casp8*$^{IEC\text{-}KO}$ mice revealed that combined deletion of XBP1 and Casp8 led to increased death of IECs causing blunted and thinned villi, crypt hyperplasia, near complete loss of Paneth cells, an increased presence of immune cells in lamina propria (Figure 2-14A), similar to the manifestation of ileitis in *Casp8*$^{IEC\text{-}KO}$ mice. Immunostaining with Lysozyme, Ki-67 and CD45 antibodies showed that *Casp8*$^{IEC\text{-}KO}$ and *Xbp1*$^{IEC\text{-}KO}$ *Casp8*$^{IEC\text{-}KO}$ mice had strongly diminished numbers of Paneth cells, severe hyperplasia, and inflammation (Figure 2-14A). quantitative PCR with reverse transcription (qRT-PCR) analysis showed that mice lacking Casp8 or XBP1 and Casp8 had reduced expression of *Lyz* as well as two important Paneth cell associated defensins[227], *Defa5* and *Defa-rs10*, confirming the Paneth cell impairment in the ilea of *Casp8*$^{IEC\text{-}KO}$ and *Xbp1*$^{IEC\text{-}KO}$ *Casp8*$^{IEC\text{-}KO}$ mice (Figure 2-14B). Side-by-side histopathological scoring and qRT-PCR analysis of mRNA expression of inflammatory genes such as *Il1b*, *Ccl2* and *Cxcl1* revealed that *Casp8*$^{IEC\text{-}KO}$ and *Xbp1*$^{IEC\text{-}KO}$ *Casp8*$^{IEC\text{-}KO}$ mice had similar level of ileal pathology (Figure 2-14C and 2-14D). Taken together, these results show that additional deletion of XBP1 in *Casp8*$^{IEC\text{-}KO}$ mice did not exaggerate the severity of ileitis.

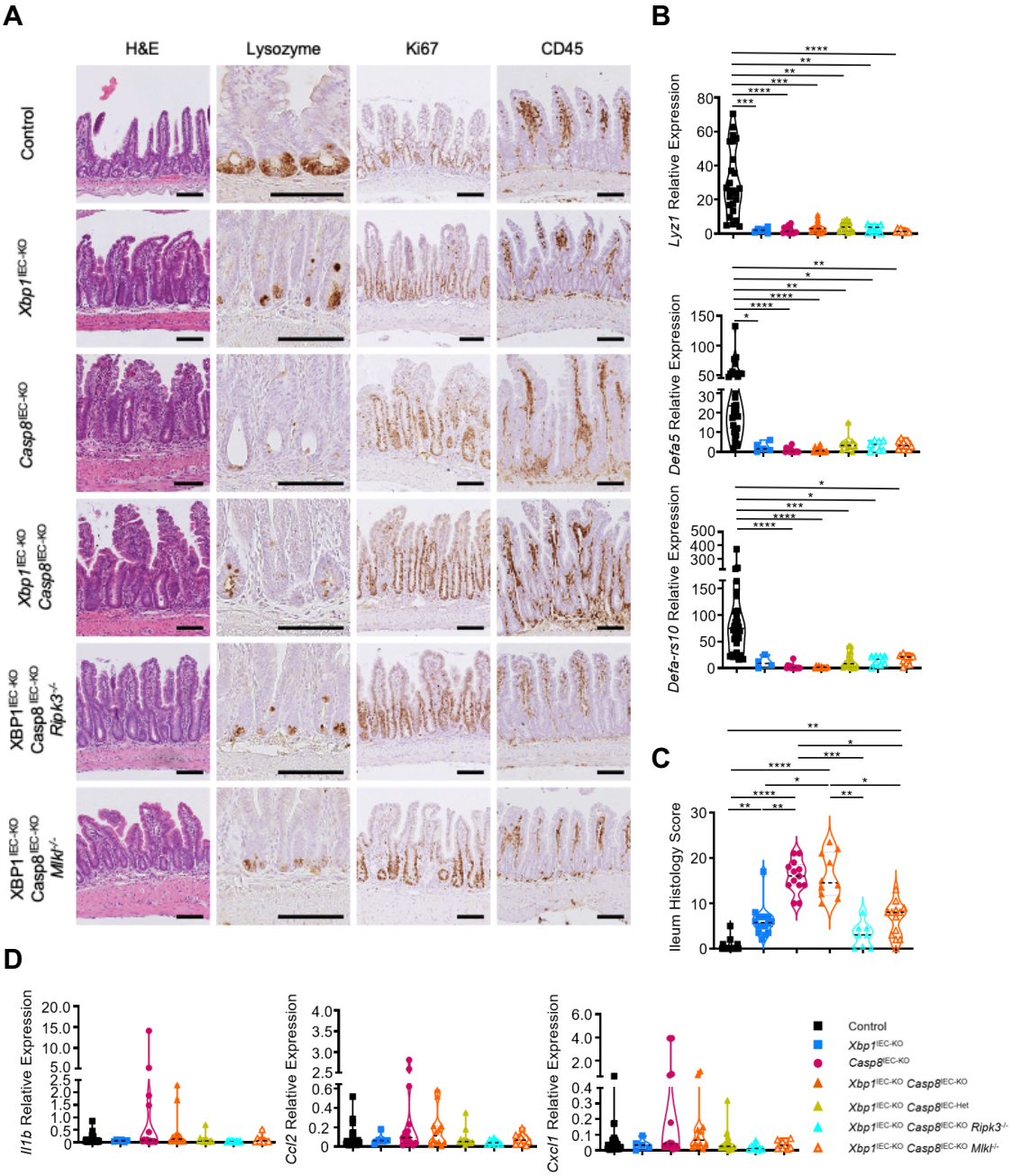

Figure 2-14 Epithelial-specific XBP1 ablation does not exaggerate necroptosis-induced ileitis in *Casp8*$^{IEC-KO}$ mice.

(A) Representative images of Swiss-roll ileal sections from 8-12 week-old mice with the indicated genotypes stained with H&E or immunostained for Lysozyme, CD45, Ki67. Scale bars, 100 μm. **(B)** Graphs showing relative mRNA expression of *Lyz1*, *Defa5*, *Defa-rs10* in the colons of 8-12 week-old mice with the indicated genotypes. **(C)** Graph depicting ileitis histology scores from 8-12 weeks old mice with indicated genotypes. **(D)** Graphs depicting qRT-PCR analysis results for *Il1b*, *Ccl2*, *Cxcl1*. Each dot represents one mouse. $*p < 0.05$, $**p < 0.01$, $***p < 0.005$, $****p < 0.0001$.(One-way ANOVA).

2.3.2 Epithelial XBP1 does not protect from severe ileitis in *Fadd*$^{IEC\text{-}KO}$ mice

IEC-specific deletion of FADD leads to spontaneous ileitis[309]. As the *Xbp1*$^{IEC\text{-}KO}$ *Fadd*$^{IEC\text{-}KO}$ mouse line was already established, it was asked whether IEC-specific ablation of XBP1 could increase the severity of ileitis in *Fadd*$^{IEC\text{-}KO}$ mice. To study this, ileal sections from *Fadd*$^{IEC\text{-}KO}$ and *Xbp1*$^{IEC\text{-}KO}$ *Fadd*$^{IEC\text{-}KO}$ mice were assessed. Examination of H&E-stained sections revealed that *Fadd*$^{IEC\text{-}KO}$ and *Xbp1*$^{IEC\text{-}KO}$ *Fadd*$^{IEC\text{-}KO}$ mice developed spontaneous ileitis which was characterised by the absence of Paneth cell-associated granules, hyperplastic epithelium, increased influx of immune cells into lamina propria, and increased IEC death which leads to epithelial injury with blunted villi (Figure 2-15A). These observations were confirmed by immunostaining the ileal sections with antibodies raised against Lysozyme, Ki-67 and CD45 (Figure 2-15A). Histological ileitis scoring revealed that *Fadd*$^{IEC\text{-}KO}$ and *Xbp1*$^{IEC\text{-}KO}$ *Fadd*$^{IEC\text{-}KO}$ mice had similar levels of ileitis scores (Figure 2-15B). Altogether, these results show that deletion of IEC-specific XBP1 does not aggravate ileitis in *Casp8*$^{IEC\text{-}KO}$ and *Fadd*$^{IEC\text{-}KO}$ mice.

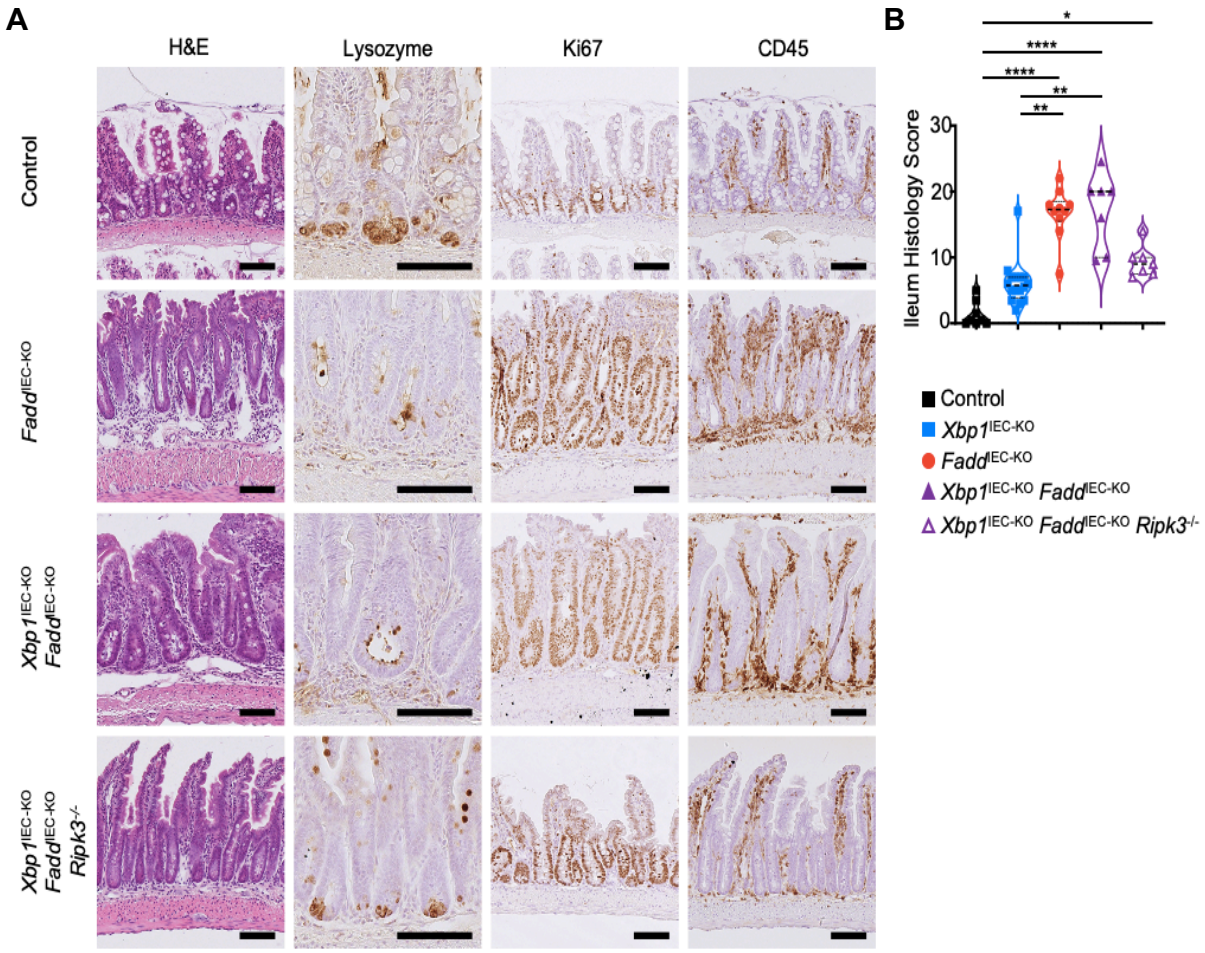

Figure 2-15 Epithelial XBP1 does not play an important role in ileitis in *Fadd*$^{IEC-KO}$ mice.

(A) Representative images of Swiss-roll ileal sections from 8-12 week-old mice with the indicated genotypes stained with H&E or immunostained for Lysozyme, CD45, Ki67. **(B)** Graphs showing ileum histology score from 8-12 weeks old mice with indicated genotypes. Each dot represents one mouse. $*p < 0.05$, $**p < 0.01$, $***p < 0.005$, $****p < 0.0001$.(One-way ANOVA). Scale bars, 100 μm.

2.3.3 IEC-specific XBP1 deficiency leads to Paneth cell impairment and crypt hyperplasia independent of extrinsic apoptosis and necroptosis

Small intestinal sections from *Xbp1*$^{IEC-KO}$ mice were found to have increased numbers of IECs that were positively stained with active caspase-3 (or cleaved caspase-3) and TdT-mediated dUTP nick end labelling (TUNEL, demonstrating the DNA fragmentation[349]). Moreover, Tamoxifen-induced acute XBP1 deletion in IECs leads to increased number of TUNEL$^+$ IECs[323], suggesting epithelial apoptosis contributes to intestinal pathology including Paneth cell impairment in XBP1 deficiency. Meanwhile, the spontaneous ileitis as well as Paneth cell loss in *Casp8*$^{IEC-KO}$ mice is prevented by ablating RIPK3 or

MLKL[307,311], demonstrating that IEC-specific deletion of Casp8 leads to necroptosis-induced ileitis. To address genetically whether extrinsic apoptosis and/or necroptosis plays a role in Paneth cell impairment and crypt hyperplasia in XBP1 deficiency, ileal sections from *Xbp1*$^{IEC\text{-}KO}$ *Casp8*$^{IEC\text{-}KO}$ *Ripk3*$^{-/-}$ and *Xbp1*$^{IEC\text{-}KO}$ *Casp8*$^{IEC\text{-}KO}$ *Mlkl*$^{-/-}$ mice were examined. Ablation of RIPK3 or MLKL prevented death of IECs and suppressed the severity of ileitis in *Xbp1*$^{IEC\text{-}KO}$ *Casp8*$^{IEC\text{-}KO}$ mice to ileitis levels in *Xbp1*$^{IEC\text{-}KO}$ (Figure 2-14A, 2-14C-D). Immunostaining for Lysozyme and Ki67 as well as qRT-PCR gene expression analysis revealed that combined deficiency of Casp8 and RIPK3 or Casp8 and MLKL did not rescue Paneth cell impairment and hyperplastic ilea in *Xbp1*$^{IEC\text{-}KO}$ *Casp8*$^{IEC\text{-}KO}$ mice (Figure 2-14A-B).

Ubiquitous [309] as well as IEC-specific RIPK3 deletion [307] restores Paneth cell loss and strongly suppresses ileitis in *Fadd*$^{IEC\text{-}KO}$ mice. To answer whether combined deletion of FADD and RIPK3 could restore impairment of Paneth cell in *Xbp1*$^{IEC\text{-}KO}$ mice, distal ileal sections from *Xbp1*$^{IEC\text{-}KO}$ *Fadd*$^{IEC\text{-}KO}$ *Ripk3*$^{-/-}$ mice were examined. Histological assessment of H&E-stained sections revealed that RIPK3 deletion strongly suppressed epithelial cell death and inflammation in the small intestines of *Xbp1*$^{IEC\text{-}KO}$ *Fadd*$^{IEC\text{-}KO}$ mice (Figure 2-15). However, *Fadd*$^{IEC\text{-}KO}$ *Ripk3*$^{-/-}$ background failed to rescue the Paneth cell impairment as well as crypt hyperplasia in XBP1 deficiency (Figure 2-15). Taken together, FADD-Casp8-mediated apoptosis and RIPK3-MLKL-dependent necroptosis do not play a role in the Paneth cell impairment and crypt hyperplasia in *Xbp1*$^{IEC\text{-}KO}$ mice.

To check whether impairment in Paneth cells and ileal hyperplasia in *Xbp1*$^{IEC\text{-}KO}$ mice could be mediated by type of cell death independent of FADD-Casp8 and RIPK3-MLKL, ileal sections from *Xbp1*$^{IEC\text{-}KO}$, *Xbp1*$^{IEC\text{-}KO}$ *Casp8*$^{IEC\text{-}KO}$ *Ripk3*$^{-/-}$, *Xbp1*$^{IEC\text{-}KO}$ *Casp8*$^{IEC\text{-}KO}$ *Mlkl*$^{-/-}$ and *Xbp1*$^{IEC\text{-}KO}$ *Fadd*$^{IEC\text{-}KO}$ *Ripk3*$^{-/-}$ mice were immunostained with antibodies against cleaved-Caspase-3 and stained for TUNEL. Strikingly, *Xbp1*$^{IEC\text{-}KO}$ mice did not exhibit increased numbers of cleaved-Caspase-3^{+} or TUNEL^{+} IECs in the ileum compared to control mice (Figure 2-16). Moreover, *Xbp1*$^{IEC\text{-}KO}$ *Casp8*$^{IEC\text{-}KO}$ *Ripk3*$^{-/-}$ and *Xbp1*$^{IEC\text{-}KO}$ *Casp8*$^{IEC\text{-}KO}$ *Mlkl*$^{-/-}$ mice did not show increased numbers of IECs positively stained with cleaved-Caspase-3 or TUNEL in the ileum compared to conrol mice (Figure 2-16). Importantly, IEC-specific RIPK3 ablation strongly suppresses but does not completely prevent IEC death in *Fadd*$^{IEC\text{-}KO}$ mice [307]. In line with this, *Xbp1*$^{IEC\text{-}KO}$ *Fadd*$^{IEC\text{-}KO}$ *Ripk3*$^{-/-}$ mice showed an increased number of CC3^{+} and TUNEL^{+} IECs compared to control mice (Figure 2-16). Taken together, these results show that IEC-specific XBP1 ablation-induced

Paneth cell impairment and ileal hyperplasia are independent of FADD-Casp8-mediated apoptosis and RIPK3-MLKL-dependent necroptosis.

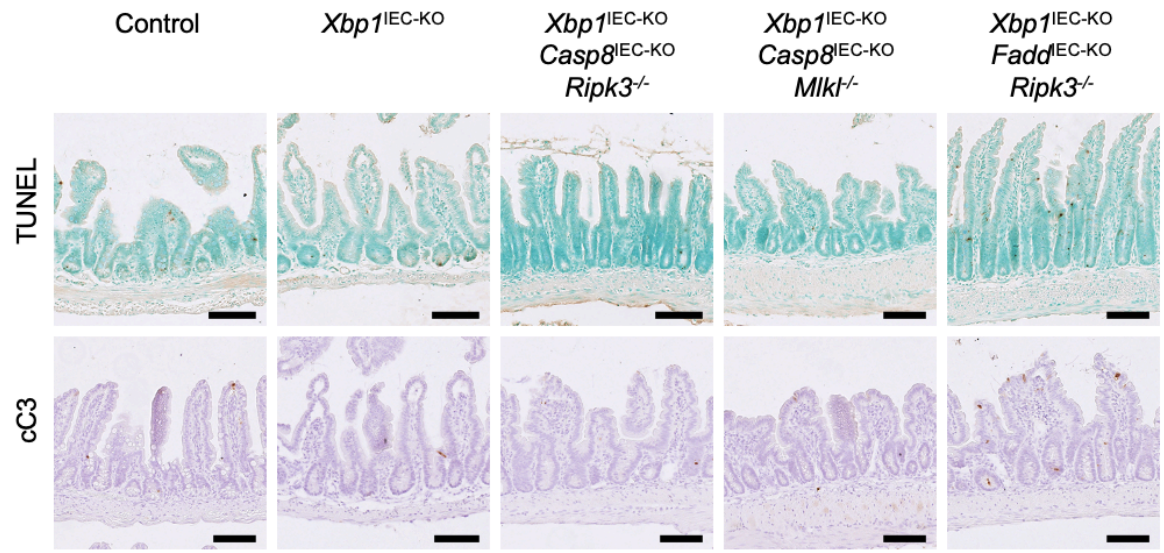

Figure 2-16 Chronic deficiency of XBP1 does not cause an increased number of CC3- and TUNEL-positive IECs in the ileum.

Representative images of Swiss-roll ileal sections from 8-12 week-old mice with the indicated genotypes immunostained for cleaved-Caspase-3 (CC3) or stained for TUNEL. Scale bars, 100 μm.

2.4 The contribution of IEC-specific TNF and TNFR1 to necroptosis-induced intestinal inflammation in *Xbp1*$^{IEC\text{-}KO}$ *Casp8*$^{IEC\text{-}KO}$ mice

2.4.1 Epithelial TNFR1 drives the exacerbated colitis in *Xbp1*$^{IEC\text{-}KO}$ *Casp8*$^{IEC\text{-}KO}$ mice

XBP1 deficient IECs were shown to have increased p65 and IκBα phosphorylation, indicating NF-κB activation in the ilea of *Xbp1*$^{IEC\text{-}KO}$ mice. Thus, increased TNF production from IECs could be the culprit of exaggerated colitis in *Xbp1*$^{IEC\text{-}KO}$ *Casp8*$^{IEC\text{-}KO}$ mice. To address this, IEC-specific TNF was deleted by crossing *Xbp1*$^{IEC\text{-}KO}$ *Casp8*$^{IEC\text{-}KO}$ mice to mice carrying transgenic *Tnf* flanked by two *LoxP* sites[350]. Histopathological assessment of the colon sections from mice lacking XBP1, Casp8 and TNF specifically in IECs (*Xbp1*$^{IEC\text{-}KO}$ *Casp8*$^{IEC\text{-}KO}$ *Tnf*$^{IEC\text{-}KO}$) revealed that these mice developed colitis which

manifested itself by hyperplastic epithelium, increased immune cell infiltration into mucosa and submucosa as well as increased epithelial cell death leading to severe epithelial injury with extensive ulcerations (Figure 2-17). The sections immunostained with Ki-67 and CD45 antibodies confirmed crypt hyperplasia and an influx of immune cells into colon layers, respectively (Figure 2-17). The histopathological scoring revealed that *Xbp1*$^{IEC\text{-}KO}$ *Casp8*$^{IEC\text{-}KO}$ and *Xbp1*$^{IEC\text{-}KO}$ *Casp8*$^{IEC\text{-}KO}$ *Tnf*$^{IEC\text{-}KO}$ mice had similar levels of colitis. Furthermore, around 85% of *Xbp1*$^{IEC\text{-}KO}$ *Casp8*$^{IEC\text{-}KO}$ *Tnf*$^{IEC\text{-}KO}$ mice exhibited ulcers scattered throughout the entire colon, similar to *Xbp1*$^{IEC\text{-}KO}$ *Casp8*$^{IEC\text{-}KO}$ mice (Figure 2-18A-B). Hence, TNF produced by epithelial cells does not play an important role in severe colitis in *Xbp1*$^{IEC\text{-}KO}$ *Casp8*$^{IEC\text{-}KO}$ mice.

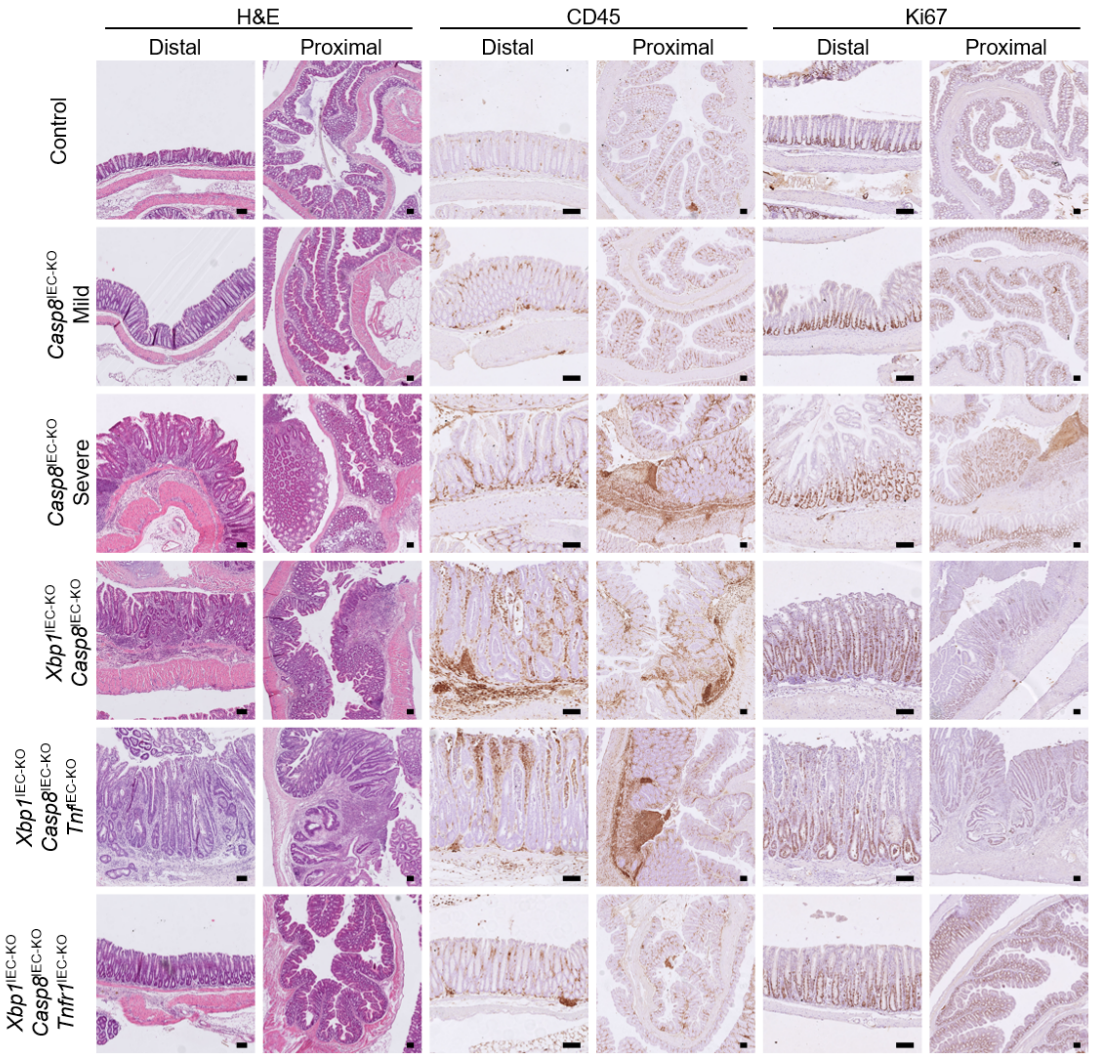

Figure 2-17 IEC-specific TNFR1 but not TNF drives the exacerbation of colitis in *Xbp1*$^{IEC\text{-}KO}$ *Casp8*$^{IEC\text{-}KO}$ mice.

Representative images of Swiss-roll ileal sections from 8-12 week-old mice with the indicated genotypes stained with H&E or immunostained for CD45, Ki67. Scale bars, 100 μm.

The ablation of epithelial-intrinsic TNFR1 completely prevents ulcer formation and strongly diminishes colitis in *Casp8*$^{IEC\text{-}KO}$ as well as in *Fadd*$^{IEC\text{-}KO}$ mice, showing TNFR1 in IECs is one of the major drivers of necroptosis-induced colon inflammation[307]. To address whether XBP1 ablation exaggerates the necroptosis-induced colitis in a TNFR1-driven manner, *Xbp1*$^{IEC\text{-}KO}$ *Casp8*$^{IEC\text{-}KO}$ mice were crossed to mice possessing two *loxP* sites spanning exon 2 to exon 5 in *Tnfr1*[351]. Upon IEC-specific transgenic CRE expression, frameshift mutation occurs at *Tnfr1* leading to XBP1, Casp8 and TNFR1 deficiency in IECs (hereafter, *Xbp1*$^{IEC\text{-}KO}$ *Casp8*$^{IEC\text{-}KO}$ *Tnfr1*$^{IEC\text{-}KO}$). H&E-stained colon sections from *Xbp1*$^{IEC\text{-}}$

KO *Casp8*$^{IEC-KO}$ *Tnfr1*$^{IEC-KO}$ mice revealed that mice lacking XBP1, Casp8 and TFNR1 in intestinal epithelium developed mild colitis which manifested itself by IEC death leading to minimal epithelial erosion and rare ulcerations found between transverse and proximal regions, mild crypt hyperplasia and mild influx of immune cells, infiltrating in mucosa without leading to abundant crypt abscesses (Figure 2-17). Immunostaining for CD45 and Ki-67 confirmed the mucosal inflammation and mild hyperplasia in the colons of *Xbp1*$^{IEC-KO}$ *Casp8*$^{IEC-KO}$ *Tnfr1*$^{IEC-KO}$ mice, respectively (Figure 2-17). Histopathological assessment and RNA sequencing demonstrated that ablation of epithelial-specific TNFR1 strongly suppressed the colitis in *Xbp1*$^{IEC-KO}$ *Casp8*$^{IEC-KO}$ mice (Figure 2-18). Taken together, epithelial-specific TNFR1, independent of TNF produced by IECs, drives the exacerbation of colitis in *Xbp1*$^{IEC-KO}$ *Casp8*$^{IEC-KO}$ mice.

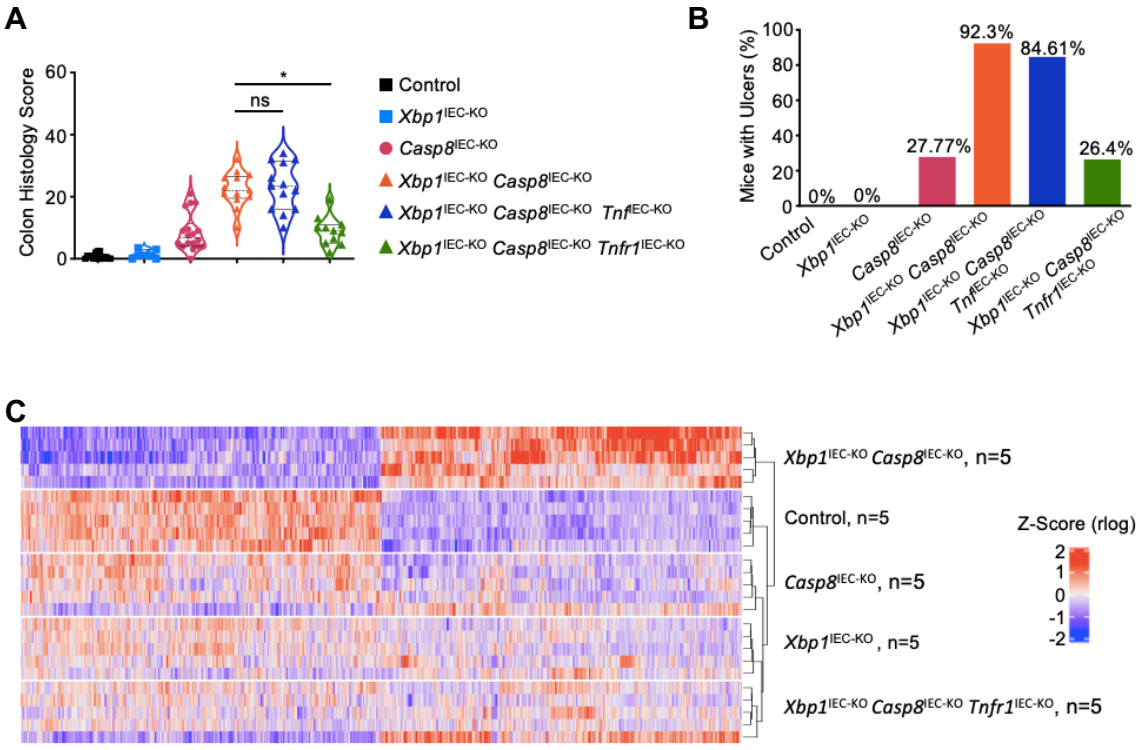

Figure 2-18 Histopathological assessment and RNA sequencing analysis of colons from *Xbp1*$^{IEC-KO}$ *Casp8*$^{IEC-KO}$ *Tnf*$^{IEC-KO}$ and *Xbp1*$^{IEC-KO}$ *Casp8*$^{IEC-KO}$ *Tnfr1*$^{IEC-KO}$ mice.

Graphs showing colon histology score (left), percent of the mice with colonic ulcers (right) from 8-12 weeks old mice with indicated genotypes. Each dot represents one mouse. $*p < 0.05$, $**p < 0.01$, $***p < 0.005$, $****p < 0.0001$.(One-way ANOVA).

2.4.2 Epithelial cell-intrinsic TNF and TNFR1 do not drive necroptosis-induced ileitis in *Xbp1*$^{IEC-KO}$ *Casp8*$^{IEC-KO}$ mice

A report demonstrated that small intestinal organoids isolated from *Casp8*$^{IEC-KO}$ mice showed increased cell death 24 hours after TNF treatment. Moreover, the observed cell death in organoids was blocked when organoids were pre-treated with an inhibitor targeting the kinase activity of RIPK1, claiming TNF induces necroptosis in caspase-8 deficient IECs [308].

However, the genetic evidence was provided by another study that IEC-specific ablation of TNFR1 did not alleviate the severity of ileitis in *Casp8*$^{IEC-KO}$ mice, showing epithelial-specific TNFR1-signalling does not contribute to the ileitis in mice lacking Casp8. Whereas XBP1 does not play an important role in necroptosis-induced ileitis in *Casp8*$^{IEC-KO}$ (Figure 2-14), the contribution of IEC-specific TNF and TNFR1 to ileitis in *Xbp1*$^{IEC-KO}$ *Casp8*$^{IEC-KO}$ mice could be demonstrated as *Xbp1*$^{IEC-KO}$ *Casp8*$^{IEC-KO}$ *Tnf*$^{IEC-KO}$ and *Xbp1*$^{IEC-KO}$ *Casp8*$^{IEC-KO}$ *Tnfr1*$^{IEC-KO}$ mice lines were already established. Examination of H&E-stained ileal sections from *Xbp1*$^{IEC-KO}$ *Casp8*$^{IEC-KO}$ *Tnf*$^{IEC-KO}$ and *Xbp1*$^{IEC-KO}$ *Casp8*$^{IEC-KO}$ *Tnfr1*$^{IEC-KO}$ mice showed that these mice exhibited IEC death without leading to ulceration, absence of Paneth cell-associated granules, crypt hyperplasia and increased immune cell presence in lamina propria, similar to *Casp8*$^{IEC-KO}$ and *Xbp1*$^{IEC-KO}$ *Casp8*$^{IEC-KO}$ mice (Figure 2-19A). These observations were confirmed by immunostaining the ileal sections with Lysozyme, Ki-67 and CD45 antibodies (Figure 2-19A). Side-by-side and blind histopathological scoring demonstrated that *Casp8*$^{IEC-KO}$, *Xbp1*$^{IEC-KO}$ *Casp8*$^{IEC-KO}$, *Xbp1*$^{IEC-KO}$ *Casp8*$^{IEC-KO}$ *Tnf*$^{IEC-KO}$ and *Xbp1*$^{IEC-KO}$ *Casp8*$^{IEC-KO}$ *Tnfr1*$^{IEC-KO}$ mice have similar levels of ileitis (Figure 2-19B). All in all, these genetic results show TNF and TNFR1 in IECs do not play a role in small intestinal inflammation of *Xbp1*$^{IEC-KO}$ *Casp8*$^{IEC-KO}$ mice.

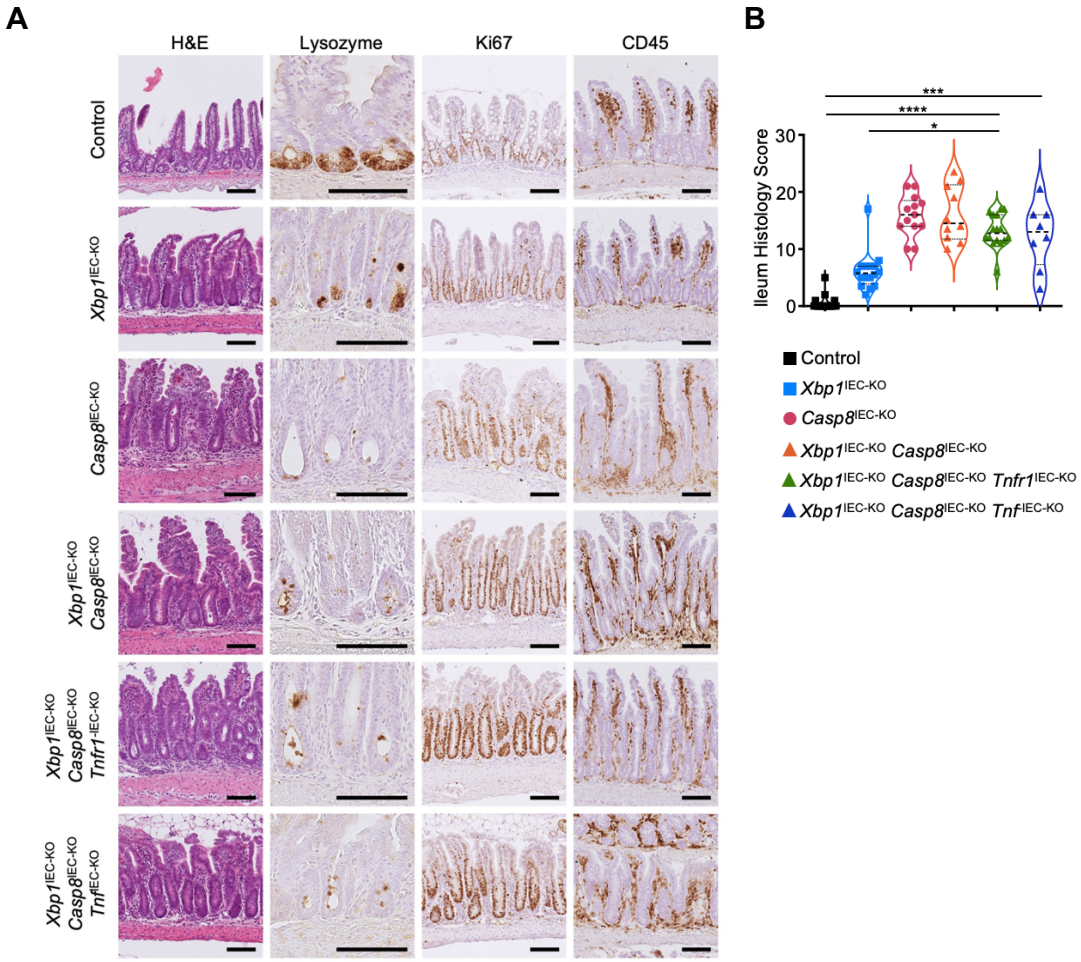

Figure 2-19 IEC-Specific TNF and TNFR1 do not contribute to ileitis in *Xbp1*$^{IEC-KO}$ *Casp8*$^{IEC-KO}$ mice.

(A) Representative images of Swiss-roll ileal sections from 8-12 week-old mice with the indicated genotypes stained with H&E or immunostained for Lysozyme, CD45, Ki67. **(B)** Graphs showing ileum histology score from 8-12 weeks old mice with indicated genotypes. Each dot represents one mouse. ∗p < 0.05, ∗∗p < 0.01, ∗∗∗p < 0.005, ∗∗∗∗p < 0.0001.(One-way ANOVA). Scale bars, 100 µm.

2.5 Epithelial-specific XBP1 is required for the formation of the functional mucus layer in the colon

2.5.1 MUC2 is strongly reduced in the colons of *Xbp1*$^{IEC-KO}$ mice

The results of the genetic mouse model in this thesis prompted a consideration that physiological and/or anatomical features of the large intestine could be the culprit of exaggerated necroptosis-induced colitis upon XBP1 deletion in *Casp8*$^{IEC-KO}$ and *Fadd*$^{IEC-KO}$ mice. Examination of RNA sequencing analysis revealed that *Mucin-2 (Muc2)* was the

only robustly downregulated gene in the colons of *Xbp1*$^{IEC\text{-}KO}$ mice compared to controls (Figure 2-20A). qRT-PCR analysis confirmed that *Muc2* expression was reduced in the colons of *Xbp1*$^{IEC\text{-}KO}$ mice (Figure 2-20B).

MUC2 is the most abundantly secreted mucin in the intestine[352,353]. *Muc2*$^{-/-}$ mice lack the mucus layer and fail to separate luminal bacteria from the colonocytes, showing that MUC2 is the indispensable backbone of the mucus layer in the colon[244]. Furthermore, MUC2-deficient mice develop spontaneous colitis [248] as well as age-progressive colorectal cancer[354]. It was demonstrated that the mucus layer exists in the small intestine, however, it is not stratified and does not provide a clear separation of luminal bacteria from small intestinal epithelium [246,355]. It was postulated that diminished *Muc2* expression could lead to a complete or partial loss of mucus layer in the colons of *Xbp1*$^{IEC\text{-}KO}$ mice, causing luminal bacteria to come in contact with colonic IECs and contributing tod the deterioration of colitis in *Casp8*$^{IEC\text{-}KO}$ and *Fadd*$^{IEC\text{-}KO}$ mice.

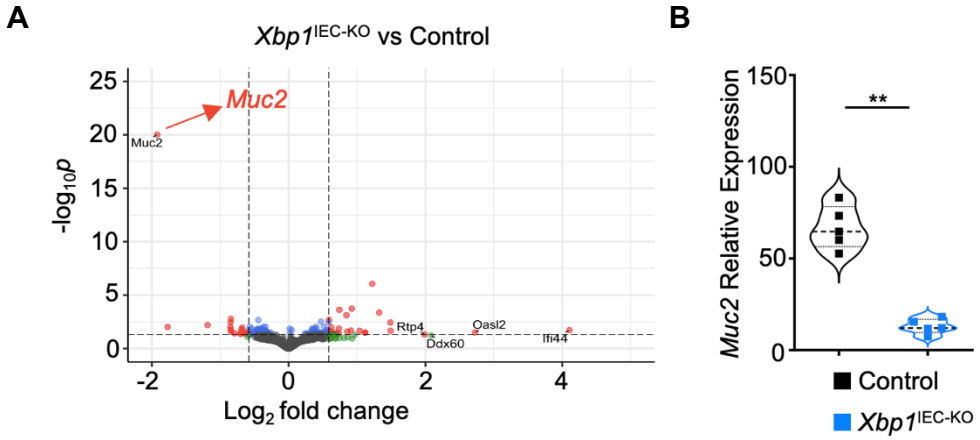

Figure 2-20 Ablation of XBP1 in IECs causes diminished *Muc2* expression in the colon.

(A) Volcano plot showing 3'mRNA sequencing analysis differentially regulated genes in the colons of *Xbp1*$^{IEC\text{-}KO}$ mice compared to control mice. Grey circles: genes are not significant; light green circles: genes with Log2 Fold Change ≥1.5 or ≤1.5; light blue circles: genes with *p* value of ≤0.05; light red circles: genes with Log2 Fold Change ≥1.5 or ≤1.5 and *p* value of ≤0.05. 5 mice per mouse line were analysed. **(B)** Violin box graph depicting qRT-PCR analysis of *Mucin2* gene expression in the colons of *Xbp1*$^{IEC\text{-}KO}$ and control mice. *Tbp* was used as a housekeeping gene to calculate the relative expression of *Muc2*. $2^{-\Delta CT}$ method was performed. Each dot represents one mouse. ns: not significant, $^{**}p < 0.01$.

The Production of MUC2 is regulated at different stages of its synthesis. Therefore, RNA and protein expression of the *Mucin2* gene could show alterations [202]. To check whether

MUC2 production is reduced upon IEC-specific XBP1 ablation, colon sections from *Xbp1*$^{IEC-KO}$ and control mice were immunostained with antibodies that are specific to MUC2. Consistent with the downregulation of *Muc2* mRNA expression, immunohistochemistry results revealed that MUC2 expression was strongly diminished in the distal colons of *Xbp1*$^{IEC-KO}$ mice compared to control mice (Figure 2-21). To further validate this result, Alcian Blue followed by PAS staining (Alcian Blue-PAS) was employed. Alcian Blue-PAS stains mucin-filled Goblet cell-associated granulae, thereby visualising mucin production[244]. Performing Alcian Blue-PAS staining on colon sections from *Xbp1*$^{IEC-KO}$ and control mice demonstrated that XBP1 ablation led to a robust reduction in mucin production. Taken together, these results demonstrate that IEC-intrinsic XBP1 is indispensable for MUC2 and mucin production in the colon.

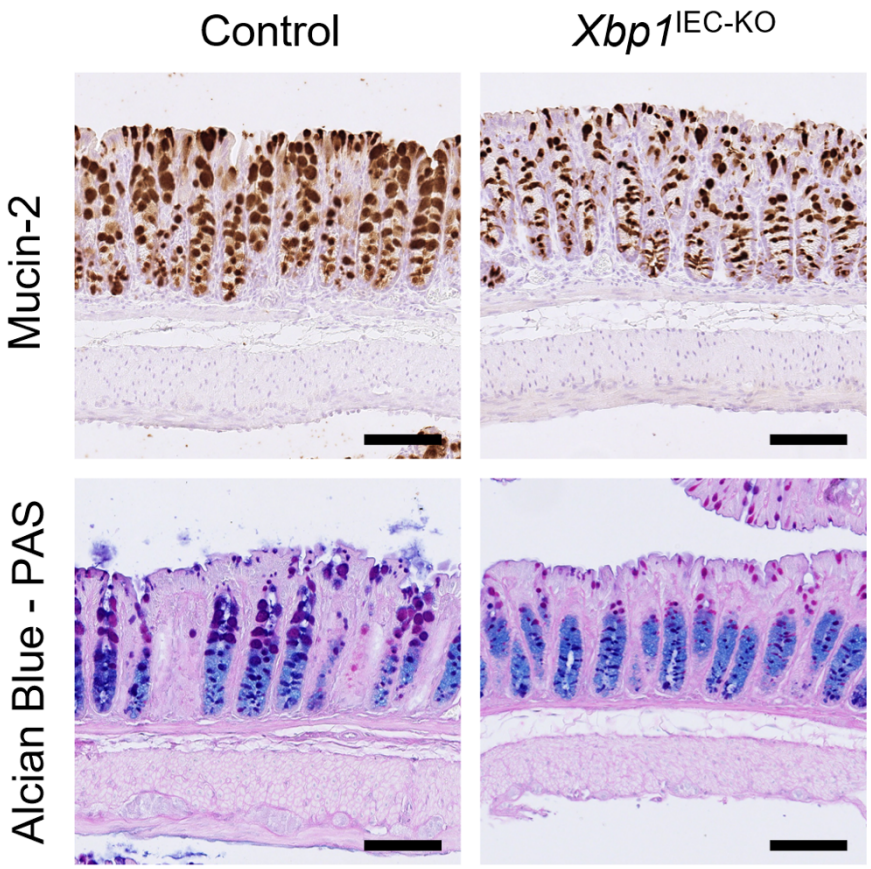

Figure 2-21 Epithelial XBP1 regulates the production of MUC2 in the colon.

Representative images of Swiss-roll colon sections from 8-12 week-old mice with the indicated genotypes immunostained for Mucin-2 or stained with Alcian Blue-PAS. Scale bar, 100μm.

2.5.2 XBP1 deficiency impairs the inner mucus layer in the colon

Mucins are hydrophilic, rendering the mucus layer to shrink upon utilization of fixatives dissolved in water such as PFA. Therefore, the mucus layer in the colon that are fixed in water-based fixatives cannot be properly visualised[356]. To visualise the mucus layers, a non-water-based fixative (Carnoy's fixative) was employed. Moreover, the mucus layer can only be visualised when part of a colon containing faecal material is fixed and processed [356]. To investigate whether *Xbp1*$^{IEC\text{-}KO}$ mice have disrupted mucus layers, distal colon segments containing faecal material from *Xbp1*$^{IEC\text{-}KO}$ and WT mice were collected, fixed in Carnoy's fixative and stained with Alcian Blue-PAS. Results revealed that epithelium and faecal material were separated by, a light purple-coloured, thick mucus layer in the colons of control mice (Figure 2-22A). However, the thicknesses of the mucus layer in the colons of *Xbp1*$^{IEC\text{-}KO}$ mice were severely reduced (Figure 2-22A, middle) and in certain areas, the mucus layers do not exist at all (Figure 2-22A, right). To uniformly assess the mucus barrier impairment in *Xbp1*$^{IEC\text{-}KO}$ mice, the mucus area of each mouse was calculated and divided by the periphery of its lumen. Indeed, calculations revealed that robust reduction in the overall thickness of the mucus layer in the colons of *Xbp1*$^{IEC\text{-}KO}$ mice (Figure 2-22B).

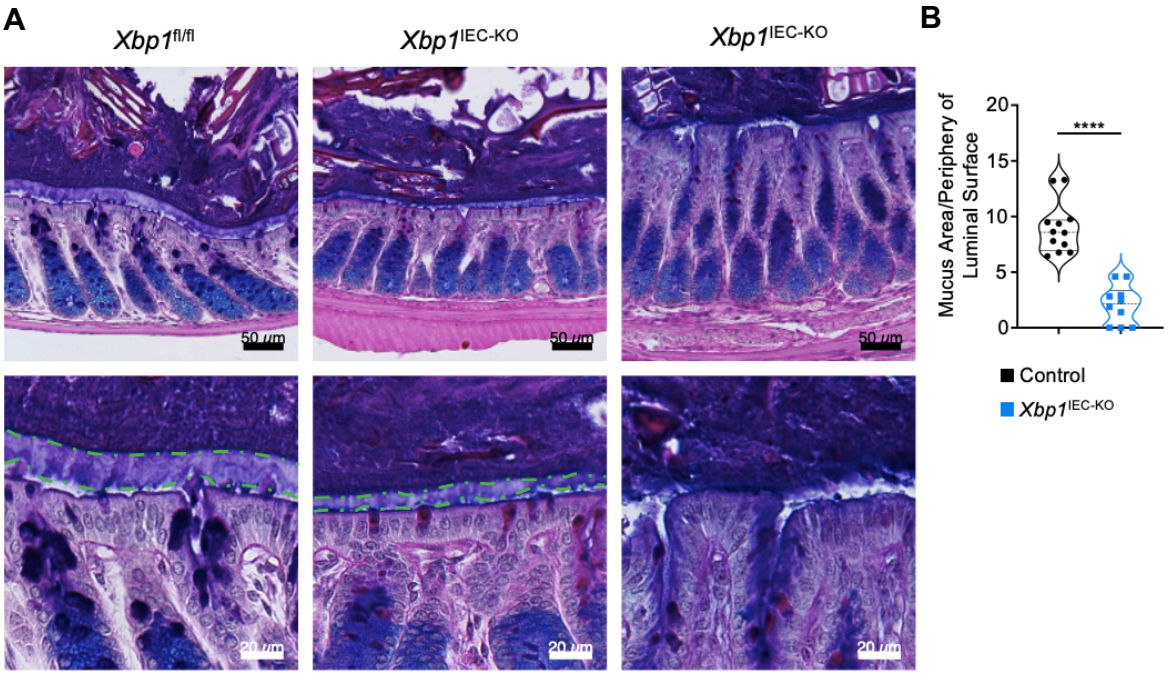

Figure 2-22 *Xbp1*$^{IEC-KO}$ mice have impaired inner mucus layer in the colon.

(A) Representative images of Alcian Blue-PAS stained distal colon tissues fixed in Carnoy's fixed from 11-week-old mice with indicated genotypes. The representative images stated as *Xbp1*$^{IEC-KO}$ (middle and right) are from the same mouse. **(B)** Quantification of mucus layers is shown in (A). The inner mucus layers were labelled with green dashed lines. Each dot represents one mouse. $^{****}p < 0.0001$. Each corresponding scale bar is indicated in the pictures.

The inner mucus layer forms a barrier between luminal bacteria and colonic epithelium[244]. Thus, an improperly formed colonic mucus layer in *Xbp1*$^{IEC-KO}$ mice is expected to show the failed separation of luminal bacteria from the epithelium. To uncover this, fluorescence *in situ* hybridization (FISH) by using a DNA probe, which is specific for 16s ribosomal RNA of eubacteria (EUB338)[244], was performed. To visualise the mucus layer, FISH staining was followed by immunofluorescence (IF) using lectin from *Ulex europaeus* (UEA-I), specifically binds to α-linked fucose residues on glycoproteins[357]. Therefore, combining FISH and IF allowed the visualization of luminal bacteria and mucus layer, respectively. Results showed the existence of thick mucus layers, which separated the luminal bacteria from the epithelium in the colons of control mice. In contrast, luminal bacteria permeated into the compromised mucus layer and came in contact with the apical regions of colonic epithelium in *Xbp1*$^{IEC-KO}$ mice (Figure 2-23).

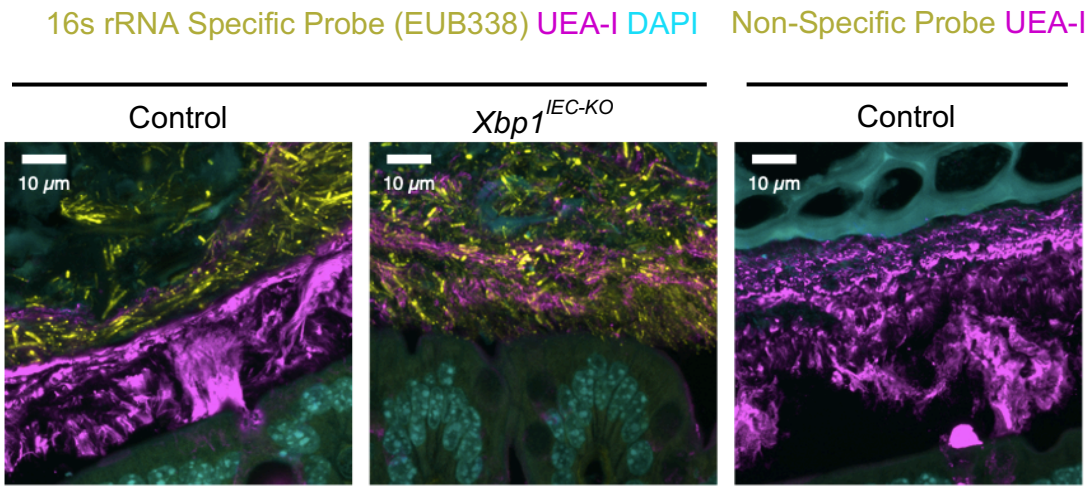

Figure 2-23 Luminal bacteria are not separated from the colonic epithelial cells with XBP1 deficiency.

Representative images of Carnoy's-fixed colon sections from 11-week-old mice with indicated genotypes stained with bacterial 16S rRNA *in situ* hybridization probe EUB338 (yellow) or non-specific control hybridization probe. Mucus was stained with UEA-I (purple), and nuclei were stained with DAPI (Aqua). Scale bars are indicated on pictures.

Whereas MUC2 is the major gel-forming mucin in the intestinal tract, other mucins, or mucus-associated proteins such as MUC12[358], ZG16[359] and TFF3[251] are produced and secreted by Goblet cells as well. To investigate whether deletion of XBP1 in IECs could lead to a reduction in the expression of other mucins and mucus-associated genes, *Zg16* and *Tff3* mRNA expression were analysed from colon tissues of *Xbp1*$^{IEC\text{-}KO}$ and control mice. The results revealed that neither *Zg16* nor *Tff3* expression was reduced in the colons of *Xbp1*$^{IEC\text{-}KO}$ mice compared to control mice (Figure 2-24A). In contrast, immunostaining the colon sections from *Xbp1*$^{IEC\text{-}KO}$ and control mice with the antibodies recognizing ZG16 protein demonstrated that the production of ZG16 was robustly reduced in the colons of *Xbp1*$^{IEC\text{-}KO}$ mice compared to control mice (Figure 2-24B). Taken together, these results demonstrate that IEC-specific XBP1 is essential for the mucus layer formation and separation of luminal bacteria from the colonic epithelium.

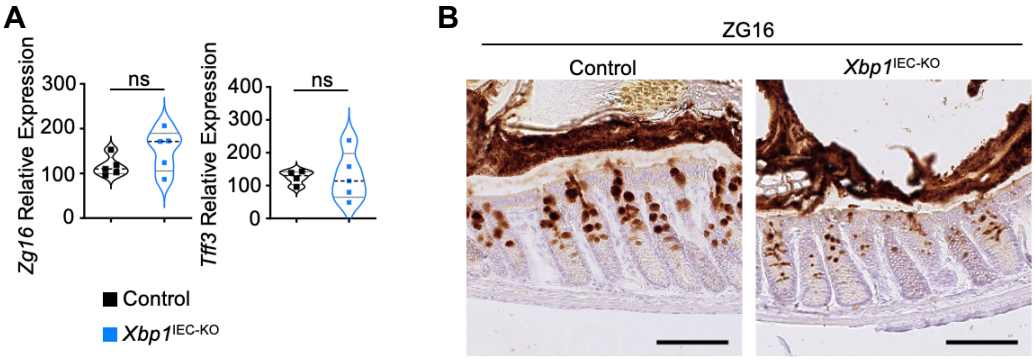

Figure 2-24 ZG16 production is reduced in the colons of *Xbp1*$^{IEC-KO}$ mice.

(A) Graphs showing relative mRNA expression of *Zg16* and *Tff3* in the colons of *Xbp1*$^{IEC-KO}$ and control mice. *Tbp* was used as a housekeeping gene to calculate the relative expression of genes of interest. $2^{-\Delta CT}$ method was performed. **(B)** Representative images of Carnoy's-fixed colon sections from 11-week-old mice with indicated genotypes immunostained for ZG16. Scale bars, 100μm. Each dot represents one mouse. ns: not significant.

2.5.3 Epithelial-specific XBP1 but not Casp8 regulates mucin levels in the colon

The reduction in MUC2 expression was reported in the colons of mice with IEC-specific ablation of Casp8 [312]. Therefore, this could challenge the hypothesis above explaining how additional deletion of XBP1 exaggerated the severity of colitis in *Casp8*$^{IEC-KO}$ mice. To check whether *Casp8*$^{IEC-KO}$ mice had reduced MUC2, total RNA isolated from distal colons of *Casp8*$^{IEC-KO}$ mice were analysed for *Muc2* expression. qRT-PCR analysis revealed that the colons from *Casp8*$^{IEC-KO}$ mice did not have reduced expression of *Muc2* compared to control mice. In stark contrast, *Xbp1*$^{IEC-KO}$ *Casp8*$^{IEC-KO}$ mice had strongly downregulated *Muc2* expression in the colon (Figure 2-25A).

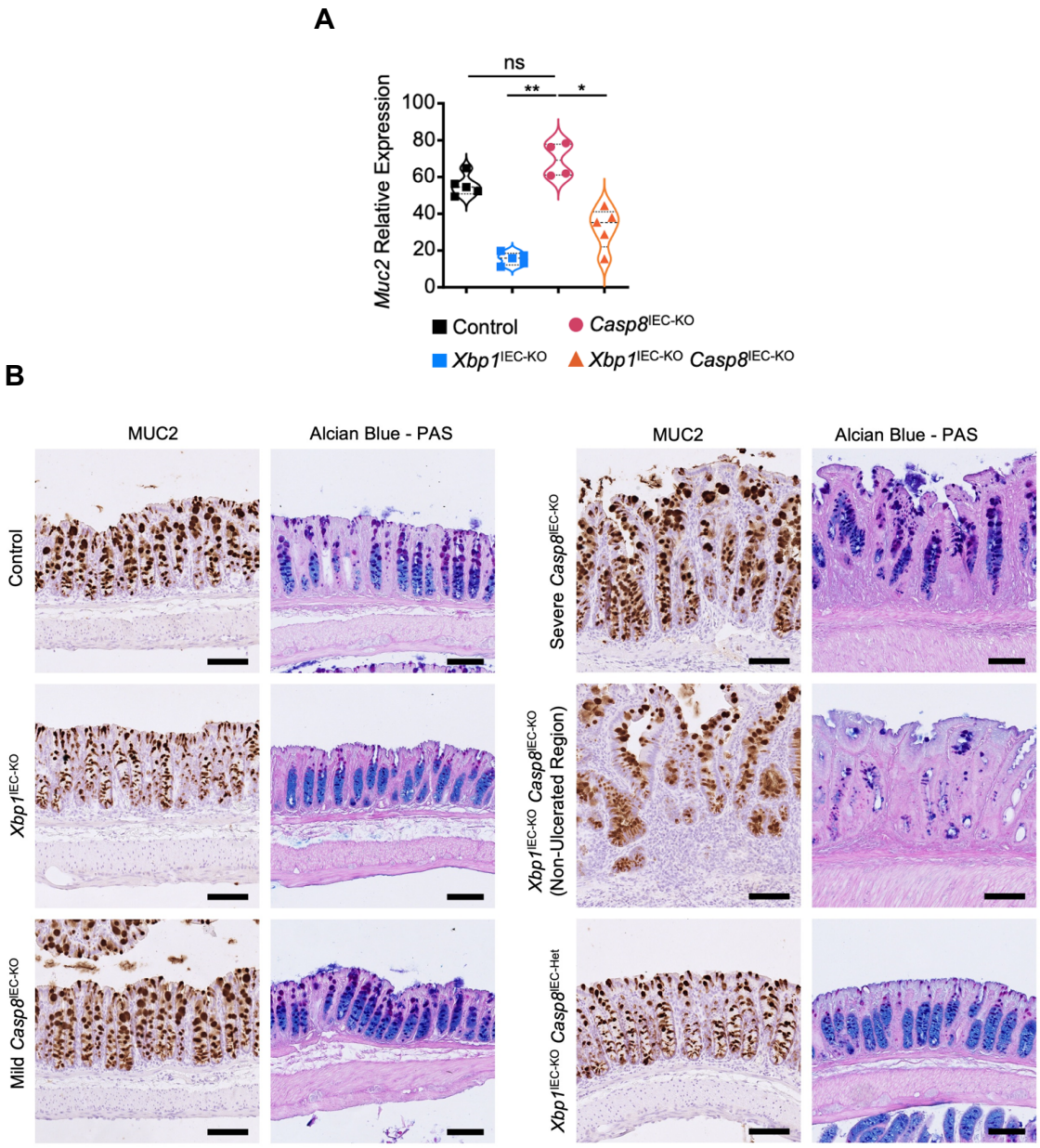

Figure 2-25 Deficiency of XBP1 but not caspase-8 reduces MUC2 expression in the colonic epithelium.

(A) Violin graph showing relative mRNA expression of *Muc2* measured by qRT-PCR analysis in the colons of *Xbp1*$^{IEC\text{-}KO}$ and control mice. *Tbp* was used as a housekeeping gene to calculate the relative expression of genes of interest. $2^{-\Delta CT}$ method was performed. **(B)** Representative images of Swiss-roll colon sections from 8-12 week-old mice with the indicated genotypes immunostained for Mucin-2 or stained with Alcian Blue-PAS. Each dot represents one mouse. ns: not significant, $^{*}p < 0.05$, $^{**}p < 0.01$. Scale bar, 100μm.

To assess whether MUC2 expression in the colon could be impaired by deletion of Casp8 in IECs, colon sections from control, *Xbp1*$^{IEC\text{-}KO}$, *Casp8*$^{IEC\text{-}KO}$, *Xbp1*$^{IEC\text{-}KO}$ *Casp8*$^{IEC\text{-}KO}$ and *Xbp1*$^{IEC\text{-}KO}$ *Casp8*$^{IEC\text{-}Het}$ were stained with Alcian blue-PAS and immunostained with antibodies raised against MUC2. Results demonstrated that *Xbp1*$^{IEC\text{-}KO}$, *Xbp1*$^{IEC\text{-}KO}$

Casp8$^{IEC\text{-}KO}$, *Xbp1*$^{IEC\text{-}KO}$ *Casp8*$^{IEC\text{-}Het}$ but not *Casp8*$^{IEC\text{-}KO}$ mice showed diminished mucin and MUC2 expression compared to control mice (Figure 2-25B). Therefore, these data show that the absence of XBP1 but not caspase-8 in IECs leads to reduced mucin expression in the colons of *Xbp1*$^{IEC\text{-}KO}$ *Casp8*$^{IEC\text{-}KO}$ mice.

2.5.4 XBP1 suppresses the translocation of luminal bacteria into colonic sublayers and prevents systemic inflammation in *Casp8*$^{IEC\text{-}KO}$ mice

It was postulated that XBP1-deficiency-induced impaired mucus layer accompanied by the loss of intestinal epithelial integrity, caused by caspase-8 ablation, could allow penetration of bacteria into the layers of the colonic epithelium in *Xbp1*$^{IEC\text{-}KO}$ *Casp8*$^{IEC\text{-}KO}$ mice. To show the translocation of bacteria from the lumen into the colon layers in mice with XBP1 and caspase-8 deficiency, colon sections from *Xbp1*$^{IEC\text{-}KO}$, *Casp8*$^{IEC\text{-}KO}$ and *Xbp1*$^{IEC\text{-}KO}$ *Casp8*$^{IEC\text{-}KO}$ mice were incubated with fluorophore-conjugated DNA probes specific to bacterial ribosomal RNA (16s rRNA). Whereas *Xbp1*$^{IEC\text{-}KO}$ mice had impaired mucus layer (Figures 2-23 and 2-24), FISH results did not reveal the presence of bacteria within the colonic sublayers of *Xbp1*$^{IEC\text{-}KO}$ mice (Figure 2-26A). Importantly, FISH performed on the colon sections from *Casp8*$^{IEC\text{-}KO}$ mice revealed that some mice showed the presence of bacteria in the sublayers of the colon, in line with the expected consequence of necroptosis-induced epithelial barrier dysfunction (Figure 2-26A). Strikingly, almost all *Xbp1*$^{IEC\text{-}KO}$ *Casp8*$^{IEC\text{-}KO}$ mice showed translocation of luminal bacteria into sublayers of the colon (Figure 2-26A). To objectively assess the degree of bacterial translocation into the colon layers and compare it between mouse lines, the numbers of mice with bacterial presence in the submucosa were counted. Whereas 37.5% of *Casp8*$^{IEC\text{-}KO}$ mice (9 out of 24) exhibited bacterial presence in the submucosa, 10 out of 11 *Xbp1*$^{IEC\text{-}KO}$ *Casp8*$^{IEC\text{-}KO}$ mice (≈91%) harboured bacteria in their submucosa layer (Figure 2-26B), providing critical evidence that XBP1 alleviates penetration of luminal bacteria into the sublayers of the colon.

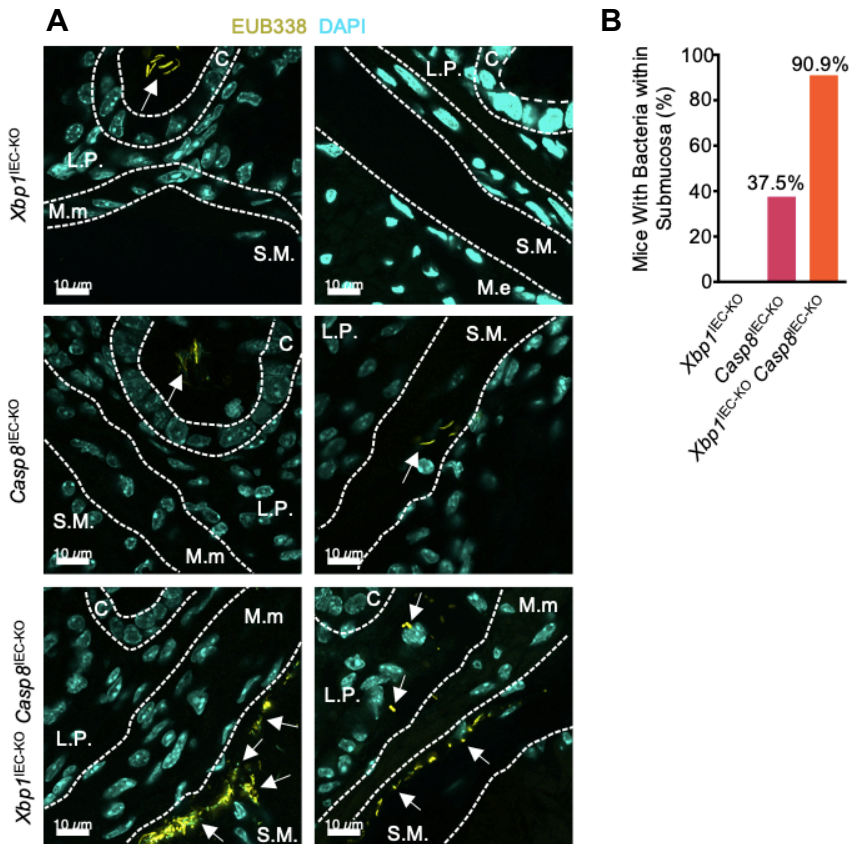

Figure 2-26 Epithelial-specific XBP1 restricts bacterial translocation into colonic submucosa in *Casp8*$^{IEC-KO}$ mice.

(A) Representative images of Swiss-roll colon sections from 8-12 week-old mice with the indicated genotypes stained with 16S rRNA *in situ* hybridization probe EUB338 (Yellow). Nuclei were stained with DAPI (Aqua). White arrows indicate bacteria. Each colonic structure and layer were labelled with white dashed lines. C: Crypt, L.P: Lamina propria, M.m: Muscularis mucosae, S.M: Submucosa, M.e: Muscularis externa. **(B)** Bar graph depicting the percentage of *Xbp1*$^{IEC-KO}$, *Casp8*$^{IEC-KO}$ and *Xbp1*$^{IEC-KO}$ *Casp8*$^{IEC-KO}$ mice with EUB338 signal in Submucosa. Scale bars are indicated in the pictures.

Increased bacterial translocation into the subepithelial layers of the colon could prompt an immune response at the systemic level. Therefore, it is sought to check the indicators of systemic inflammation in *Xbp1*$^{IEC-KO}$ *Casp8*$^{IEC-KO}$ mice. *Xbp1*$^{IEC-KO}$ *Casp8*$^{IEC-KO}$ mice had elevated spleen weight compared to *Casp8*$^{IEC-KO}$ (Figure 2-27). Importantly, *Xbp1*$^{IEC-KO}$, *Casp8*$^{IEC-KO}$ and *Xbp1*$^{IEC-KO}$ *Casp8*$^{IEC-Het}$ mice did not have significantly increased spleen weight compared to controls. Consistently, peripheral blood analysis revealed that *Xbp1*$^{IEC-KO}$ *Casp8*$^{IEC-KO}$ mice showed increased numbers of circulating granulocytes and monocytes compared to *Casp8*$^{IEC-KO}$, *Xbp1*$^{IEC-KO}$ *Casp8*$^{IEC-Het}$, *Xbp1*$^{IEC-KO}$ and control mice (Figure 2-27). Taken together, these data show that XBP1 suppresses the translocation

of luminal bacteria into sublayers of the colon and prevents systemic inflammation in *Casp8*$^{IEC-KO}$ mice.

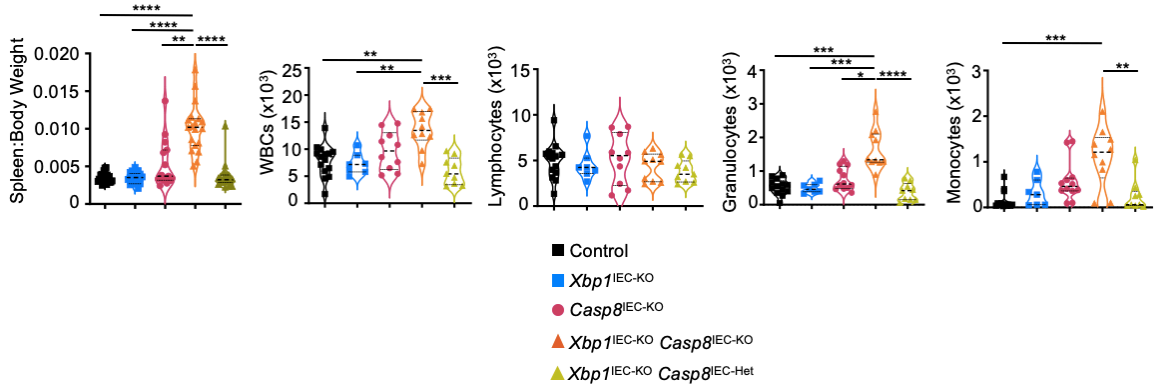

Figure 2-27 *Xbp1*$^{IEC-KO}$ *Caps8*$^{IEC-KO}$ mice exhibit markers of systemic inflammation.

Violin graphs showing spleen to body weight ratio and peripheral blood analysis of 8-12 week-old mice with indicated genotypes. Each dot represents one mouse. ns: not significant, *p < 0.05, **p < 0.01, ***p < 0.005, ****p < 0.0001.

2.6 XBP1 deficiency leads to the dysfunctional mucus layer independent of extrinsic apoptosis, necroptosis and TNFR1 signalling in IECs

2.6.1 Combined inhibition of extrinsic apoptosis and necroptosis do not restore the mucus barrier impairment

Goblet cells are the only source of mucin production and secretion in the colon [202,352,353]. Therefore, it was hypothesized that the absence of XBP1 in IECs could induce Goblet cell death, indirectly causing the compromised mucus layer in the colon. To check the presence of caspase-3-mediated cell death, colon sections from *Xbp1*$^{IEC-KO}$ and control mice were immunostained for active/cleaved-caspase-3 (CC3). Interestingly, results did not reveal an increased number of CC3^{+} IECs in *Xbp1*$^{IEC-KO}$ mice compared to control mice (Figure 2-28). Chromosomal DNA can be fragmented in various cell death modalities, and the presence of DNA fragmentation can be used as a broad marker for cell death[118]. To this end, TUNEL staining was performed on the colon sections from WT and *Xbp1*$^{IEC-KO}$

mice. Consistently, *Xbp1*$^{IEC-KO}$ mice did not have increased numbers of TUNEL^{+} IECs in the colon compared to controls (Figure 2-28), suggesting that chronic XBP1 deficiency does not lead to Goblet cell apoptosis.

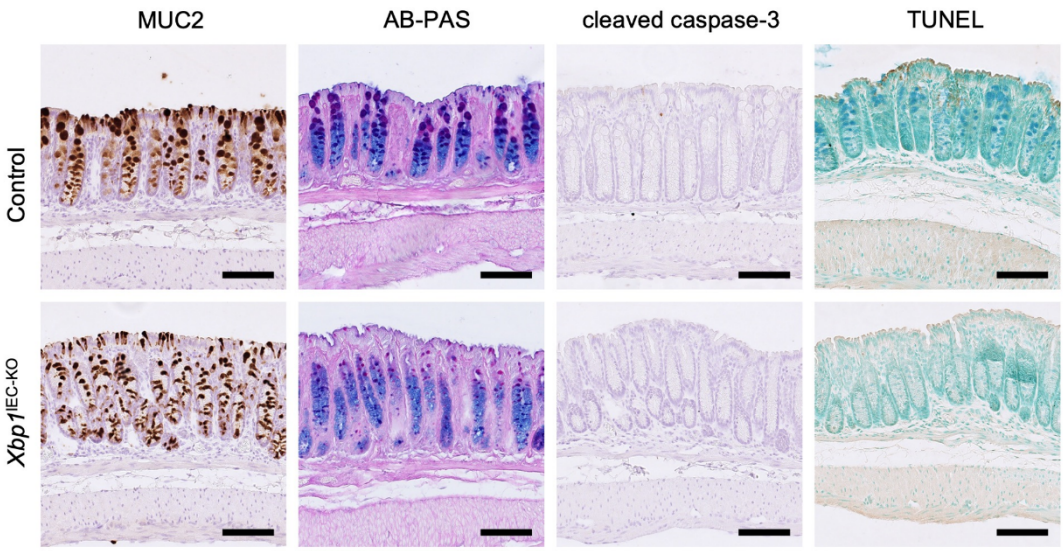

Figure 2-28 XBP1 deficiency does not lead to increased caspase-3- and TUNEL-positive IECs in the colon compared to control mice.

Representative images of Swiss-roll colon sections from 8-12 week-old mice with the indicated genotypes stained with Alcian Blue-Pas or immunostained for MUC2, cleaved-caspase-3 and TUNEL. Scale bars, 100μm.

To uncover whether XBP1 deficiency induces caspase-8-mediated death and/or RIPK3-MLKL-dependent necroptosis of Goblet cells, colon sections from *Xbp1*$^{IEC-KO}$ *Casp8*$^{IEC-KO}$ *Ripk3*$^{-/-}$ and *Xbp1*$^{IEC-KO}$ *Casp8*$^{IEC-KO}$ *Mlkl*$^{-/-}$ mice were stained with Alcian blue-PAS and immunostained for MUC2. Interestingly, results revealed that *Xbp1*$^{IEC-KO}$ *Casp8*$^{IEC-KO}$ *Ripk3*$^{-/-}$ as well as *Xbp1*$^{IEC-KO}$ *Casp8*$^{IEC-KO}$ *Mlkl*$^{-/-}$ mice had reduced mucin expression in the colon (Figure 2-29A). Consistent with this, staining colon segments containing faecal material with Alcian blue-PAS demonstrated that *Xbp1*$^{IEC-KO}$ *Casp8*$^{IEC-KO}$ *Ripk3*$^{-/-}$ and *Xbp1*$^{IEC-KO}$ *Casp8*$^{IEC-KO}$ *Mlkl*$^{-/-}$ had impaired mucus layer (Figure 2-29B), similar to *Xbp1*$^{IEC-KO}$ mice (Figure 2-29C).

Of note, it was reported that the content of the microbiota, which varies between different mouse colonies fed with the same food within the same facility, could alter the permeability as well as the thickness of the mucus layer[360]. However, neither *Xbp1*$^{IEC-KO}$ *Casp8*$^{IEC-KO}$ *Ripk3*$^{-/-}$ nor *Xbp1*$^{IEC-KO}$ *Casp8*$^{IEC-KO}$ *Mlkl*$^{-/-}$ mice from different cages had immense variability in mucus layer thicknesses. Nonetheless, representative pictures of Alcian Blue-

PAS and bacterial FISH staining were selected from cohoused littermates of each corresponding experimental mouse line (Figure 2-29B).

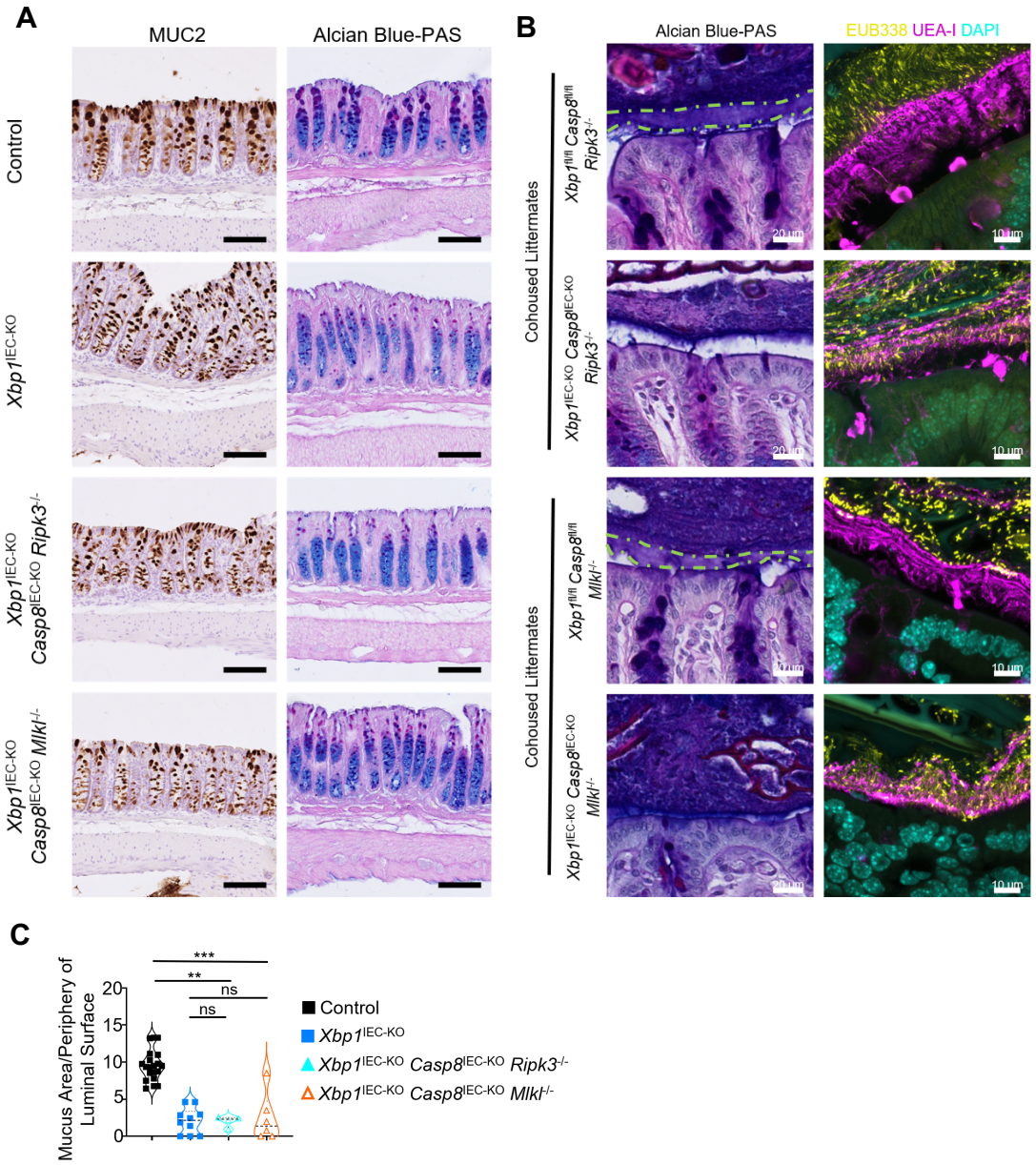

Figure 2-29 Extrinsic apoptosis and necroptosis do not contribute to the formation of the impaired mucus barrier in the colons of *Xbp1*$^{IEC-KO}$ mice.

(A) Representative images of Swiss-roll colon sections from 8-12 week-old mice with the indicated genotypes immunostained for Mucin-2 or stained with Alcian Blue-PAS. **(B)** Representative images of Carnoy's-fixed colon sections from 11-week-old mice with indicated genotypes stained with Alcian Blue-PAS or bacterial 16S rRNA *in situ* hybridization probe EUB338 (yellow) followed by immunostaining with UEA-I (purple). **(C)** Violin graph showing the quantification of mucus layers in (B). The inner mucus layers were labelled with green dashed lines. Each dot represents one mouse. ns: not significant, $^{**}p < 0.01$, $^{***}p < 0.005$. Scale bars in (A), 100μm. Scale bars in (B) are indicated on the pictures.

To uncover whether IEC-specific XBP1 deletion could induce death of Goblet cells independent of FADD-caspase-8 and RIPK3-MLKL, colon sections from *Xbp1*$^{IEC\text{-}KO}$ *Casp8*$^{IEC\text{-}KO}$ *Ripk3*$^{-/-}$ and *Xbp1*$^{IEC\text{-}KO}$ *Casp8*$^{IEC\text{-}KO}$ *Mlkl*$^{-/-}$ mice were analysed for the presence of IEC death. Immunostaining with antibodies raised against cleaved-caspase-3 and performing TUNEL staining revealed that *Xbp1*$^{IEC\text{-}KO}$ *Casp8*$^{IEC\text{-}KO}$ *Ripk3*$^{-/-}$ and *Xbp1*$^{IEC\text{-}KO}$ *Casp8*$^{IEC\text{-}KO}$ *Mlkl*$^{-/-}$ mice did not have increased numbers of CC3^{+} and TUNEL^{+} IECs (Figure 2-30). Taken together, these results show that XBP1 deficiency causes the dysfunctional mucus layer in the colon independent of extrinsic apoptosis and necroptosis.

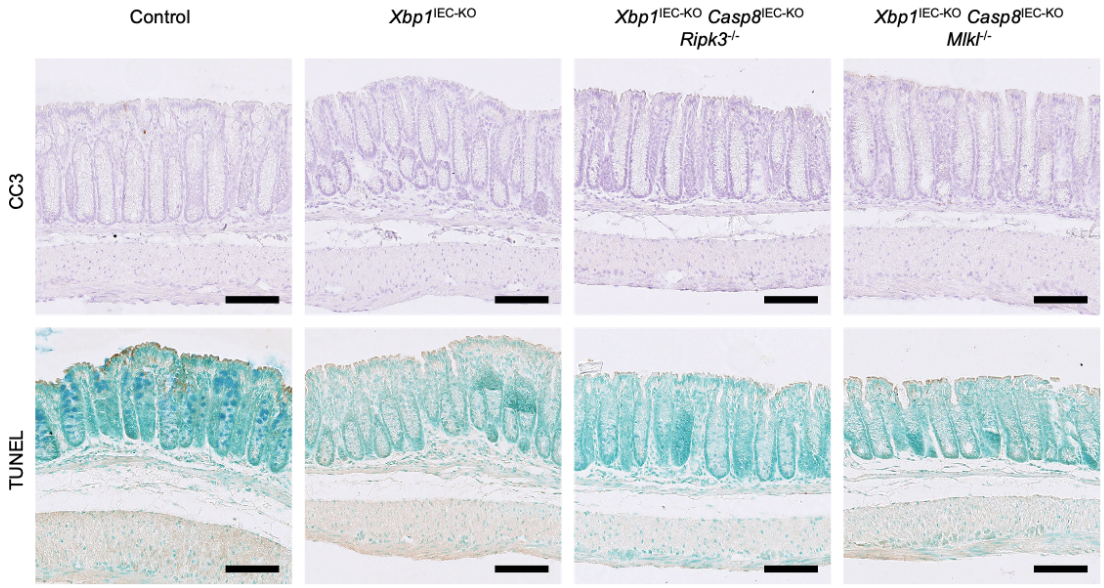

Figure 2-30 *Xbp1*$^{IEC\text{-}KO}$ *Casp8*$^{IEC\text{-}KO}$ *Ripk3*$^{-/-}$ and *Xbp1*$^{IEC\text{-}KO}$ *Casp8*$^{IEC\text{-}KO}$ *Mlkl*$^{-/-}$ mice do not show increased numbers of cleaved caspase-3- and TUNEL-positive colonic IECs compared to control mice.

Representative images of Swiss-roll colon sections from 8-12 week-old mice with the indicated genotypes immunostained for DNA fragmentation (TUNEL) or cleaved-Caspase-3 (cC3). Scale bars, 100 µm.

2.6.2 IEC-specific TNFR1 does not contribute to the impairment of the mucus layer in *Xbp1*$^{IEC\text{-}KO}$ mice

Ablation of TNFR1 specifically in IECs strongly suppresses the severity of colitis and the epithelial barrier impairment in *Xbp1*$^{IEC\text{-}KO}$ *Casp8*$^{IEC\text{-}KO}$ mice (Figure 2-17). Moreover, it was suggested that mice show TNFR1-dependent Goblet cell dysfunction upon TNF

injection[361]. Therefore, these could raise the question of whether epithelial-intrinsic TNFR1 deletion suppresses colitis in *Xbp1*$^{IEC\text{-}KO}$ *Casp8*$^{IEC\text{-}KO}$ by normalizing mucin production and recovering the impaired mucus layer caused by IEC-specific XBP1 ablation. To this end, mice deficient in epithelial-specific XBP1 and TNFR1 (hereafter, *Xbp1*$^{IEC\text{-}KO}$ *Tnfr1*$^{IEC\text{-}KO}$) were generated. Colon sections from control, *Xbp1*$^{IEC\text{-}KO}$ and *Xbp1*$^{IEC\text{-}KO}$ *Tnfr1*$^{IEC\text{-}KO}$ mice were immunostained with MUC2 antibodies. Interestingly, results demonstrated that the colons of *Xbp1*$^{IEC\text{-}KO}$ *Tnfr1*$^{IEC\text{-}KO}$ mice showed strongly reduced MUC2 production compared to control mice, similar to *Xbp1*$^{IEC\text{-}KO}$ mice (Figure 2-31). Diminished mucin expression in the colons of *Xbp1*$^{IEC\text{-}KO}$ *Tnfr1*$^{IEC\text{-}KO}$ mice was further confirmed by Alcian Blue-PAS staining (Figure 2-31). Similar to *Xbp1*$^{IEC\text{-}KO}$ mice which showed reduced ZG16 production in the colon (Figure 2-24B), epithelial-specific TNFR1 deletion did not restore the diminished ZG16 production in the colons of *Xbp1*$^{IEC\text{-}KO}$ mice (Figure 2-31).

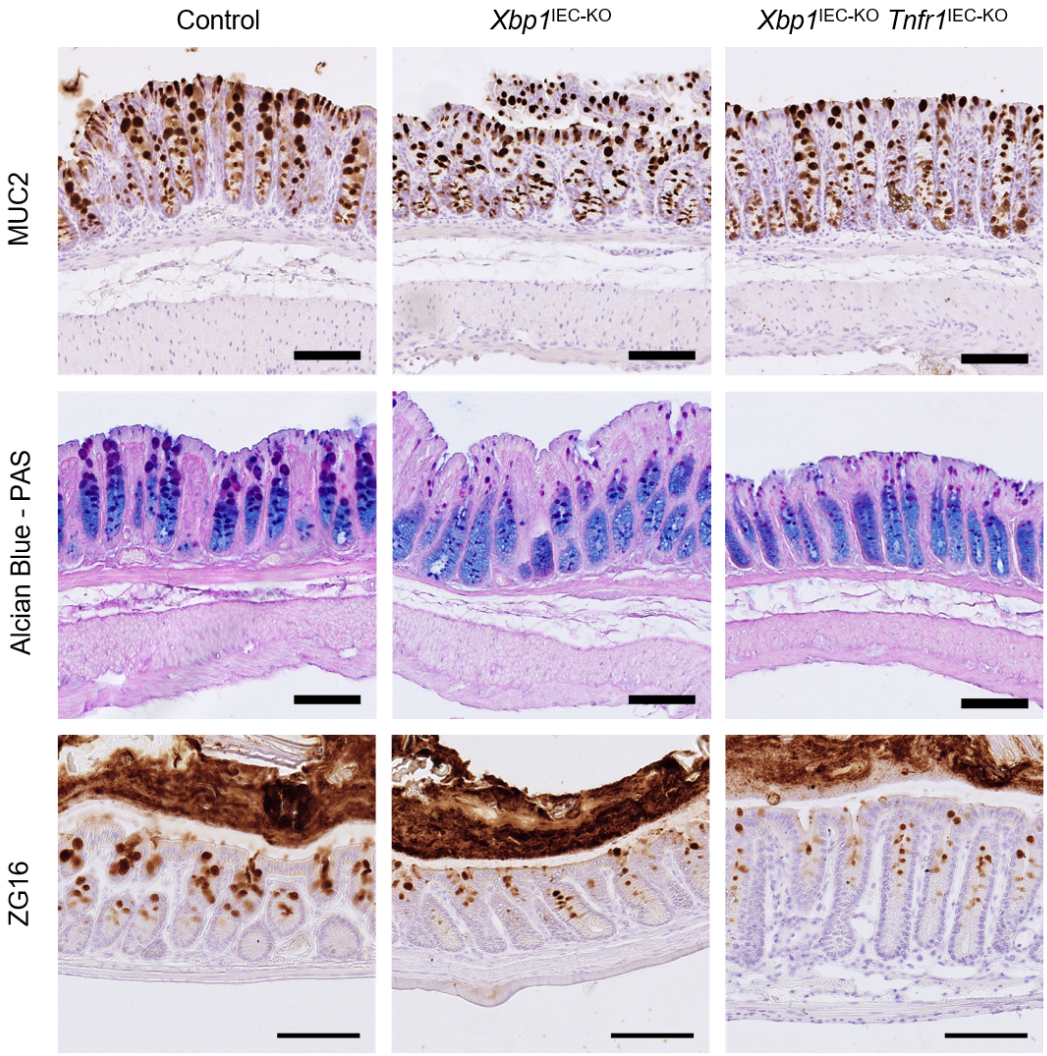

Figure 2-31 TNFR1 signalling in epithelium does not play an important role in reduced mucin production in the colons of *Xbp1*$^{IEC-KO}$ mice.

Representative images of Carnoy's-fixed colon sections from 11-week-old mice with indicated genotypes stained with Alcian Blue-PAS or immunostained for Mucin-2 and ZG16. Scale bar, 100μm.

To uncover whether ablation of TNFR1 in IECs could restore improperly formed mucus layer in *Xbp1*$^{IEC-KO}$ mice, distal colon tissues containing faecal material from *Xbp1*$^{IEC-KO}$ *Tnfr1*$^{IEC-KO}$ mice were collected and fixed in Carnoy's fixative. Mucus layers in the colons of control, *Xbp1*$^{IEC-KO}$ and *Xbp1*$^{IEC-KO}$ *Tnfr1*$^{IEC-KO}$ mice were visualised by performing Alcian Blue-PAS staining. Consistent with the diminished mucin production, histological assessment and quantification of the mucus layer demonstrated that *Xbp1*$^{IEC-KO}$ *Tnfr1*$^{IEC-KO}$ mice had the impaired mucus layer (Figure 2-32). All in all, these results demonstrate

that the ablation of TNFR1 in epithelium suppresses necroptosis-induced colitis in *Xbp1*$^{IEC-KO}$ *Casp8*$^{IEC-KO}$ mice without improving the mucus layer impairment.

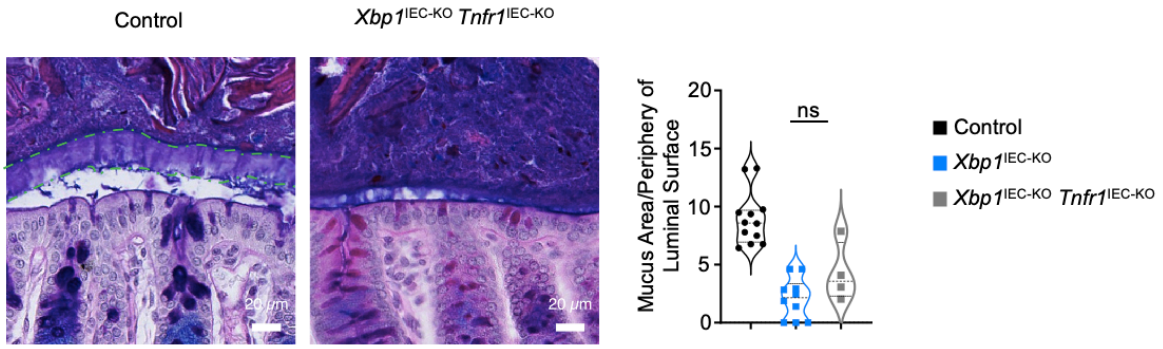

Figure 2-32 *Xbp1*$^{IEC-KO}$ *Tnfr1*$^{IEC-KO}$ mice show an impaired mucus layer in the colon.

Representative images of Carnoy's-fixed colon sections from 11-week-old mice with indicated genotypes stained with Alcian Blue-PAS. Violin graph showing the quantification of mucus layers. The inner mucus layers were labelled with green dashed lines. Each dot represents one mouse. ns: not significant, $^{**}p < 0.01$, $^{***}p < 0.005$. Scale bars are indicated in the pictures.

2.6.3 Glycosylation reactions are not completely lost in the colons of mice lacking XBP1

Diverse glycosylation modifications on mucins are taught to be critical for their functionality[247], as the enzymes catalysing glycosylation reactions were shown to regulate mucin production[362,363]. The majority of the carbohydrates are incorporated into proteins in cis-, medial- and trans-Golgi, however, the reactions commence in ER[247]. Therefore, it was asked whether the deficiency of XBP1-mediated UPR could lead to a complete defect in one of the glycosylation reactions in Goblet cells, indirectly causing the reduction in MUC2 expression. To address this, lectins were employed. Plants, animals as well as microorganisms synthesize a family of proteins, called lectins. They can recognize specific glycan(s) without possessing an enzymatic activity. Thus, some lectins purified from plant species have been utilised in glycobiology[364]. Colon sections from *Xbp1*$^{IEC-KO}$ and WT mice were incubated with biotin-conjugated lectins from different plant species, recognizing various types of glycosylation (Figure 2-33). Visualizing biotinylated lectins by incubating them with chromogen 3,3'Diaminobenzidine (DAB) demonstrated that none of

the stained glycoproteins was absent in Goblet cells (Figure 2-33), arguing against the hypothesis that XBP1 deletion could render specific steps in MUC2 glycosylation completely impaired.

Lectin	Sugar specificity
WGA	N-Acetylglucosamine
Con A	Mannose
MAL II	Sialic acid
SNA	Sialic acid linked to *N*-Acetylgalactosamine Sialic acid linked to galactose
RCA_{120}	Galactose, *N*-Acetylgalactosamine
UEA I	Fucose

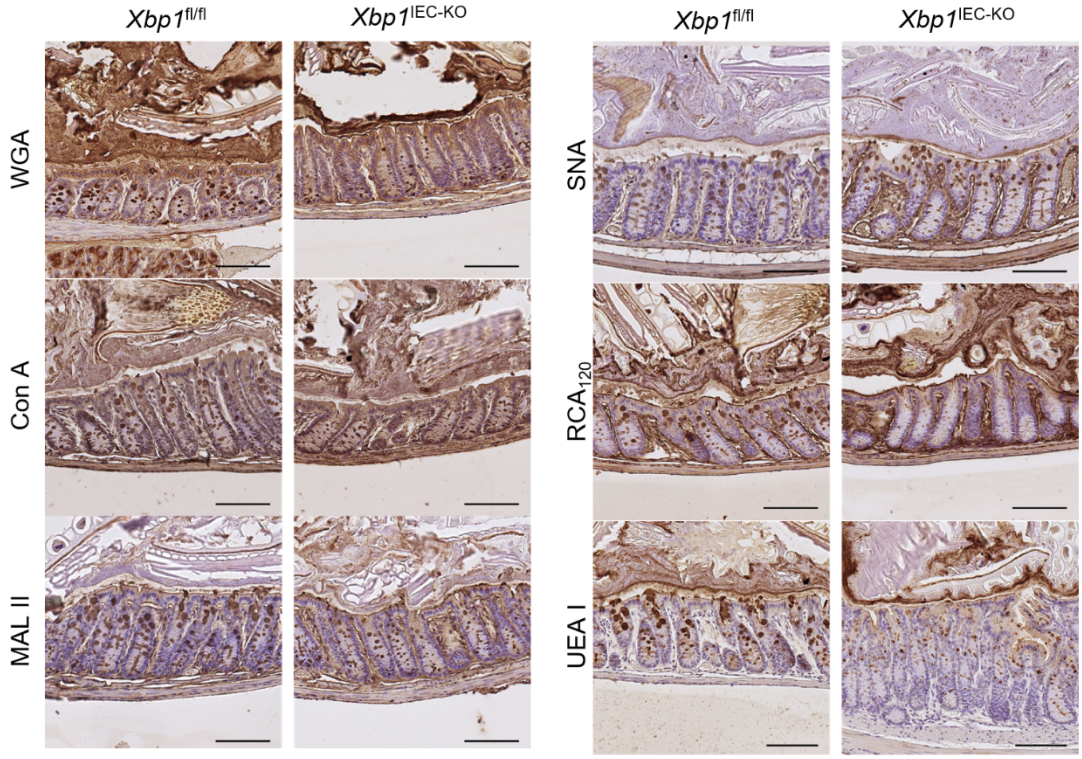

Figure 2-33 XBP1 deficiency does not lead to complete loss of certain glycosylation reactions in Goblet cells.

(A) Table showing the employed lectins and their corresponding sugar specificity. The information was taken from the manual provided by the manufacturer. **(B)** Representative images of Carnoy's-fixed colon sections from 11-week-old mice with indicated genotypes stained with WGA, ConA, MAL II, SNA, RCA_{120}, UEA-I lectins.

2.6.3.1 XBP1 regulates *Muc2* expression independent of cell-extrinsic factors

Presence[365], IEC-specific Myd88-dependent sensing[366], and composition of colonic microbiota[360] play critical roles in MUC2 production and regulation of the mucus layer in the colon. In an attempt to study whether IEC-extrinsic factors such as intestinal microbiota could lead to impaired mucin production in XBP1 deficiency, colon organoids from control

and *Xbp1*$^{IEC-KO}$ mice were established[333]. Similar to the controls, crypts lacking XBP1 were capable of forming colon organoids, that were in spheroid morphology (stem cell state) and did not show any growth defect as they could be passaged (Figure 2-34A). Notch signalling is a critical regulator of the self-renewal of the intestinal epithelium[367]. Importantly, inhibition of Notch signalling was shown to induce Goblet cell differentiation[368]. To differentiate colon organoids into Goblet cells, control and XBP1-deficient colonoids were incubated with N-[N-(3,5-Difluorphenacetyl)-L-alanyl]-S-phenylglycin-tert-butylester (DAPT)[369], which inhibits the activation of the Notch signalling pathway[370,371]. After 6 days of DAPT incubation, control and XBP1-deficient organoids showed loss of spheroid morphology, which was maintained in DMSO treatment, indicating conversion into Goblet cells upon DAPT treatment (Figure 2-34A). Investigation of mRNA expression by performing qRT-PCR analysis showed that DAPT treatment led to robust *Muc2* expression in control colonoids. Consistent with *in vivo* results (Figure 2-21), XBP1-deficient organoids treated with DAPT had strongly diminished Muc2 expression compared to control organoids treated with DAPT (Figure 2-34B).

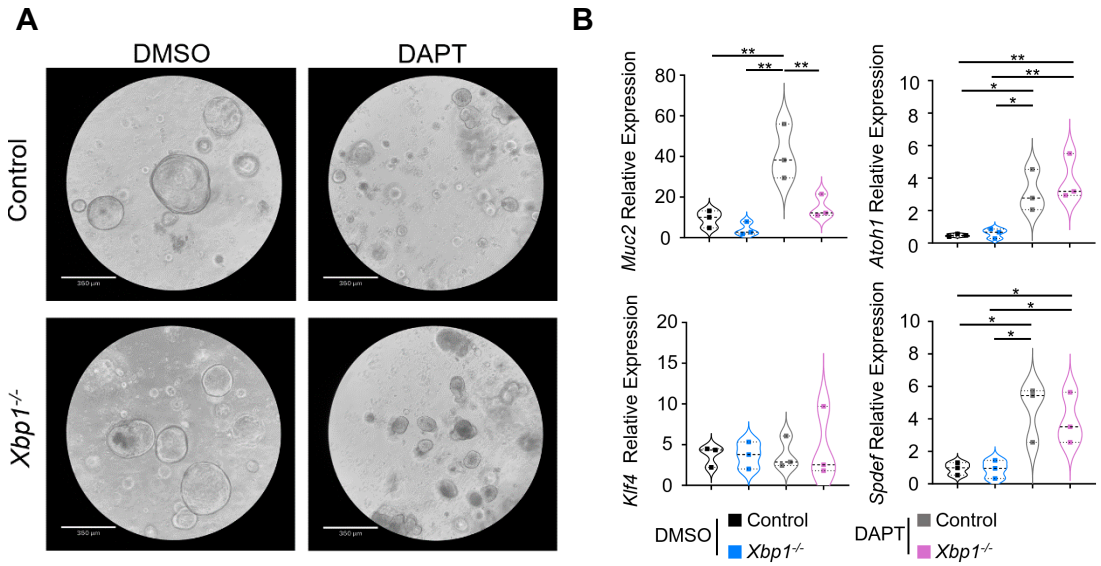

Figure 2-34 XBP1-deficient colon organoids have strongly reduced *Muc2* expression upon differentiation into Goblet cells.

(A) Representative images of mouse colon organoids from control and *Xbp1*$^{IEC-KO}$ mice treated with DMSO or DAPT for 6 days. **(B)** Graphs showing relative mRNA expression of *Muc2, Atoh1, Klf4* and *Spdef* measured by qRT-PCR analysis from colon organoids with indicated genotypes and treatments.

It was asked whether deficiency of XBP1 could impair Goblet cell differentiation, indirectly leading to reduced *Muc2* expression. To study this, we assessed the expression of early, *Atoh1* (*Math1*)[372,373], and terminal, *Klf4*[374], *Spdef*[375] transcriptional factors that are critical for the lineage fate determination of intestinal secretory cells. Consistent with RNA sequencing results obtained from *in vivo* (Figure 2-21), qRT-PCR analysis revealed that control and Xbp1$^{-/-}$ organoids treated with DAPT had similar *Atoh1*, *Klf4* and *Spdef* mRNA expression (Figure 2-34B), showing Goblet cell differentiation were intact and did not contribute to reduced *Muc2* expression in the colons of *Xbp1*$^{IEC\text{-}KO}$ mice. Taken together, XBP1 deficiency in intestinal epithelium does not affect Goblet cell differentiation and causes reduced *Muc2* expression independent of intestinal microbiota.

2.7 Increased bacterial translocation and systemic inflammation in *Xbp1*$^{IEC\text{-}KO}$ *Casp8*$^{IEC\text{-}KO}$ mice depends on IEC necroptosis

Considering *Casp8*$^{IEC\text{-}KO}$ and *Xbp1*$^{IEC\text{-}KO}$ *Casp8*$^{IEC\text{-}KO}$ but not *Xbp1*$^{IEC\text{-}KO}$ mice show the presence of bacteria in the subepithelial layers of the colon (Figure 2-26), it was hypothesized that the dysfunctional mucus layer in mice lacking XBP1 could amplify penetration of luminal bacteria into colonic sublayers in *Casp8*$^{IEC\text{-}KO}$ mice during ongoing IEC-necroptosis. Therefore, blocking IEC necroptosis by deleting of RIPK3 or MLKL in *Xbp1*$^{IEC\text{-}KO}$ *Casp8*$^{IEC\text{-}KO}$ mice were expected to prevent bacterial translocation into the sublayers of colon. To address this, FISH specifically targeting bacterial 16s rRNA was performed on the colon sections from *Xbp1*$^{IEC\text{-}KO}$ *Casp8*$^{IEC\text{-}KO}$ *Ripk3*$^{-/-}$ and *Xbp1*$^{IEC\text{-}KO}$ *Casp8*$^{IEC\text{-}KO}$ *Mlkl*$^{-/-}$ mice. Fluorescence microscopy analysis revealed that *Xbp1*$^{IEC\text{-}KO}$ *Casp8*$^{IEC\text{-}KO}$ *Ripk3*$^{-/-}$ and *Xbp1*$^{IEC\text{-}KO}$ *Casp8*$^{IEC\text{-}KO}$ *Mlkl*$^{-/-}$ mice did not show bacterial presence within the sublayers of the colon (Figure 2-35A).

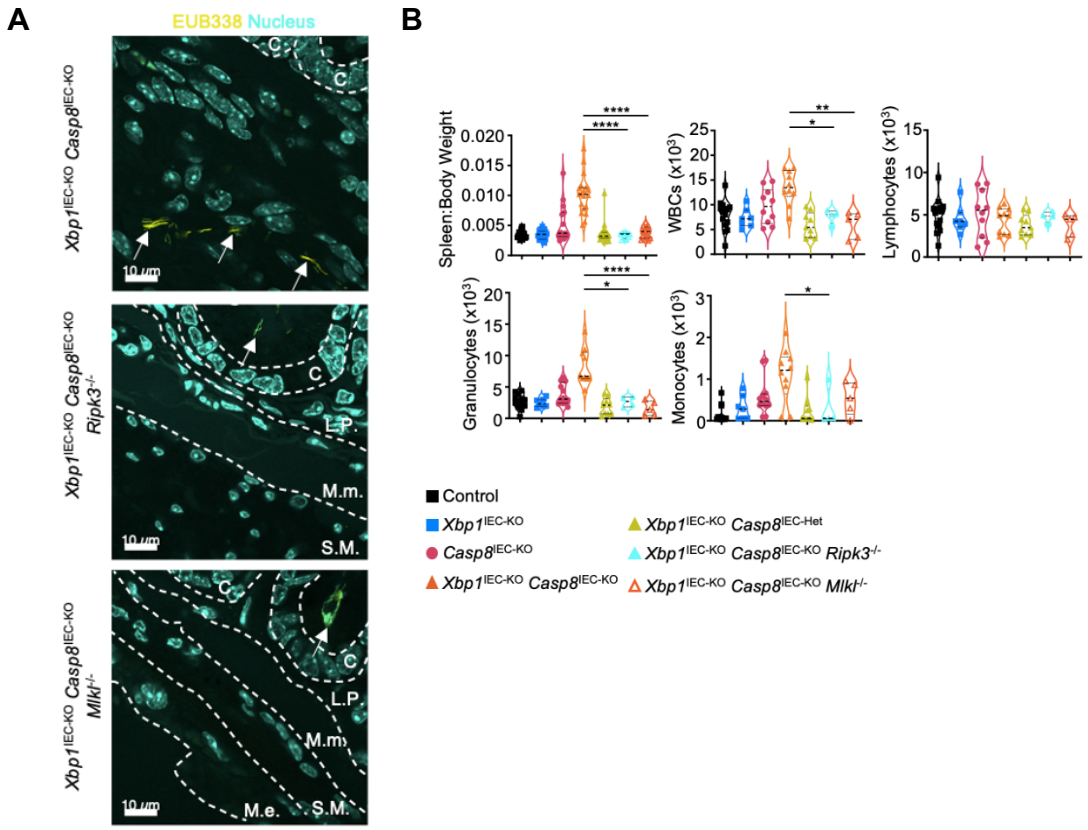

Figure 2-35 Inhibition of IEC necroptosis prevents bacterial translocation into the colonic sublayers and systemic inflammation in *Xbp1*$^{IEC\text{-}KO}$ *Casp8*$^{IEC\text{-}KO}$ mice.

(A) Representative images of PFA-fixed Swiss rolled colon tissues from mice with indicated genotypes stained with 16S rRNA in situ hybridization probe EUB338 (Yellow). Nuclei were stained with DAPI (Aqua). White arrows indicate bacteria. Each colonic structure and layer were labelled with white dashed lines. C: Crypt, L.P: Lamina propria, M.m: Muscularis mucosae, S.M: Submucosa, M.e: Muscularis externa. Scale bars are indicated on the pictures. **(B)** Violin graphs showing spleen to body weight ration and analysed circulating blood of 8-12 weeks old mice with indicated genotypes. Each dot represents one mouse. ns: not significant, $^{*}p < 0.05$, $^{**}p < 0.01$, $^{***}p < 0.005$, $^{****}p < 0.0001$.

As the inhibition of epithelial necroptosis prevented the translocation of luminal bacteria into the submucosa, RIPK3 or MLKL deletion in *Xbp1*$^{IEC\text{-}KO}$ *Casp8*$^{IEC\text{-}KO}$ mice was expected to inhibit systemic inflammation. Indeed, *Xbp1*$^{IEC\text{-}KO}$ *Casp8*$^{IEC\text{-}KO}$ *Ripk3*$^{-/-}$ and *Xbp1*$^{IEC\text{-}KO}$ *Casp8*$^{IEC\text{-}KO}$ *Mlkl*$^{-/-}$ mice did not show markers of systemic inflammation (Figure 2-35B). Collectively, these results show that epithelial cell-intrinsic XBP1 restricts luminal bacterial translocation into the subepithelial layers of the colon and prevents systemic inflammation in the loss of epithelial barrier integrity triggered by IEC necroptosis.

2.8 Epithelial XBP1 deficiency causes reduced mucin production in the ileum independent of extrinsic apoptosis and necroptosis

IEC-specific XBP1 deficiency leads to diminished mucin production in the colon (Figure 2-21-24). In addition to the colon, Goblet cells exist in the small intestine and produce mucins[202]. Therefore, it was asked whether the ablation of XBP1 in IECs could lead to diminished mucin production in the small intestine. To investigate this, ileal sections from control and *Xbp1*$^{IEC\text{-}KO}$ mice were stained with Alcian Blue-PAS. The results revealed that Goblet cells in the ilea of control mice show dark-purple stained vacuoles. In stark contrast, XBP1 ablation caused a reduction in the sizes of vacuoles positively stained for Alcian Blue-PAS, showing that mucin production was diminished in the ilea of *Xbp1*$^{IEC\text{-}KO}$ mice (Figure 2-36A). Indeed, qRT-PCR results confirmed that *Muc2* expression was strongly reduced in the small intestines of *Xbp1*$^{IEC\text{-}KO}$ mice compared to control mice (Figure 2-36B). Consistent with the findings in the colon, the combined deletion of Casp8 and RIP3 or Casp8 and MLKL did not normalise the mucin expression in the small intestines of Xbp1$^{IEC\text{-}KO}$ mice (Figure 2-36).

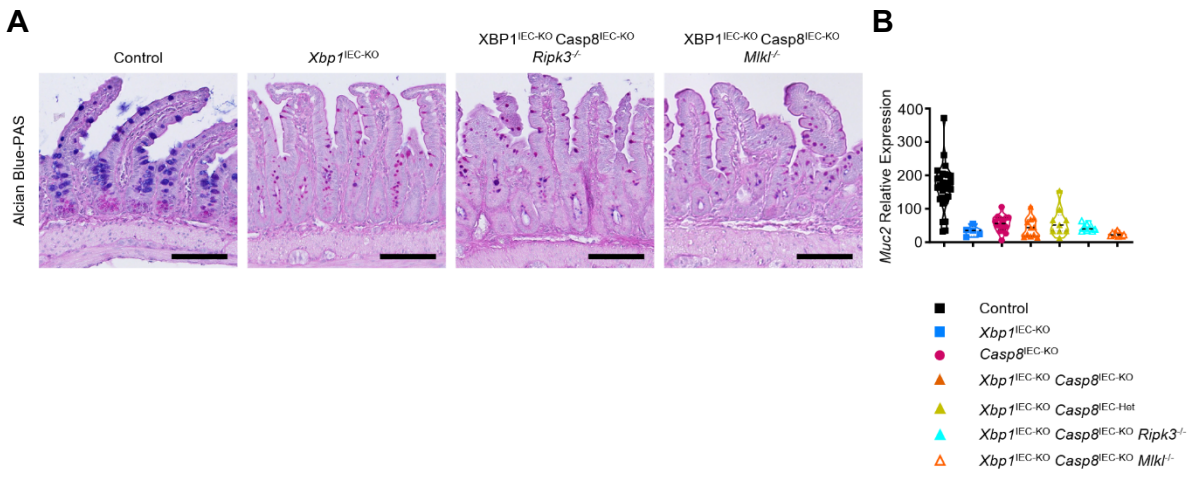

Figure 2-36 XBP1 deficiency results in impaired mucin production in the ileum independent of extrinsic apoptosis and necroptosis.

(A) Representative images of ileal sections from 8-12 week-old mice with indicated genotypes stained with Alcian Blue-PAS. **(B)** Graph showing qRT-PCR analysis of *Mucin2* gene expression in ilea of 8-12 old weeks mice with indicated genotypes. *Tbp* was used as a housekeeping gene to calculate the relative expression of *Muc2*. $2^{-\Delta CT}$ method was performed. Each dot represents one mouse. Scale bar, 100μm.

Of note, studies demonstrated that Paneth cells express mucins as indicated by Alcian Blue^{+}, PAS^{+} and MUC2^{+} cells in ileal crypts [376,377]. In line with this, small intestinal sections stained with Alcian blue-PAS showed the presence of a magenta-purple colour at the bottom of the crypts in control mice, demonstrating the existence of Paneth cells (Figure 2-36A). In contrast, small intestinal sections from mice lacking XBP1 in IECs showed profoundly reduced numbers of Alcian blue-PAS-positive cells in the crypts, which was not restored upon combined inhibition of extrinsic apoptosis and necroptosis (Figure 2-19). All in all, these results show that epithelial XBP1 regulates the expression of mucins in the small intestine independent of FADD-caspase-8-mediated apoptosis and RIPK3-MLKL-dependent necroptosis.

3. Discussion

3.1 XBP1 suppresses necroptosis-induced colitis by regulating the formation of bacteria-impermeable mucus barrier

3.1.1 XBP1-deletion-induced impaired mucus barrier per se aggravates necroptosis-induced colitis

IBD is a complex disease which is thought to be rooted in the combination of multiple factors including the host's genetic background[266,277,281-283]. Assessment of an individual's multiple variants is considered a critical identification of genetic predisposition to IBD[329]. However, the impact of crosstalk between multiple genes and their pathways on the pathogenesis of IBD is largely unknown. In this study, we revealed a previously unidentified link between ER stress and necroptosis in the intestinal epithelium. Our results showed that epithelial XBP1 deficiency exaggerated TNFR1-driven necroptosis-induced colitis in *Casp8*$^{IEC-KO}$ or *Fadd*$^{IEC-KO}$ mice. Critically, the strong synergistic effect of the loss of XBP1-mediated UPR and intestinal epithelial necroptosis is confined to the colon as necroptosis-induced or -mediated ileitis is not exacerbated upon XBP1 ablation in mice with Casp8 or FADD deficiency.

We found that MUC2, the major constituent of the mucus layer[202], was strongly downregulated in the colons of *Xbp1*$^{IEC-KO}$ mice. Consistent with MUC2 being the major backbone of the mucus layer, mice with XBP1 deficiency show an impaired colonic mucus layer and the failed separation of luminal bacteria from colonic epithelium, similar to a recent report[264]. This constitutes the main mechanism of action that we propose to explain how deletion of XBP1 aggravates colitis in mice with epithelial caspase-8 or FADD deficiency (Figure 3-1). Previous studies demonstrated that the mucus layer in the colon provides an essential barrier regulating the intestinal inflammatory responses against microbiota[246,248,354,378]. While caspase-8 or FADD ablation drives IEC necroptosis and causes the epithelial barrier breach manifested by ulcerations in the colon, XBP1 deficiency, through impairing the colonic mucus layer, causes the failure of the separation of luminal bacteria, leading to increased contact between luminal bacteria and necroptotic epithelial cells which could worsen the severity of necroptosis-induced colitis in Casp8 or FADD deficient mice (Figure 3-1). In line with this proposed mechanism, the development of colitis in *Casp8*$^{IEC-KO}$ and *Fadd*$^{IEC-KO}$ mice depends on the presence of luminal microbiota[309,312], and *Xbp1*$^{IEC-KO}$ mice show microbiota-driven severe colitis upon DSS

administration, supporting the role of luminal microbiota in our proposed model. In contrast, the tightly layered, bacteria-impermeable mucus layer does not exist in the small intestine, and the contact between luminal bacteria and small intestinal IECs is not clearly prevented[202,379]. Critically, luminal microbiota does not drive ileitis in mice with caspase-8 or FADD deficiency[309,312].

PAMPs can be sensed by the host's cells via TLR4- and TLR3-induced TRIF-mediated pathway[12]. TRIF contains the RHIM domain and was shown to induce (RIPK1-)RIPK3-MLKL-dependent necroptosis upon caspase inhibition[380-382]. Therefore, increased contact between luminal bacteria and colonic epithelial cells caused by XBP1 deletion might be increasing the severity of necroptosis in *Casp8*$^{\text{IEC-KO}}$ and *Fadd*$^{\text{IEC-KO}}$ mice by promoting the induction of TRIF-(RIPK1)-RIPK3-MLKL-mediated necroptosis. To address this, mice lacking epithelial-specific XBP1, Casp8 and TRIF (also known as TICAM) could be generated, and the severity of colitis in *Xbp1*$^{\text{IEC-KO}}$ *Casp8*$^{\text{IEC-KO}}$ and *Xbp1*$^{\text{IEC-KO}}$ *Casp8*$^{\text{IEC-KO}}$ *Ticam*$^{\text{IEC-KO}}$ can be assessed side-by-side. Whereas Myd88-dependent signalling contributes to mucin secretion and mucus layer formation[366], the role of TRIF reinforcing the mucus barrier is not known. Therefore, TRIF ablation in IECs might not interfere with the interpretation of results from *Xbp1*$^{\text{IEC-KO}}$ *Casp8*$^{\text{IEC-KO}}$ *Ticam*$^{\text{IEC-KO}}$ mice. Of note, the colons of *Xbp1*$^{\text{IEC-KO}}$ mice show upregulation of IFN-inducible genes[383] including *Ifi44*, *Oasl2* and *Rtp4* (Figure 2-20). Pathogen sensing via TLR3 and TLR4 induce TRIF-mediated type I IFN responses[32-35], and the colonic epithelium with XBP1 deficiency has increased contact with luminal bacteria. Therefore, IFN-inducible genes might be upregulated by TRIF-mediated sensing of luminal bacteria by colonic IECs in *Xbp1*$^{\text{IEC-KO}}$ mice.

It is critical to emphasise that *Xbp1*$^{\text{IEC-KO}}$ mice do not develop colon inflammation. In contrast, *Muc2*$^{-/-}$ mice are completely devoid of the mucus layer and show spontaneous colitis[248], and *Casp8*$^{\text{IEC-KO}}$ as well as *Fadd*$^{\text{IEC-KO}}$ mice develop colitis, demonstrating that either the complete loss of bacteria-impermeable mucus layer or the failure in the epithelial barrier integrity is required to initiate colitis. Our results suggest that the combined failure of the mucus layer and epithelial barrier synergizes and leads to severe colitis. All in all, here we propose a mechanism (Figure 3-1) by which XBP1 suppresses IEC-necroptosis-dependent colitis but does not play a role in necroptosis-induced ileitis in mice models of intestinal inflammation.

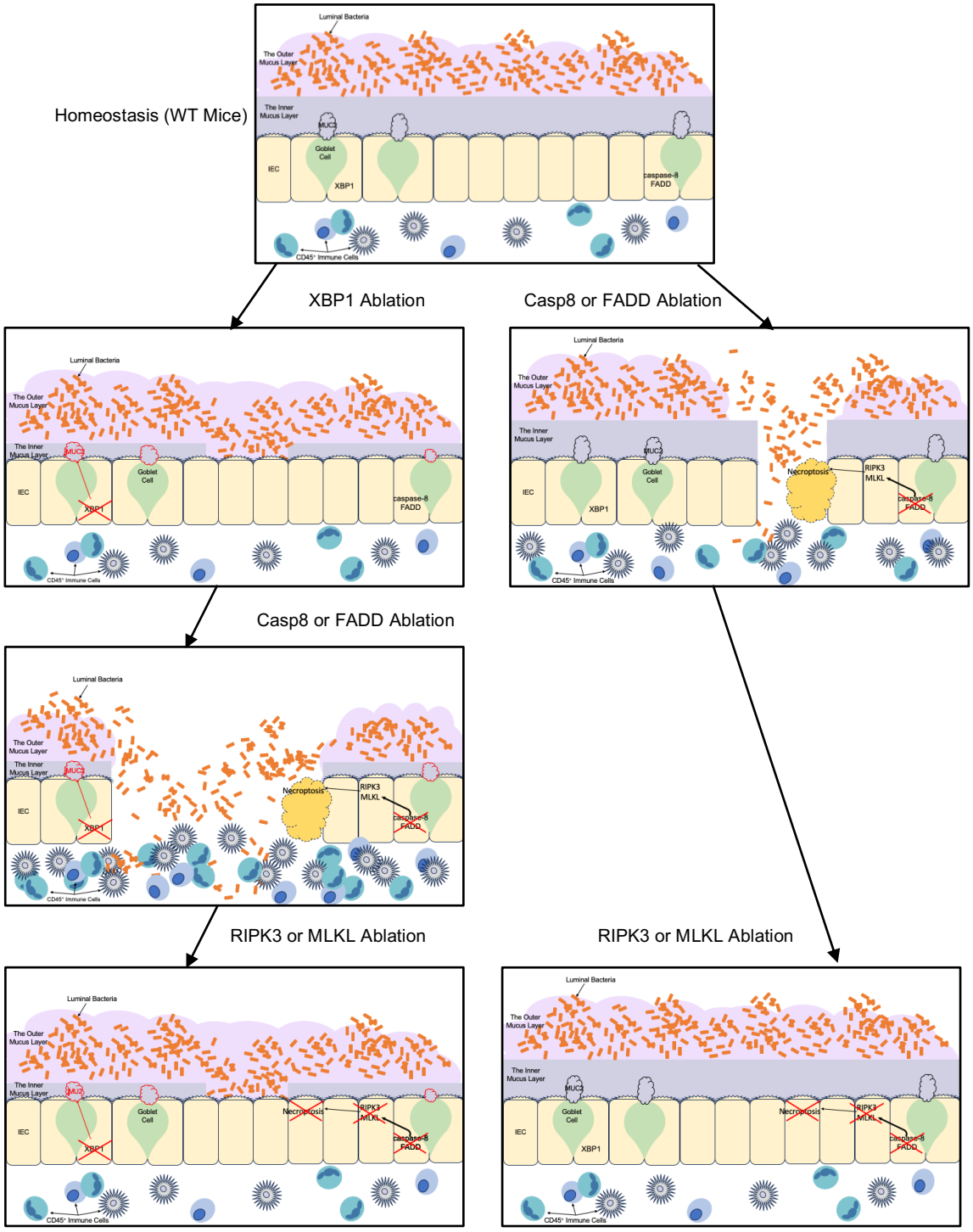

Figure 3-1 The main proposed mechanism by which epithelial-specific XBP1 protects from severe necroptosis-induced colitis in mice with IEC-Specific Casp8 or FADD deficiency.

IEC-Specific XBP1 ablation leads to a dysfunctional bacteria-impermeable mucus layer as indicated by increased contact between luminal bacteria and colonic epithelium. Epithelial Casp8 or FADD deficiency leads to necroptosis-induced colitis. XBP1-deletion-induced impaired mucus layer causes luminal bacteria to come in contact with IEC lacking Casp8 or FADD and aggravates the necroptosis-induced colitis. Inhibition of epithelial necroptosis completely prevents severe colitis in mice lacking XBP1 and Casp8 or XBP1 and FADD, however, the impaired mucus barrier is independent of FADD-Casp8-mediated apoptosis and RIPK3-MLKL-dependent necroptosis in XBP1 deficient mice.

In this proposed mechanism (Figure 3-1), luminal bacteria play an essential role in the exacerbation of colitis in mice lacking XBP1 and Casp8 or XBP1 and FADD. However, the results in this thesis do not provide direct evidence demonstrating IEC-specific XBP1 deficiency exaggerated colitis in *Casp8*$^{IEC\text{-}KO}$ and *Fadd*$^{IEC\text{-}KO}$ mice microbiota-mediated manner. To show this, broad-spectrum antibiotics can be administrated to *Casp8*$^{IEC\text{-}KO}$, *Xbp1*$^{IEC\text{-}KO}$ *Casp8*$^{IEC\text{-}KO}$ and control mice (or *Fadd*$^{IEC\text{-}KO}$, *Xbp1*$^{IEC\text{-}KO}$ *Fadd*$^{IEC\text{-}KO}$), followed by histopathological analysis of the colons. After the antibiotic regimen, *Casp8*$^{IEC\text{-}KO}$ and *Xbp1*$^{IEC\text{-}KO}$ *Casp8*$^{IEC\text{-}KO}$ (or *Fadd*$^{IEC\text{-}KO}$ and *Xbp1*$^{IEC\text{-}KO}$ *Fadd*$^{IEC\text{-}KO}$) mice are expected to have similar levels of colitis. Similar to antibiotic treatment, raising these mice under germ-free conditions and assessing the colon sections would provide direct evidence that microbiota drives the exacerbation of the phenotype in this model. Employing colon organoids from control, *Casp8*$^{IEC\text{-}KO}$, and *Xbp1*$^{IEC\text{-}KO}$ *Casp8*$^{IEC\text{-}KO}$ mice would provide another approach. Specifically, culturing isolated colonic crypts from *Casp8*$^{IEC\text{-}KO}$ and *Xbp1*$^{IEC\text{-}KO}$ *Casp8*$^{IEC\text{-}KO}$ mice are expected to form organoids as they are devoid of microbiota. Moreover, colon organoids do not have a mucus layer even though Goblet cells exist and secrete mucins in these cultures[384]. Thus, organoids from *Casp8*$^{IEC\text{-}KO}$ and *Xbp1*$^{IEC\text{-}KO}$ *Casp8*$^{IEC\text{-}KO}$ mice are hypothesized to die at similar levels upon coculturing them with bacteria species such as *Lactobacillus* [385].

Providing unambiguous evidence demonstrating that XBP1 deficiency-induced impaired mucus barrier is the culprit of exacerbated colitis in *Xbp1*$^{IEC\text{-}KO}$ *Casp8*$^{IEC\text{-}KO}$ or *Xbp1*$^{IEC\text{-}KO}$ *Fadd*$^{IEC\text{-}KO}$ mice might be more difficult. Generating mice with Goblet cell overexpressing *Muc2*, and crossing these mice to *Xbp1*$^{IEC\text{-}KO}$ *Casp8*$^{IEC\text{-}KO}$ mice would be the most direct approach showing XBP1-deletion induced impaired mucus layer exaggerates colitis in *Casp8*$^{IEC\text{-}KO}$ mice. To perform this, knock-in mice carrying *Muc2* preceded with Stop codon flanked by two *Frt* sites can be generated[386]. Since we have already employed the CRE-*loxP* system to delete XBP1 and Casp8 or XBP1 and FADD in IECs, the utilization of FLPo-FRT system[387] is critical to avoid the *Muc2* induction in non-Goblet cells in the intestinal epithelium. However, the generation of mice expressing *Muc2* might not be straightforward. One drawback is that MUC2 is a big protein (roughly 5200 amino acids) containing many repeats[247]. Therefore, usual cloning strategies would not suffice to generate mice with inducible MUC2. In addition, ablation of XBP1 perturbates ER[162], the overexpression of MUC2 might not be achieved at all. Nevertheless, one feasible approach could be mucus transfer. A recent report claimed that delivering the mucus

isolated from wild-type mice to the mice with thinner mucus layer alleviated the DSS-induced colitis[363]. However, it is quite vague how the complex three-dimensional structure of mucus can still be preserved after the isolation procedure and the route of administration (the gastrointestinal tract) having an immensely dynamic environment in terms of pH and salt concentration[388,389]. In line with this, it was reported that native mucus structure cannot be established upon the introduction of water to commercially available mucus[390]. Therefore, simple isolation and transfer of mucus raises a question of validity. Meanwhile, there has been ongoing research on developing mucus mimetics, which are synthetic hydrogels or nanoparticles to reinforce mucosal barriers by acting as native mucus[391]. This might be the most feasible way to provide direct evidence that the XBP1-deletion-induced dysfunctional mucus layer exacerbates necroptosis-induced colitis.

3.1.2 Epithelial XBP1 deficiency might alter the composition of colonic microbiota driving the exaggeration of necroptosis-induced Colitis

Mucins are heavily glycosylated, and it was reported that some bacteria species exploit this carbohydrate-rich environment as an energy source[245,247]. The reduction in MUC2 expression and the impaired mucus layer upon XBP1 ablation might lead to dysbiosis in the colon. Studies also showed that alteration of microbiota by faecal transplantation could worsen colitis in mouse models[392-394]. Therefore, XBP1-deficiency might lead to the exaggeration of necroptosis-induced colitis by altering the composition of gut microbiota in *Casp8*$^{IEC\text{-}KO}$ mice. To address this, the first 16S rRNA sequencing can be performed from bacteria isolated from *Xbp1*$^{IEC\text{-}KO}$ and *Xbp1*$^{fl/fl}$ littermates that are cohoused and raised in the same cages. In case of substantial microbiota alteration in *Xbp1*$^{IEC\text{-}KO}$ mice compared to *Xbp1*$^{fl/fl}$ mice, microbiota isolated from faeces of *Xbp1*$^{IEC\text{-}KO}$ mice can be transplanted to *Casp8*$^{IEC\text{-}KO}$ mice received antibiotics or raised under germ-free conditions. Transferring microbiota from *Casp8*$^{IEC\text{-}KO}$ to *Casp8*$^{IEC\text{-}KO}$ mice should be included in this experimental set-up as an important control. If the altered composition of microbiota contributes to the severity of colitis in *Xbp1*$^{IEC\text{-}KO}$ *Casp8*$^{IEC\text{-}KO}$ mice, *Casp8*$^{IEC\text{-}KO}$ mice that received microbiota transfer from *Xbp1*$^{IEC\text{-}KO}$ mice are expected to show more severe colitis compared to *Casp8*$^{IEC\text{-}KO}$ mice transplanted with microbiota from *Casp8*$^{IEC\text{-}KO}$ mice.

3.2 The possible mechanisms by which XBP1 deficiency impairs the mucus layer

3.2.1 Death of Goblet cells and mucus layer

Ubiquitous RIPK3 or MLKL deletion in *Xbp1*$^{IEC\text{-}KO}$ *Casp8*$^{IEC\text{-}KO}$ mice revealed that severe colitis in mice lacking XBP1 and Casp8 depends on IEC-necroptosis. Having generated these mouse lines, we found that the impaired mucus layer in XBP1 deficiency is independent of FADD-caspase-8-mediated apoptosis and RIPK3-MLKL-dependent necroptosis.

Chemically controllable prolonged activation of IRE1α (bearing I642G mutation) shows a protective effect on cell viability in response to thapsigargin/tunicamycin-induced ER stress conditions[395]. However, cell death upon ER stress induction is well-documented[396,397]. Specifically, the endonuclease domain of IRE1 is suggested to contribute to ER stress-induced cell death[395] by altering mRNA expression death receptor 5 (DR5)[398,399]. Moreover, under certain conditions, it was shown that ER stress can induce intrinsic apoptosis[400]. We failed to detect the increased presence of activated caspase-3 and DNA fragmentation in the colons of *Xbp1*$^{IEC\text{-}KO}$, *Xbp1*$^{IEC\text{-}KO}$ *Casp8*$^{IEC\text{-}KO}$ *Ripk3*$^{-/-}$, *Xbp1*$^{IEC\text{-}KO}$ *Casp8*$^{IEC\text{-}KO}$ *Mlkl*$^{-/-}$ mice, suggesting defective mucus layer in *Xbp1*$^{IEC\text{-}KO}$ mice is independent of Goblet cell death. However, it could be possible that we could not detect the regulated death of Goblet cells in our model as the intestinal sections represent snapshots of certain moments of mice with chronic XBP1 deficiency. In addition, it was shown that induction of ER stress in cells could undergo caspase-2-dependent apoptosis[401] or Gasdermin-E-dependent pyroptosis[402] or increased cytosolic Ca^{+2}-mediated apoptosis[403] or caspase-1-mediated pyroptosis[404-406]. It is unclear whether these results can be translated to our model. Nevertheless, performing immunoblot analysis for Gasdermin-E, cleaved caspase-1/2 cleavage from proteins isolated from IECs could reveal whether the XBP1 deficiency indirectly leads to impairment in the mucus layer by inducing Goblet cell death.

Colon organoids lacking XBP1 are capable of differentiating into Goblet cells without showing the reduced expression of early and late differentiation markers, demonstrating that epithelial-specific XBP1 deficiency does not interfere with the Goblet cell differentiation. Considering this, protein expression of early (ATOH1[372,373]) or terminal (SPDEF[375]) Goblet cell differentiation markers could be quantified from the protein extracts

of colonic IECs isolated from control and XBP1-deficient mice. Since our data suggest that chronic XBP1 deficiency does not lead to the death of Goblet cells, immunoblot or flow-cytometry-based protein analysis of control and XBP1 deficient IECs is expected to show similar ATOH1 and SPDEF levels.

3.2.2 Contribution of the cell death-independent pathways to the impaired mucus layer in XBP1 deficiency

3.2.2.1 XBP1 regulates *Muc2* expression in a cell-intrinsic manner

Goblet cells express TLRs (TLR1,2,3,4 and 5) as well as NLRP6 and were shown to drastically induce production as well as secretion of mucins upon PRR-ligand engagement[407-409]. Moreover, the mucus layer is known to be fine-tuned by the composition of the luminal microbiota[360,365,366]. Therefore, it is plausible to ask whether microbiota mediates the impairment of the mucus layer in XBP1-deficient mice. We found that colonoids lacking XBP1 exhibit reduced *Muc2* expression, showing that XBP1 deficiency leads to diminished *Muc2* independent of luminal microbiota. Importantly, our organoid experiments also show the IEC-intrinsic effect of XBP1 ablation on MUC2 as organoids lack immune and stromal cells[410-412]. Furthermore, our results demonstrate that organoids deficient in XBP1 do differentiate into Goblet cells, showing that XBP1 is not required for the differentiation of Goblet cells. Recently, a group reported that organoids lacking ERN2 (IRE1β), a paralog of IRE1α[166,167] is expressed in epithelial cells of the intestine[168], capable of splicing *Xbp1*[413-415] and protects mice from severe DSS-induced colitis[168], show impaired Goblet cell differentiation[264]. Our results contradict their claim that is IRE1β controls MUC2 production through XBP1[264]. Whereas they included *Xbp1*$^{\text{IEC-KO}}$ mice in their study, they did not provide organoid experiments from mice lacking XBP1 in IECs. Another important point lies within the experimental set-up of the colonoid differentiation. Organoids lacking ERN2 were differentiated with DAPT incubation for 24 hours[264]. However, in our study, we incubated XBP1-deficient organoids with the same Notch inhibitor for 6 days. The fundamental reason why we prolonged the differentiation duration is that the Goblet cell abundance percentage rate was found to be 90 only after 4 days of differentiation[416]. Therefore, we interpret that XBP1 and IRE1β regulate MUC2 expression and Goblet cell physiology thorough different mechanisms.

3.2.2.2 The potential role of IRE1- and XBP1s-mediated UPR pathways in the regulation of MUC2

Previous reports as well as results in this thesis show that deficiency of XBP1 leads to IRE1α activation as indicated by the increased number of pIRE1α$^+$ IECs and the strong *Xbp1u* splicing activity[162,239]. Dramatic activation of IRE1α might mediate the formation of the dysfunctional mucus barrier in XBP1 deficiency by possibly initiating *Muc2* mRNA decay via its Rnase domain (Figure 3-2A). To answer this, IRE1α can be deleted in colon organoids lacking XBP1. Of note, mice with IEC-specific IRE1α deficiency do not show reduced mucin production[239]. After generating organoids deficient in IRE1α and XBP1, they can be differentiated into Goblet cells, and their *Muc2* expression can be analysed. It is critical to draw attention that the colon organoid culture would not be an optimal platform to perform the series of these experiments as they show immense variability in transfection efficiency upon laborious and expensive techniques[417,418]. Nevertheless, the DAPT-induced Goblet cell differentiation experiment can be performed with the colonoids isolated from *Ire1*$^{IEC\text{-}KO}$ *Xbp1*$^{IEC\text{-}KO}$ mice as this mouse line was already generated by another group[239,419]. Whereas inhibition of IRE1α endonuclease domain can be achieved by chemical compounds, those inhibitors might be interfering with the RIDD activity of IRE1β. For example, a chemical compound, 4μ8c[420], was thought to inhibit the endonuclease activity of IRE1α. A recent study employed domain-swap experiments and showed that the RIDD activities of IRE1α as well as IRE1β were inhibited upon 4μ8c incubation[421]. Nevertheless, incubating Goblet cell differentiated colon organoids with 4μ8c in the presence/absence of transcription inhibitors, and assessment of *Muc2* expression would be a critical experiment, addressing the potential contribution of RIDD to the reduction of *Muc2 in* XBP1 deficiency. Including IRE1 kinase inhibitors would be an important control in this experimental setup. In the case of *Muc2* upregulation upon 4μ8c as well as IRE1α kinase inhibitor (Endonuclease activity of IRE1 preceded by the kinase activity of it), it could be concluded that XBP1 deletion-induced increased endonuclease activity of IRE1α drives the degradation of *Muc2* mRNA. However, it could be that IRE1α kinase inhibitors but not 4μ8c rescues the *Muc2* phenotype of organoids lacking XBP1, showing IRE1 reduces *Muc2* expression independent of its endonuclease activity (Figure 3-2B).

Importantly, a previous report put forward that IRE1β, possibly via its endonuclease domain, play a critical role in the *Muc2* expression[265]. Therefore, RIDD activity of ERN1

as well as ERN2 together may contribute to reduced mucin production in XBP1 deficiency. Considering organoids lacking ERN2 cannot differentiate into Goblet cells, knock-out constructs targeting *Ern2* would not be an option for the organoid platform. Yet, utilization of inhibitors of IRE1, known to inhibit both ERN1 and ERN2, can be the way to answer whether IRE1α coupled with IRE1β impairs mucin production upon XBP1 ablation. Moreover, ERN2-targeted knock-down studies followed by MUC2 expression assessment can be performed in human Goblet-like cell lines, which will be discussed below. Critically, XBP1 deletion activates the Rnase domain of IRE1α and to a lesser extent Rnase domain of IRE1β, as indicated by different levels of *Xbp1u* and *Xbp1s* in the epithelial cells of *Ern1*$^{\text{IEC-KO}}$ *Xbp1*$^{\text{IEC-KO}}$ and *Ern2*$^{\text{IEC-KO}}$ *Xbp1*$^{\text{IEC-KO}}$ mice[239]. Therefore, IRE1α-mediated RIDD could be the main regulator of *Muc2* expression in XBP1 deficiency.

While the RIDD activity provides a solid explanation of the mechanism by which *Muc2* is downregulated in the absence of XBP1, it is critical to consider that we found ZG16 is downregulated in the colons of *Xbp1*$^{\text{IEC-KO}}$ mice, showing XBP1-mediated UPR is critical for the production of other mucus-associated proteins as well(discussed also in section 3.2.3). However, we were unable to check the protein levels of other mucins and mucus-associated proteins due to a lack of commercially available antibodies. Endonuclease domains of IRE1α and IRE1β perform RIDD after a certain base sequence of mRNAs possessing two stem-loop tertiary structures as well as other physical properties, which potentially contribute to translational stalling[175,176,178]. It remains to be elucidated whether *Muc2* and *Zg16* (as well as other mucins and mucus-associated mRNAs) can be targets of RIDD activity upon XBP1 deletion. Importantly, the mucus-associated proteins including ZG16 are stored in Goblet cell granulae and secreted into the lumen together with MUC2[202,245]. It could be possible that reduced MUC2 production-storage-secretion culminates in diminished production of ZG16 via a feedback mechanism, indirectly leading to the decline of mucus-associated proteins in XBP1 deficiency.

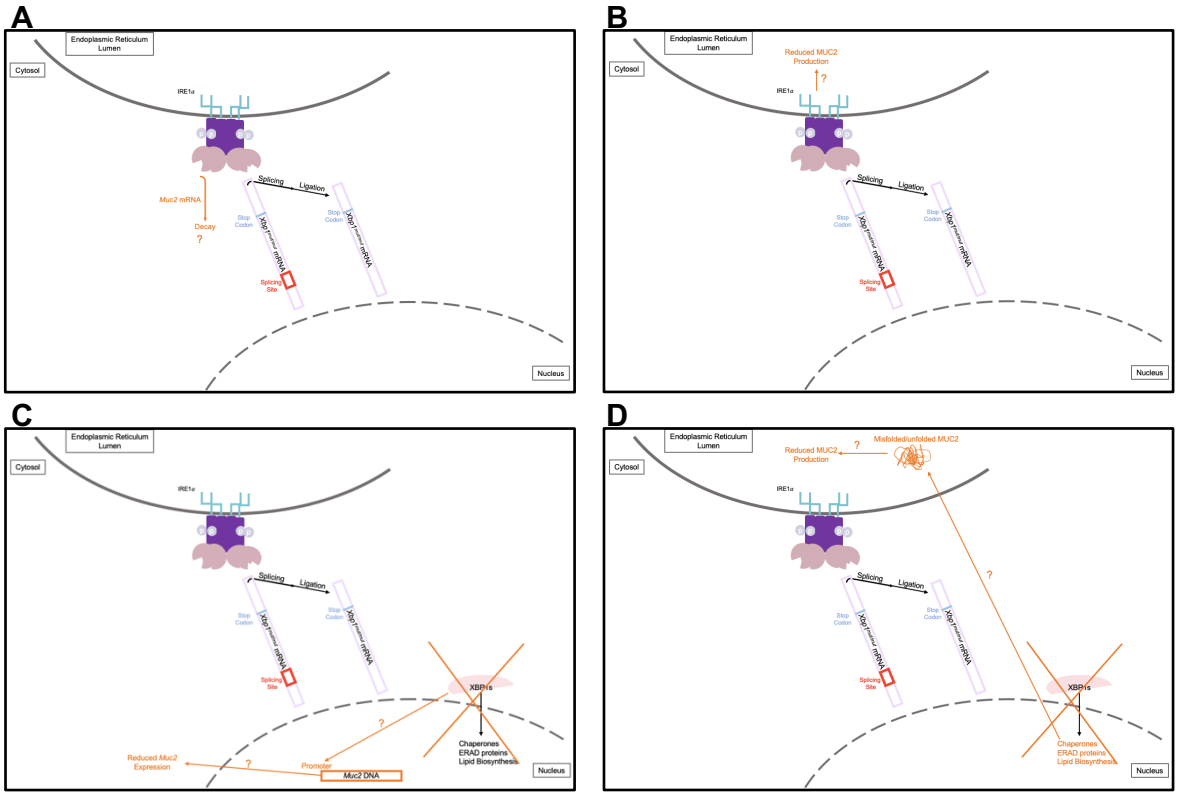

Figure 3-2 The possible mechanisms by which XBP1 deletion in IECs could lead to reduced MUC2 production.

(A) XBP1-deletion-induced activated IRE1α (and/or IRE1β) decaying the *Muc2* mRNA by RIDD. **(B)** Activated IRE1α (and/or IRE1β), independent of its endonuclease activity and XBP1s, could lead to a reduction in MUC2 production by leading to dysregulated ER such as impaired glycosylation reactions or other posttranslational modifications. **(C)** Upon ablation of XBP1, the XBP1s transcription factor could not bind to the promoter of *Muc2* and promote its expression. **(D)** In XBP1 deficient cells, the target genes of XBP1 including chaperones, protein disulphide isomerase and ER-associated protein degradation (ERAD) proteins could not be expressed. The absence of these critical proteins could cause an impairment in the MUC2 protein production process and lead to diminished levels of it.

Another possible mechanism by which XBP1 regulates the expression of MUC2 is the deficiency of XBP1s per se could reduce the Muc2 expression. XBP1s is a transcription factor, which might bind the *Muc2* promoter and contribute to the expression of *Muc2* (Figure 3-2C). To study this, XBP1s-specific chromatin immunoprecipitation followed by DNA sequencing (ChIP-seq) can be performed on colonic IECs isolated from control and *Xbp1*$^{IEC\text{-}KO}$ mice. If XBP1s is capable of binding the promoter region of *Muc2*, sequencing

analysis of immunoprecipitated DNA from control but not XBP1 deficient IECs is expected to show 5' regions of *Muc2*. Of note, the critical promoter regions of *Muc2* that are required to induce its expression differ between ileal and colonic Goblet cells[422]. Therefore, this disparity should be considered during the analysis of ChIP-seq data. In addition to the direct role of XBP1s in the regulation of the *Muc2* expression, upon activation of IRE1α, and to a lesser extent ERN2[423], spliced XBP1 protein induces transcription of UPR genes, which are critical for protein synthesis and secretion[424]. Specifically, XBP1s protein induces the expression of ER resident chaperones, proteins involved in ER-associated protein degradation (ERAD) and a protein playing a role in disulphide bond formation (protein disulphide isomerase, PDI)[158]. As MUC2 containing repetitive domains[247] is produced in copious amounts[202], and its structure is maintained by disulphide bonds[425], it might be possible that XBP1 deficient Goblet cells might not provide the adequate amounts of ER-resident chaperones, PDI and ERAD proteins. Healthy functioning ER in IECs was demonstrated to play an essential role in providing adequate levels of MUC2 and its assembly[168,260-263]. Therefore, target genes of XBP1s might be required to perform at least one of the routes that MUC2 takes such as protein folding, post-translational modifications, and secretion (Figure 3-2D). A series of *in vitro* over-expression studies could be conducted to test this hypothesis. As it was discussed above, intestinal organoid culture may not be a feasible approach to perform these. Nevertheless, colorectal cancer cell lines can be employed in this context such as HT-29 or LS174T cells. Incubating HT-29 cell lines with methotrexate (MTX) differentiates them into mucin-secreting Goblet-like cells (HT-29-MTX-E12), capable of establishing tight junctions between each other, and provides a mucus layer in the culture[426,427]. However, it was reported that *Muc2* expression in LS174T cells is higher compared to HT-29 cells[428,429]. Whereas LS174T cells do not form the mucus layer in contrast to HT-29-MTX-E12 cells, utilization of LS174T cells would be a better option for a Goblet cell-like model to investigate. After performing the knockdown of XBP1 in these cells, qRT-PCR analysis for *Muc2* and Alcian Blue-PAS can be performed. Upon XBP1 deletion, mucus production is expected to be reduced in these cells as well. To show chaperons, ERAD proteins and PDI are essential for mucin production, cells can be transfected with the plasmids containing six genes (and different combinations of them) whose expression is critically induced by XBP1s[158]. Then, qRT-PCR analysis and Alcian blue-PAS staining can be performed on these cells to check whether MUC2 and mucin production is normalized. Of note, in this experimental set-up, ERDJ5, one of the XBP1-induced ER chaperone[158], should not be included in the

overexpression plasmids, as mice lacking ERDJ5 do not have reduced MUC2 production, even though they have increased sensitivity to DSS-induced colitis[430].

3.2.2.3 The potential contribution of impaired glycosylation reactions to MUC2 reduction

MUCIN2 is subjected to extensive glycosylation reactions including *N*- and *O*-glycosylations, and the glycosylations on MUC2 are thought to be critical for its structure and functionality. *O*-glycosylation of sugar moieties[247] could alter the net electrical charge of the proteins[431,432]. Alcian Blue is a basic dye that stains mucins with carboxyl groups (acidic) which appear light blue while PAS stains mucins with hydroxyl groups (both acidic and neutral glycoproteins) appearing as magenta[433]. In our study, Goblet cells of *Xbp1*$^{IEC-KO}$ mice exhibited reduced dark-blue stained granules while red-magenta-coloured vacuoles were prominent in XBP1 deficient Goblet cells (Figure 2-21 and 2-22), especially in the upper parts of colonic crypts (intercryptic Goblet cells[434]), implicating XBP1-deletion could lead to the impaired decoration of MUC2 with acidic moieties. Sialic acid is one of the most prominent acidic modifications on mucins[247]. We checked the presence of various glycosylations including sialic acid in the colons by performing lectin-based staining and found that mice with XBP1 ablation showed diminished levels of glycosylations without leading to a complete absence of these modifications. Moreover, RNA-sequencing results did not show altered expression of enzymes involved in these pathways. Even though our experiments reveal certain glycosylations are not perished by XBP1 ablation in the colon, we did not conduct the experiments, providing a quantitative assessment of the glycosylations on mucins. To study this, mucus can be isolated from *Xbp1*$^{IEC-KO}$ mice and analyzed by mass-spectroscopy[250]. It is important to note that the recent report studied *Xbp1*$^{IEC-KO}$ and *Ern2*$^{-/-}$ mice side by side[264] showed differential staining patterns of Alcian Blue-PAS on the colon sections. Specifically, *Ern2*$^{-/-}$ mice had a dramatic reduction in the number of Goblet cell vacuoles positively stained with Alcian blue-PAS compared to wild-type mice. Meanwhile, their results showed a staining pattern in *Xbp1*$^{IEC-KO}$ mice, similar to our observations (less dark blue staining, prominent magenta colour). Therefore, XBP1 in Goblet cells might play a role in the glycosylation pathways of secreted proteins. These further implicate that XBP1 and ERN2 act differentially on Goblet cell physiology and MUC2 regulation.

3.2.3 The regulatory role of epithelial XBP1 in other mucins and mucus-associated proteins

In addition to secreted mucins, there are several mucins anchored on the apical regions of IECs (MUCIN-13[253], MUCIN-17[254,255]), and it might be interesting to check whether protein expression of transmembrane mucins in the colon could be diminished upon IEC-specific XBP1 deficiency.

Interestingly, our results also showed that colons of *Xbp1*$^{IEC\text{-}KO}$ mice had reduced protein but not mRNA expression of ZG16. ZG16 plays a critical role in defence against gram-positive bacteria[252]. ZG16 and MUC2 might have different feedback pathways at transcriptional as well as translational levels, and this could be a potential explanation for why we detected a discrepancy in the mRNA expression levels of *Zg16* and *Muc2*.

3.3 Differential effects of epithelial TNFR1 and TNF on necroptosis-induced colitis

It was previously demonstrated that chemical induction of ER stress in cells leads to IRE1α-TRAF2-axis-mediated autocrine-TNF production which contributes to ER-stress-induced cell death[435]. In addition, IECs with XBP1 deficiency showed increased NF-κB activation[162], suggesting TNF derived from IECs could contribute to the severe colitis in *Xbp1*$^{IEC\text{-}KO}$ *Casp8*$^{IEC\text{-}KO}$ mice. We found that IEC-derived TNF does not play an important role in colitis in *Xbp1*$^{IEC\text{-}KO}$ *Casp8*$^{IEC\text{-}KO}$ mice. Of note, it is not shown whether IEC-specific TNF drives colitis in *Casp8*$^{IEC\text{-}KO}$ mice. The generation of mice with combined caspase-8 and TNF ablation in IECs would answer this question. However, it was shown that full-body TNF deletion alleviates colitis in *Fadd*$^{IEC\text{-}KO}$ mice[309]. The effect of knocking out TNF ubiquitously however could be different than ablating it only in IECs as immune cell-derived TNF could contribute to colitis as well.

It was reported that roughly one-third of IBD patients receiving anti-TNF are irresponsive to the therapy, and the alleviating effect of anti-TNF wears off in some IBD patients, ranging between 23-46%, in the course of the therapy[436,437]. It was suggested that the genetic background of the host could contribute to the resistance against anti-TNF theraphy[437]. Therefore, it would be interesting to investigate whether IBD patients with hypomorphic mutations in *XBP1* show resistance against anti-TNF therapy.

It was previously shown that IEC-specific TNFR1 deletion profoundly suppresses colitis and completely rescues the epithelial barrier breach in *Casp8*$^{IEC\text{-}KO}$ and *Fadd*$^{IEC\text{-}KO}$ mice[307]. Consistent with this, in this study we revealed that epithelial-specific TNFR1 drives severe colitis in mice lacking XBP1 and Casp8 in IECs. In addition, we showed that epithelial-specific TNFR1 signalling does not contribute to the impaired mucus layer in XBP1 deficiency, arguing against the role of TNFR1-mediated Goblet cell dysfunction[361]. These results show that ablation of TNFR1 in IECs alleviates the severity of colitis in mice with combined XBP1 and caspase-8 deficiency by suppressing epithelial necroptosis without improving the dysfunctional mucus layer caused by XBP1 deficiency.

Homotrimers of Lymphotoxin-α, a member TNF superfamily, were shown to bind TNFR1 and induce its signalling[438]. Furthermore, another report showed that Lymphotoxin-α and TNF can induce TNFR1-dependent necroptosis at a similar level[439]. Therefore, it remains to be addressed whether Lymphotoxin-α produced from IECs could contribute to the pathology of colitis in *Xbp1*$^{IEC\text{-}KO}$ *Casp8*$^{IEC\text{-}KO}$ *Tnf*$^{IEC\text{-}KO}$ mice. This can be achieved in two different ways. Administration of neutralizing antibodies against Lymphotoxin-α[440,441] into *Xbp1*$^{IEC\text{-}KO}$ *Casp8*$^{IEC\text{-}KO}$ *Tnf*$^{IEC\text{-}KO}$ mice might be one approach to address this. In addition, crossing *Lta*$^{-/-}$ mice to *Xbp1*$^{IEC\text{-}KO}$ *Casp8*$^{IEC\text{-}KO}$ *Tnf*$^{IEC\text{-}KO}$ mice would be a genetic approach. However, mice lacking Lymphotoxin-α have impaired Peyer's patches as well as lymph nodes[442], which could potentially interfere with the interpretation of results from this experimental system. Neutralizing or deleting Lymphotoxin-α leads to another drawback as both methods target Lymphotoxin-α derived from immune cells as well[443,444]. Thus, even if these methods would show that Lymphotoxin-α plays a critical role in this model, a blunted immune system by blocking LTA derived from immune cells would raise questions. Generation of *Lta*$^{fl/fl}$ mice and crossing this mouse line to *Xbp1*$^{IEC\text{-}KO}$ *Casp8*$^{IEC\text{-}KO}$ *Tnf*$^{IEC\text{-}KO}$ mice would be the best yet challenging solution.

One report demonstrated that L929 cells are capable of undergoing chemically induced ER-stress-mediated necroptosis[445]. Whereas depleting TNFR1 by siRNA-mediated knock-down strategy in L929 cells strongly suppressed necroptosis, neither knock-down of TNF nor Lymphotoxin-α in L929 cells reduced cell death levels, suggesting ER-stress induces TNFR1-dependent but ligand-independent necroptosis. Whereas brefeldin-A was utilized to induce ER stress in cells, which is a compound leading to the accumulation of proteins in ER by preventing them from being transported to Golgi[446], we achieved ER stress by deleting XBP1, inducing ER-Stress by inhibition of XBP1s-mediated UPR.

Therefore, it is unclear whether their interpretation and hypothesis could be translated into our study.

3.4 Effect of epithelial-specific XBP1 on ileitis in *Casp8*$^{IEC-KO}$ and *Fadd*$^{IEC-KO}$ mice

In our study, we did not observe a profound ileitis in mice lacking XBP1 in IECs, in contrast to the first paper which revealed the critical role of XBP1 in the intestinal inflammation[323]. A further study by the same group reported that the extent of ileal pathology in these mice showed variability when they were raised in different animal facilities, showing the effect of microbiota on the development of ileal pathology in the XBP1 model[162]. Therefore, the differential composition of microbiota could explain why *Xbp1*$^{IEC-KO}$ mice generated in our animal facility do not develop extensive enteritis. In addition, it has been known that the same genetic alteration in mice with different genetic backgrounds can result in disparate phenotypes[447,448]. Whereas in our study *Xbp1*$^{IEC-KO}$ mice are C57BL/6N, the first report defining the role of XBP1 in enteritis and IBD utilized mice with 129;C57BL/6N;balb/c backgrounds[323]. Therefore, the difference in genetic background could also explain why *Xbp1*$^{IEC-KO}$ mice generated in our study do not show profound inflammation in the intestine. Meanwhile, a study showed that mice with IEC-specific XBP1 deficiency have an increased number of Immunoglobulin A-positive (IgA^{+}) Plasma cells in Lamina propria and elevated levels of total IgA in ilea[449]. As we assessed intestinal inflammation by performing blind histopathological scoring and immunostaining for CD45-positive cells, we might have missed the surge in IgA-positive B-cells in the mucosa. To comprehensively investigate inflammation depth in the ilea of *Xbp1*$^{IEC-KO}$ mice, immune cells from lamina propria could be isolated and analysed by flow cytometry.

Mice lacking caspase-8 or FADD do develop necroptosis-induced ileitis independent of microbiota[309,312]. In our study, we detected spontaneous terminal ileitis with an increased number of dying IECs and severe Paneth cell loss. Importantly, combined deficiency of XBP1 and Casp8 or XBP1 and FADD did not lead to more severe ileitis compared to their respective single knockouts. These results show that XBP1 deletion-induced ER stress and necroptosis pathways do not interact in the ileum as we discussed our proposed mechanism above (Section 3.1).

Immunostaining with antibodies raised against Lysozyme and Pro-cryptdin revealed that mice lacking XBP1 in IECs have almost no Paneth Cells[323]. Electron microscopy was employed in the same study, and results showed the presence of a few Paneth cells with perturbated ER and store granules. In a follow-up study, the same groups generated mice (C57BL/6N background) lacking XBP1 specifically in Paneth cells (*Xbp1*$^{fl/fl}$ x *D6-Cre*), and these mice showed severe structural defects in Paneth cells including the reduction in number and density of the secretory granules[162]. In line with these, immunostaining as well as RNA expression analysis in our study demonstrated that Paneth cells were severely affected without complete loss. Importantly, Paneth cell impairment was not rescued by combined inhibition of extrinsic apoptosis and necroptosis. Furthermore, we failed to detect increased numbers of IECs positively stained for cleaved caspase-3 and TUNEL in small intestines of *Xbp1*$^{IEC\text{-}KO}$ mice, *Xbp1*$^{IEC\text{-}KO}$ *Casp8*$^{IEC\text{-}KO}$ *Ripk3*$^{-/-}$ and *Xbp1*$^{IEC\text{-}KO}$ *Casp8*$^{IEC\text{-}KO}$ *Mlkl*$^{-/-}$ mice. Therefore, it is plausible to suggest that XBP1-deletion causes structural defects in Paneth cells without inducing cell death.

Xbp1$^{IEC\text{-}KO}$ mice show hyperplasia in the small intestine[162,323,419,449]. It was shown that hyperplastic small intestinal epithelium in *Xbp1*$^{IEC\text{-}KO}$ mice is independent of IRE1α and JNK pathway[419]. Paneth cells play a critical role in the replenishment of intestinal epithelium by secreting WNT, EGF and NOTCH ligands including WNT11[238]. XBP1 ablation leads to increased *Wnt11* expression in the ileum, and it was suggested to drive epithelial regenerative responses in *Xbp1*$^{IEC\text{-}KO}$ mice[419]. In our study, we provide evidence that FADD-caspase-8-mediated apoptosis and RIPK3-MLKL-dependent necroptosis do not contribute to small intestinal hyperplasia in mice lacking XBP1.

Here we revealed that neither TNF nor TNFR1 in IECs plays a critical role in small intestinal pathology in mice lacking both XBP1 and caspase-8. These results are consistent with the previous publication, demonstrating TNFR1 does not contribute to ileal pathology in *Casp8*$^{IEC\text{-}KO}$ mice[307].

4. Concluding Remarks

This study reveals the previously unidentified role of XBP1-mediated UPR in intestinal epithelium suppressing necroptosis-induced colon inflammation. Genetic susceptibility including the interaction of multiple genes is thought to be an important contributor to the predisposition to IBD[328]. Hypomorphic mutations in *XBP1* gene[323] are identified in IBD patients, and the humans deficient in CASP8[303] show intestinal inflammation. In the case of identification of patients harbouring mutations in both *XBP1* and *CASP8* (or other proteins regulating the cell death pathways) genes, our data could be an important to understand and untangle the intricate cross-talk between UPR and cell death in intestinal inflammatory diseases. Moreover, the data in this thesis suggest that the defective mucus layer is the culprit of exacerbated colitis upon XBP1 deficiency. In the translational aspect, this work can provide pivotal insights into the mucus layer regulating the inflammation in the intestine as the mucus layer is found to be perturbated in ulcerative colitis patients[378]. Further investigations on how precisely XBP1 deficiency dampens mucin production would be critical for the development and utilization of new therapies reinforcing mucus layer in IBD patients.

5. Materials and Methods

5.1 Materials

5.1.1 Antibodies, chemicals, commercial kits and equipment

The following materials were employed in this study:

REAGENT	SOURCE	Catalog Number/IDENTIFIER
Antibodies		
Anti-CD45	Thermo Fisher Scientific	Cat# 14-0451-82, RRID: AB_467251
Anti-cleaved-Caspase-3	Cell Signaling Technology	Cat# 9661, RRID: AB_2341188
Anti-Lysozyme	Dako	Cat# F0372
Anti-Ki67	Abcam	Cat# ab15580, RRID: AB_443209
Anti-MUC2	Abcam	Cat# ab272692, RRID: AB_2888616
Anti-ZG16	Abcam	Cat# ab185483
Anti-IRE1 (pS724)	Abcam	Cat# ab48187, RRID:AB_873899
Anti-Rabbit-IgG (H+L), Biotin-XX	Thermo Fisher Scientific	Cat# B-2770, RRID: AB_2536431
Anti-Rat IgG (H+L), DSB-X Biotin	Thermo Fisher Scientific	Cat# D-20697, RRID: AB_2536518

Chemicals, proteins, Oligonucleotides		
Ulex Europaeus Agglutinin I (UEA I), Biotinylated	Vector Laboratories	Cat# B-1065, RRID: AB_2336766
Streptavidin, Alexa Fluor™ 488	Thermo Fisher Scientific	Cat# S11223
ReadyProbes™ In Situ Hybridization (ISH) Blocking Solution (5x)	Thermo Fisher Scientific	Cat# R37620
3dGRO® Wnt3a Conditioned Media Supplement	Sigma-Aldrich	Cat# SCM112
Matrigel® Growth Factor Reduced (GFR) Basement Membrane Matrix	Corning	Cat# 354230
DMEM/F-12 with 15 mM HEPES	StemCell	Cat# 36254
Y-27632 (Dihydrochloride)	StemCell	Cat# 72304
DAPT	StemCell	Cat# 72082
Trypsin-EDTA (0.05%), phenol red	Thermo Fisher Scientific	Cat# 25300054

SuperBlock™ T20 (TBS) Blocking-Buffer	Thermo Fisher Scientific	Cat# 37536
ProLong™ Diamond Antifade Mountant with DAPI	Thermo Fisher Scientific	Cat# P36962
Methanol, 99.9%, Extra Dry	Thermo Fisher Scientific	Cat# 326950010
Chloroform 99.0-99.4%	AnalaR NORMAPUR ACS	Cat# 22711290
Acetic acid, glacial 99.7+%	Thermo Fisher Scientific	Cat# 36289.AP
EUB338: 5TexRd-XN/GCTGCCTCCCGTAGGAGT	IDT	
Non-EUB338: 5TexRd-XN/ACTCCTACGGGAGGCAGC	IDT	
Höchst 3342	Invitrogen	H3570
TaqMan Probes		
Muc2	Thermo Fisher Scientific	Assay ID: Mm01276696_m1
Defars10	Thermo Fisher Scientific	Assay ID: Mm00833275_g1

Defa5	Thermo Fisher Scientific	Assay ID: Mm00651548_g1
Lyz1	Thermo Fisher Scientific	Assay ID: Mm00657323_m1
Zg16	Thermo Fisher Scientific	Assay ID: Mm00459035_m1
Tff3	Thermo Fisher Scientific	Assay ID: Mm00495590_m1
Ccl2	Thermo Fisher Scientific	Assay ID: Mm00441242_m1
Cxcl1	Thermo Fisher Scientific	Assay ID: Mm00445235_m1
Il1b	Thermo Fisher Scientific	Assay ID: Mm00434228_m1
Atoh1	Thermo Fisher Scientific	Assay ID: Mm00476035_s1
Klf4	Thermo Fisher Scientific	Assay ID: Mm00516104_m1
Spdef	Thermo Fisher Scientific	Assay ID: Mm00600221_m1
Tbp	Thermo Fisher Scientific	Assay ID: Mm00446973_m1
Commercial kits		
Streptavidin/Biotin Blocking Kit	Vector Laboratories	Cat# SP-2002
Lectin Kit I, Biotinylated	Vector Laboratories	Cat# BK-1000

ABC-HRP Kit, Peroxidase (Standard)	Vector Laboratories	Cat# PK-6100
DAB Substrate Kit	Abcam	Cat# ab64238
TrueVIEW® Autofluorescence Quenching Kit	Vector Laboratories	Cat# SP-8500-15
Alcian Blue PAS Stain Kit	Abcam	Cat# ab245876
TUNEL Assay Kit	Abcam	Cat# ab206386
IntestiCult™ Organoid Growth Medium	StemCell	Cat#06005
Direct-zol RNA Miniprep Kit	Zymo research	R2050
Equipment		
Tissue retriever 2100	PickCell	
Tissue processor	Leica	TP1020
Rotary Microtome	Leica	RM2255
Modular tissue embedding centre	Leica	EG1150C

LSM980 Airyscan 2	Carl Zeiss	

Table 5-1. Antibodies, chemicals, commercial kits, and equipment used in this thesis.

5.1.2 Buffers and solutions

Tail Lysis Buffer: Tris-HCl (pH 8.5) [100 mM], EDTA [5 mM], NaCl [200 mM], SDS 0.2% (w/v)

TE Buffer: Tris-HCl (pH 8) 10 mM, EDTA (pH 8) 1 mM

10X TBS: 200 mM Tris and 1500 mM NaCl, pH 7.6 at room temperature.

TBS-T: 1X TBS supplemented with 0.05% Tween-20

Carnoy's fixative: 60% (v/v) Extra Dry Methanol, 30% (v/v) Chloroform, 10% (v/v) Glacial Acetic Acid

Peroxidase blocking buffer: 0.04 M Sodium Citrate, 0.121 M Na_2HPO_2, 0.03M NaN_3, 3% H_2O_2

TEX-buffer: 50 mM Tris, 1 mM EDTA, 0.5 % Triton X-100, pH 8.0

FISH hybridization solution: 20 mM Tris-HCl, pH 7.4; 0.9 M NaCl; 0.1% (w/v); Sodium Dodecylsulfate (SDS) in nuclease-free water

FISH washing buffer: 20 mM Tris-HCl, pH 7.4; 0.9 M NaCl; 0.1% (w/v)

Colonic crypt isolation Buffer: Na_2HPO_4 [5.6 mM], KH_2PO_4 [8mM], NaCl [96 mM], KCl [1.6 mM], Sucrose [44 mM], D-sorbitol [54.8 mM], DL-dithiothreitol [0.5 mM], EDTA [5 mM]

5.1.3 Software

Endnote 20.6 was employed to cite the previous studies that provided scientific information. Microsoft Office programs including Word, Excel and Power Point were

utilized for writing and arrangement of acquired experimental data. OMERO was used to prepare histological figures. Prism GraphPad was utilized to construct graphs and perform statistical analysis.

5.2 Methods

5.2.1 Animal Experiments

All mice lines were kept in pathogen-specific-free (SPF) conditions, which were regularly screened by the CECAD animal facility, Institute for Genetics, University of Cologne. Mice were kept 1-5 mice per cage, which were individually ventilated. Depending on the cage space availability, female mice were pooled in the same cages without any other parameter. All mice lived at 22-24°C under 12 hours of light and dark conditions with water and food, *ad libitum*.

All mice breedings and sacrificing were approved by local federal authorities (Landesamt für Natur, Umwelt und Verbrauchschutz, NRW, Germany). All of the performed animal experiments followed the rules and instructions of European, national and local guidelines. Except for the animals in need of medical examination, no mice were excluded from the study.

The generation of the following mice was already described: *Casp8*$^{fl/fl}$ [337], *Fadd*$^{fl/fl}$ [450], *Villin*-cre [331], *Tnfr1*$^{fl/fl}$ [351], *Tnf*$^{fl/fl}$ [350], *Mlkl*$^{-/-}$ [343] and *Ripk3*$^{-/-}$ [341]. *Xbp1*$^{tm1a(EUCOMM)Wtsi}$ mice were crossed to mice carrying *FLPe-Deleter* [451], leading to the generation of *Xbp1*$^{fl/fl}$ mice without FRT-flanking cassette. To generate *Xbp1*$^{IEC\text{-}KO}$ mice, *Xbp1*$^{fl/fl}$ mice were crossed to mice carrying P1 bacteriophage cyclization recombination (*Cre*) under *Villin-1* [331] promoter.

5.2.1.1 Tissue preparation

After the mice were euthanised by cervical dislocation, mice weights were assessed and opened longitudinally. The intestinal fragments were excised and placed into ice-cold PBS until the histology was performed. For mucus layer-associated studies, the pieces were not put into PBS, and the subsequent steps were directly performed.

2-3 mm pieces of intestine from each mouse were excised before performing histological analysis. The pieces were directly frozen by liquid nitrogen and kept at -80°C until RNA extractions were performed.

5.2.1.2 Blood Analysis

After the euthanasia, mice were quickly opened longitudinally. 100 µl peripheral blood was collected from the left ventricle and directly put into tubes containing EDTA. The collected peripheral blood was analysed by the Abacus Junior Vet Analyser machine according to the manufacturer's guidelines.

5.2.2 Histology

5.2.2.1 Intestinal Swiss roll and histology assessment

The intestinal pieces were cleared from surrounding fat tissues. They were opened longitudinally, and luminal content was cleaned by PBS. By using needles, the intestines were Swiss rolled and then rolled pieces were put into histology cassettes to fix in 4% paraformaldehyde at 4°C for 18-20 hours. The histology cassettes were subjected to gradually increasing ethanol concentrations (30-50-70-96-100% (v/v)) for 2 hours each, followed by incubation in xylol for 2 hours. Then, cassettes were put into liquified paraffin, followed by the embedding procedure.

The sections with 3 µm thickness were hydrated: in Xylol for 20 minutes, in 100-96-75% (v/v) ethanol gradient for 2 minutes for each, followed by incubation in water for 5 min. The slides were visualised by Haematoxylin staining for 1 minute, followed by incubation in tap water for 15-20 minutes. Then, the slides were further stained with Eosin for 1 minute. Then, the sections were dehydrated by increasing the ethanol gradient 75-96-100% (v/v) for 1 minute for each and 1 minute in Xylol incubation. Then, coverslips were mounted by utilizing Entellan.

H&E-stained sections were assessed blindly. The assessment was based on four main parameters: crypt hyperplasia, epithelial injury, IEC death and intestinal inflammation. Each section was divided into 4 areas. These areas were random and had a score spectrum between 0 and 4. Thus, for each parameter, one section can get 16 points, hypothetically. In total, the maximum hypothetical score for a section was 64. Hyperplasia

was assessed based on the ratio of crypt to villi in the small intestine, and length of the crypt region in the colon. The severity of the epithelial injury was decided based on the integrity of the intestinal barrier where the highest damage was ulcer formation. Based on the amount of dying cells in the crypt region, IEC death was assessed. The severity of inflammation was based on the amount of the infiltrated immune cells as well as their localization (mucosa-submucosa-serosa).

5.2.2.2 Immunohistochemistry and Immunofluorescence

3 µm thick intestinal sections were rehydrated: Xylol for 20 minutes, in 100-96-75% (v/v) ethanol gradient for 2 minutes for each, followed by incubation in TBS for 5 minutes (Section 5.1.2). To block endogenous peroxidase, sections were incubated with 1X Peroxidase Blocking Buffer (Section 5.1.2) for 10 minutes. After washing with TBS 3 times for 5 minutes, Antigen retrieval was performed. Depending on different antibodies, different buffer was employed. (CD45 IHC: Proteinase K in TEX Buffer (Section 5.1.2); Ki67, ZG16, cleaved caspase-3 IHC: Citrate Buffer (Section 5.1.2); MUC2 IHC: Tris-EDTA Buffer (Section 5.1.2).). Except for proteinase K-mediated antigen retrieval, antigen retrieval was performed with the corresponding buffers in the pressure cooker for 20 minutes. The sections were allowed to cool down and washed with TBS-T (Section 5.1.2). To block endogenous proteins and biotin, sections were incubated with commercial blocking Buffer supplemented with 0.3% Triton-X and 1:100 diluted avidin from Avidin/Biotin blocking kit (Vector labs) for 1 hour. After the blocking, the sections were briefly washed with the TBS-T and incubated with primary antibodies (All antibodies except MUC2 were diluted 1:1000 in Commercial blocking Buffer (Thermo Scientific); the dilution of MUC2 was 1:5000) for 16-18 hours at 4°C. Excess primary antibodies were washed away by TBS-T washing step 3 times for 5 minutes each. Then, the sections were incubated with secondary antibodies diluted in commercial blocking buffer (Thermo Scientific) for 1 hour (Secondary antibodies were diluted 1:1000. Secondary antibody for CD45: Anti-Rat IgG (H+L), DSB-X Biotin; for other stainings: Anti-Rabbit IgG (H+L), DSB-X Biotin were used (Table 5-1).). After washing with TBS-T, the sections were incubated with Avidin-Biotin-HRP complex (Vector Labs) for 1 hour at room temperature. The sections were washed and visualized by the DAB substrate kit (Abcam). The visualizations were examined under a microscope and were halted upon the sufficient signal intensity was reached. To stop the DAB reaction, the sections were washed in tap water. To

perform the counterstaining, nuclei were stained with Haematoxylin for 5-30 seconds. After 15 minutes of water incubation, the sections were dehydrated and mounted with Entellan.

To detect bacterial translocation into the sublayers of colon, the sections with 3 µm thickness were employed. After the rehydration, the sections were incubated with 0.5 µg EUB338 or non-specific probes (Table 5-1), dissolved in FISH hybridization solution (Section 5.1.2) at 50°C for 3 hours. After washing with FISH washing solution, the sections were quenched for the non-specific signal by using commercial kit TrueVIEW® Autofluorescence Quenching Kit (Vector Labs), (Table 5-1). After washing with TBS, the nuclei staining was enhanced by using Höchst 3342 (Invitrogen, H3570) in TBS. Then, the sections were mounted with ProLong™ Diamond Antifade Mountant (Invitrogen). Representative images were taken using LSM980 Airyscan 2 (Carl Zeiss).

5.2.2.3 Mucus Layer staining and FISH

The most distal colon pieces containing faecal material were carefully excised from the rest of the colon and directly fixed in Carnoy's fixative (Section 5.1.2). After 1 week of fixation at 4°C, the pieces were put into the histology cassettes and washed with dry methanol (Table 5-1) 2 times for 30 minutes each. Then, tissues were incubated in absolute ethanol two times for 20 minutes each. Tissues were cleared by xylene incubation two times for 15 minutes each. After tissues were exposed to paraffin for 15 minutes, they were embedded. The sections were cut for 5 µm thickness. Alcian Blue-PAS, lectin stainings and FISH. Note that Alcian Blue-PAS staining was also performed on the 3 µm thick sections with the exact protocol described below.

The sections were rehydrated as described above. To perform Alcian Blue-PAS staining, the commercially available kit was employed (Table 5-1). The sections were incubated with 3% Acetic acid for 2 minutes. Excess Acetic Acid was removed, and sections were incubated with Alcian Blue for 3-5 minutes. The sections were washed with tap water 2 times for 5 minutes and incubated with Periodic acid for 5 minutes. After washing with tap water, Schiff's solution was applied on the sections for 2-5 minutes. To get rid of excess staining, the sections were washed under the running tap water, followed by Haematoxylin staining for 5-30 seconds. Sections were dehydrated and mounted with Entellan as described above.

To perform FISH, the sections were deparaffinized by pre-warmed Xylene (60°C) for 10 minutes. The slides were incubated in absolute ethanol for 5 min. The sections were incubated with either 0.5 μg EUB338 or non-specific probes (Table 5-1) prepared in FISH hybridization solution (Section 5.1.2) at 50°C for 3 hours. After hybridization, the excess oligomers were washed with FISH washing solution (Section 5.1.2) at 50°C for 5 minutes. Then, the sections were incubated with Biotinylated *Ulex europaeus* agglutinin I (UEA-I) (Vector Labs) (1:1000 dilution in TBS (Section 5.1.2) at room temperature for 1 hour. The excess UEA-I was washed with TBS, followed by the secondary antibody incubation, Streptavidin-Alexa Fluor™ 488 conjugate (Invitrogen) at room temperature for 1 hour. The sections were washed and mounted with ProLong™ Diamond Antifade Mountant (Invitrogen). The mouting step was at room temperature in the dark for 16-18 hours. Analysis and representative picture acquisition were performed by utilization of LSM980 Airyscan 2 (Carl Zeiss).

5.2.3 Molecular Biology

5.2.3.1 Isolation of Genomic DNA and genotyping PCR

Tail biopsies from 2-3 weeks old mice were first lysed in 100-200µl lysis buffer (Section 5.1.2) supplemented with proteinase K at 54°C (10mg/ml for 16 hours or 50mg/ml for 1-2 hours.). To precipitate the genomic DNA, 100-200µl of isopropanol was added, and samples were centrifuged at the highest speed for 1 minutes. Supernatants were carefully discarded, and pellets were washed with 70% ethanol (v/v), followed by the highest speed for 1 minutes. After ethanol was discarded, pellets were incubated at room temperate until they were dry. Genomic DNAs were suspended in TE buffer (Section 5.1.2).

Each PCR is composed of 12.5µl Master Mix (VWR), 2µl (3µM) of primer mix (Table 5-2), 10µl of molecular grade water. The PCRs were performed depending on the conditions of each primer sets (Table 5-2). After PCRs were complete, the products were resolved in agarose gels. Agarose gels were made by adding 2% agarose (w/v) in 1X TAE buffer (section 5.1.2) and boiling them. To visualize DNAs, 0.5mg/ml Ethidium bromide was added before pouring gels. Gels were run for 1-2 hours at 120-140 mV.

PCR	**Primer Sequences (5'-3')**	**Expected Band sizes**
Villin Cre	P1: ACAGGCACTAAGGGAGCCAATG P2: ATTGCAGGTCAGAAAGAGGTCACAG P3: GTTCTTGCGAACCTCATCACTC	Transgenic: 350 base pairs WT: 900 base pairs
Xbp1	P1: CGGATATCGCTCTAGCAAGG P2: TACAGAGGGTGGGAGGATTG	Flx: 950 base pairs WT: 740 base pairs Deletion: 316 base pairs
Casp8	P1: TCCTGTACCATATCTGCCTGAACGCT P2: ATAATTCCCCCAAATCCTCGCATC	Flx: 656 base pairs WT: 750 base pairs Deletion: 200 base pairs
Fadd	P1: CACCGTTGCTCTTTGTCTAC P2: GTAATCTCTGTAGGGAGCCCT P3: AAGGCATCAGCAAGAGCAGT	Flx: 206 base pairs WT: 280 base pairs Deletion: 380 base pairs
Ripk3	P1: CGCTTTAGAAGCCTTCAGGTTGAC P2: GCCTGCCCATCAGCAACTC P3: CCAGAGGCCACTTGTGTAGCG	WT: 485 base pairs Deletion: 320 base pairs
Mlkl	P1: CATCAAGTTAGGCCAGCTCA P2: TCTGCTGGTTAGCCTCCTTC	WT: 204 base pairs

		Deletion: 173 base pairs
Tnfr1	P1: CAAGTGCTTGGGGTTCAGGG P2: CGTCCTGGAGAAAGGGAAAG	Flx: 195 base pairs WT: 134 base pairs
Tnf	P1: TGAGTCTGTCTTAACTAACC P2: GAAATCTTACCTACGACGTG P3: CTCTTAAGACCCACTTGCTC	Flx: 400 base pairs WT: 350 base pairs Deletion: 450 base pairs

Table 5-2 Genotyping PCR primers and the expected band sizes of the genotyping PCRs.

The following PCR programs were used:

Villin Cre: Initiation 94°C for 3 minutes; denaturing 94°C for 60 seconds; annealing 67°C for 60 seconds; elongation 72°C for 60 seconds for 35 cycles. Final elongation at 72°C for 5 minutes.

Xbp1: Initiation 95°C for 10 minutes; denaturing 94°C for 30 seconds; annealing 60°C for 30 seconds; elongation 72°C for 40 seconds for 40 cycles. Final elongation at 72°C for 5 minutes.

Casp8: Initiation 95°C for 3 minutes; denaturing 94°C for 30 seconds; annealing 62°C for 30 seconds; elongation 72°C for 30 seconds for 30 cycles. Final elongation at 72°C for 5 minutes.

Fadd: Initiation 94°C for 3 minutes; denaturing 94°C for 30 seconds; annealing 60°C for 45 seconds; elongation 72°C for 30 seconds for 35 cycles. Final elongation at 72°C for 3 minutes.

Ripk3: Initiation 94°C for 4 minutes; denaturing 94°C for 60 seconds; annealing 60°C for 30 seconds; elongation 72°C for 60 seconds for 30 cycles. Final elongation at 72°C for 10 minutes.

Mlkl: Initiation 94°C for 3 minutes; denaturing 94°C for 30 seconds; annealing 58°C for 30 seconds; elongation 72°C for 60 seconds for 35 cycles. Final elongation at 72°C for 3 minutes.

Tnfr1: Initiation 94°C for 3 minutes; denaturing 94°C for 30 seconds; annealing 60°C for 60 seconds; elongation 72°C for 60 seconds for 29 cycles. Final elongation at 72°C for 5 minutes.

Tnf: Initiation 94°C for 3 minutes; denaturing 94°C for 30 seconds; annealing 60°C for 45 seconds; elongation 72°C for 45 seconds for 35 cycles. Final elongation at 72°C for 5 minutes.

5.2.3.2 mRNA expression experiments

5.2.3.2.1 RNA isolation, cDNA synthesis and gene expression analysis by quantitative RT-PCR

Pieces from small intestine or colon were snap frozen in liquid nitrogen and stored at -80°C until they were used. Tissues were first homogenized by employing Precellys24 system. After samples were lysed in RNAzol® RT (Sigma-Aldrich, R4533), RNAs were purified with Direct-zol RNA Miniprep Kit (Zymo research, R2050) according to manufacturer's guidelines. cDNAs were synthesized from 1 µg of template RNA in 20µl volume of reaction by using LunaScript® RT SuperMix Kit (New England Biolabs, E3010).

After cDNAs were diluted 4 times with Nuclease free water, quantitative RT-PCR were done by using TaqMan probes and Luna Universal Probe qPCR Master Mix (New England Biolabs, M3004X) in a QuantStudio 5 Real-Time PCR System (ABI). Each reaction composed of 8

TaqMan probes in this study were purchased from Thermo Fisher Scientific: Muc2 (Mm01276696_m1), Defars10 (Mm00833275_g1), Defa5 (Mm00651548_g1), Lyz1 (Mm00657323_m1), Zg16 (Mm00459035_m1), Tff3 (Mm00495590_m1), Ccl2

(Mm00441242_m1), Cxcl1 (Mm00445235_m1), Il1b (Mm00434228_m1), Tbp (Mm00446973_m1).

5.2.3.2.2 3'mRNA sequencing

After total RNA was extracted as described above, 2µg total RNAs that met the following parameters were used for 3'mRNA sequencing: OD260/280 = 1.8-2.1, OD260/230 > 1.5 and RIN > 7.

As Ulrike Göbel performed the rest of the procedure, it was described by Ulrike Göbel:

''The library preparation was performed using the QuantSeq 3′ mRNA-Seq Library Prep Kit FWD for Illumina (Lexogen). Single-end RNA-seq reads were produced by the Lexogen QuantSeq FWD protocol and sequenced on a NovaSeq 6000 instrument. Reads of the same sample sequenced on different lanes of the instrument were merged without correction for a batch effect. The Illumina TruSeq adapter and poly-A runs of length ³ 18 were removed from the sequenced reads using cutadapt version 3.2. Reads were aligned against Mus_musculus GRCm38 (Ensembl v100) plus the ERCC92 spike-in sequences. The subread suite of programs [452] version 2.0.1 was used to produce a table of read counts per gene, with Ensembl Mus_musculus.GRCm38.100.gtf as the genome annotation. Parameters for subread-align were -t 0 --multiMapping -B 5 –sortReadsByCoordinates. Parameters for featureCounts were -F "GTF" -t "exon" -g "gene_id" --minOverlap 20 -M --primary -O --fraction -J -Q 30. Differential gene expression and Gene Ontology over-representation analyses were performed within the R programming environment version 4.0.0, using packages of the Bioconductor system [453] version 3.11. The initial set of 55579 genes was reduced to 15458 genes by the filter function of the Bioconductor package edgeR [454] version 3.30.3, with default parameters. DESeq2 [455] version 1.28.1 was subsequently run on the filtered count table. The raw log2 fold changes from this analysis were "shrunken" using the apeglm method [456] provided with the DESeq2 package. (Shrinkage pushes the log2 fold changes of highly variable genes towards zero.) Normalized read counts were generated by DESeq2's "counts" function with the parameter "normalized=TRUE". This function divides the raw counts by sample-specific size factors, thereby correcting for sample-specific library sizes. Variance stabilized counts on the log scale for use in heatmaps were generated by the "rlog" function of DESeq2 with parameter blind=FALSE. For Gene Ontology over-representation analysis (ORA), genes with a DESeq2 adjusted p-value < 0.05 and an absolute value of the shrunken log2 fold change > log2(1.5) were selected and divided into an up-regulated and a down-regulated set. Both sets were separately used to query the Biological Process, Molecular Function, and Cellular Component sections of the Gene Ontology database, as provided by the Bioconductor annotation package

org.Mm.eg.db version 3.12.0 The enrichGO function of the clusterProfiler [457] version 3.16.1, which is provided with Bioconductor, was used for the queries. All visualizations (heatmaps, volcano plots and Gene Ontology concept networks ("emapplots")) were prepared in R-4.1.0, using Bioconductor version 3.14, for reasons of better graphics quality. Heatmaps of z-score-normalized rlog values were drawn using the Bioconductor package ComplexHeatmap [458] version 2.10.0. All heatmaps were restricted to genes with a DESeq2 adjusted p-value < 0.05 and an absolute value of the shrunken log2 fold change > log2(1.5) in the contrast *Xbp1*$^{IEC\text{-}KO}$ *Casp8*$^{IEC\text{-}KO}$ versus control. Note that rlog values were computed on the full matrix, before extracting the sub-matrix containing the genes of interest. ORA results were visualized as concept networks ("emapplots"), using the enrichplot package version 1.14.1, which is part of clusterProfiler.''

5.2.3.3 XBP1 splicing Assay

After total RNAs were extracted and cDNA synthesis was performed from colon organoids, 1μl of undiluted cDNA was used for the reaction. Each PCR is composed of 12.5μl Master Mix (VWR), 2μl (3μM) of XBP1 splicing primer mix: (Primer 1: ACACGCTTGGGAATGGACAC; Primer 2: CCATGGGAAGATGTTCTGGG; 5' to 3'), 10μl of molecular grade water. Then, the following PCR program was used: Initiation 94°C for 2 minutes; denaturing 94°C for 30 seconds; annealing 60°C for 30 seconds; elongation 72°C for 30 seconds. The cycle was done for 35 times, followed by final elongation at 72°C for 2 minutes. PCR products were resolved on 2% (v/w) agarose gel. Expected band sizes were: XBP1 unspliced: 171 base pairs, XBP1 spliced:145 base pairs.

5.2.4 Cell Culture

5.2.4.1 Isolation of Colonic Crypts and Colon organoid culture

Mice were sacrificed, and their colon tissues were harvested carefully. The colon tissues were opened longitudinally, and the luminal content was cleaned in ice-cold dPBS two times. Then, samples were cut into small pieces (2-5 mm), which were collected in ice-cold dPBS in 50 ml tubes. The rest of the steps were performed in cell culture. Colon pieces were allowed to settle down and the dPBS as supernatants were disposed by serological pipets. Then, fresh 10ml ice-cold dPBS was put into the tubes containing pieces. Pieces were washed gently by performing 'up-down' with serological pipets 5

times. After the pieces settled down, supernatant dPBS were discarded. This step was performed 15-20 times depending on the samples until the supernatant looked clear. To isolate crypts, colon pieces were put into 20 ml of ice-cold colonic isolation buffer (Section 5.1.2) and incubated on a rocker at 4°C for 1 hour. After the incubation, the colon pieces were allowed to settle down, and the supernatants were discarded. Pieces were suspended in 10 ml ice-cold dBPS containing 10% FCS. After the colon pieces in solution were pipetted up and down 3-4 times with a serological pipet, the pieces were allowed to settle down and supernatants were collected and filtered by 70μM filter into 50ml falcon. This first collection was labelled as 'Fraction-1' and put on ice. Then, the colon pieces were suspended in 10ml of dBPS with 10% FCS again, and the whole step was repeated 3-5 times, depending on the amount of the crypts recovered (visually assessed by the cloudiness of the solution). The collected fractions were centrifuged at 150 x *g* for 5 minutes at 4°C. Supernatants were discarded and resuspended in 5 ml DMEM/F-12 with 15 mM HEPES. From each fraction, 1 ml was put into 6-well plates and assessed under the microscope. The fractions of the same mouse containing less than 50 crypts were pooled. Then the fractions were transferred into 15 ml falcons and centrifuged at 100 x *g* for 5 minutes at 4°C. After centrifugation, the isolated crypts were resuspended in room temperature IntestiCult™ Organoid Growth Medium (StemCell) which was supplemented with Wnt3a conditioned medium (Sigma-Aldrich) (For each 10 ml of IntestiCult™ Organoid Growth Medium, 2.4 ml Wnt3a conditioned medium was added). Then, crypts were mixed with ice-cold Matrigel (Corning) at a 1:1.5 ratio and directly seeded on 48 well or 6-well plates (Each drop consisted of 20μl of crypt. Each well from 48-well had one drop, while 6-well had 10-12 drops). Then, to form domes and prevent crypts from sedimenting to the bottom of the plates, the plates were inverted and incubated within the sterile hood for 2-5 minutes. After the incubation, the plates were incubated inside the incubators for 30 minutes at 37°C. For 48-well 250μl, for 6-well plate 20ml of IntestiCult™ Organoid Growth Medium was put. To prevent anoikis, the media were supplemented with 10μM Y-27632-Dihydrochloride (StemCell) for the first and second days of incubation after the isolation. Every two to three days, the media was replenished without Y-27632. Depending on the colonoids conditions (7-11 days), passaging was performed. Briefly, the media was discarded and 1 ml of ice-cold DMEM/F-12 with 15 mM HEPES (2 ml for the 6-well plate) was put on the top of the domes. Then, plates were put on the ice and incubated for 5-10 minutes. Then, the domes were scraped from plates by micropipette while performing up-down for DMEM. Organoids were collected in 15 ml tubes and centrifuged at 100 x *g* for 5 min. The supernatants were discarded carefully, and the pellets were resuspended in 2

ml of Trypsin-EDTA (0.05%), phenol red (Thermo Fisher Scientific). The tubes were incubated at 37°C for 10 minutes. After the incubation, suspensions were mixed thoroughly with a micropipette. To the stop dissociation reaction by Trypsin-EDTA, 5 ml of ice-cold dBPS containing 10% FCS was added. The tubes were centrifuged at 100 x *g* for 5 min at 4°C. The supernatants were discarded, and the pellets were dissolved in IntestiCult™ Organoid Growth Medium. The rest of the procedure was similar to that described above.

5.2.4.2 Differentiation of Colon Organoids into Goblet cells and RNA isolation

To perform the differentiation of colon organoids into Goblet cells, the organoid culture was expanded. Therefore, the following procedure was performed in colonoids after the second or third passages. After 24 hours of passaging, the media of colonoids were replaced by media containing DMSO (1:1000) or DAPT (10μM) or G03089668 (10μM, Genentech, this compound was only used for XBP1 splicing assay in this thesis.). Every 2-3 days, the media was replenished. On the 6th day of differentiation, the media were discarded, and domes were lysed directly by putting RNAzol® RT (Sigma-Aldrich, 250μl for the 48-well plate, 500μl for the 6-well plate.). The plates were incubated at -80°C until the rest of the procedure was performed. To carry on with the RNA isolation, plates were incubated at room temperature until they were completely liquefied. The solutions were put into 1.5 ml tubes, and proteins were separated by adding molecular-grade water (200μl per 1 ml of RNAzol® RT), followed by centrifugation at 12,000 x *g* for 15 minutes. The supernatants containing total RNAs were collected, and the rest of the procedure was performed as it was described in total RNA isolation (Section 5.2.3.2.1).

6. References

1. Carpenter, S., and O'Neill, L.A.J. (2024). From periphery to center stage: 50 years of advancements in innate immunity. Cell *187*, 2030-2051. 10.1016/j.cell.2024.03.036.

2. Janeway, C.A., Jr. (1989). Approaching the asymptote? Evolution and revolution in immunology. Cold Spring Harb Symp Quant Biol *54 Pt 1*, 1-13. 10.1101/sqb.1989.054.01.003.

3. Lemaitre, B., Nicolas, E., Michaut, L., Reichhart, J.M., and Hoffmann, J.A. (1996). The dorsoventral regulatory gene cassette spatzle/Toll/cactus controls the potent antifungal response in Drosophila adults. Cell *86*, 973-983. 10.1016/s0092-8674(00)80172-5.

4. Medzhitov, R., Preston-Hurlburt, P., and Janeway, C.A., Jr. (1997). A human homologue of the Drosophila Toll protein signals activation of adaptive immunity. Nature *388*, 394-397. 10.1038/41131.

5. Poltorak, A., He, X., Smirnova, I., Liu, M.Y., Van Huffel, C., Du, X., Birdwell, D., Alejos, E., Silva, M., Galanos, C., et al. (1998). Defective LPS signaling in C3H/HeJ and C57BL/10ScCr mice: mutations in Tlr4 gene. Science *282*, 2085-2088. 10.1126/science.282.5396.2085.

6. Hoffman, H.M., Mueller, J.L., Broide, D.H., Wanderer, A.A., and Kolodner, R.D. (2001). Mutation of a new gene encoding a putative pyrin-like protein causes familial cold autoinflammatory syndrome and Muckle-Wells syndrome. Nat Genet *29*, 301-305. 10.1038/ng756.

7. Aksentijevich, I., Nowak, M., Mallah, M., Chae, J.J., Watford, W.T., Hofmann, S.R., Stein, L., Russo, R., Goldsmith, D., Dent, P., et al. (2002). De novo CIAS1 mutations, cytokine activation, and evidence for genetic heterogeneity in patients with neonatal-onset multisystem inflammatory disease (NOMID): a new member of the expanding family of pyrin-associated autoinflammatory diseases. Arthritis Rheum *46*, 3340-3348. 10.1002/art.10688.

8. Martinon, F., Burns, K., and Tschopp, J. (2002). The inflammasome: a molecular platform triggering activation of inflammatory caspases and processing of proIL-beta. Mol Cell *10*, 417-426. 10.1016/s1097-2765(02)00599-3.

9. Akira, S., Uematsu, S., and Takeuchi, O. (2006). Pathogen recognition and innate immunity. Cell *124*, 783-801. 10.1016/j.cell.2006.02.015.

10. Medzhitov, R., Preston-Hurlburt, P., Kopp, E., Stadlen, A., Chen, C., Ghosh, S., and Janeway, C.A., Jr. (1998). MyD88 is an adaptor protein in the hToll/IL-1 receptor family signaling pathways. Mol Cell *2*, 253-258. 10.1016/s1097-2765(00)80136-7.

11. Yamamoto, M., Sato, S., Mori, K., Hoshino, K., Takeuchi, O., Takeda, K., and Akira, S. (2002). Cutting edge: a novel Toll/IL-1 receptor domain-containing adapter that preferentially activates the IFN-beta promoter in the Toll-like receptor signaling. J Immunol *169*, 6668-6672. 10.4049/jimmunol.169.12.6668.

12. Kawai, T., Ikegawa, M., Ori, D., and Akira, S. (2024). Decoding Toll-like receptors: Recent insights and perspectives in innate immunity. Immunity *57*, 649-673. 10.1016/j.immuni.2024.03.004.

13. Watanabe, S., Zenke, K., and Muroi, M. (2023). Lipoteichoic Acid Inhibits Lipopolysaccharide-Induced TLR4 Signaling by Forming an Inactive TLR4/MD-2 Complex Dimer. J Immunol *210*, 1386-1395. 10.4049/jimmunol.2200872.

14. Sahasrabudhe, N.M., Dokter-Fokkens, J., and de Vos, P. (2016). Particulate beta-glucans synergistically activate TLR4 and Dectin-1 in human dendritic cells. Mol Nutr Food Res *60*, 2514-2522. 10.1002/mnfr.201600356.

15. Hoshino, K., Takeuchi, O., Kawai, T., Sanjo, H., Ogawa, T., Takeda, Y., Takeda, K., and Akira, S. (1999). Cutting edge: Toll-like receptor 4 (TLR4)-deficient mice are hyporesponsive to lipopolysaccharide: evidence for TLR4 as the Lps gene product. J Immunol *162*, 3749-3752.

16. Muzio, M., Natoli, G., Saccani, S., Levrero, M., and Mantovani, A. (1998). The human toll signaling pathway: divergence of nuclear factor kappaB and JNK/SAPK activation upstream of tumor necrosis factor receptor-associated factor 6 (TRAF6). J Exp Med *187*, 2097-2101. 10.1084/jem.187.12.2097.

17. Kawai, T., Adachi, O., Ogawa, T., Takeda, K., and Akira, S. (1999). Unresponsiveness of MyD88-deficient mice to endotoxin. Immunity *11*, 115-122. 10.1016/s1074-7613(00)80086-2.

18. Kagan, J.C., and Medzhitov, R. (2006). Phosphoinositide-mediated adaptor recruitment controls Toll-like receptor signaling. Cell *125*, 943-955. 10.1016/j.cell.2006.03.047.

19. Motshwene, P.G., Moncrieffe, M.C., Grossmann, J.G., Kao, C., Ayaluru, M., Sandercock, A.M., Robinson, C.V., Latz, E., and Gay, N.J. (2009). An oligomeric signaling platform formed by the Toll-like receptor signal transducers MyD88 and IRAK-4. J Biol Chem *284*, 25404-25411. 10.1074/jbc.M109.022392.

20. Lin, S.C., Lo, Y.C., and Wu, H. (2010). Helical assembly in the MyD88-IRAK4-IRAK2 complex in TLR/IL-1R signalling. Nature *465*, 885-890. 10.1038/nature09121.

21. Deng, L., Wang, C., Spencer, E., Yang, L., Braun, A., You, J., Slaughter, C., Pickart, C., and Chen, Z.J. (2000). Activation of the IkappaB kinase complex by TRAF6 requires a dimeric ubiquitin-conjugating enzyme complex and a unique polyubiquitin chain. Cell *103*, 351-361. 10.1016/s0092-8674(00)00126-4.

22. Ikeda, F., Deribe, Y.L., Skanland, S.S., Stieglitz, B., Grabbe, C., Franz-Wachtel, M., van Wijk, S.J., Goswami, P., Nagy, V., Terzic, J., et al. (2011). SHARPIN forms a linear ubiquitin ligase complex regulating NF-kappaB activity and apoptosis. Nature *471*, 637-641. 10.1038/nature09814.

23. Gerlach, B., Cordier, S.M., Schmukle, A.C., Emmerich, C.H., Rieser, E., Haas, T.L., Webb, A.I., Rickard, J.A., Anderton, H., Wong, W.W., et al. (2011). Linear ubiquitination prevents inflammation and regulates immune signalling. Nature *471*, 591-596. 10.1038/nature09816.

24. Tokunaga, F., Nakagawa, T., Nakahara, M., Saeki, Y., Taniguchi, M., Sakata, S., Tanaka, K., Nakano, H., and Iwai, K. (2011). SHARPIN is a component of the NF-kappaB-activating linear ubiquitin chain assembly complex. Nature *471*, 633-636. 10.1038/nature09815.

25. Rahighi, S., Ikeda, F., Kawasaki, M., Akutsu, M., Suzuki, N., Kato, R., Kensche, T., Uejima, T., Bloor, S., Komander, D., et al. (2009). Specific recognition of linear ubiquitin chains by NEMO is important for NF-kappaB activation. Cell *136*, 1098-1109. 10.1016/j.cell.2009.03.007.

26. Emmerich, C.H., Ordureau, A., Strickson, S., Arthur, J.S., Pedrioli, P.G., Komander, D., and Cohen, P. (2013). Activation of the canonical IKK complex by K63/M1-linked hybrid ubiquitin chains. Proc Natl Acad Sci U S A *110*, 15247-15252. 10.1073/pnas.1314715110.

27. Karin, M., and Greten, F.R. (2005). NF-kappaB: linking inflammation and immunity to cancer development and progression. Nat Rev Immunol *5*, 749-759. 10.1038/nri1703.

28. Pasparakis, M. (2009). Regulation of tissue homeostasis by NF-kappaB signalling: implications for inflammatory diseases. Nat Rev Immunol *9*, 778-788. 10.1038/nri2655.

29. Oeckinghaus, A., and Ghosh, S. (2009). The NF-kappaB family of transcription factors and its regulation. Cold Spring Harb Perspect Biol *1*, a000034. 10.1101/cshperspect.a000034.

30. Kawai, T., Takeuchi, O., Fujita, T., Inoue, J., Muhlradt, P.F., Sato, S., Hoshino, K., and Akira, S. (2001). Lipopolysaccharide stimulates the MyD88-independent pathway and results in

activation of IFN-regulatory factor 3 and the expression of a subset of lipopolysaccharide-inducible genes. J Immunol *167*, 5887-5894. 10.4049/jimmunol.167.10.5887.

31. Hoshino, K., Kaisho, T., Iwabe, T., Takeuchi, O., and Akira, S. (2002). Differential involvement of IFN-beta in Toll-like receptor-stimulated dendritic cell activation. Int Immunol *14*, 1225-1231. 10.1093/intimm/dxf089.

32. Oganesyan, G., Saha, S.K., Guo, B., He, J.Q., Shahangian, A., Zarnegar, B., Perry, A., and Cheng, G. (2006). Critical role of TRAF3 in the Toll-like receptor-dependent and -independent antiviral response. Nature *439*, 208-211. 10.1038/nature04374.

33. Hacker, H., Redecke, V., Blagoev, B., Kratchmarova, I., Hsu, L.C., Wang, G.G., Kamps, M.P., Raz, E., Wagner, H., Hacker, G., et al. (2006). Specificity in Toll-like receptor signalling through distinct effector functions of TRAF3 and TRAF6. Nature *439*, 204-207. 10.1038/nature04369.

34. Hemmi, H., Takeuchi, O., Sato, S., Yamamoto, M., Kaisho, T., Sanjo, H., Kawai, T., Hoshino, K., Takeda, K., and Akira, S. (2004). The roles of two IkappaB kinase-related kinases in lipopolysaccharide and double stranded RNA signaling and viral infection. J Exp Med *199*, 1641-1650. 10.1084/jem.20040520.

35. Fitzgerald, K.A., McWhirter, S.M., Faia, K.L., Rowe, D.C., Latz, E., Golenbock, D.T., Coyle, A.J., Liao, S.M., and Maniatis, T. (2003). IKKepsilon and TBK1 are essential components of the IRF3 signaling pathway. Nat Immunol *4*, 491-496. 10.1038/ni921.

36. Sato, S., Sugiyama, M., Yamamoto, M., Watanabe, Y., Kawai, T., Takeda, K., and Akira, S. (2003). Toll/IL-1 receptor domain-containing adaptor inducing IFN-beta (TRIF) associates with TNF receptor-associated factor 6 and TANK-binding kinase 1, and activates two distinct transcription factors, NF-kappa B and IFN-regulatory factor-3, in the Toll-like receptor signaling. J Immunol *171*, 4304-4310. 10.4049/jimmunol.171.8.4304.

37. Kaiser, W.J., and Offermann, M.K. (2005). Apoptosis induced by the toll-like receptor adaptor TRIF is dependent on its receptor interacting protein homotypic interaction motif. J Immunol *174*, 4942-4952. 10.4049/jimmunol.174.8.4942.

38. Meylan, E., Burns, K., Hofmann, K., Blancheteau, V., Martinon, F., Kelliher, M., and Tschopp, J. (2004). RIP1 is an essential mediator of Toll-like receptor 3-induced NF-kappa B activation. Nat Immunol *5*, 503-507. 10.1038/ni1061.

39. Chen, G.Y., and Nunez, G. (2010). Sterile inflammation: sensing and reacting to damage. Nat Rev Immunol *10*, 826-837. 10.1038/nri2873.

40. Matzinger, P. (1994). Tolerance, danger, and the extended family. Annu Rev Immunol *12*, 991-1045. 10.1146/annurev.iy.12.040194.005015.

41. Matzinger, P. (2002). An innate sense of danger. Ann N Y Acad Sci *961*, 341-342. 10.1111/j.1749-6632.2002.tb03118.x.

42. Seong, S.Y., and Matzinger, P. (2004). Hydrophobicity: an ancient damage-associated molecular pattern that initiates innate immune responses. Nat Rev Immunol *4*, 469-478. 10.1038/nri1372.

43. Ma, M., Jiang, W., and Zhou, R. (2024). DAMPs and DAMP-sensing receptors in inflammation and diseases. Immunity *57*, 752-771. 10.1016/j.immuni.2024.03.002.

44. Quintana, F.J., and Cohen, I.R. (2005). Heat shock proteins as endogenous adjuvants in sterile and septic inflammation. J Immunol *175*, 2777-2782. 10.4049/jimmunol.175.5.2777.

45. Fang, H., Wu, Y., Huang, X., Wang, W., Ang, B., Cao, X., and Wan, T. (2011). Toll-like receptor 4 (TLR4) is essential for Hsp70-like protein 1 (HSP70L1) to activate dendritic cells and induce Th1 response. J Biol Chem *286*, 30393-30400. 10.1074/jbc.M111.266528.

46. Xu, J., Zhang, X., Monestier, M., Esmon, N.L., and Esmon, C.T. (2011). Extracellular histones are mediators of death through TLR2 and TLR4 in mouse fatal liver injury. J Immunol *187*, 2626-2631. 10.4049/jimmunol.1003930.

47. Galluzzi, L., Vitale, I., Aaronson, S.A., Abrams, J.M., Adam, D., Agostinis, P., Alnemri, E.S., Altucci, L., Amelio, I., Andrews, D.W., et al. (2018). Molecular mechanisms of cell death: recommendations of the Nomenclature Committee on Cell Death 2018. Cell Death Differ *25*, 486-541. 10.1038/s41418-017-0012-4.

48. Pasparakis, M., and Vandenabeele, P. (2015). Necroptosis and its role in inflammation. Nature *517*, 311-320. 10.1038/nature14191.

49. Vandenabeele, P., Bultynck, G., and Savvides, S.N. (2023). Pore-forming proteins as drivers of membrane permeabilization in cell death pathways. Nat Rev Mol Cell Biol *24*, 312-333. 10.1038/s41580-022-00564-w.

50. Julien, O., and Wells, J.A. (2017). Caspases and their substrates. Cell Death Differ *24*, 1380-1389. 10.1038/cdd.2017.44.

51. Yuan, J., and Ofengeim, D. (2024). A guide to cell death pathways. Nat Rev Mol Cell Biol *25*, 379-395. 10.1038/s41580-023-00689-6.

52. Newton, K., Strasser, A., Kayagaki, N., and Dixit, V.M. (2024). Cell death. Cell *187*, 235-256. 10.1016/j.cell.2023.11.044.

53. Murphy, J.M., Czabotar, P.E., Hildebrand, J.M., Lucet, I.S., Zhang, J.G., Alvarez-Diaz, S., Lewis, R., Lalaoui, N., Metcalf, D., Webb, A.I., et al. (2013). The pseudokinase MLKL mediates necroptosis via a molecular switch mechanism. Immunity *39*, 443-453. 10.1016/j.immuni.2013.06.018.

54. Orozco, S., Yatim, N., Werner, M.R., Tran, H., Gunja, S.Y., Tait, S.W., Albert, M.L., Green, D.R., and Oberst, A. (2014). RIPK1 both positively and negatively regulates RIPK3 oligomerization and necroptosis. Cell Death Differ *21*, 1511-1521. 10.1038/cdd.2014.76.

55. Wu, X.N., Yang, Z.H., Wang, X.K., Zhang, Y., Wan, H., Song, Y., Chen, X., Shao, J., and Han, J. (2014). Distinct roles of RIP1-RIP3 hetero- and RIP3-RIP3 homo-interaction in mediating necroptosis. Cell Death Differ *21*, 1709-1720. 10.1038/cdd.2014.77.

56. Cai, Z., Jitkaew, S., Zhao, J., Chiang, H.C., Choksi, S., Liu, J., Ward, Y., Wu, L.G., and Liu, Z.G. (2014). Plasma membrane translocation of trimerized MLKL protein is required for TNF-induced necroptosis. Nat Cell Biol *16*, 55-65. 10.1038/ncb2883.

57. Chen, X., Li, W., Ren, J., Huang, D., He, W.T., Song, Y., Yang, C., Li, W., Zheng, X., Chen, P., and Han, J. (2014). Translocation of mixed lineage kinase domain-like protein to plasma membrane leads to necrotic cell death. Cell Res *24*, 105-121. 10.1038/cr.2013.171.

58. Su, L., Quade, B., Wang, H., Sun, L., Wang, X., and Rizo, J. (2014). A plug release mechanism for membrane permeation by MLKL. Structure *22*, 1489-1500. 10.1016/j.str.2014.07.014.

59. Dondelinger, Y., Declercq, W., Montessuit, S., Roelandt, R., Goncalves, A., Bruggeman, I., Hulpiau, P., Weber, K., Sehon, C.A., Marquis, R.W., et al. (2014). MLKL compromises plasma membrane integrity by binding to phosphatidylinositol phosphates. Cell Rep *7*, 971-981. 10.1016/j.celrep.2014.04.026.

60. Wang, H., Sun, L., Su, L., Rizo, J., Liu, L., Wang, L.F., Wang, F.S., and Wang, X. (2014). Mixed lineage kinase domain-like protein MLKL causes necrotic membrane disruption upon phosphorylation by RIP3. Mol Cell *54*, 133-146. 10.1016/j.molcel.2014.03.003.

61. Wilson, N.S., Dixit, V., and Ashkenazi, A. (2009). Death receptor signal transducers: nodes of coordination in immune signaling networks. Nat Immunol *10*, 348-355. 10.1038/ni.1714.

62. Ashkenazi, A., and Dixit, V.M. (1998). Death receptors: signaling and modulation. Science *281*, 1305-1308. 10.1126/science.281.5381.1305.

63. Ermolaeva, M.A., Michallet, M.C., Papadopoulou, N., Utermohlen, O., Kranidioti, K., Kollias, G., Tschopp, J., and Pasparakis, M. (2008). Function of TRADD in tumor necrosis factor receptor 1 signaling and in TRIF-dependent inflammatory responses. Nat Immunol *9*, 1037-1046. 10.1038/ni.1638.

64. Haas, T.L., Emmerich, C.H., Gerlach, B., Schmukle, A.C., Cordier, S.M., Rieser, E., Feltham, R., Vince, J., Warnken, U., Wenger, T., et al. (2009). Recruitment of the linear ubiquitin chain assembly complex stabilizes the TNF-R1 signaling complex and is required for TNF-mediated gene induction. Mol Cell *36*, 831-844. 10.1016/j.molcel.2009.10.013.

65. Micheau, O., and Tschopp, J. (2003). Induction of TNF receptor I-mediated apoptosis via two sequential signaling complexes. Cell *114*, 181-190. 10.1016/s0092-8674(03)00521-x.

66. Hsu, H., Huang, J., Shu, H.B., Baichwal, V., and Goeddel, D.V. (1996). TNF-dependent recruitment of the protein kinase RIP to the TNF receptor-1 signaling complex. Immunity *4*, 387-396. 10.1016/s1074-7613(00)80252-6.

67. Rothe, M., Pan, M.G., Henzel, W.J., Ayres, T.M., and Goeddel, D.V. (1995). The TNFR2-TRAF signaling complex contains two novel proteins related to baculoviral inhibitor of apoptosis proteins. Cell *83*, 1243-1252. 10.1016/0092-8674(95)90149-3.

68. Wang, C.Y., Mayo, M.W., Korneluk, R.G., Goeddel, D.V., and Baldwin, A.S., Jr. (1998). NF-kappaB antiapoptosis: induction of TRAF1 and TRAF2 and c-IAP1 and c-IAP2 to suppress caspase-8 activation. Science *281*, 1680-1683. 10.1126/science.281.5383.1680.

69. Bertrand, M.J., Milutinovic, S., Dickson, K.M., Ho, W.C., Boudreault, A., Durkin, J., Gillard, J.W., Jaquith, J.B., Morris, S.J., and Barker, P.A. (2008). cIAP1 and cIAP2 facilitate cancer cell survival by functioning as E3 ligases that promote RIP1 ubiquitination. Mol Cell *30*, 689-700. 10.1016/j.molcel.2008.05.014.

70. Mahoney, D.J., Cheung, H.H., Mrad, R.L., Plenchette, S., Simard, C., Enwere, E., Arora, V., Mak, T.W., Lacasse, E.C., Waring, J., and Korneluk, R.G. (2008). Both cIAP1 and cIAP2 regulate TNFalpha-mediated NF-kappaB activation. Proc Natl Acad Sci U S A *105*, 11778-11783. 10.1073/pnas.0711122105.

71. Varfolomeev, E., Goncharov, T., Fedorova, A.V., Dynek, J.N., Zobel, K., Deshayes, K., Fairbrother, W.J., and Vucic, D. (2008). c-IAP1 and c-IAP2 are critical mediators of tumor necrosis factor alpha (TNFalpha)-induced NF-kappaB activation. J Biol Chem *283*, 24295-24299. 10.1074/jbc.C800128200.

72. Draber, P., Kupka, S., Reichert, M., Draberova, H., Lafont, E., de Miguel, D., Spilgies, L., Surinova, S., Taraborrelli, L., Hartwig, T., et al. (2015). LUBAC-Recruited CYLD and A20 Regulate Gene Activation and Cell Death by Exerting Opposing Effects on Linear Ubiquitin in Signaling Complexes. Cell Rep *13*, 2258-2272. 10.1016/j.celrep.2015.11.009.

73. Tokunaga, F., Sakata, S., Saeki, Y., Satomi, Y., Kirisako, T., Kamei, K., Nakagawa, T., Kato, M., Murata, S., Yamaoka, S., et al. (2009). Involvement of linear polyubiquitylation of NEMO in NF-kappaB activation. Nat Cell Biol *11*, 123-132. 10.1038/ncb1821.

74. Poyet, J.L., Srinivasula, S.M., Lin, J.H., Fernandes-Alnemri, T., Yamaoka, S., Tsichlis, P.N., and Alnemri, E.S. (2000). Activation of the Ikappa B kinases by RIP via IKKgamma /NEMO-mediated oligomerization. J Biol Chem *275*, 37966-37977. 10.1074/jbc.M006643200.

75. Zhang, S.Q., Kovalenko, A., Cantarella, G., and Wallach, D. (2000). Recruitment of the IKK signalosome to the p55 TNF receptor: RIP and A20 bind to NEMO (IKKgamma) upon receptor stimulation. Immunity *12*, 301-311. 10.1016/s1074-7613(00)80183-1.

76. Lafont, E., Draber, P., Rieser, E., Reichert, M., Kupka, S., de Miguel, D., Draberova, H., von Massenhausen, A., Bhamra, A., Henderson, S., et al. (2018). TBK1 and IKKepsilon prevent TNF-induced cell death by RIPK1 phosphorylation. Nat Cell Biol *20*, 1389-1399. 10.1038/s41556-018-0229-6.

77. Dondelinger, Y., Aguileta, M.A., Goossens, V., Dubuisson, C., Grootjans, S., Dejardin, E., Vandenabeele, P., and Bertrand, M.J. (2013). RIPK3 contributes to TNFR1-mediated RIPK1 kinase-dependent apoptosis in conditions of cIAP1/2 depletion or TAK1 kinase inhibition. Cell Death Differ *20*, 1381-1392. 10.1038/cdd.2013.94.

78. Geng, J., Ito, Y., Shi, L., Amin, P., Chu, J., Ouchida, A.T., Mookhtiar, A.K., Zhao, H., Xu, D., Shan, B., et al. (2017). Regulation of RIPK1 activation by TAK1-mediated phosphorylation dictates apoptosis and necroptosis. Nat Commun *8*, 359. 10.1038/s41467-017-00406-w.

79. Dondelinger, Y., Jouan-Lanhouet, S., Divert, T., Theatre, E., Bertin, J., Gough, P.J., Giansanti, P., Heck, A.J., Dejardin, E., Vandenabeele, P., and Bertrand, M.J. (2015). NF-kappaB-Independent Role of IKKalpha/IKKbeta in Preventing RIPK1 Kinase-Dependent Apoptotic and Necroptotic Cell Death during TNF Signaling. Mol Cell *60*, 63-76. 10.1016/j.molcel.2015.07.032.

80. Huyghe, J., Priem, D., and Bertrand, M.J.M. (2023). Cell death checkpoints in the TNF pathway. Trends Immunol *44*, 628-643. 10.1016/j.it.2023.05.007.

81. Kreuz, S., Siegmund, D., Scheurich, P., and Wajant, H. (2001). NF-kappaB inducers upregulate cFLIP, a cycloheximide-sensitive inhibitor of death receptor signaling. Mol Cell Biol *21*, 3964-3973. 10.1128/MCB.21.12.3964-3973.2001.

82. Micheau, O., Lens, S., Gaide, O., Alevizopoulos, K., and Tschopp, J. (2001). NF-kappaB signals induce the expression of c-FLIP. Mol Cell Biol *21*, 5299-5305. 10.1128/MCB.21.16.5299-5305.2001.

83. Irmler, M., Thome, M., Hahne, M., Schneider, P., Hofmann, K., Steiner, V., Bodmer, J.L., Schroter, M., Burns, K., Mattmann, C., et al. (1997). Inhibition of death receptor signals by cellular FLIP. Nature *388*, 190-195. 10.1038/40657.

84. Wang, L., Du, F., and Wang, X. (2008). TNF-alpha induces two distinct caspase-8 activation pathways. Cell *133*, 693-703. 10.1016/j.cell.2008.03.036.

85. Peltzer, N., and Walczak, H. (2019). Cell Death and Inflammation - A Vital but Dangerous Liaison. Trends Immunol *40*, 387-402. 10.1016/j.it.2019.03.006.

86. Newton, K. (2020). Multitasking Kinase RIPK1 Regulates Cell Death and Inflammation. Cold Spring Harb Perspect Biol *12*. 10.1101/cshperspect.a036368.

87. Moulin, M., Anderton, H., Voss, A.K., Thomas, T., Wong, W.W., Bankovacki, A., Feltham, R., Chau, D., Cook, W.D., Silke, J., and Vaux, D.L. (2012). IAPs limit activation of RIP kinases by TNF receptor 1 during development. EMBO J *31*, 1679-1691. 10.1038/emboj.2012.18.

88. Zhang, J., Webster, J.D., Dugger, D.L., Goncharov, T., Roose-Girma, M., Hung, J., Kwon, Y.C., Vucic, D., Newton, K., and Dixit, V.M. (2019). Ubiquitin Ligases cIAP1 and cIAP2 Limit Cell Death to Prevent Inflammation. Cell Rep *27*, 2679-2689 e2673. 10.1016/j.celrep.2019.04.111.

89. Tang, Y., Tu, H., Zhang, J., Zhao, X., Wang, Y., Qin, J., and Lin, X. (2019). K63-linked ubiquitination regulates RIPK1 kinase activity to prevent cell death during embryogenesis and inflammation. Nat Commun *10*, 4157. 10.1038/s41467-019-12033-8.

90. Kist, M., Komuves, L.G., Goncharov, T., Dugger, D.L., Yu, C., Roose-Girma, M., Newton, K., Webster, J.D., and Vucic, D. (2021). Impaired RIPK1 ubiquitination sensitizes mice to TNF toxicity and inflammatory cell death. Cell Death Differ *28*, 985-1000. 10.1038/s41418-020-00629-3.

91. Peltzer, N., Darding, M., Montinaro, A., Draber, P., Draberova, H., Kupka, S., Rieser, E., Fisher, A., Hutchinson, C., Taraborrelli, L., et al. (2018). LUBAC is essential for embryogenesis by preventing cell death and enabling haematopoiesis. Nature *557*, 112-117. 10.1038/s41586-018-0064-8.

92. Peltzer, N., Rieser, E., Taraborrelli, L., Draber, P., Darding, M., Pernaute, B., Shimizu, Y., Sarr, A., Draberova, H., Montinaro, A., et al. (2014). HOIP deficiency causes embryonic lethality by aberrant TNFR1-mediated endothelial cell death. Cell Rep *9*, 153-165. 10.1016/j.celrep.2014.08.066.

93. Kumari, S., Redouane, Y., Lopez-Mosqueda, J., Shiraishi, R., Romanowska, M., Lutzmayer, S., Kuiper, J., Martinez, C., Dikic, I., Pasparakis, M., and Ikeda, F. (2014). Sharpin prevents skin inflammation by inhibiting TNFR1-induced keratinocyte apoptosis. Elife *3*. 10.7554/eLife.03422.

94. Rickard, J.A., Anderton, H., Etemadi, N., Nachbur, U., Darding, M., Peltzer, N., Lalaoui, N., Lawlor, K.E., Vanyai, H., Hall, C., et al. (2014). TNFR1-dependent cell death drives inflammation in Sharpin-deficient mice. Elife *3*. 10.7554/eLife.03464.

95. Berger, S.B., Kasparcova, V., Hoffman, S., Swift, B., Dare, L., Schaeffer, M., Capriotti, C., Cook, M., Finger, J., Hughes-Earle, A., et al. (2014). Cutting Edge: RIP1 kinase activity is dispensable for normal development but is a key regulator of inflammation in SHARPIN-deficient mice. J Immunol *192*, 5476-5480. 10.4049/jimmunol.1400499.

96. Laurien, L., Nagata, M., Schunke, H., Delanghe, T., Wiederstein, J.L., Kumari, S., Schwarzer, R., Corona, T., Kruger, M., Bertrand, M.J.M., et al. (2020). Autophosphorylation at serine 166 regulates RIP kinase 1-mediated cell death and inflammation. Nat Commun *11*, 1747. 10.1038/s41467-020-15466-8.

97. Dondelinger, Y., Delanghe, T., Priem, D., Wynosky-Dolfi, M.A., Sorobetea, D., Rojas-Rivera, D., Giansanti, P., Roelandt, R., Gropengiesser, J., Ruckdeschel, K., et al. (2019). Serine 25 phosphorylation inhibits RIPK1 kinase-dependent cell death in models of infection and inflammation. Nat Commun *10*, 1729. 10.1038/s41467-019-09690-0.

98. Degterev, A., Hitomi, J., Germscheid, M., Ch'en, I.L., Korkina, O., Teng, X., Abbott, D., Cuny, G.D., Yuan, C., Wagner, G., et al. (2008). Identification of RIP1 kinase as a specific cellular target of necrostatins. Nat Chem Biol *4*, 313-321. 10.1038/nchembio.83.

99. Zhang, Y., Su, S.S., Zhao, S., Yang, Z., Zhong, C.Q., Chen, X., Cai, Q., Yang, Z.H., Huang, D., Wu, R., and Han, J. (2017). RIP1 autophosphorylation is promoted by mitochondrial ROS and is essential for RIP3 recruitment into necrosome. Nat Commun *8*, 14329. 10.1038/ncomms14329.

100. Cho, Y.S., Challa, S., Moquin, D., Genga, R., Ray, T.D., Guildford, M., and Chan, F.K. (2009). Phosphorylation-driven assembly of the RIP1-RIP3 complex regulates programmed necrosis and virus-induced inflammation. Cell *137*, 1112-1123. 10.1016/j.cell.2009.05.037.

101. Wegner, K.W., Saleh, D., and Degterev, A. (2017). Complex Pathologic Roles of RIPK1 and RIPK3: Moving Beyond Necroptosis. Trends Pharmacol Sci *38*, 202-225. 10.1016/j.tips.2016.12.005.

102. Varfolomeev, E.E., Schuchmann, M., Luria, V., Chiannilkulchai, N., Beckmann, J.S., Mett, I.L., Rebrikov, D., Brodianski, V.M., Kemper, O.C., Kollet, O., et al. (1998). Targeted disruption of the mouse Caspase 8 gene ablates cell death induction by the TNF receptors, Fas/Apo1, and DR3 and is lethal prenatally. Immunity *9*, 267-276. 10.1016/s1074-7613(00)80609-3.

103. Yeh, W.C., de la Pompa, J.L., McCurrach, M.E., Shu, H.B., Elia, A.J., Shahinian, A., Ng, M., Wakeham, A., Khoo, W., Mitchell, K., et al. (1998). FADD: essential for embryo development and signaling from some, but not all, inducers of apoptosis. Science *279*, 1954-1958. 10.1126/science.279.5358.1954.

104. Kaiser, W.J., Upton, J.W., Long, A.B., Livingston-Rosanoff, D., Daley-Bauer, L.P., Hakem, R., Caspary, T., and Mocarski, E.S. (2011). RIP3 mediates the embryonic lethality of caspase-8-deficient mice. Nature *471*, 368-372. 10.1038/nature09857.

105. Oberst, A., Dillon, C.P., Weinlich, R., McCormick, L.L., Fitzgerald, P., Pop, C., Hakem, R., Salvesen, G.S., and Green, D.R. (2011). Catalytic activity of the caspase-8-FLIP(L) complex inhibits RIPK3-dependent necrosis. Nature *471*, 363-367. 10.1038/nature09852.

106. Alvarez-Diaz, S., Dillon, C.P., Lalaoui, N., Tanzer, M.C., Rodriguez, D.A., Lin, A., Lebois, M., Hakem, R., Josefsson, E.C., O'Reilly, L.A., et al. (2016). The Pseudokinase MLKL and the Kinase RIPK3 Have Distinct Roles in Autoimmune Disease Caused by Loss of Death-Receptor-Induced Apoptosis. Immunity *45*, 513-526. 10.1016/j.immuni.2016.07.016.

107. Zhang, H., Zhou, X., McQuade, T., Li, J., Chan, F.K., and Zhang, J. (2011). Functional complementation between FADD and RIP1 in embryos and lymphocytes. Nature *471*, 373-376. 10.1038/nature09878.

108. Dillon, C.P., Oberst, A., Weinlich, R., Janke, L.J., Kang, T.B., Ben-Moshe, T., Mak, T.W., Wallach, D., and Green, D.R. (2012). Survival function of the FADD-CASPASE-8-cFLIP(L) complex. Cell Rep *1*, 401-407. 10.1016/j.celrep.2012.03.010.

109. He, S., Wang, L., Miao, L., Wang, T., Du, F., Zhao, L., and Wang, X. (2009). Receptor interacting protein kinase-3 determines cellular necrotic response to TNF-alpha. Cell *137*, 1100-1111. 10.1016/j.cell.2009.05.021.

110. Li, J., McQuade, T., Siemer, A.B., Napetschnig, J., Moriwaki, K., Hsiao, Y.S., Damko, E., Moquin, D., Walz, T., McDermott, A., et al. (2012). The RIP1/RIP3 necrosome forms a functional amyloid signaling complex required for programmed necrosis. Cell *150*, 339-350. 10.1016/j.cell.2012.06.019.

111. Wu, X., Ma, Y., Zhao, K., Zhang, J., Sun, Y., Li, Y., Dong, X., Hu, H., Liu, J., Wang, J., et al. (2021). The structure of a minimum amyloid fibril core formed by necroptosis-mediating RHIM of human RIPK3. Proc Natl Acad Sci U S A *118*. 10.1073/pnas.2022933118.

112. Sun, L., Wang, H., Wang, Z., He, S., Chen, S., Liao, D., Wang, L., Yan, J., Liu, W., Lei, X., and Wang, X. (2012). Mixed lineage kinase domain-like protein mediates necrosis signaling downstream of RIP3 kinase. Cell *148*, 213-227. 10.1016/j.cell.2011.11.031.

113. Hildebrand, J.M., Tanzer, M.C., Lucet, I.S., Young, S.N., Spall, S.K., Sharma, P., Pierotti, C., Garnier, J.M., Dobson, R.C., Webb, A.I., et al. (2014). Activation of the pseudokinase MLKL unleashes the four-helix bundle domain to induce membrane localization and necroptotic cell death. Proc Natl Acad Sci U S A *111*, 15072-15077. 10.1073/pnas.1408987111.

114. Fritsch, M., Gunther, S.D., Schwarzer, R., Albert, M.C., Schorn, F., Werthenbach, J.P., Schiffmann, L.M., Stair, N., Stocks, H., Seeger, J.M., et al. (2019). Caspase-8 is the molecular switch for apoptosis, necroptosis and pyroptosis. Nature *575*, 683-687. 10.1038/s41586-019-1770-6.

115. Newton, K., Wickliffe, K.E., Maltzman, A., Dugger, D.L., Reja, R., Zhang, Y., Roose-Girma, M., Modrusan, Z., Sagolla, M.S., Webster, J.D., and Dixit, V.M. (2019). Activity of caspase-8 determines plasticity between cell death pathways. Nature *575*, 679-682. 10.1038/s41586-019-1752-8.

116. Newton, K., Wickliffe, K.E., Dugger, D.L., Maltzman, A., Roose-Girma, M., Dohse, M., Komuves, L., Webster, J.D., and Dixit, V.M. (2019). Cleavage of RIPK1 by caspase-8 is crucial for limiting apoptosis and necroptosis. Nature *574*, 428-431. 10.1038/s41586-019-1548-x.

117. Frisch, S.M., and Francis, H. (1994). Disruption of epithelial cell-matrix interactions induces apoptosis. J Cell Biol *124*, 619-626. 10.1083/jcb.124.4.619.

118. Kist, M., and Vucic, D. (2021). Cell death pathways: intricate connections and disease implications. EMBO J *40*, e106700. 10.15252/embj.2020106700.

119. Kale, J., Osterlund, E.J., and Andrews, D.W. (2018). BCL-2 family proteins: changing partners in the dance towards death. Cell Death Differ *25*, 65-80. 10.1038/cdd.2017.186.

120. Edlich, F., Banerjee, S., Suzuki, M., Cleland, M.M., Arnoult, D., Wang, C., Neutzner, A., Tjandra, N., and Youle, R.J. (2011). Bcl-x(L) retrotranslocates Bax from the mitochondria into the cytosol. Cell *145*, 104-116. 10.1016/j.cell.2011.02.034.

121. Schellenberg, B., Wang, P., Keeble, J.A., Rodriguez-Enriquez, R., Walker, S., Owens, T.W., Foster, F., Tanianis-Hughes, J., Brennan, K., Streuli, C.H., and Gilmore, A.P. (2013). Bax exists in a dynamic equilibrium between the cytosol and mitochondria to control apoptotic priming. Mol Cell *49*, 959-971. 10.1016/j.molcel.2012.12.022.

122. Todt, F., Cakir, Z., Reichenbach, F., Emschermann, F., Lauterwasser, J., Kaiser, A., Ichim, G., Tait, S.W., Frank, S., Langer, H.F., and Edlich, F. (2015). Differential retrotranslocation of mitochondrial Bax and Bak. EMBO J *34*, 67-80. 10.15252/embj.201488806.

123. Nechushtan, A., Smith, C.L., Lamensdorf, I., Yoon, S.H., and Youle, R.J. (2001). Bax and Bak coalesce into novel mitochondria-associated clusters during apoptosis. J Cell Biol *153*, 1265-1276. 10.1083/jcb.153.6.1265.

124. Rehm, M., Dussmann, H., and Prehn, J.H. (2003). Real-time single cell analysis of Smac/DIABLO release during apoptosis. J Cell Biol *162*, 1031-1043. 10.1083/jcb.200303123.

125. Zhou, L.L., Zhou, L.Y., Luo, K.Q., and Chang, D.C. (2005). Smac/DIABLO and cytochrome c are released from mitochondria through a similar mechanism during UV-induced apoptosis. Apoptosis *10*, 289-299. 10.1007/s10495-005-0803-9.

126. Li, Y., Zhou, M., Hu, Q., Bai, X.C., Huang, W., Scheres, S.H., and Shi, Y. (2017). Mechanistic insights into caspase-9 activation by the structure of the apoptosome holoenzyme. Proc Natl Acad Sci U S A *114*, 1542-1547. 10.1073/pnas.1620626114.

127. Riedl, S.J., and Salvesen, G.S. (2007). The apoptosome: signalling platform of cell death. Nat Rev Mol Cell Biol *8*, 405-413. 10.1038/nrm2153.

128. Yuan, S., Yu, X., Asara, J.M., Heuser, J.E., Ludtke, S.J., and Akey, C.W. (2011). The holo-apoptosome: activation of procaspase-9 and interactions with caspase-3. Structure *19*, 1084-1096. 10.1016/j.str.2011.07.001.

129. Singh, R., Letai, A., and Sarosiek, K. (2019). Regulation of apoptosis in health and disease: the balancing act of BCL-2 family proteins. Nat Rev Mol Cell Biol *20*, 175-193. 10.1038/s41580-018-0089-8.

130. Llambi, F., Wang, Y.M., Victor, B., Yang, M., Schneider, D.M., Gingras, S., Parsons, M.J., Zheng, J.H., Brown, S.A., Pelletier, S., et al. (2016). BOK Is a Non-canonical BCL-2 Family Effector of Apoptosis Regulated by ER-Associated Degradation. Cell *165*, 421-433. 10.1016/j.cell.2016.02.026.

131. Ke, F.F.S., Vanyai, H.K., Cowan, A.D., Delbridge, A.R.D., Whitehead, L., Grabow, S., Czabotar, P.E., Voss, A.K., and Strasser, A. (2018). Embryogenesis and Adult Life in the Absence of Intrinsic Apoptosis Effectors BAX, BAK, and BOK. Cell *173*, 1217-1230 e1217. 10.1016/j.cell.2018.04.036.

132. Lindsten, T., Ross, A.J., King, A., Zong, W.X., Rathmell, J.C., Shiels, H.A., Ulrich, E., Waymire, K.G., Mahar, P., Frauwirth, K., et al. (2000). The combined functions of proapoptotic Bcl-2 family members bak and bax are essential for normal development of multiple tissues. Mol Cell *6*, 1389-1399. 10.1016/s1097-2765(00)00136-2.

133. Li, H., Zhu, H., Xu, C.J., and Yuan, J. (1998). Cleavage of BID by caspase 8 mediates the mitochondrial damage in the Fas pathway of apoptosis. Cell *94*, 491-501. 10.1016/s0092-8674(00)81590-1.

134. McArthur, K., Whitehead, L.W., Heddleston, J.M., Li, L., Padman, B.S., Oorschot, V., Geoghegan, N.D., Chappaz, S., Davidson, S., San Chin, H., et al. (2018). BAK/BAX macropores facilitate mitochondrial herniation and mtDNA efflux during apoptosis. Science *359*. 10.1126/science.aao6047.

135. Riley, J.S., Quarato, G., Cloix, C., Lopez, J., O'Prey, J., Pearson, M., Chapman, J., Sesaki, H., Carlin, L.M., Passos, J.F., et al. (2018). Mitochondrial inner membrane permeabilisation enables mtDNA release during apoptosis. EMBO J *37*. 10.15252/embj.201899238.

136. Cosentino, K., Hertlein, V., Jenner, A., Dellmann, T., Gojkovic, M., Pena-Blanco, A., Dadsena, S., Wajngarten, N., Danial, J.S.H., Thevathasan, J.V., et al. (2022). The interplay between BAX and BAK tunes apoptotic pore growth to control mitochondrial-DNA-mediated inflammation. Mol Cell *82*, 933-949 e939. 10.1016/j.molcel.2022.01.008.

137. Porter, K.R., Claude, A., and Fullam, E.F. (1945). A Study of Tissue Culture Cells by Electron Microscopy : Methods and Preliminary Observations. J Exp Med *81*, 233-246. 10.1084/jem.81.3.233.

138. Porter, K.R., and Thompson, H.P. (1948). A particulate body associated with epithelial cells cultured from mammary carcinomas of mice of a milkfactor strain. J Exp Med *88*, 15-24. 10.1084/jem.88.1.15.

139. Porter, K.R., and Kallman, F.L. (1952). Significance of cell particulates as seen by electron microscopy. Ann N Y Acad Sci *54*, 882-891. 10.1111/j.1749-6632.1952.tb39963.x.

140. Palade, G.E., and Porter, K.R. (1954). Studies on the endoplasmic reticulum. I. Its identification in cells in situ. J Exp Med *100*, 641-656. 10.1084/jem.100.6.641.

141. Borgese, N., Francolini, M., and Snapp, E. (2006). Endoplasmic reticulum architecture: structures in flux. Curr Opin Cell Biol *18*, 358-364. 10.1016/j.ceb.2006.06.008.

142. Shibata, Y., Voeltz, G.K., and Rapoport, T.A. (2006). Rough sheets and smooth tubules. Cell *126*, 435-439. 10.1016/j.cell.2006.07.019.

143. Almanza, A., Carlesso, A., Chintha, C., Creedican, S., Doultsinos, D., Leuzzi, B., Luis, A., McCarthy, N., Montibeller, L., More, S., et al. (2019). Endoplasmic reticulum stress signalling - from basic mechanisms to clinical applications. FEBS J *286*, 241-278. 10.1111/febs.14608.

144. Phillips, M.J., and Voeltz, G.K. (2016). Structure and function of ER membrane contact sites with other organelles. Nat Rev Mol Cell Biol *17*, 69-82. 10.1038/nrm.2015.8.

145. Friedman, J.R., Lackner, L.L., West, M., DiBenedetto, J.R., Nunnari, J., and Voeltz, G.K. (2011). ER tubules mark sites of mitochondrial division. Science *334*, 358-362. 10.1126/science.1207385.

146. Kaufman, R.J. (2004). Regulation of mRNA translation by protein folding in the endoplasmic reticulum. Trends Biochem Sci *29*, 152-158. 10.1016/j.tibs.2004.01.004.

147. Hebert, D.N., and Molinari, M. (2007). In and out of the ER: protein folding, quality control, degradation, and related human diseases. Physiol Rev *87*, 1377-1408. 10.1152/physrev.00050.2006.

148. Ogle, J.M., and Ramakrishnan, V. (2005). Structural insights into translational fidelity. Annu Rev Biochem *74*, 129-177. 10.1146/annurev.biochem.74.061903.155440.

149. Cochella, L., and Green, R. (2005). Fidelity in protein synthesis. Curr Biol *15*, R536-540. 10.1016/j.cub.2005.07.018.

150. Poothong, J., Jang, I., and Kaufman, R.J. (2021). Defects in Protein Folding and/or Quality Control Cause Protein Aggregation in the Endoplasmic Reticulum. Prog Mol Subcell Biol *59*, 115-143. 10.1007/978-3-030-67696-4_6.

151. Wang, M., and Kaufman, R.J. (2016). Protein misfolding in the endoplasmic reticulum as a conduit to human disease. Nature *529*, 326-335. 10.1038/nature17041.

152. Hetz, C., Zhang, K., and Kaufman, R.J. (2020). Mechanisms, regulation and functions of the unfolded protein response. Nat Rev Mol Cell Biol *21*, 421-438. 10.1038/s41580-020-0250-z.

153. Zhang, K., Wong, H.N., Song, B., Miller, C.N., Scheuner, D., and Kaufman, R.J. (2005). The unfolded protein response sensor IRE1alpha is required at 2 distinct steps in B cell lymphopoiesis. J Clin Invest *115*, 268-281. 10.1172/JCI21848.

154. Iwawaki, T., Akai, R., Yamanaka, S., and Kohno, K. (2009). Function of IRE1 alpha in the placenta is essential for placental development and embryonic viability. Proc Natl Acad Sci U S A *106*, 16657-16662. 10.1073/pnas.0903775106.

155. Walter, P., and Ron, D. (2011). The unfolded protein response: from stress pathway to homeostatic regulation. Science *334*, 1081-1086. 10.1126/science.1209038.

156. Harding, H.P., Zhang, Y., and Ron, D. (1999). Protein translation and folding are coupled by an endoplasmic-reticulum-resident kinase. Nature *397*, 271-274. 10.1038/16729.

157. Shi, Y., Vattem, K.M., Sood, R., An, J., Liang, J., Stramm, L., and Wek, R.C. (1998). Identification and characterization of pancreatic eukaryotic initiation factor 2 alpha-subunit kinase, PEK, involved in translational control. Mol Cell Biol *18*, 7499-7509. 10.1128/MCB.18.12.7499.

158. Lee, A.H., Iwakoshi, N.N., and Glimcher, L.H. (2003). XBP-1 regulates a subset of endoplasmic reticulum resident chaperone genes in the unfolded protein response. Mol Cell Biol *23*, 7448-7459. 10.1128/MCB.23.21.7448-7459.2003.

159. Acosta-Alvear, D., Zhou, Y., Blais, A., Tsikitis, M., Lents, N.H., Arias, C., Lennon, C.J., Kluger, Y., and Dynlacht, B.D. (2007). XBP1 controls diverse cell type- and condition-specific transcriptional regulatory networks. Mol Cell *27*, 53-66. 10.1016/j.molcel.2007.06.011.

160. Schuck, S., Prinz, W.A., Thorn, K.S., Voss, C., and Walter, P. (2009). Membrane expansion alleviates endoplasmic reticulum stress independently of the unfolded protein response. J Cell Biol *187*, 525-536. 10.1083/jcb.200907074.

161. Lee, A.H., Scapa, E.F., Cohen, D.E., and Glimcher, L.H. (2008). Regulation of hepatic lipogenesis by the transcription factor XBP1. Science *320*, 1492-1496. 10.1126/science.1158042.

162. Adolph, T.E., Tomczak, M.F., Niederreiter, L., Ko, H.J., Bock, J., Martinez-Naves, E., Glickman, J.N., Tschurtschenthaler, M., Hartwig, J., Hosomi, S., et al. (2013). Paneth cells as a site of origin for intestinal inflammation. Nature *503*, 272-276. 10.1038/nature12599.

163. Travers, K.J., Patil, C.K., Wodicka, L., Lockhart, D.J., Weissman, J.S., and Walter, P. (2000). Functional and genomic analyses reveal an essential coordination between the unfolded protein response and ER-associated degradation. Cell *101*, 249-258. 10.1016/s0092-8674(00)80835-1.

164. Cox, J.S., Shamu, C.E., and Walter, P. (1993). Transcriptional induction of genes encoding endoplasmic reticulum resident proteins requires a transmembrane protein kinase. Cell *73*, 1197-1206. 10.1016/0092-8674(93)90648-a.

165. Mori, K., Ma, W., Gething, M.J., and Sambrook, J. (1993). A transmembrane protein with a cdc2+/CDC28-related kinase activity is required for signaling from the ER to the nucleus. Cell *74*, 743-756. 10.1016/0092-8674(93)90521-q.

166. Tirasophon, W., Welihinda, A.A., and Kaufman, R.J. (1998). A stress response pathway from the endoplasmic reticulum to the nucleus requires a novel bifunctional protein kinase/endoribonuclease (Ire1p) in mammalian cells. Genes Dev *12*, 1812-1824. 10.1101/gad.12.12.1812.

167. Wang, X.Z., Harding, H.P., Zhang, Y., Jolicoeur, E.M., Kuroda, M., and Ron, D. (1998). Cloning of mammalian Ire1 reveals diversity in the ER stress responses. EMBO J *17*, 5708-5717. 10.1093/emboj/17.19.5708.

168. Bertolotti, A., Wang, X., Novoa, I., Jungreis, R., Schlessinger, K., Cho, J.H., West, A.B., and Ron, D. (2001). Increased sensitivity to dextran sodium sulfate colitis in IRE1beta-deficient mice. J Clin Invest *107*, 585-593. 10.1172/JCI11476.

169. Yoshida, H., Haze, K., Yanagi, H., Yura, T., and Mori, K. (1998). Identification of the cis-acting endoplasmic reticulum stress response element responsible for transcriptional induction of mammalian glucose-regulated proteins. Involvement of basic leucine zipper transcription factors. J Biol Chem *273*, 33741-33749. 10.1074/jbc.273.50.33741.

170. Urra, H., Pihan, P., and Hetz, C. (2020). The UPRosome - decoding novel biological outputs of IRE1alpha function. J Cell Sci *133*. 10.1242/jcs.218107.

171. Karagoz, G.E., Acosta-Alvear, D., Nguyen, H.T., Lee, C.P., Chu, F., and Walter, P. (2017). An unfolded protein-induced conformational switch activates mammalian IRE1. Elife *6*. 10.7554/eLife.30700.

172. Bertolotti, A., Zhang, Y., Hendershot, L.M., Harding, H.P., and Ron, D. (2000). Dynamic interaction of BiP and ER stress transducers in the unfolded-protein response. Nat Cell Biol *2*, 326-332. 10.1038/35014014.

173. Prischi, F., Nowak, P.R., Carrara, M., and Ali, M.M. (2014). Phosphoregulation of Ire1 RNase splicing activity. Nat Commun *5*, 3554. 10.1038/ncomms4554.

174. Karagoz, G.E., Acosta-Alvear, D., and Walter, P. (2019). The Unfolded Protein Response: Detecting and Responding to Fluctuations in the Protein-Folding Capacity of the Endoplasmic Reticulum. Cold Spring Harb Perspect Biol *11*. 10.1101/cshperspect.a033886.

175. Yoshida, H., Matsui, T., Yamamoto, A., Okada, T., and Mori, K. (2001). XBP1 mRNA is induced by ATF6 and spliced by IRE1 in response to ER stress to produce a highly active transcription factor. Cell *107*, 881-891. 10.1016/s0092-8674(01)00611-0.

176. Hollien, J., Lin, J.H., Li, H., Stevens, N., Walter, P., and Weissman, J.S. (2009). Regulated Ire1-dependent decay of messenger RNAs in mammalian cells. J Cell Biol *186*, 323-331. 10.1083/jcb.200903014.

177. Almanza, A., Mnich, K., Blomme, A., Robinson, C.M., Rodriguez-Blanco, G., Kierszniowska, S., McGrath, E.P., Le Gallo, M., Pilalis, E., Swinnen, J.V., et al. (2022). Regulated IRE1alpha-dependent decay (RIDD)-mediated reprograming of lipid metabolism in cancer. Nat Commun *13*, 2493. 10.1038/s41467-022-30159-0.

178. Hollien, J., and Weissman, J.S. (2006). Decay of endoplasmic reticulum-localized mRNAs during the unfolded protein response. Science *313*, 104-107. 10.1126/science.1129631.

179. Moore, K., and Hollien, J. (2015). Ire1-mediated decay in mammalian cells relies on mRNA sequence, structure, and translational status. Mol Biol Cell *26*, 2873-2884. 10.1091/mbc.E15-02-0074.

180. Urano, F., Wang, X., Bertolotti, A., Zhang, Y., Chung, P., Harding, H.P., and Ron, D. (2000). Coupling of stress in the ER to activation of JNK protein kinases by transmembrane protein kinase IRE1. Science *287*, 664-666. 10.1126/science.287.5453.664.

181. Turner, J.R. (2009). Intestinal mucosal barrier function in health and disease. Nat Rev Immunol *9*, 799-809. 10.1038/nri2653.

182. Hooper, L.V. (2009). Do symbiotic bacteria subvert host immunity? Nat Rev Microbiol *7*, 367-374. 10.1038/nrmicro2114.

183. Hooper, L.V., Littman, D.R., and Macpherson, A.J. (2012). Interactions Between the Microbiota and the Immune System. Science *336*, 1268-1273. 10.1126/science.1223490.

184. Rao, J.N., and Wang, J.Y. (2010). In Regulation of Gastrointestinal Mucosal Growth. 10.4199/C00028ED1V01Y201103ISP015.

185. Kiela, P.R., and Ghishan, F.K. (2016). Physiology of Intestinal Absorption and Secretion. Best Pract Res Clin Gastroenterol *30*, 145-159. 10.1016/j.bpg.2016.02.007.

186. Gehart, H., and Clevers, H. (2019). Tales from the crypt: new insights into intestinal stem cells. Nat Rev Gastroenterol Hepatol *16*, 19-34. 10.1038/s41575-018-0081-y.

187. Clevers, H.C., and Bevins, C.L. (2013). Paneth cells: maestros of the small intestinal crypts. Annu Rev Physiol *75*, 289-311. 10.1146/annurev-physiol-030212-183744.

188. Allaire, J.M., Crowley, S.M., Law, H.T., Chang, S.Y., Ko, H.J., and Vallance, B.A. (2019). The Intestinal Epithelium: Central Coordinator of Mucosal Immunity: (Trends in Immunology 39, 677-696, 2018). Trends Immunol *40*, 174. 10.1016/j.it.2018.12.008.

189. Rodriguez-Boulan, E., and Macara, I.G. (2014). Organization and execution of the epithelial polarity programme. Nat Rev Mol Cell Biol *15*, 225-242. 10.1038/nrm3775.

190. Mukherjee, T.M., and Williams, A.W. (1967). A comparative study of the ultrastructure of microvilli in the epithelium of small and large intestine of mice. J Cell Biol *34*, 447-461. 10.1083/jcb.34.2.447.

191. Niess, J.H., and Reinecker, H.C. (2006). Dendritic cells in the recognition of intestinal microbiota. Cell Microbiol *8*, 558-564. 10.1111/j.1462-5822.2006.00694.x.

192. Macdonald, T.T., and Monteleone, G. (2005). Immunity, inflammation, and allergy in the gut. Science *307*, 1920-1925. 10.1126/science.1106442.

193. Helander, H.F., and Fandriks, L. (2014). Surface area of the digestive tract - revisited. Scand J Gastroenterol *49*, 681-689. 10.3109/00365521.2014.898326.

194. Reyes, A., Haynes, M., Hanson, N., Angly, F.E., Heath, A.C., Rohwer, F., and Gordon, J.I. (2010). Viruses in the faecal microbiota of monozygotic twins and their mothers. Nature *466*, 334-338. 10.1038/nature09199.

195. Lozupone, C.A., Stombaugh, J.I., Gordon, J.I., Jansson, J.K., and Knight, R. (2012). Diversity, stability and resilience of the human gut microbiota. Nature *489*, 220-230. 10.1038/nature11550.

196. Okumura, R., and Takeda, K. (2017). Roles of intestinal epithelial cells in the maintenance of gut homeostasis. Exp Mol Med *49*, e338. 10.1038/emm.2017.20.

197. Macpherson, A.J., and Uhr, T. (2004). Induction of protective IgA by intestinal dendritic cells carrying commensal bacteria. Science *303*, 1662-1665. 10.1126/science.1091334.

198. Kelsall, B. (2008). Recent progress in understanding the phenotype and function of intestinal dendritic cells and macrophages. Mucosal Immunol *1*, 460-469. 10.1038/mi.2008.61.

199. Barker, N., van Es, J.H., Kuipers, J., Kujala, P., van den Born, M., Cozijnsen, M., Haegebarth, A., Korving, J., Begthel, H., Peters, P.J., and Clevers, H. (2007). Identification of stem cells in small intestine and colon by marker gene Lgr5. Nature *449*, 1003-1007. 10.1038/nature06196.

200. Sato, T., Vries, R.G., Snippert, H.J., van de Wetering, M., Barker, N., Stange, D.E., van Es, J.H., Abo, A., Kujala, P., Peters, P.J., and Clevers, H. (2009). Single Lgr5 stem cells build crypt-villus structures in vitro without a mesenchymal niche. Nature *459*, 262-265. 10.1038/nature07935.

201. Basak, O., van de Born, M., Korving, J., Beumer, J., van der Elst, S., van Es, J.H., and Clevers, H. (2014). Mapping early fate determination in Lgr5+ crypt stem cells using a novel Ki67-RFP allele. EMBO J *33*, 2057-2068. 10.15252/embj.201488017.

202. Johansson, M.E., and Hansson, G.C. (2016). Immunological aspects of intestinal mucus and mucins. Nat Rev Immunol *16*, 639-649. 10.1038/nri.2016.88.

203. von Moltke, J., Ji, M., Liang, H.E., and Locksley, R.M. (2016). Tuft-cell-derived IL-25 regulates an intestinal ILC2-epithelial response circuit. Nature *529*, 221-225. 10.1038/nature16161.

204. Howitt, M.R., Lavoie, S., Michaud, M., Blum, A.M., Tran, S.V., Weinstock, J.V., Gallini, C.A., Redding, K., Margolskee, R.F., Osborne, L.C., et al. (2016). Tuft cells, taste-chemosensory cells, orchestrate parasite type 2 immunity in the gut. Science *351*, 1329-1333. 10.1126/science.aaf1648.

205. Gerbe, F., Sidot, E., Smyth, D.J., Ohmoto, M., Matsumoto, I., Dardalhon, V., Cesses, P., Garnier, L., Pouzolles, M., Brulin, B., et al. (2016). Intestinal epithelial tuft cells initiate type 2 mucosal immunity to helminth parasites. Nature *529*, 226-230. 10.1038/nature16527.

206. Gribble, F.M., and Reimann, F. (2019). Function and mechanisms of enteroendocrine cells and gut hormones in metabolism. Nat Rev Endocrinol *15*, 226-237. 10.1038/s41574-019-0168-8.

207. de Lau, W., Kujala, P., Schneeberger, K., Middendorp, S., Li, V.S., Barker, N., Martens, A., Hofhuis, F., DeKoter, R.P., Peters, P.J., et al. (2012). Peyer's patch M cells derived from Lgr5(+) stem cells require SpiB and are induced by RankL in cultured "miniguts". Mol Cell Biol *32*, 3639-3647. 10.1128/MCB.00434-12.

208. Knoop, K.A., Kumar, N., Butler, B.R., Sakthivel, S.K., Taylor, R.T., Nochi, T., Akiba, H., Yagita, H., Kiyono, H., and Williams, I.R. (2009). RANKL is necessary and sufficient to initiate development of antigen-sampling M cells in the intestinal epithelium. J Immunol *183*, 5738-5747. 10.4049/jimmunol.0901563.

209. Kanaya, T., Hase, K., Takahashi, D., Fukuda, S., Hoshino, K., Sasaki, I., Hemmi, H., Knoop, K.A., Kumar, N., Sato, M., et al. (2012). The Ets transcription factor Spi-B is essential for the differentiation of intestinal microfold cells. Nat Immunol *13*, 729-736. 10.1038/ni.2352.

210. Kraehenbuhl, J.P., and Neutra, M.R. (2000). Epithelial M cells: differentiation and function. Annu Rev Cell Dev Biol *16*, 301-332. 10.1146/annurev.cellbio.16.1.301.

211. Mowat, A.M., and Agace, W.W. (2014). Regional specialization within the intestinal immune system. Nat Rev Immunol *14*, 667-685. 10.1038/nri3738.

212. Kanaya, T., Williams, I.R., and Ohno, H. (2020). Intestinal M cells: Tireless samplers of enteric microbiota. Traffic *21*, 34-44. 10.1111/tra.12707.

213. Gebert, A., Rothkotter, H.J., and Pabst, R. (1996). M cells in Peyer's patches of the intestine. Int Rev Cytol *167*, 91-159. 10.1016/s0074-7696(08)61346-7.

214. Hase, K., Kawano, K., Nochi, T., Pontes, G.S., Fukuda, S., Ebisawa, M., Kadokura, K., Tobe, T., Fujimura, Y., Kawano, S., et al. (2009). Uptake through glycoprotein 2 of FimH(+) bacteria by M cells initiates mucosal immune response. Nature *462*, 226-230. 10.1038/nature08529.

215. Darwich, A.S., Aslam, U., Ashcroft, D.M., and Rostami-Hodjegan, A. (2014). Meta-analysis of the turnover of intestinal epithelia in preclinical animal species and humans. Drug Metab Dispos *42*, 2016-2022. 10.1124/dmd.114.058404.

216. Beumer, J., and Clevers, H. (2021). Cell fate specification and differentiation in the adult mammalian intestine. Nat Rev Mol Cell Biol *22*, 39-53. 10.1038/s41580-020-0278-0.

217. Ritsma, L., Ellenbroek, S.I.J., Zomer, A., Snippert, H.J., de Sauvage, F.J., Simons, B.D., Clevers, H., and van Rheenen, J. (2014). Intestinal crypt homeostasis revealed at single-stem-cell level by in vivo live imaging. Nature *507*, 362-365. 10.1038/nature12972.

218. Snippert, H.J., van der Flier, L.G., Sato, T., van Es, J.H., van den Born, M., Kroon-Veenboer, C., Barker, N., Klein, A.M., van Rheenen, J., Simons, B.D., and Clevers, H. (2010). Intestinal crypt homeostasis results from neutral competition between symmetrically dividing Lgr5 stem cells. Cell *143*, 134-144. 10.1016/j.cell.2010.09.016.

219. Hageman, J.H., Heinz, M.C., Kretzschmar, K., van der Vaart, J., Clevers, H., and Snippert, H.J.G. (2020). Intestinal Regeneration: Regulation by the Microenvironment. Dev Cell *54*, 435-446. 10.1016/j.devcel.2020.07.009.

220. Koch, U., Lehal, R., and Radtke, F. (2013). Stem cells living with a Notch. Development *140*, 689-704. 10.1242/dev.080614.

221. Shibahara, T., Sato, N., Waguri, S., Iwanaga, T., Nakahara, A., Fukutomi, H., and Uchiyama, Y. (1995). The fate of effete epithelial cells at the villus tips of the human small intestine. Arch Histol Cytol *58*, 205-219. 10.1679/aohc.58.205.

222. Madara, J.L. (1990). Maintenance of the macromolecular barrier at cell extrusion sites in intestinal epithelium: physiological rearrangement of tight junctions. J Membr Biol *116*, 177-184. 10.1007/BF01868675.

223. Marchiando, A.M., Shen, L., Graham, W.V., Edelblum, K.L., Duckworth, C.A., Guan, Y., Montrose, M.H., Turner, J.R., and Watson, A.J. (2011). The epithelial barrier is maintained by in vivo tight junction expansion during pathologic intestinal epithelial shedding. Gastroenterology *140*, 1208-1218 e1201-1202. 10.1053/j.gastro.2011.01.004.

224. Buczacki, S.J., Zecchini, H.I., Nicholson, A.M., Russell, R., Vermeulen, L., Kemp, R., and Winton, D.J. (2013). Intestinal label-retaining cells are secretory precursors expressing Lgr5. Nature *495*, 65-69. 10.1038/nature11965.

225. Wilson, C.L., Ouellette, A.J., Satchell, D.P., Ayabe, T., Lopez-Boado, Y.S., Stratman, J.L., Hultgren, S.J., Matrisian, L.M., and Parks, W.C. (1999). Regulation of intestinal alpha-defensin activation by the metalloproteinase matrilysin in innate host defense. Science *286*, 113-117. 10.1126/science.286.5437.113.

226. Salzman, N.H., Ghosh, D., Huttner, K.M., Paterson, Y., and Bevins, C.L. (2003). Protection against enteric salmonellosis in transgenic mice expressing a human intestinal defensin. Nature *422*, 522-526. 10.1038/nature01520.

227. Salzman, N.H., Underwood, M.A., and Bevins, C.L. (2007). Paneth cells, defensins, and the commensal microbiota: a hypothesis on intimate interplay at the intestinal mucosa. Semin Immunol *19*, 70-83. 10.1016/j.smim.2007.04.002.

228. Vaishnava, S., Behrendt, C.L., Ismail, A.S., Eckmann, L., and Hooper, L.V. (2008). Paneth cells directly sense gut commensals and maintain homeostasis at the intestinal host-microbial interface. Proc Natl Acad Sci U S A *105*, 20858-20863. 10.1073/pnas.0808723105.

229. Kobayashi, K.S., Chamaillard, M., Ogura, Y., Henegariu, O., Inohara, N., Nunez, G., and Flavell, R.A. (2005). Nod2-dependent regulation of innate and adaptive immunity in the intestinal tract. Science *307*, 731-734. 10.1126/science.1104911.

230. Tan, G., Zeng, B., and Zhi, F.C. (2015). Regulation of human enteric alpha-defensins by NOD2 in the Paneth cell lineage. Eur J Cell Biol *94*, 60-66. 10.1016/j.ejcb.2014.10.007.

231. Ayabe, T., Satchell, D.P., Wilson, C.L., Parks, W.C., Selsted, M.E., and Ouellette, A.J. (2000). Secretion of microbicidal alpha-defensins by intestinal Paneth cells in response to bacteria. Nat Immunol *1*, 113-118. 10.1038/77783.

232. Wallaeys, C., Garcia-Gonzalez, N., and Libert, C. (2023). Paneth cells as the cornerstones of intestinal and organismal health: a primer. EMBO Mol Med *15*, e16427. 10.15252/emmm.202216427.

233. Salzman, N.H., Hung, K., Haribhai, D., Chu, H., Karlsson-Sjoberg, J., Amir, E., Teggatz, P., Barman, M., Hayward, M., Eastwood, D., et al. (2010). Enteric defensins are essential regulators of intestinal microbial ecology. Nat Immunol *11*, 76-83. 10.1038/ni.1825.

234. Powell, D.W., Pinchuk, I.V., Saada, J.I., Chen, X., and Mifflin, R.C. (2011). Mesenchymal cells of the intestinal lamina propria. Annu Rev Physiol *73*, 213-237. 10.1146/annurev.physiol.70.113006.100646.

235. Valenta, T., Degirmenci, B., Moor, A.E., Herr, P., Zimmerli, D., Moor, M.B., Hausmann, G., Cantu, C., Aguet, M., and Basler, K. (2016). Wnt Ligands Secreted by Subepithelial Mesenchymal Cells Are Essential for the Survival of Intestinal Stem Cells and Gut Homeostasis. Cell Rep *15*, 911-918. 10.1016/j.celrep.2016.03.088.

236. Stzepourginski, I., Nigro, G., Jacob, J.M., Dulauroy, S., Sansonetti, P.J., Eberl, G., and Peduto, L. (2017). CD34+ mesenchymal cells are a major component of the intestinal stem cells niche at homeostasis and after injury. Proc Natl Acad Sci U S A *114*, E506-E513. 10.1073/pnas.1620059114.

237. Kosinski, C., Li, V.S., Chan, A.S., Zhang, J., Ho, C., Tsui, W.Y., Chan, T.L., Mifflin, R.C., Powell, D.W., Yuen, S.T., et al. (2007). Gene expression patterns of human colon tops and basal crypts and BMP antagonists as intestinal stem cell niche factors. Proc Natl Acad Sci U S A *104*, 15418-15423. 10.1073/pnas.0707210104.

238. Sato, T., van Es, J.H., Snippert, H.J., Stange, D.E., Vries, R.G., van den Born, M., Barker, N., Shroyer, N.F., van de Wetering, M., and Clevers, H. (2011). Paneth cells constitute the niche for Lgr5 stem cells in intestinal crypts. Nature *469*, 415-418. 10.1038/nature09637.

239. Tschurtschenthaler, M., Adolph, T.E., Ashcroft, J.W., Niederreiter, L., Bharti, R., Saveljeva, S., Bhattacharyya, J., Flak, M.B., Shih, D.Q., Fuhler, G.M., et al. (2017). Defective ATG16L1-mediated removal of IRE1alpha drives Crohn's disease-like ileitis. J Exp Med *214*, 401-422. 10.1084/jem.20160791.

240. Burger, E., Araujo, A., Lopez-Yglesias, A., Rajala, M.W., Geng, L., Levine, B., Hooper, L.V., Burstein, E., and Yarovinsky, F. (2018). Loss of Paneth Cell Autophagy Causes Acute Susceptibility to Toxoplasma gondii-Mediated Inflammation. Cell Host Microbe *23*, 177-190 e174. 10.1016/j.chom.2018.01.001.

241. Cadwell, K., Liu, J.Y., Brown, S.L., Miyoshi, H., Loh, J., Lennerz, J.K., Kishi, C., Kc, W., Carrero, J.A., Hunt, S., et al. (2008). A key role for autophagy and the autophagy gene Atg16l1 in mouse and human intestinal Paneth cells. Nature *456*, 259-263. 10.1038/nature07416.

242. Cadwell, K., Patel, K.K., Komatsu, M., Virgin, H.W.t., and Stappenbeck, T.S. (2009). A common role for Atg16L1, Atg5 and Atg7 in small intestinal Paneth cells and Crohn disease. Autophagy *5*, 250-252. 10.4161/auto.5.2.7560.

243. Ireland, H., Houghton, C., Howard, L., and Winton, D.J. (2005). Cellular inheritance of a Cre-activated reporter gene to determine Paneth cell longevity in the murine small intestine. Dev Dyn *233*, 1332-1336. 10.1002/dvdy.20446.

244. Johansson, M.E., Phillipson, M., Petersson, J., Velcich, A., Holm, L., and Hansson, G.C. (2008). The inner of the two Muc2 mucin-dependent mucus layers in colon is devoid of bacteria. Proc Natl Acad Sci U S A *105*, 15064-15069. 10.1073/pnas.0803124105.

245. Luis, A.S., and Hansson, G.C. (2023). Intestinal mucus and their glycans: A habitat for thriving microbiota. Cell Host Microbe *31*, 1087-1100. 10.1016/j.chom.2023.05.026.

246. Ermund, A., Schutte, A., Johansson, M.E., Gustafsson, J.K., and Hansson, G.C. (2013). Studies of mucus in mouse stomach, small intestine, and colon. I. Gastrointestinal mucus layers have different properties depending on location as well as over the Peyer's patches. Am J Physiol Gastrointest Liver Physiol *305*, G341-347. 10.1152/ajpgi.00046.2013.

247. Hansson, G.C. (2020). Mucins and the Microbiome. Annu Rev Biochem *89*, 769-793. 10.1146/annurev-biochem-011520-105053.

248. Van der Sluis, M., De Koning, B.A., De Bruijn, A.C., Velcich, A., Meijerink, J.P., Van Goudoever, J.B., Buller, H.A., Dekker, J., Van Seuningen, I., Renes, I.B., and Einerhand, A.W. (2006). Muc2-deficient mice spontaneously develop colitis, indicating that MUC2 is critical for colonic protection. Gastroenterology *131*, 117-129. 10.1053/j.gastro.2006.04.020.

249. Gruber, A.D., Elble, R.C., Ji, H.L., Schreur, K.D., Fuller, C.M., and Pauli, B.U. (1998). Genomic cloning, molecular characterization, and functional analysis of human CLCA1, the first human member of the family of Ca2+-activated Cl- channel proteins. Genomics *54*, 200-214. 10.1006/geno.1998.5562.

250. Johansson, M.E., Thomsson, K.A., and Hansson, G.C. (2009). Proteomic analyses of the two mucus layers of the colon barrier reveal that their main component, the Muc2 mucin, is strongly bound to the Fcgbp protein. J Proteome Res *8*, 3549-3557. 10.1021/pr9002504.

251. Madsen, J., Nielsen, O., Tornoe, I., Thim, L., and Holmskov, U. (2007). Tissue localization of human trefoil factors 1, 2, and 3. J Histochem Cytochem *55*, 505-513. 10.1369/jhc.6A7100.2007.

252. Bergstrom, J.H., Birchenough, G.M., Katona, G., Schroeder, B.O., Schutte, A., Ermund, A., Johansson, M.E., and Hansson, G.C. (2016). Gram-positive bacteria are held at a distance in the colon mucus by the lectin-like protein ZG16. Proc Natl Acad Sci U S A *113*, 13833-13838. 10.1073/pnas.1611400113.

253. Williams, S.J., Wreschner, D.H., Tran, M., Eyre, H.J., Sutherland, G.R., and McGuckin, M.A. (2001). Muc13, a novel human cell surface mucin expressed by epithelial and hemopoietic cells. J Biol Chem *276*, 18327-18336. 10.1074/jbc.M008850200.

254. Gum, J.R., Jr., Crawley, S.C., Hicks, J.W., Szymkowski, D.E., and Kim, Y.S. (2002). MUC17, a novel membrane-tethered mucin. Biochem Biophys Res Commun *291*, 466-475. 10.1006/bbrc.2002.6475.

255. Pelaseyed, T., Gustafsson, J.K., Gustafsson, I.J., Ermund, A., and Hansson, G.C. (2013). Carbachol-induced MUC17 endocytosis is concomitant with NHE3 internalization and CFTR membrane recruitment in enterocytes. Am J Physiol Cell Physiol *305*, C457-467. 10.1152/ajpcell.00141.2013.

256. McDole, J.R., Wheeler, L.W., McDonald, K.G., Wang, B., Konjufca, V., Knoop, K.A., Newberry, R.D., and Miller, M.J. (2012). Goblet cells deliver luminal antigen to CD103+ dendritic cells in the small intestine. Nature *483*, 345-349. 10.1038/nature10863.

257. Javitt, G., Khmelnitsky, L., Albert, L., Bigman, L.S., Elad, N., Morgenstern, D., Ilani, T., Levy, Y., Diskin, R., and Fass, D. (2020). Assembly Mechanism of Mucin and von Willebrand Factor Polymers. Cell *183*, 717-729 e716. 10.1016/j.cell.2020.09.021.

258. Bennett, E.P., Mandel, U., Clausen, H., Gerken, T.A., Fritz, T.A., and Tabak, L.A. (2012). Control of mucin-type O-glycosylation: a classification of the polypeptide GalNAc-transferase gene family. Glycobiology *22*, 736-756. 10.1093/glycob/cwr182.

259. Axelsson, M.A., Karlsson, N.G., Steel, D.M., Ouwendijk, J., Nilsson, T., and Hansson, G.C. (2001). Neutralization of pH in the Golgi apparatus causes redistribution of glycosyltransferases and changes in the O-glycosylation of mucins. Glycobiology *11*, 633-644. 10.1093/glycob/11.8.633.

260. Heazlewood, C.K., Cook, M.C., Eri, R., Price, G.R., Tauro, S.B., Taupin, D., Thornton, D.J., Png, C.W., Crockford, T.L., Cornall, R.J., et al. (2008). Aberrant mucin assembly in mice causes endoplasmic reticulum stress and spontaneous inflammation resembling ulcerative colitis. PLoS Med *5*, e54. 10.1371/journal.pmed.0050054.

261. Brandl, K., Rutschmann, S., Li, X., Du, X., Xiao, N., Schnabl, B., Brenner, D.A., and Beutler, B. (2009). Enhanced sensitivity to DSS colitis caused by a hypomorphic Mbtps1 mutation disrupting the ATF6-driven unfolded protein response. Proc Natl Acad Sci U S A *106*, 3300-3305. 10.1073/pnas.0813036106.

262. Zhao, F., Edwards, R., Dizon, D., Afrasiabi, K., Mastroianni, J.R., Geyfman, M., Ouellette, A.J., Andersen, B., and Lipkin, S.M. (2010). Disruption of Paneth and goblet cell homeostasis and increased endoplasmic reticulum stress in Agr2-/- mice. Dev Biol *338*, 270-279. 10.1016/j.ydbio.2009.12.008.

263. Coleman, O.I., Lobner, E.M., Bierwirth, S., Sorbie, A., Waldschmitt, N., Rath, E., Berger, E., Lagkouvardos, I., Clavel, T., McCoy, K.D., et al. (2018). Activated ATF6 Induces Intestinal Dysbiosis and Innate Immune Response to Promote Colorectal Tumorigenesis. Gastroenterology *155*, 1539-1552 e1512. 10.1053/j.gastro.2018.07.028.

264. Grey, M.J., De Luca, H., Ward, D.V., Kreulen, I.A., Bugda Gwilt, K., Foley, S.E., Thiagarajah, J.R., McCormick, B.A., Turner, J.R., and Lencer, W.I. (2022). The epithelial-specific ER stress sensor ERN2/IRE1beta enables host-microbiota crosstalk to affect colon goblet cell development. J Clin Invest *132*. 10.1172/JCI153519.

265. Tsuru, A., Fujimoto, N., Takahashi, S., Saito, M., Nakamura, D., Iwano, M., Iwawaki, T., Kadokura, H., Ron, D., and Kohno, K. (2013). Negative feedback by IRE1beta optimizes mucin production in goblet cells. Proc Natl Acad Sci U S A *110*, 2864-2869. 10.1073/pnas.1212484110.

266. Chang, J.T. (2020). Pathophysiology of Inflammatory Bowel Diseases. N Engl J Med *383*, 2652-2664. 10.1056/NEJMra2002697.

267. Kaser, A., Zeissig, S., and Blumberg, R.S. (2010). Inflammatory bowel disease. Annu Rev Immunol *28*, 573-621. 10.1146/annurev-immunol-030409-101225.

268. Halme, L., Paavola-Sakki, P., Turunen, U., Lappalainen, M., Farkkila, M., and Kontula, K. (2006). Family and twin studies in inflammatory bowel disease. World J Gastroenterol *12*, 3668-3672. 10.3748/wjg.v12.i23.3668.

269. Probert, C.S., Jayanthi, V., Hughes, A.O., Thompson, J.R., Wicks, A.C., and Mayberry, J.F. (1993). Prevalence and family risk of ulcerative colitis and Crohn's disease: an epidemiological study among Europeans and south Asians in Leicestershire. Gut *34*, 1547-1551. 10.1136/gut.34.11.1547.

270. Orholm, M., Munkholm, P., Langholz, E., Nielsen, O.H., Sorensen, T.I., and Binder, V. (1991). Familial occurrence of inflammatory bowel disease. N Engl J Med *324*, 84-88. 10.1056/NEJM199101103240203.

271. Freeman, H.J. (2002). Familial Crohn's disease in single or multiple first-degree relatives. J Clin Gastroenterol *35*, 9-13. 10.1097/00004836-200207000-00004.

272. Halme, L., Turunen, U., Helio, T., Paavola, P., Walle, T., Miettinen, A., Jarvinen, H., Kontula, K., and Farkkila, M. (2002). Familial and sporadic inflammatory bowel disease: comparison of clinical features and serological markers in a genetically homogeneous population. Scand J Gastroenterol *37*, 692-698. 10.1080/00365520212511.

273. Carbonnel, F., Macaigne, G., Beaugerie, L., Gendre, J.P., and Cosnes, J. (1999). Crohn's disease severity in familial and sporadic cases. Gut *44*, 91-95. 10.1136/gut.44.1.91.

274. Peeters, M., Nevens, H., Baert, F., Hiele, M., de Meyer, A.M., Vlietinck, R., and Rutgeerts, P. (1996). Familial aggregation in Crohn's disease: increased age-adjusted risk and concordance in clinical characteristics. Gastroenterology *111*, 597-603. 10.1053/gast.1996.v111.pm8780562.

275. Bayless, T.M., Tokayer, A.Z., Polito, J.M., 2nd, Quaskey, S.A., Mellits, E.D., and Harris, M.L. (1996). Crohn's disease: concordance for site and clinical type in affected family members--potential hereditary influences. Gastroenterology *111*, 573-579. 10.1053/gast.1996.v111.pm8780559.

276. Graham, D.B., and Xavier, R.J. (2020). Pathway paradigms revealed from the genetics of inflammatory bowel disease. Nature *578*, 527-539. 10.1038/s41586-020-2025-2.

277. Jostins, L., Ripke, S., Weersma, R.K., Duerr, R.H., McGovern, D.P., Hui, K.Y., Lee, J.C., Schumm, L.P., Sharma, Y., Anderson, C.A., et al. (2012). Host-microbe interactions have shaped the genetic architecture of inflammatory bowel disease. Nature *491*, 119-124. 10.1038/nature11582.

278. Halfvarson, J., Bodin, L., Tysk, C., Lindberg, E., and Jarnerot, G. (2003). Inflammatory bowel disease in a Swedish twin cohort: a long-term follow-up of concordance and clinical characteristics. Gastroenterology *124*, 1767-1773. 10.1016/s0016-5085(03)00385-8.

279. Orholm, M., Binder, V., Sorensen, T.I., Rasmussen, L.P., and Kyvik, K.O. (2000). Concordance of inflammatory bowel disease among Danish twins. Results of a nationwide study. Scand J Gastroenterol *35*, 1075-1081. 10.1080/003655200451207.

280. Thompson, N.P., Driscoll, R., Pounder, R.E., and Wakefield, A.J. (1996). Genetics versus environment in inflammatory bowel disease: results of a British twin study. BMJ *312*, 95-96. 10.1136/bmj.312.7023.95.

281. Kaplan, G.G., and Windsor, J.W. (2021). The four epidemiological stages in the global evolution of inflammatory bowel disease. Nat Rev Gastroenterol Hepatol *18*, 56-66. 10.1038/s41575-020-00360-x.

282. Frank, D.N., St Amand, A.L., Feldman, R.A., Boedeker, E.C., Harpaz, N., and Pace, N.R. (2007). Molecular-phylogenetic characterization of microbial community imbalances in human inflammatory bowel diseases. Proc Natl Acad Sci U S A *104*, 13780-13785. 10.1073/pnas.0706625104.

283. Norman, J.M., Handley, S.A., Baldridge, M.T., Droit, L., Liu, C.Y., Keller, B.C., Kambal, A., Monaco, C.L., Zhao, G., Fleshner, P., et al. (2015). Disease-specific alterations in the enteric virome in inflammatory bowel disease. Cell *160*, 447-460. 10.1016/j.cell.2015.01.002.

284. Collaborators, G.B.D.I.B.D. (2020). The global, regional, and national burden of inflammatory bowel disease in 195 countries and territories, 1990-2017: a systematic analysis for the Global

Burden of Disease Study 2017. Lancet Gastroenterol Hepatol *5*, 17-30. 10.1016/S2468-1253(19)30333-4.

285. Ni, J., Wu, G.D., Albenberg, L., and Tomov, V.T. (2017). Gut microbiota and IBD: causation or correlation? Nat Rev Gastroenterol Hepatol *14*, 573-584. 10.1038/nrgastro.2017.88.

286. Patankar, J.V., and Becker, C. (2020). Cell death in the gut epithelium and implications for chronic inflammation. Nat Rev Gastroenterol Hepatol *17*, 543-556. 10.1038/s41575-020-0326-4.

287. Ghazavi, F., Huysentruyt, J., De Coninck, J., Kourula, S., Martens, S., Hassannia, B., Wartewig, T., Divert, T., Roelandt, R., Popper, B., et al. (2022). Executioner caspases 3 and 7 are dispensable for intestinal epithelium turnover and homeostasis at steady state. Proc Natl Acad Sci U S A *119*. 10.1073/pnas.2024508119.

288. Dannappel, M., Vlantis, K., Kumari, S., Polykratis, A., Kim, C., Wachsmuth, L., Eftychi, C., Lin, J., Corona, T., Hermance, N., et al. (2014). RIPK1 maintains epithelial homeostasis by inhibiting apoptosis and necroptosis. Nature *513*, 90-94. 10.1038/nature13608.

289. Takahashi, N., Vereecke, L., Bertrand, M.J., Duprez, L., Berger, S.B., Divert, T., Goncalves, A., Sze, M., Gilbert, B., Kourula, S., et al. (2014). RIPK1 ensures intestinal homeostasis by protecting the epithelium against apoptosis. Nature *513*, 95-99. 10.1038/nature13706.

290. Mitchell, P.S., Roncaioli, J.L., Turcotte, E.A., Goers, L., Chavez, R.A., Lee, A.Y., Lesser, C.F., Rauch, I., and Vance, R.E. (2020). NAIP-NLRC4-deficient mice are susceptible to shigellosis. Elife *9*. 10.7554/eLife.59022.

291. Roncaioli, J.L., Babirye, J.P., Chavez, R.A., Liu, F.L., Turcotte, E.A., Lee, A.Y., Lesser, C.F., and Vance, R.E. (2023). A hierarchy of cell death pathways confers layered resistance to shigellosis in mice. Elife *12*. 10.7554/eLife.83639.

292. Fattinger, S.A., Maurer, L., Geiser, P., Bernard, E.M., Enz, U., Ganguillet, S., Gul, E., Kroon, S., Demarco, B., Mack, V., et al. (2023). Gasdermin D is the only Gasdermin that provides protection against acute Salmonella gut infection in mice. Proc Natl Acad Sci U S A *120*, e2315503120. 10.1073/pnas.2315503120.

293. Katz, K.D., Hollander, D., Vadheim, C.M., McElree, C., Delahunty, T., Dadufalza, V.D., Krugliak, P., and Rotter, J.I. (1989). Intestinal permeability in patients with Crohn's disease and their healthy relatives. Gastroenterology *97*, 927-931. 10.1016/0016-5085(89)91499-6.

294. Teahon, K., Smethurst, P., Levi, A.J., Menzies, I.S., and Bjarnason, I. (1992). Intestinal permeability in patients with Crohn's disease and their first degree relatives. Gut *33*, 320-323. 10.1136/gut.33.3.320.

295. Yacyshyn, B.R., and Meddings, J.B. (1995). CD45RO expression on circulating CD19+ B cells in Crohn's disease correlates with intestinal permeability. Gastroenterology *108*, 132-137. 10.1016/0016-5085(95)90017-9.

296. Peeters, M., Geypens, B., Claus, D., Nevens, H., Ghoos, Y., Verbeke, G., Baert, F., Vermeire, S., Vlietinck, R., and Rutgeerts, P. (1997). Clustering of increased small intestinal permeability in families with Crohn's disease. Gastroenterology *113*, 802-807. 10.1016/s0016-5085(97)70174-4.

297. Soderholm, J.D., Olaison, G., Lindberg, E., Hannestad, U., Vindels, A., Tysk, C., Jarnerot, G., and Sjodahl, R. (1999). Different intestinal permeability patterns in relatives and spouses of patients with Crohn's disease: an inherited defect in mucosal defence? Gut *44*, 96-100. 10.1136/gut.44.1.96.

298. Buhner, S., Buning, C., Genschel, J., Kling, K., Herrmann, D., Dignass, A., Kuechler, I., Krueger, S., Schmidt, H.H., and Lochs, H. (2006). Genetic basis for increased intestinal

permeability in families with Crohn's disease: role of CARD15 3020insC mutation? Gut *55*, 342-347. 10.1136/gut.2005.065557.

299. Wyatt, J., Vogelsang, H., Hubl, W., Waldhoer, T., and Lochs, H. (1993). Intestinal permeability and the prediction of relapse in Crohn's disease. Lancet *341*, 1437-1439. 10.1016/0140-6736(93)90882-h.

300. Iwamoto, M., Koji, T., Makiyama, K., Kobayashi, N., and Nakane, P.K. (1996). Apoptosis of crypt epithelial cells in ulcerative colitis. J Pathol *180*, 152-159. 10.1002/(SICI)1096-9896(199610)180:2<152::AID-PATH649>3.0.CO;2-Y.

301. Di Sabatino, A., Ciccocioppo, R., Luinetti, O., Ricevuti, L., Morera, R., Cifone, M.G., Solcia, E., and Corazza, G.R. (2003). Increased enterocyte apoptosis in inflamed areas of Crohn's disease. Dis Colon Rectum *46*, 1498-1507. 10.1007/s10350-004-6802-z.

302. Hagiwara, C., Tanaka, M., and Kudo, H. (2002). Increase in colorectal epithelial apoptotic cells in patients with ulcerative colitis ultimately requiring surgery. J Gastroenterol Hepatol *17*, 758-764. 10.1046/j.1440-1746.2002.02791.x.

303. Lehle, A.S., Farin, H.F., Marquardt, B., Michels, B.E., Magg, T., Li, Y., Liu, Y., Ghalandary, M., Lammens, K., Hollizeck, S., et al. (2019). Intestinal Inflammation and Dysregulated Immunity in Patients With Inherited Caspase-8 Deficiency. Gastroenterology *156*, 275-278. 10.1053/j.gastro.2018.09.041.

304. Nenci, A., Becker, C., Wullaert, A., Gareus, R., van Loo, G., Danese, S., Huth, M., Nikolaev, A., Neufert, C., Madison, B., et al. (2007). Epithelial NEMO links innate immunity to chronic intestinal inflammation. Nature *446*, 557-561. 10.1038/nature05698.

305. Vlantis, K., Wullaert, A., Polykratis, A., Kondylis, V., Dannappel, M., Schwarzer, R., Welz, P., Corona, T., Walczak, H., Weih, F., et al. (2016). NEMO Prevents RIP Kinase 1-Mediated Epithelial Cell Death and Chronic Intestinal Inflammation by NF-kappaB-Dependent and -Independent Functions. Immunity *44*, 553-567. 10.1016/j.immuni.2016.02.020.

306. Eftychi, C., Schwarzer, R., Vlantis, K., Wachsmuth, L., Basic, M., Wagle, P., Neurath, M.F., Becker, C., Bleich, A., and Pasparakis, M. (2019). Temporally Distinct Functions of the Cytokines IL-12 and IL-23 Drive Chronic Colon Inflammation in Response to Intestinal Barrier Impairment. Immunity *51*, 367-380 e364. 10.1016/j.immuni.2019.06.008.

307. Schwarzer, R., Jiao, H., Wachsmuth, L., Tresch, A., and Pasparakis, M. (2020). FADD and Caspase-8 Regulate Gut Homeostasis and Inflammation by Controlling MLKL- and GSDMD-Mediated Death of Intestinal Epithelial Cells. Immunity *52*, 978-993 e976. 10.1016/j.immuni.2020.04.002.

308. Gunther, C., Martini, E., Wittkopf, N., Amann, K., Weigmann, B., Neumann, H., Waldner, M.J., Hedrick, S.M., Tenzer, S., Neurath, M.F., and Becker, C. (2011). Caspase-8 regulates TNF-alpha-induced epithelial necroptosis and terminal ileitis. Nature *477*, 335-339. 10.1038/nature10400.

309. Welz, P.S., Wullaert, A., Vlantis, K., Kondylis, V., Fernandez-Majada, V., Ermolaeva, M., Kirsch, P., Sterner-Kock, A., van Loo, G., and Pasparakis, M. (2011). FADD prevents RIP3-mediated epithelial cell necrosis and chronic intestinal inflammation. Nature *477*, 330-334. 10.1038/nature10273.

310. Weinlich, R., Oberst, A., Dillon, C.P., Janke, L.J., Milasta, S., Lukens, J.R., Rodriguez, D.A., Gurung, P., Savage, C., Kanneganti, T.D., and Green, D.R. (2013). Protective roles for caspase-8 and cFLIP in adult homeostasis. Cell Rep *5*, 340-348. 10.1016/j.celrep.2013.08.045.

311. Wittkopf, N., Gunther, C., Martini, E., He, G., Amann, K., He, Y.W., Schuchmann, M., Neurath, M.F., and Becker, C. (2013). Cellular FLICE-like inhibitory protein secures intestinal epithelial

cell survival and immune homeostasis by regulating caspase-8. Gastroenterology *145*, 1369-1379. 10.1053/j.gastro.2013.08.059.

312. Stolzer, I., Kaden-Volynets, V., Ruder, B., Letizia, M., Bittel, M., Rausch, P., Basic, M., Bleich, A., Baines, J.F., Neurath, M.F., et al. (2020). Environmental Microbial Factors Determine the Pattern of Inflammatory Lesions in a Murine Model of Crohn's Disease-Like Inflammation. Inflamm Bowel Dis *26*, 66-79. 10.1093/ibd/izz142.

313. Cuchet-Lourenco, D., Eletto, D., Wu, C., Plagnol, V., Papapietro, O., Curtis, J., Ceron-Gutierrez, L., Bacon, C.M., Hackett, S., Alsaleem, B., et al. (2018). Biallelic RIPK1 mutations in humans cause severe immunodeficiency, arthritis, and intestinal inflammation. Science *361*, 810-813. 10.1126/science.aar2641.

314. Uchiyama, Y., Kim, C.A., Pastorino, A.C., Ceroni, J., Lima, P.P., de Barros Dorna, M., Honjo, R.S., Bertola, D., Hamanaka, K., Fujita, A., et al. (2019). Primary immunodeficiency with chronic enteropathy and developmental delay in a boy arising from a novel homozygous RIPK1 variant. J Hum Genet *64*, 955-960. 10.1038/s10038-019-0631-3.

315. Sultan, M., Adawi, M., Kol, N., McCourt, B., Adawi, I., Baram, L., Tal, N., Werner, L., Lev, A., Snapper, S.B., et al. (2022). RIPK1 mutations causing infantile-onset IBD with inflammatory and fistulizing features. Front Immunol *13*, 1041315. 10.3389/fimmu.2022.1041315.

316. Bazgir, N., Tahvildari, A., Chavoshzade, Z., Jamee, M., Golchehre, Z., Karimi, A., Dara, N., Fallahi, M., Keramatipour, M., Karamzade, A., and Sharafian, S. (2023). A rare immunological disease, caspase 8 deficiency: case report and literature review. Allergy Asthma Clin Immunol *19*, 29. 10.1186/s13223-023-00778-3.

317. Treton, X., Pedruzzi, E., Cazals-Hatem, D., Grodet, A., Panis, Y., Groyer, A., Moreau, R., Bouhnik, Y., Daniel, F., and Ogier-Denis, E. (2011). Altered endoplasmic reticulum stress affects translation in inactive colon tissue from patients with ulcerative colitis. Gastroenterology *141*, 1024-1035. 10.1053/j.gastro.2011.05.033.

318. Deuring, J.J., de Haar, C., Koelewijn, C.L., Kuipers, E.J., Peppelenbosch, M.P., and van der Woude, C.J. (2012). Absence of ABCG2-mediated mucosal detoxification in patients with active inflammatory bowel disease is due to impeded protein folding. Biochem J *441*, 87-93. 10.1042/BJ20111281.

319. Hodin, C.M., Verdam, F.J., Grootjans, J., Rensen, S.S., Verheyen, F.K., Dejong, C.H., Buurman, W.A., Greve, J.W., and Lenaerts, K. (2011). Reduced Paneth cell antimicrobial protein levels correlate with activation of the unfolded protein response in the gut of obese individuals. J Pathol *225*, 276-284. 10.1002/path.2917.

320. Barrett, J.C., Hansoul, S., Nicolae, D.L., Cho, J.H., Duerr, R.H., Rioux, J.D., Brant, S.R., Silverberg, M.S., Taylor, K.D., Barmada, M.M., et al. (2008). Genome-wide association defines more than 30 distinct susceptibility loci for Crohn's disease. Nat Genet *40*, 955-962. 10.1038/ng.175.

321. McGovern, D.P., Gardet, A., Torkvist, L., Goyette, P., Essers, J., Taylor, K.D., Neale, B.M., Ong, R.T., Lagace, C., Li, C., et al. (2010). Genome-wide association identifies multiple ulcerative colitis susceptibility loci. Nat Genet *42*, 332-337. 10.1038/ng.549.

322. Zheng, W., Rosenstiel, P., Huse, K., Sina, C., Valentonyte, R., Mah, N., Zeitlmann, L., Grosse, J., Ruf, N., Nurnberg, P., et al. (2006). Evaluation of AGR2 and AGR3 as candidate genes for inflammatory bowel disease. Genes Immun *7*, 11-18. 10.1038/sj.gene.6364263.

323. Kaser, A., Lee, A.H., Franke, A., Glickman, J.N., Zeissig, S., Tilg, H., Nieuwenhuis, E.E., Higgins, D.E., Schreiber, S., Glimcher, L.H., and Blumberg, R.S. (2008). XBP1 links ER stress to intestinal inflammation and confers genetic risk for human inflammatory bowel disease. Cell *134*, 743-756. 10.1016/j.cell.2008.07.021.

324. van der Post, S., Jabbar, K.S., Birchenough, G., Arike, L., Akhtar, N., Sjovall, H., Johansson, M.E.V., and Hansson, G.C. (2019). Structural weakening of the colonic mucus barrier is an early event in ulcerative colitis pathogenesis. Gut *68*, 2142-2151. 10.1136/gutjnl-2018-317571.

325. Kaser, A., Adolph, T.E., and Blumberg, R.S. (2013). The unfolded protein response and gastrointestinal disease. Semin Immunopathol *35*, 307-319. 10.1007/s00281-013-0377-5.

326. Bergstrom, J.H., Berg, K.A., Rodriguez-Pineiro, A.M., Stecher, B., Johansson, M.E., and Hansson, G.C. (2014). AGR2, an endoplasmic reticulum protein, is secreted into the gastrointestinal mucus. PLoS One *9*, e104186. 10.1371/journal.pone.0104186.

327. Park, S.W., Zhen, G., Verhaeghe, C., Nakagami, Y., Nguyenvu, L.T., Barczak, A.J., Killeen, N., and Erle, D.J. (2009). The protein disulfide isomerase AGR2 is essential for production of intestinal mucus. Proc Natl Acad Sci U S A *106*, 6950-6955. 10.1073/pnas.0808722106.

328. Yamamoto-Furusho, J.K. (2007). Genetic factors associated with the development of inflammatory bowel disease. World J Gastroenterol *13*, 5594-5597. 10.3748/wjg.v13.i42.5594.

329. Ananthakrishnan, A.N. (2021). IBD risk prediction using multi-ethnic polygenic risk scores. Nat Rev Gastroenterol Hepatol *18*, 217-218. 10.1038/s41575-021-00425-5.

330. Rajewsky, K., Gu, H., Kuhn, R., Betz, U.A., Muller, W., Roes, J., and Schwenk, F. (1996). Conditional gene targeting. J Clin Invest *98*, 600-603. 10.1172/JCI118828.

331. Madison, B.B., Dunbar, L., Qiao, X.T., Braunstein, K., Braunstein, E., and Gumucio, D.L. (2002). Cis elements of the villin gene control expression in restricted domains of the vertical (crypt) and horizontal (duodenum, cecum) axes of the intestine. J Biol Chem *277*, 33275-33283. 10.1074/jbc.M204935200.

332. Maunoury, R., Robine, S., Pringault, E., Leonard, N., Gaillard, J.A., and Louvard, D. (1992). Developmental regulation of villin gene expression in the epithelial cell lineages of mouse digestive and urogenital tracts. Development *115*, 717-728. 10.1242/dev.115.3.717.

333. Sato, T., Stange, D.E., Ferrante, M., Vries, R.G., Van Es, J.H., Van den Brink, S., Van Houdt, W.J., Pronk, A., Van Gorp, J., Siersema, P.D., and Clevers, H. (2011). Long-term expansion of epithelial organoids from human colon, adenoma, adenocarcinoma, and Barrett's epithelium. Gastroenterology *141*, 1762-1772. 10.1053/j.gastro.2011.07.050.

334. Guttman, O., Le Thomas, A., Marsters, S., Lawrence, D.A., Gutgesell, L., Zuazo-Gaztelu, I., Harnoss, J.M., Haag, S.M., Murthy, A., Strasser, G., et al. (2022). Antigen-derived peptides engage the ER stress sensor IRE1alpha to curb dendritic cell cross-presentation. J Cell Biol *221*. 10.1083/jcb.202111068.

335. Gerdes, J., Lemke, H., Baisch, H., Wacker, H.H., Schwab, U., and Stein, H. (1984). Cell cycle analysis of a cell proliferation-associated human nuclear antigen defined by the monoclonal antibody Ki-67. J Immunol *133*, 1710-1715.

336. Erlandsen, S.L., Parsons, J.A., and Taylor, T.D. (1974). Ultrastructural immunocytochemical localization of lysozyme in the Paneth cells of man. J Histochem Cytochem *22*, 401-413. 10.1177/22.6.401.

337. Beisner, D.R., Ch'en, I.L., Kolla, R.V., Hoffmann, A., and Hedrick, S.M. (2005). Cutting edge: innate immunity conferred by B cells is regulated by caspase-8. J Immunol *175*, 3469-3473. 10.4049/jimmunol.175.6.3469.

338. Lalaoui, N., Boyden, S.E., Oda, H., Wood, G.M., Stone, D.L., Chau, D., Liu, L., Stoffels, M., Kratina, T., Lawlor, K.E., et al. (2020). Mutations that prevent caspase cleavage of RIPK1 cause autoinflammatory disease. Nature *577*, 103-108. 10.1038/s41586-019-1828-5.

339. Lin, Y., Devin, A., Rodriguez, Y., and Liu, Z.G. (1999). Cleavage of the death domain kinase RIP by caspase-8 prompts TNF-induced apoptosis. Genes Dev *13*, 2514-2526. 10.1101/gad.13.19.2514.

340. Tao, P., Sun, J., Wu, Z., Wang, S., Wang, J., Li, W., Pan, H., Bai, R., Zhang, J., Wang, Y., et al. (2020). A dominant autoinflammatory disease caused by non-cleavable variants of RIPK1. Nature *577*, 109-114. 10.1038/s41586-019-1830-y.

341. Newton, K., Sun, X., and Dixit, V.M. (2004). Kinase RIP3 is dispensable for normal NF-kappa Bs, signaling by the B-cell and T-cell receptors, tumor necrosis factor receptor 1, and Toll-like receptors 2 and 4. Mol Cell Biol *24*, 1464-1469. 10.1128/MCB.24.4.1464-1469.2004.

342. Moriwaki, K., Balaji, S., McQuade, T., Malhotra, N., Kang, J., and Chan, F.K. (2014). The necroptosis adaptor RIPK3 promotes injury-induced cytokine expression and tissue repair. Immunity *41*, 567-578. 10.1016/j.immuni.2014.09.016.

343. Lin, J., Kumari, S., Kim, C., Van, T.M., Wachsmuth, L., Polykratis, A., and Pasparakis, M. (2016). RIPK1 counteracts ZBP1-mediated necroptosis to inhibit inflammation. Nature *540*, 124-128. 10.1038/nature20558.

344. Zhao, J., Jitkaew, S., Cai, Z., Choksi, S., Li, Q., Luo, J., and Liu, Z.G. (2012). Mixed lineage kinase domain-like is a key receptor interacting protein 3 downstream component of TNF-induced necrosis. Proc Natl Acad Sci U S A *109*, 5322-5327. 10.1073/pnas.1200012109.

345. Chinnaiyan, A.M., O'Rourke, K., Tewari, M., and Dixit, V.M. (1995). FADD, a novel death domain-containing protein, interacts with the death domain of Fas and initiates apoptosis. Cell *81*, 505-512. 10.1016/0092-8674(95)90071-3.

346. Boldin, M.P., Varfolomeev, E.E., Pancer, Z., Mett, I.L., Camonis, J.H., and Wallach, D. (1995). A novel protein that interacts with the death domain of Fas/APO1 contains a sequence motif related to the death domain. J Biol Chem *270*, 7795-7798. 10.1074/jbc.270.14.7795.

347. Bell, B.D., Leverrier, S., Weist, B.M., Newton, R.H., Arechiga, A.F., Luhrs, K.A., Morrissette, N.S., and Walsh, C.M. (2008). FADD and caspase-8 control the outcome of autophagic signaling in proliferating T cells. Proc Natl Acad Sci U S A *105*, 16677-16682. 10.1073/pnas.0808597105.

348. Osborn, S.L., Diehl, G., Han, S.J., Xue, L., Kurd, N., Hsieh, K., Cado, D., Robey, E.A., and Winoto, A. (2010). Fas-associated death domain (FADD) is a negative regulator of T-cell receptor-mediated necroptosis. Proc Natl Acad Sci U S A *107*, 13034-13039. 10.1073/pnas.1005997107.

349. Gavrieli, Y., Sherman, Y., and Ben-Sasson, S.A. (1992). Identification of programmed cell death in situ via specific labeling of nuclear DNA fragmentation. J Cell Biol *119*, 493-501. 10.1083/jcb.119.3.493.

350. Grivennikov, S.I., Tumanov, A.V., Liepinsh, D.J., Kruglov, A.A., Marakusha, B.I., Shakhov, A.N., Murakami, T., Drutskaya, L.N., Forster, I., Clausen, B.E., et al. (2005). Distinct and nonredundant in vivo functions of TNF produced by t cells and macrophages/neutrophils: protective and deleterious effects. Immunity *22*, 93-104. 10.1016/j.immuni.2004.11.016.

351. Van Hauwermeiren, F., Armaka, M., Karagianni, N., Kranidioti, K., Vandenbroucke, R.E., Loges, S., Van Roy, M., Staelens, J., Puimege, L., Palagani, A., et al. (2013). Safe TNF-based antitumor therapy following p55TNFR reduction in intestinal epithelium. J Clin Invest *123*, 2590-2603. 10.1172/JCI65624.

352. Audie, J.P., Janin, A., Porchet, N., Copin, M.C., Gosselin, B., and Aubert, J.P. (1993). Expression of human mucin genes in respiratory, digestive, and reproductive tracts ascertained by in situ hybridization. J Histochem Cytochem *41*, 1479-1485. 10.1177/41.10.8245407.

353. Weiss, A.A., Babyatsky, M.W., Ogata, S., Chen, A., and Itzkowitz, S.H. (1996). Expression of MUC2 and MUC3 mRNA in human normal, malignant, and inflammatory intestinal tissues. J Histochem Cytochem *44*, 1161-1166. 10.1177/44.10.8813081.

354. Velcich, A., Yang, W., Heyer, J., Fragale, A., Nicholas, C., Viani, S., Kucherlapati, R., Lipkin, M., Yang, K., and Augenlicht, L. (2002). Colorectal cancer in mice genetically deficient in the mucin Muc2. Science *295*, 1726-1729. 10.1126/science.1069094.

355. Atuma, C., Strugala, V., Allen, A., and Holm, L. (2001). The adherent gastrointestinal mucus gel layer: thickness and physical state in vivo. Am J Physiol Gastrointest Liver Physiol *280*, G922-929. 10.1152/ajpgi.2001.280.5.G922.

356. Johansson, M.E., and Hansson, G.C. (2012). Preservation of mucus in histological sections, immunostaining of mucins in fixed tissue, and localization of bacteria with FISH. Methods Mol Biol *842*, 229-235. 10.1007/978-1-61779-513-8_13.

357. Kandori, H., Hirayama, K., Takeda, M., and Doi, K. (1996). Histochemical, lectin-histochemical and morphometrical characteristics of intestinal goblet cells of germfree and conventional mice. Exp Anim *45*, 155-160. 10.1538/expanim.45.155.

358. Williams, S.J., McGuckin, M.A., Gotley, D.C., Eyre, H.J., Sutherland, G.R., and Antalis, T.M. (1999). Two novel mucin genes down-regulated in colorectal cancer identified by differential display. Cancer Res *59*, 4083-4089.

359. Tateno, H., Yabe, R., Sato, T., Shibazaki, A., Shikanai, T., Gonoi, T., Narimatsu, H., and Hirabayashi, J. (2012). Human ZG16p recognizes pathogenic fungi through non-self polyvalent mannose in the digestive system. Glycobiology *22*, 210-220. 10.1093/glycob/cwr130.

360. Jakobsson, H.E., Rodriguez-Pineiro, A.M., Schutte, A., Ermund, A., Boysen, P., Bemark, M., Sommer, F., Backhed, F., Hansson, G.C., and Johansson, M.E. (2015). The composition of the gut microbiota shapes the colon mucus barrier. EMBO Rep *16*, 164-177. 10.15252/embr.201439263.

361. Van Hauwermeiren, F., Vandenbroucke, R.E., Grine, L., Lodens, S., Van Wonterghem, E., De Rycke, R., De Geest, N., Hassan, B., and Libert, C. (2015). TNFR1-induced lethal inflammation is mediated by goblet and Paneth cell dysfunction. Mucosal Immunol *8*, 828-840. 10.1038/mi.2014.112.

362. Ilani, T., Reznik, N., Yeshaya, N., Feldman, T., Vilela, P., Lansky, Z., Javitt, G., Shemesh, M., Brenner, O., Elkis, Y., et al. (2023). The disulfide catalyst QSOX1 maintains the colon mucosal barrier by regulating Golgi glycosyltransferases. EMBO J *42*, e111869. 10.15252/embj.2022111869.

363. Yao, Y., Kim, G., Shafer, S., Chen, Z., Kubo, S., Ji, Y., Luo, J., Yang, W., Perner, S.P., Kanellopoulou, C., et al. (2022). Mucus sialylation determines intestinal host-commensal homeostasis. Cell *185*, 1172-1188 e1128. 10.1016/j.cell.2022.02.013.

364. Reily, C., Stewart, T.J., Renfrow, M.B., and Novak, J. (2019). Glycosylation in health and disease. Nat Rev Nephrol *15*, 346-366. 10.1038/s41581-019-0129-4.

365. Johansson, M.E., Jakobsson, H.E., Holmen-Larsson, J., Schutte, A., Ermund, A., Rodriguez-Pineiro, A.M., Arike, L., Wising, C., Svensson, F., Backhed, F., and Hansson, G.C. (2015). Normalization of Host Intestinal Mucus Layers Requires Long-Term Microbial Colonization. Cell Host Microbe *18*, 582-592. 10.1016/j.chom.2015.10.007.

366. Frantz, A.L., Rogier, E.W., Weber, C.R., Shen, L., Cohen, D.A., Fenton, L.A., Bruno, M.E., and Kaetzel, C.S. (2012). Targeted deletion of MyD88 in intestinal epithelial cells results in compromised antibacterial immunity associated with downregulation of polymeric immunoglobulin receptor, mucin-2, and antibacterial peptides. Mucosal Immunol *5*, 501-512. 10.1038/mi.2012.23.

367. Fre, S., Huyghe, M., Mourikis, P., Robine, S., Louvard, D., and Artavanis-Tsakonas, S. (2005). Notch signals control the fate of immature progenitor cells in the intestine. Nature *435*, 964-968. 10.1038/nature03589.

368. van Es, J.H., van Gijn, M.E., Riccio, O., van den Born, M., Vooijs, M., Begthel, H., Cozijnsen, M., Robine, S., Winton, D.J., Radtke, F., and Clevers, H. (2005). Notch/gamma-secretase inhibition turns proliferative cells in intestinal crypts and adenomas into goblet cells. Nature *435*, 959-963. 10.1038/nature03659.

369. Dovey, H.F., John, V., Anderson, J.P., Chen, L.Z., de Saint Andrieu, P., Fang, L.Y., Freedman, S.B., Folmer, B., Goldbach, E., Holsztynska, E.J., et al. (2001). Functional gamma-secretase inhibitors reduce beta-amyloid peptide levels in brain. J Neurochem *76*, 173-181. 10.1046/j.1471-4159.2001.00012.x.

370. Geling, A., Steiner, H., Willem, M., Bally-Cuif, L., and Haass, C. (2002). A gamma-secretase inhibitor blocks Notch signaling in vivo and causes a severe neurogenic phenotype in zebrafish. EMBO Rep *3*, 688-694. 10.1093/embo-reports/kvf124.

371. Bray, S.J. (2016). Notch signalling in context. Nat Rev Mol Cell Biol *17*, 722-735. 10.1038/nrm.2016.94.

372. Shroyer, N.F., Helmrath, M.A., Wang, V.Y., Antalffy, B., Henning, S.J., and Zoghbi, H.Y. (2007). Intestine-specific ablation of mouse atonal homolog 1 (Math1) reveals a role in cellular homeostasis. Gastroenterology *132*, 2478-2488. 10.1053/j.gastro.2007.03.047.

373. Yang, Q., Bermingham, N.A., Finegold, M.J., and Zoghbi, H.Y. (2001). Requirement of Math1 for secretory cell lineage commitment in the mouse intestine. Science *294*, 2155-2158. 10.1126/science.1065718.

374. Katz, J.P., Perreault, N., Goldstein, B.G., Lee, C.S., Labosky, P.A., Yang, V.W., and Kaestner, K.H. (2002). The zinc-finger transcription factor Klf4 is required for terminal differentiation of goblet cells in the colon. Development *129*, 2619-2628. 10.1242/dev.129.11.2619.

375. Gregorieff, A., Stange, D.E., Kujala, P., Begthel, H., van den Born, M., Korving, J., Peters, P.J., and Clevers, H. (2009). The ets-domain transcription factor Spdef promotes maturation of goblet and paneth cells in the intestinal epithelium. Gastroenterology *137*, 1333-1345 e1331-1333. 10.1053/j.gastro.2009.06.044.

376. Spicer, S.S., Staley, M.W., Wetzel, M.G., and Wetzel, B.K. (1967). Acid mucosubstance and basic protein in mouse Paneth cells. J Histochem Cytochem *15*, 225-242. 10.1177/15.4.225.

377. Stahl, M., Tremblay, S., Montero, M., Vogl, W., Xia, L., Jacobson, K., Menendez, A., and Vallance, B.A. (2018). The Muc2 mucin coats murine Paneth cell granules and facilitates their content release and dispersion. Am J Physiol Gastrointest Liver Physiol *315*, G195-G205. 10.1152/ajpgi.00264.2017.

378. Johansson, M.E., Gustafsson, J.K., Holmen-Larsson, J., Jabbar, K.S., Xia, L., Xu, H., Ghishan, F.K., Carvalho, F.A., Gewirtz, A.T., Sjovall, H., and Hansson, G.C. (2014). Bacteria penetrate the normally impenetrable inner colon mucus layer in both murine colitis models and patients with ulcerative colitis. Gut *63*, 281-291. 10.1136/gutjnl-2012-303207.

379. Gustafsson, J.K., and Johansson, M.E.V. (2022). The role of goblet cells and mucus in intestinal homeostasis. Nat Rev Gastroenterol Hepatol *19*, 785-803. 10.1038/s41575-022-00675-x.

380. He, S., Liang, Y., Shao, F., and Wang, X. (2011). Toll-like receptors activate programmed necrosis in macrophages through a receptor-interacting kinase-3-mediated pathway. Proc Natl Acad Sci U S A *108*, 20054-20059. 10.1073/pnas.1116302108.

381. Kaiser, W.J., Sridharan, H., Huang, C., Mandal, P., Upton, J.W., Gough, P.J., Sehon, C.A., Marquis, R.W., Bertin, J., and Mocarski, E.S. (2013). Toll-like receptor 3-mediated necrosis via TRIF, RIP3, and MLKL. J Biol Chem *288*, 31268-31279. 10.1074/jbc.M113.462341.

382. Polykratis, A., Hermance, N., Zelic, M., Roderick, J., Kim, C., Van, T.M., Lee, T.H., Chan, F.K.M., Pasparakis, M., and Kelliher, M.A. (2014). Cutting edge: RIPK1 Kinase inactive mice are viable and protected from TNF-induced necroptosis in vivo. J Immunol *193*, 1539-1543. 10.4049/jimmunol.1400590.

383. McNab, F., Mayer-Barber, K., Sher, A., Wack, A., and O'Garra, A. (2015). Type I interferons in infectious disease. Nat Rev Immunol *15*, 87-103. 10.1038/nri3787.

384. Hentschel, V., Seufferlein, T., and Armacki, M. (2021). Intestinal organoids in coculture: redefining the boundaries of gut mucosa ex vivo modeling. Am J Physiol Gastrointest Liver Physiol *321*, G693-G704. 10.1152/ajpgi.00043.2021.

385. Puschhof, J., Pleguezuelos-Manzano, C., Martinez-Silgado, A., Akkerman, N., Saftien, A., Boot, C., de Waal, A., Beumer, J., Dutta, D., Heo, I., and Clevers, H. (2021). Intestinal organoid cocultures with microbes. Nat Protoc *16*, 4633-4649. 10.1038/s41596-021-00589-z.

386. O'Gorman, S., Fox, D.T., and Wahl, G.M. (1991). Recombinase-mediated gene activation and site-specific integration in mammalian cells. Science *251*, 1351-1355. 10.1126/science.1900642.

387. Raymond, C.S., and Soriano, P. (2007). High-efficiency FLP and PhiC31 site-specific recombination in mammalian cells. PLoS One *2*, e162. 10.1371/journal.pone.0000162.

388. Datta, S.S., Preska Steinberg, A., and Ismagilov, R.F. (2016). Polymers in the gut compress the colonic mucus hydrogel. Proc Natl Acad Sci U S A *113*, 7041-7046. 10.1073/pnas.1602789113.

389. Nishikawa, M., Hasegawa, S., Yamashita, F., Takakura, Y., and Hashida, M. (2002). Electrical charge on protein regulates its absorption from the rat small intestine. Am J Physiol Gastrointest Liver Physiol *282*, G711-719. 10.1152/ajpgi.00358.2001.

390. Kocevar-Nared, J., Kristl, J., and Smid-Korbar, J. (1997). Comparative rheological investigation of crude gastric mucin and natural gastric mucus. Biomaterials *18*, 677-681. 10.1016/s0142-9612(96)00180-9.

391. Bej, R., and Haag, R. (2022). Mucus-Inspired Dynamic Hydrogels: Synthesis and Future Perspectives. J Am Chem Soc *144*, 20137-20152. 10.1021/jacs.1c13547.

392. Garrett, W.S., Gallini, C.A., Yatsunenko, T., Michaud, M., DuBois, A., Delaney, M.L., Punit, S., Karlsson, M., Bry, L., Glickman, J.N., et al. (2010). Enterobacteriaceae act in concert with the gut microbiota to induce spontaneous and maternally transmitted colitis. Cell Host Microbe *8*, 292-300. 10.1016/j.chom.2010.08.004.

393. Zhu, W., Winter, M.G., Byndloss, M.X., Spiga, L., Duerkop, B.A., Hughes, E.R., Buttner, L., de Lima Romao, E., Behrendt, C.L., Lopez, C.A., et al. (2018). Precision editing of the gut microbiota ameliorates colitis. Nature *553*, 208-211. 10.1038/nature25172.

394. Schulfer, A.F., Battaglia, T., Alvarez, Y., Bijnens, L., Ruiz, V.E., Ho, M., Robinson, S., Ward, T., Cox, L.M., Rogers, A.B., et al. (2018). Intergenerational transfer of antibiotic-perturbed microbiota enhances colitis in susceptible mice. Nat Microbiol *3*, 234-242. 10.1038/s41564-017-0075-5.

395. Lin, J.H., Li, H., Yasumura, D., Cohen, H.R., Zhang, C., Panning, B., Shokat, K.M., Lavail, M.M., and Walter, P. (2007). IRE1 signaling affects cell fate during the unfolded protein response. Science *318*, 944-949. 10.1126/science.1146361.

396. Back, S.H., Scheuner, D., Han, J., Song, B., Ribick, M., Wang, J., Gildersleeve, R.D., Pennathur, S., and Kaufman, R.J. (2009). Translation attenuation through eIF2alpha phosphorylation prevents oxidative stress and maintains the differentiated state in beta cells. Cell Metab *10*, 13-26. 10.1016/j.cmet.2009.06.002.

397. Han, J., Song, B., Kim, J., Kodali, V.K., Pottekat, A., Wang, M., Hassler, J., Wang, S., Pennathur, S., Back, S.H., et al. (2015). Antioxidants Complement the Requirement for Protein Chaperone Function to Maintain beta-Cell Function and Glucose Homeostasis. Diabetes *64*, 2892-2904. 10.2337/db14-1357.

398. Lu, M., Lawrence, D.A., Marsters, S., Acosta-Alvear, D., Kimmig, P., Mendez, A.S., Paton, A.W., Paton, J.C., Walter, P., and Ashkenazi, A. (2014). Opposing unfolded-protein-response signals converge on death receptor 5 to control apoptosis. Science *345*, 98-101. 10.1126/science.1254312.

399. Chang, T.K., Lawrence, D.A., Lu, M., Tan, J., Harnoss, J.M., Marsters, S.A., Liu, P., Sandoval, W., Martin, S.E., and Ashkenazi, A. (2018). Coordination between Two Branches of the Unfolded Protein Response Determines Apoptotic Cell Fate. Mol Cell *71*, 629-636 e625. 10.1016/j.molcel.2018.06.038.

400. Puthalakath, H., O'Reilly, L.A., Gunn, P., Lee, L., Kelly, P.N., Huntington, N.D., Hughes, P.D., Michalak, E.M., McKimm-Breschkin, J., Motoyama, N., et al. (2007). ER stress triggers apoptosis by activating BH3-only protein Bim. Cell *129*, 1337-1349. 10.1016/j.cell.2007.04.027.

401. Upton, J.P., Wang, L., Han, D., Wang, E.S., Huskey, N.E., Lim, L., Truitt, M., McManus, M.T., Ruggero, D., Goga, A., et al. (2012). IRE1alpha cleaves select microRNAs during ER stress to derepress translation of proapoptotic Caspase-2. Science *338*, 818-822. 10.1126/science.1226191.

402. Ren, F., Narita, R., Rashidi, A.S., Fruhwurth, S., Gao, Z., Bak, R.O., Thomsen, M.K., Verjans, G.M., Reinert, L.S., and Paludan, S.R. (2023). ER stress induces caspase-2-tBID-GSDME-dependent cell death in neurons lytically infected with herpes simplex virus type 2. EMBO J, e113118. 10.15252/embj.2022113118.

403. Rojas-Rivera, D., Armisen, R., Colombo, A., Martinez, G., Eguiguren, A.L., Diaz, A., Kiviluoto, S., Rodriguez, D., Patron, M., Rizzuto, R., et al. (2012). TMBIM3/GRINA is a novel unfolded protein response (UPR) target gene that controls apoptosis through the modulation of ER calcium homeostasis. Cell Death Differ *19*, 1013-1026. 10.1038/cdd.2011.189.

404. Oslowski, C.M., Hara, T., O'Sullivan-Murphy, B., Kanekura, K., Lu, S., Hara, M., Ishigaki, S., Zhu, L.J., Hayashi, E., Hui, S.T., et al. (2012). Thioredoxin-interacting protein mediates ER stress-induced beta cell death through initiation of the inflammasome. Cell Metab *16*, 265-273. 10.1016/j.cmet.2012.07.005.

405. Lerner, A.G., Upton, J.P., Praveen, P.V., Ghosh, R., Nakagawa, Y., Igbaria, A., Shen, S., Nguyen, V., Backes, B.J., Heiman, M., et al. (2012). IRE1alpha induces thioredoxin-interacting protein to activate the NLRP3 inflammasome and promote programmed cell death under irremediable ER stress. Cell Metab *16*, 250-264. 10.1016/j.cmet.2012.07.007.

406. Bronner, D.N., Abuaita, B.H., Chen, X., Fitzgerald, K.A., Nunez, G., He, Y., Yin, X.M., and O'Riordan, M.X. (2015). Endoplasmic Reticulum Stress Activates the Inflammasome via NLRP3- and Caspase-2-Driven Mitochondrial Damage. Immunity *43*, 451-462. 10.1016/j.immuni.2015.08.008.

407. Birchenough, G.M., Nystrom, E.E., Johansson, M.E., and Hansson, G.C. (2016). A sentinel goblet cell guards the colonic crypt by triggering Nlrp6-dependent Muc2 secretion. Science *352*, 1535-1542. 10.1126/science.aaf7419.

408. Knoop, K.A., McDonald, K.G., McCrate, S., McDole, J.R., and Newberry, R.D. (2015). Microbial sensing by goblet cells controls immune surveillance of luminal antigens in the colon. Mucosal Immunol *8*, 198-210. 10.1038/mi.2014.58.

409. Wlodarska, M., Thaiss, C.A., Nowarski, R., Henao-Mejia, J., Zhang, J.P., Brown, E.M., Frankel, G., Levy, M., Katz, M.N., Philbrick, W.M., et al. (2014). NLRP6 inflammasome orchestrates the colonic host-microbial interface by regulating goblet cell mucus secretion. Cell *156*, 1045-1059. 10.1016/j.cell.2014.01.026.

410. Evans, G.S., Flint, N., Somers, A.S., Eyden, B., and Potten, C.S. (1992). The development of a method for the preparation of rat intestinal epithelial cell primary cultures. J Cell Sci *101 (Pt 1)*, 219-231. 10.1242/jcs.101.1.219.

411. Whitehead, R.H., Demmler, K., Rockman, S.P., and Watson, N.K. (1999). Clonogenic growth of epithelial cells from normal colonic mucosa from both mice and humans. Gastroenterology *117*, 858-865. 10.1016/s0016-5085(99)70344-6.

412. Fukamachi, H. (1992). Proliferation and differentiation of fetal rat intestinal epithelial cells in primary serum-free culture. J Cell Sci *103 (Pt 2)*, 511-519. 10.1242/jcs.103.2.511.

413. Feldman, H.C., Vidadala, V.N., Potter, Z.E., Papa, F.R., Backes, B.J., and Maly, D.J. (2019). Development of a Chemical Toolset for Studying the Paralog-Specific Function of IRE1. ACS Chem Biol *14*, 2595-2605. 10.1021/acschembio.9b00482.

414. Calfon, M., Zeng, H., Urano, F., Till, J.H., Hubbard, S.R., Harding, H.P., Clark, S.G., and Ron, D. (2002). IRE1 couples endoplasmic reticulum load to secretory capacity by processing the XBP-1 mRNA. Nature *415*, 92-96. 10.1038/415092a.

415. Grey, M.J., Cloots, E., Simpson, M.S., LeDuc, N., Serebrenik, Y.V., De Luca, H., De Sutter, D., Luong, P., Thiagarajah, J.R., Paton, A.W., et al. (2020). IRE1beta negatively regulates IRE1alpha signaling in response to endoplasmic reticulum stress. J Cell Biol *219*. 10.1083/jcb.201904048.

416. Yin, X., Farin, H.F., van Es, J.H., Clevers, H., Langer, R., and Karp, J.M. (2014). Niche-independent high-purity cultures of Lgr5+ intestinal stem cells and their progeny. Nat Methods *11*, 106-112. 10.1038/nmeth.2737.

417. Menche, C., and Farin, H.F. (2021). Strategies for genetic manipulation of adult stem cell-derived organoids. Exp Mol Med *53*, 1483-1494. 10.1038/s12276-021-00609-8.

418. Martinez-Silgado, A., Yousef Yengej, F.A., Puschhof, J., Geurts, V., Boot, C., Geurts, M.H., Rookmaaker, M.B., Verhaar, M.C., Beumer, J., and Clevers, H. (2022). Differentiation and CRISPR-Cas9-mediated genetic engineering of human intestinal organoids. STAR Protoc *3*, 101639. 10.1016/j.xpro.2022.101639.

419. Niederreiter, L., Fritz, T.M., Adolph, T.E., Krismer, A.M., Offner, F.A., Tschurtschenthaler, M., Flak, M.B., Hosomi, S., Tomczak, M.F., Kaneider, N.C., et al. (2013). ER stress transcription factor Xbp1 suppresses intestinal tumorigenesis and directs intestinal stem cells. J Exp Med *210*, 2041-2056. 10.1084/jem.20122341.

420. Cross, B.C., Bond, P.J., Sadowski, P.G., Jha, B.K., Zak, J., Goodman, J.M., Silverman, R.H., Neubert, T.A., Baxendale, I.R., Ron, D., and Harding, H.P. (2012). The molecular basis for selective inhibition of unconventional mRNA splicing by an IRE1-binding small molecule. Proc Natl Acad Sci U S A *109*, E869-878. 10.1073/pnas.1115623109.

421. Neidhardt, L., Cloots, E., Friemel, N., Weiss, C.A.M., Harding, H.P., McLaughlin, S.H., Janssens, S., and Ron, D. (2024). The IRE1beta-mediated unfolded protein response is repressed by the chaperone AGR2 in mucin producing cells. EMBO J *43*, 719-753. 10.1038/s44318-023-00014-z.

422. Gum, J.R., Jr., Hicks, J.W., Gillespie, A.M., Carlson, E.J., Komuves, L., Karnik, S., Hong, J.C., Epstein, C.J., and Kim, Y.S. (1999). Goblet cell-specific expression mediated by the MUC2 mucin gene promoter in the intestine of transgenic mice. Am J Physiol *276*, G666-676. 10.1152/ajpgi.1999.276.3.G666.

423. Cloots, E., Simpson, M.S., De Nolf, C., Lencer, W.I., Janssens, S., and Grey, M.J. (2021). Evolution and function of the epithelial cell-specific ER stress sensor IRE1beta. Mucosal Immunol *14*, 1235-1246. 10.1038/s41385-021-00412-8.

424. Todd, D.J., Lee, A.H., and Glimcher, L.H. (2008). The endoplasmic reticulum stress response in immunity and autoimmunity. Nat Rev Immunol *8*, 663-674. 10.1038/nri2359.

425. Javitt, G., Calvo, M.L.G., Albert, L., Reznik, N., Ilani, T., Diskin, R., and Fass, D. (2019). Intestinal Gel-Forming Mucins Polymerize by Disulfide-Mediated Dimerization of D3 Domains. J Mol Biol *431*, 3740-3752. 10.1016/j.jmb.2019.07.018.

426. Lesuffleur, T., Barbat, A., Dussaulx, E., and Zweibaum, A. (1990). Growth adaptation to methotrexate of HT-29 human colon carcinoma cells is associated with their ability to differentiate into columnar absorptive and mucus-secreting cells. Cancer Res *50*, 6334-6343.

427. Elzinga, J., van der Lugt, B., Belzer, C., and Steegenga, W.T. (2021). Characterization of increased mucus production of HT29-MTX-E12 cells grown under Semi-Wet interface with Mechanical Stimulation. PLoS One *16*, e0261191. 10.1371/journal.pone.0261191.

428. Hsu, H.P., Lai, M.D., Lee, J.C., Yen, M.C., Weng, T.Y., Chen, W.C., Fang, J.H., and Chen, Y.L. (2017). Mucin 2 silencing promotes colon cancer metastasis through interleukin-6 signaling. Sci Rep *7*, 5823. 10.1038/s41598-017-04952-7.

429. Bu, X.D., Li, N., Tian, X.Q., and Huang, P.L. (2011). Caco-2 and LS174T cell lines provide different models for studying mucin expression in colon cancer. Tissue Cell *43*, 201-206. 10.1016/j.tice.2011.03.002.

430. Jeong, H., Hong, E.H., Ahn, J.H., Cho, J., Jeong, J.H., Kim, C.W., Yoon, B.I., Koo, J.H., Park, Y.Y., Yang, Y.M., et al. (2023). ERdj5 protects goblet cells from endoplasmic reticulum stress-mediated apoptosis under inflammatory conditions. Exp Mol Med *55*, 401-412. 10.1038/s12276-023-00945-x.

431. Lis, H., and Sharon, N. (1993). Protein glycosylation. Structural and functional aspects. Eur J Biochem *218*, 1-27. 10.1111/j.1432-1033.1993.tb18347.x.

432. Varki, A. (2008). Sialic acids in human health and disease. Trends Mol Med *14*, 351-360. 10.1016/j.molmed.2008.06.002.

433. Mowry, R.W. (1963). Special Value of Methods That Color Both Acidic and Vicinal Hydroxl Groups in Histochemical Study of Mucins - with Revised Directions for Colloidal Iron Stain, Use of Alcian Blue G8x and Their Combinations with Periodic Acid-Schiff Reaction. Ann Ny Acad Sci *106*, 402-&.

434. Nystrom, E.E.L., Martinez-Abad, B., Arike, L., Birchenough, G.M.H., Nonnecke, E.B., Castillo, P.A., Svensson, F., Bevins, C.L., Hansson, G.C., and Johansson, M.E.V. (2021). An intercrypt subpopulation of goblet cells is essential for colonic mucus barrier function. Science *372*. 10.1126/science.abb1590.

435. Hu, P., Han, Z., Couvillon, A.D., Kaufman, R.J., and Exton, J.H. (2006). Autocrine tumor necrosis factor alpha links endoplasmic reticulum stress to the membrane death receptor pathway through IRE1alpha-mediated NF-kappaB activation and down-regulation of TRAF2 expression. Mol Cell Biol *26*, 3071-3084. 10.1128/MCB.26.8.3071-3084.2006.

436. Roda, G., Jharap, B., Neeraj, N., and Colombel, J.F. (2016). Loss of Response to Anti-TNFs: Definition, Epidemiology, and Management. Clin Transl Gastroenterol *7*, e135. 10.1038/ctg.2015.63.

437. Plichta, D.R., Graham, D.B., Subramanian, S., and Xavier, R.J. (2019). Therapeutic Opportunities in Inflammatory Bowel Disease: Mechanistic Dissection of Host-Microbiome Relationships. Cell *178*, 1041-1056. 10.1016/j.cell.2019.07.045.

438. Hass, P.E., Hotchkiss, A., Mohler, M., and Aggarwal, B.B. (1985). Characterization of Specific High-Affinity Receptors for Human-Tumor Necrosis Factor on Mouse Fibroblasts. Journal of Biological Chemistry *260*, 2214-2218.

439. Etemadi, N., Holien, J.K., Chau, D., Dewson, G., Murphy, J.M., Alexander, W.S., Parker, M.W., Silke, J., and Nachbur, U. (2013). Lymphotoxin alpha induces apoptosis, necroptosis and inflammatory signals with the same potency as tumour necrosis factor. FEBS J *280*, 5283-5297. 10.1111/febs.12419.

440. Rusu, I., Mennillo, E., Bain, J.L., Li, Z., Sun, X., Ly, K.M., Rosli, Y.Y., Naser, M., Wang, Z., Advincula, R., et al. (2022). Microbial signals, MyD88, and lymphotoxin drive TNF-independent intestinal epithelial tissue damage. J Clin Invest *132*. 10.1172/JCI154993.

441. Chiang, E.Y., Kolumam, G.A., Yu, X., Francesco, M., Ivelja, S., Peng, I., Gribling, P., Shu, J., Lee, W.P., Refino, C.J., et al. (2009). Targeted depletion of lymphotoxin-alpha-expressing TH1 and TH17 cells inhibits autoimmune disease. Nat Med *15*, 766-773. 10.1038/nm.1984.

442. De Togni, P., Goellner, J., Ruddle, N.H., Streeter, P.R., Fick, A., Mariathasan, S., Smith, S.C., Carlson, R., Shornick, L.P., Strauss-Schoenberger, J., and et al. (1994). Abnormal development of peripheral lymphoid organs in mice deficient in lymphotoxin. Science *264*, 703-707. 10.1126/science.8171322.

443. Calmon-Hamaty, F., Combe, B., Hahne, M., and Morel, J. (2011). Lymphotoxin alpha revisited: general features and implications in rheumatoid arthritis. Arthritis Res Ther *13*, 232. 10.1186/ar3376.

444. Albarbar, B., Dunnill, C., and Georgopoulos, N.T. (2015). Regulation of cell fate by lymphotoxin (LT) receptor signalling: Functional differences and similarities of the LT system to other TNF superfamily (TNFSF) members. Cytokine Growth Factor Rev *26*, 659-671. 10.1016/j.cytogfr.2015.05.001.

445. Saveljeva, S., Mc Laughlin, S.L., Vandenabeele, P., Samali, A., and Bertrand, M.J. (2015). Endoplasmic reticulum stress induces ligand-independent TNFR1-mediated necroptosis in L929 cells. Cell Death Dis *6*, e1587. 10.1038/cddis.2014.548.

446. Ktistakis, N.T., Linder, M.E., and Roth, M.G. (1992). Action of brefeldin A blocked by activation of a pertussis-toxin-sensitive G protein. Nature *356*, 344-346. 10.1038/356344a0.

447. LeCouter, J.E., Kablar, B., Whyte, P.F., Ying, C., and Rudnicki, M.A. (1998). Strain-dependent embryonic lethality in mice lacking the retinoblastoma-related p130 gene. Development *125*, 4669-4679. 10.1242/dev.125.23.4669.

448. Sibilia, M., and Wagner, E.F. (1995). Strain-dependent epithelial defects in mice lacking the EGF receptor. Science *269*, 234-238. 10.1126/science.7618085.

449. Grootjans, J., Krupka, N., Hosomi, S., Matute, J.D., Hanley, T., Saveljeva, S., Gensollen, T., Heijmans, J., Li, H., Limenitakis, J.P., et al. (2019). Epithelial endoplasmic reticulum stress orchestrates a protective IgA response. Science *363*, 993-998. 10.1126/science.aat7186.

450. Mc Guire, C., Volckaert, T., Wolke, U., Sze, M., de Rycke, R., Waisman, A., Prinz, M., Beyaert, R., Pasparakis, M., and van Loo, G. (2010). Oligodendrocyte-specific FADD deletion protects

mice from autoimmune-mediated demyelination. J Immunol *185*, 7646-7653. 10.4049/jimmunol.1000930.

451. Rodriguez, C.I., Buchholz, F., Galloway, J., Sequerra, R., Kasper, J., Ayala, R., Stewart, A.F., and Dymecki, S.M. (2000). High-efficiency deleter mice show that FLPe is an alternative to Cre-loxP. Nat Genet *25*, 139-140. 10.1038/75973.

452. Liao, Y., Smyth, G.K., and Shi, W. (2013). The Subread aligner: fast, accurate and scalable read mapping by seed-and-vote. Nucleic Acids Res *41*, e108. 10.1093/nar/gkt214.

453. Huber, W., Carey, V.J., Gentleman, R., Anders, S., Carlson, M., Carvalho, B.S., Bravo, H.C., Davis, S., Gatto, L., Girke, T., et al. (2015). Orchestrating high-throughput genomic analysis with Bioconductor. Nat Methods *12*, 115-121. 10.1038/nmeth.3252.

454. Robinson, M.D., McCarthy, D.J., and Smyth, G.K. (2010). edgeR: a Bioconductor package for differential expression analysis of digital gene expression data. Bioinformatics *26*, 139-140. 10.1093/bioinformatics/btp616.

455. Love, M.I., Huber, W., and Anders, S. (2014). Moderated estimation of fold change and dispersion for RNA-seq data with DESeq2. Genome Biol *15*, 550. 10.1186/s13059-014-0550-8.

456. Zhu, A., Ibrahim, J.G., and Love, M.I. (2019). Heavy-tailed prior distributions for sequence count data: removing the noise and preserving large differences. Bioinformatics *35*, 2084-2092. 10.1093/bioinformatics/bty895.

457. Yu, G., Wang, L.G., Han, Y., and He, Q.Y. (2012). clusterProfiler: an R package for comparing biological themes among gene clusters. OMICS *16*, 284-287. 10.1089/omi.2011.0118.

458. Gu, Z., Eils, R., and Schlesner, M. (2016). Complex heatmaps reveal patterns and correlations in multidimensional genomic data. Bioinformatics *32*, 2847-2849. 10.1093/bioinformatics/btw313.

7. Acknowledgement

First and foremost, I would like to express my sincere thanks to Prof. Dr. Manolis Pasparakis that he has given me a chance to work in his lab and trusted me. Through his years-long mentorship, I acquired critical thinking and a focused scientific approach. I am genuinely grateful for his support and guidance, helping me to become a scientist.

I would like to thank Prof. Dr. Philip Rosenstiel, Prof. Dr. Hamid Kashkar. and Prof. Dr. Matthias Hammerschmidt for agreeing to participate in the assessment of this thesis. I also thank Dr. Emmi Wachsmuth for accepting to be Beisitzenderin and helping me with bureaucratic problems that I came across over the years.

I thank Ulrike Göbel for helping us with the RNA-sequencing analysis.

I want to thank the members of the Pasparakis lab who kindly helped me and encouraged me with polite scientific/non-scientific discussions and conversations whenever I needed.

I am deeply thankful to our technicians. They made my life easier: Paul Roggan, Edeltraud Stade, Elza Gareus, Jennifer Kuth, Julia von Rhein, Nina Richter, Mathilda Hahn, Claudia Uthoff-Hachenberg, Bettina Löffelsender. I also want to thank Silke Röpke who has helped me extensively with bureaucratic process during my early days in Germany. I also thank Dr. Johannes Winkler and Dr. Martin Hafner for helping me with the bureaucratic problems that I encountered.

Contributions of previous Lab members to the study:

Dr. Robin Schwarzer, Dr. Marius Dannappel and Dr. Katerina Vlantis generated all the mouse lines used in this study. Some of the intestinal histological sections in this thesis were collected by them. Ulrike Goebel performed mRNA sequencing analysis. I performed the rest of the experiments in this study.